AD-637 506

AFFDL-TR-66-7

SONIC FATIGUE IN COMBINED ENVIRONMENT

JOHN R. BALLENTINE
HARRY E. PLUMBLEE
CECIL W. SCHNEIDER

LOCKHEED-GEORGIA COMPANY

TECHNICAL REPORT AFFDL-TR-66-7

MAY 1966

20070921456

The distribution of this document is unlimited

AIR FORCE FLIGHT DYNAMICS LABORATORY
RESEARCH AND TECHNOLOGY DIVISION
AIR FORCE SYSTEMS COMMAND
WRIGHT-PATTERSON AIR FORCE BASE, OHIO

NOTICES

When Government drawings, specifications, or other data are used for any purpose other than in connection with a definitely related Government procurement operation, the United States Government thereby incurs no responsibility nor any obligation whatsoever; and the fact that the Government may have formulated, furnished, or in any way supplied the said drawings, specifications, or other data, is not to be regarded by implication or otherwise as in any manner licensing the holder or any other person or corporation, or conveying any rights or permission to manufacture, use, or sell any patented invention that may in any way be related thereto.

Copies of this report should not be returned to the Research and Technology Division unless return is required by security considerations, contractual obligations, or notice on a specific document.

300 - July 1966 - 773-49-1087

AFFDL-TR-66-7

SONIC FATIGUE IN COMBINED ENVIRONMENT

JOHN R. BALLENTINE
HARRY E. PLUMBLEE
CECIL W. SCHNEIDER

LOCKHEED-GEORGIA COMPANY

The distribution of this document is unlimited

FOREWORD

This report was prepared by the Lockheed-Georgia Company, Marietta, Georgia for the Aero-Acoustics Branch, Vehicle Dynamics Division, Air Force Flight Dynamics Laboratory, Wright-Patterson Air Force Base, Ohio, under contract AF 33(615)-1481. The Lockheed-Georgia Company report identification number is ER-8452. The study covers the effects of combined environments (acoustical noise, heat, and low-frequency vibration) and curvature on sonic fatigue. This research is part of a continuing effort to establish tolerance levels and design criteria for sonic fatigue prevention under the Research & Technology Division, Air Force Systems Command's exploratory development program. The Project Number is 1471, "Aero-Acoustics Problems," and Task Number 147101, "Sonic Fatigue." Mr. M. J. Cote and later Mr. D. L. Smith of the Aero-Acoustics Branch were the task engineers.

The period covered by this contract is from April 1964 to December 1965. This report concludes the work on Contract AF 33(615)-1481.

The authors acknowledge the valuable and considerable assistance tendered by J. T. Mathis, F. F. Rudder, Jr., R. C. Wirthlin, H. T. Watson, T. F. Nelson, and F. W. Wagoner, all of the Lockheed-Georgia Company. In addition to Mr. M. J. Cote, Mr. D. L. Smith, Mr. J. Plzak, Mr. E. Hott, and Mr. J. McCarthy of the Flight Dynamics Laboratory provided immeasurable assistance in conducting the complex specimen tests at Wright-Patterson Air Force Base, Ohio.

Manuscript released by the authors 30 December 1965 for publication as an AFFDL Technical Report.

This technical report has been reviewed and is approved.

Walter J. Mykytow

WALTER J. MYKYTOW
Asst. for Research & Technology
Vehicle Dynamics Division

ABSTRACT

Research on sonic fatigue in combined environment is described. Emphasis is placed on determining the effects of structural curvature, low-frequency vibratory loads, and heat, both singly and collectively, on sonic fatigue. The analytical and experimental investigation is presented in two major phases:

1. An investigation of simple structural panels to determine the effect of curvature and heat cycling schemes on dynamic response and fatigue.

2. An investigation to determine the effects of high-intensity sound, heat, and low-frequency vibratory loads on curved titanium-faced honeycomb sandwich panels.

TABLE OF CONTENTS

Section	Title	Page
I	INTRODUCTION	1
II	SIMPLE SPECIMEN INVESTIGATION	2
	A. Theoretical and Analytical	2
	B. Experimental	18
	C. Comparison of Theoretical and Experimental Results	53
	D. Discussion of Results	56
III	COMPLEX SPECIMEN INVESTIGATION	76
	A. Theoretical and Analytical	76
	B. Experimental	91
	C. Comparison of Theoretical and Experimental Results	118
	D. Discussion of Results	123
IV	CONCLUSIONS	135
V	REFERENCES	136
	APPENDIX I - Design Nomogram Modifications	139
	APPENDIX II - Final Equations	142

LIST OF ILLUSTRATIONS

Figure	Title	Page
1	Curved Panel Coordinate System	4
2	General View of High Intensity Sound System	20
3	Block Diagram of High Intensity Sound System Controls, Data Collection, and Data Reduction System	21
4	Simple Test Specimen Design Details	22
5	Simple Panel Test Mounting Frame	24
6	Typical Strain Gage Locations for Determining Panel Response	25
7	Simple Panel Test Fixture and Test Specimens Installed for Test	26
8	Mode Shapes for 0.051 Panel with 48-Inch Radius	27
9	Mode Shapes for 0.032 Flat Panel	28
10	Mode Shapes for 0.032 Panel with 48-Inch Radius	29
11	Sine Sweep Excitation - Flat Panel	30
12	Sine Sweep Excitation - 96" R	31
13	Sine Sweep Excitation - 72" R	32
14	Sine Sweep Excitation - 48" R	33
15	Broad-Band Noise Excitation at 151 db - Flat Panel	35
16	Broad-Band Noise Excitation at 151 db - 96" R	36
17	Broad-Band Noise Excitation at 151 db - 72" R	37
18	Broad-Band Noise Excitation at 151 db - 48" R	38
19	Broad-Band Noise Spectra for Fatigue Tests	39
20	Spectrum Level Versus Mean Cycles-to-Failure	41
21	$\bar{\epsilon}$ - N Curves for Simple Curved Panels	42
22	Probability Distribution of Strain Peaks	43
23	View of Test Specimens Mounted in Test Section	44
24	Quartz Lamp Heaters for Elevated Temperature Tests	45

LIST OF ILLUSTRATIONS (Continued)

Figure	Title	Page
25	Thermocouple Locations	46
26	Strain Gage Locations - Elevated Temperature Tests	47
27	Sine Sweep Excitation, Ambient Temperature - Titanium	49
28	Sine Sweep Excitation, 450° F - Titanium	50
29	Sine Sweep Excitation, Ambient and 450° F - Stainless Steel	51
30	Broad-Band Noise Spectra for Elevated Temperature Tests	52
31	Non-Dimensional Frequency Solutions - Simply-Supported Edges, A = 0.50	57
32	Non-Dimensional Frequency Solutions - Simply-Supported Edges, A = 0.67	58
33	Non-Dimensional Frequency Solutions - Simply-Supported Edges, A = 1.00	59
34	Non-Dimensional Frequency Solutions - Simply-Supported Edges, A = 1.50	60
35	Non-Dimensional Frequency Solutions - Simply-Supported Edges, A = 2.00	61
36	Non-Dimensional Frequency Solutions - Clamped Edges, A = 0.50	62
37	Non-Dimensional Frequency Solutions - Clamped Edges, A = 0.67	63
38	Non-Dimensional Frequency Solutions - Clamped Edges, A = 1.00	64
39	Non-Dimensional Frequency Solutions - Clamped Edges, A = 1.50	65
40	Non-Dimensional Frequency Solutions - Clamped Edges, A = 2.00	66
41	Nomogram for Converting Non-Dimensional Frequency to Actual Frequency	68
42	1/R Versus RMS Strain	70
43	1/R Versus Mean Cycles to Failure	71
44	Typical Fatigue Crack for Curved Test Specimen	73
45	Broad-Band Noise Excitation, 162 db - 450° F	75

LIST OF ILLUSTRATIONS (Continued)

Figure	Title	Page
46	Theoretical and Actual Models of Tapered Edge Geometry	77
47	Honeycomb Sandwich Panel Coordinate System	79
48	Honeycomb Sandwich Panel Configuration and Dimensions	80
49	Titanium Honeycomb Sandwich Test Specimen	93
50	Complex Test Specimen Test Fixture	95
51	Front View - Test Fixture	96
52	Front View - Test Fixture with Hydraulic Actuator	97
53	Front View - Test Fixture with Test Panels Removed	98
54	Typical "Pilot Model" Response	99
55	Near Field Noise Survey - Microphone Locations	102
56	Overall View of Test Arrangement	103
57	Test Set-Up	104
58	Panel #3 (Front View) Time to Failure - 165 Minutes	106
59	Panel #5 (Back View) Time to Failure - 215 Minutes	106
60	Panel #9 (Front View) Time to Failure - 180 Minutes	107
61	Panel #24 (Front View) Time to Failure - 20 Minutes	107
62	Test Panel Skin Cracks	108
63	Microphone Data - 1/3 Octave Band Levels	109
64	Microphone Data - 1/3 Octave Band Levels	110
65	Microphone Data - 1/3 Octave Band Levels	111
66	Complex Test Specimen Response	112
67	Complex Test Specimen Response	113
68	Complex Test Specimen Response	114
69	Complex Test Specimen Response	115

LIST OF ILLUSTRATIONS (Continued)

Figure	Title	Page
70	Probability Distribution of Strain Peaks	119
71	Probability Distribution of Strain Peaks	120
72	Probability Distribution of Strain Peaks	121
73	Probability Distribution of Strain Peaks	122
74	Effect of Variation of Transverse Shear Modulus	124
75	Effect of One-Dimensional Variation of Transverse Shear Modulus	126
76	Effect of Curvature	127
77	Effect of Core Thickness	129
78	Effect of Skin Thickness	130
79	Effect of Varying Ratio of Inner Skin Thickness to Outer Skin Thickness	132
I-1	Effect of Curvature on Stress Ratio	140
I-2	Design Chart Skin and Rib Construction	141

LIST OF TABLES

Table	Title	Page
1	Values of ${}_2M_{ij} = {}_2N_{ij}$	10
2	Values of $\beta_i \ell = \gamma_i b$ for Clamped Boundaries	11
3	Values of M_i and N_i	14
4	Simple Specimen Test Summary	34
5	Typical Fahrenheit Temperature Distribution	53
6	Failure Summary - Titanium Specimens	54
7	Failure Summary - Stainless Steel Specimens	55
8	Frequency Studies on Curved Panel with 96" Radius	56
9	Natural Frequencies for Example Problem	67
10	Titanium Honeycomb Sandwich Panel Details	92
11	Near-Field Noise Survey, J57-P21 at Max. A/B Power	100
12	Complex Specimen Test Runs	101
13	SPL Measured at Panel Centerline	116
14	Strain Measured at Centerline of Curved Honeycomb Sandwich Panels	117
15	Natural Frequencies of Titanium Sandwich Panel	123

LIST OF SYMBOLS

a	Mid-plane radius of simple panel
A	Simple panel aspect ratio. Ratio of arc length to straight edge length.
b	Panel arc length (for simple and sandwich panel)
b_1, b_2	Honeycomb panel arc lengths (defined in Figure 48)
c/c_c	Damping ratio
C_{ij}	Elastic coefficient. Ratio of stress to strain $- \sigma_i/\epsilon_j$
E	Young's modulus for isotropic material
E_x, E_y	Young's moduli for orthotropic material
f	Frequency
G	Shear modulus for isotropic material
G_{xy}, G_{xz}, G_{yz}	Shear moduli for orthotropic material
h	Simple panel thickness
h_1, h_2, h_3, h_4	Honeycomb panel layer thicknesses (defined in Figure 48)
ℓ	Panel length (for simple and sandwich panel)
ℓ_1, ℓ_2	Honeycomb panel lengths (defined in Figure 48)
M_i, M_{mn}	Generalized modal mass
$p(x,y)$	Acoustic pressure distribution
q_r	Generalized coordinate (used to replace U, V, W, Ψ, and Φ)
Q_{mn}	Generalized force for the mn^{th} mode
R	Honeycomb panel mid-plane radius
t	Length to thickness ratio for simple panel
T	Kinetic energy
u	Mid-plane displacement in x direction
U_o	Strain energy density
U	Strain energy
U_{mn}	Generalized coordinate

v	Mid-plane displacement in y direction
V_{mn}	Generalized coordinate
w	Mid-plane displacement in radial, z, direction
x	Shell mid-plane coordinate
$X_m(x)$	Mode shape for x coordinate
y	Shell mid-plane coordinate, $y = a\varphi$
$Y_n(y)$	Mode shape for y coordinate
z	Shell mid-plane coordinate through thickness
α_m	Constant appearing in clamped mode function
β	Modal damping ratio
β_m	Constant appearing in mode function
γ_n	Constant appearing in mode function
δ	Damping ratio
δ_{ij}	Kronecker delta
ϵ_i	Strain
ζ_{mn}	Damping ratio for the mn^{th} mode
θ_n	Constant appearing in clamped mode function
λ	Non-dimensional frequency
ν	Poisson's ratio for isotropic material
ν_x, ν_y	Poisson's ratio for orthotropic material
ρ	Mass density
σ, σ_i	Stress
τ	Shear stress
φ	Shear rotation angle (in Section III); angle which defines cylindrical coordinate, y (in Section II) (generalized coordinate).
ψ	Shear rotation angle
Ψ_{mn}	Generalized coordinate
ω	Circular frequency

NOTATION

$\lfloor\ \rfloor$	Row matrix
$\{\ \}$	Column matrix
$[\ ]$	Rectangular matrix
$\lceil\ \rfloor$	Diagonal matrix
$[\,I\,]$	Identity matrix
$'$	Derivative with respect to argument
$\cdot$	Time derivative
$-$	Root mean square

I

INTRODUCTION

From the time that fatigue of flight vehicle structure was determined to be partially due to power plant generated acoustical noise, the analytical and experimental investigations have been mainly concerned with flat structure exposed only to acoustical excitation. It is logical that this approach was taken because sonic fatigue had been generally confined to secondary structure, control surfaces, and fairings. These structural components are inherently flat and generally exposed to the most severe acoustical noise environment, i.e., during on-ground operation and high gross weight takeoff. During these segments of flight vehicle operation the air-loads and aerodynamic effects are minimal.

The assumption that the useful life of a structural component can be determined from consideration of acoustical excitation alone is one that is open to considerable doubt. For example, during the sonic proof test of the B-58 Weapon System it was determined conclusively that low-frequency, wing-mode vibratory loads caused a large percentage of the fatigue damage in certain wing structure (Reference 1). Body-mode stresses are certainly more intense during taxi and high speed takeoff. It is quite possible that these dynamic loads have caused some of the so called "early" sonic fatigue failures of flight vehicle structure subjected to both types of loads. In addition to the multiple loads creating fatigue, some of the structure is immersed in the high thermal environment of the jet efflux with an attendant reduction in the allowable fatigue strength.

High performance flight vehicles will experience fatigue, significant boundary layer turbulence, aerodynamic heating, and gust or buffet effects simultaneously. If design criteria for advanced flight vehicles are to be realistic, these environmental conditions can no longer be separated as they have in the past.

To this end, the research reported herein was designed to determine the effects of structure curvature, low-frequency vibratory loads, and heat, both singly and collectively, on sonic fatigue. The overall investigation consisted of two major phases. These were:

1. An investigation of simple structural panels to determine the effect of curvature and heat cycling schemes on dynamic response and fatigue.
2. An investigation to determine the effects of high intensity sound, heat, and low-frequency vibratory loads on curved, complex structural panels representative of future flight vehicle structure.

A description of the investigations and results of the first phase is contained in Section II. The investigations and results for the complex structural panels, the second phase, are described in Section III.

II

SIMPLE SPECIMEN INVESTIGATION

A. Theoretical and Analytical

1. Statement of Problem

The method chosen for defining the basic effects of curvature on fatigue life is to test to failure the most simple curved panel specimen that could be designed. This configuration is an unstiffened, cylindrically curved panel which is fastened to a semi-rigid frame.

This section of the report is a description of the analysis which defines the panel response to an arbitrary acoustic excitation.

Three of the basic approaches which can be pursued in a response analysis of an elastic structure are:

a. the differential equations approach

b. the lumped-mass analogy, and

c. the energy approach

The differential equations approach is generally termed an "exact analysis" within the limits of linear homogeneous elasticity relationships and other simplifying assumptions which are used. The differential equations for a complex structural system can be developed by equilibrium considerations. Also, a variational approach, utilizing the Euler-Lagrange equations in conjunction with the total energy, can be used to derive the differential equations. It is exceedingly difficult, however, to obtain solutions to the differential equations for other than simply-supported boundary conditions unless approximate methods such as a finite difference or Gallerkin are utilized.

The lumped-mass analogy is also straightforward to set up and solve. This method can handle most boundary conditions, but it is useful only if a digital computer is available. It does not rely upon assumed mode shapes, but uses standard methods for generating the lumped-mass system modes. The one disadvantage of this method is that when a two-dimensional, or lattice-work structure is analyzed, even the largest computers do not have adequate capacity to solve the problem, considering the number of mass stations necessary to adequately represent the system.

The Rayleigh-Ritz energy method is exact within the limitations of the differential equations approach with one exception: a mode shape must be assumed which is not necessarily a solution to the differential equations. In cases where exact mode shapes can be assumed, the final results are exact. For boundaries such as clamped edges, inexact mode functions which satisfy only the geometric boundary conditions can be used. The Rayleigh-Ritz energy solutions have been relied upon, mainly because results are guaranteed.

The basic approach to the curved panel response has been that of solving for both the simply-supported and clamped edge conditions. Since most structural panels have edge fixities which lie between these boundary conditions, the two analyses provide an upper and lower bound for both frequency and response.

Since the modal-energy approach has been used, the problems of defining panel response logically divides into two separate problems, i.e. (a) definition of natural frequencies, mode shapes, and generalized mass, and (b) definition of response. These topics comprise the following two sections of the report.

2. Frequency Analysis

The vibration analysis of a cylindrically curved panel was made using the following assumptions:

a. The material is linearly elastic.

b. The material is orthotropic.

c. Panel thickness is much less than the major panel dimensions. (Elasticity theory of thin shells is applicable.)

For ease in accomplishing the manipulations, matrix algebra will be used throughout the analysis.

The strain energy density of an elastic system is

$$U_o = \frac{1}{2} \lfloor \sigma_i \rfloor \{\epsilon_i\} \tag{1}$$

It is necessary to express the stress, σ_i, in terms of strain, ϵ_i, and then the strain in terms of displacements. For an orthotropic elastic solid, the stress-strain relationships are

$$\{\sigma_i\} = \left[C_{ij}\right] \{\epsilon_j\} \qquad \lfloor \sigma_i \rfloor = \lfloor \epsilon_j \rfloor \; C_{ji} \tag{2}$$

where $\left[C_{ij}\right]$ is the elastic coefficient matrix. For orthotropic materials C is symmetric.

The strain displacement relationships, as derived by Love (Reference 2) are

$$\{\epsilon_i\} = \begin{bmatrix} \frac{\partial}{\partial x} & 0 & 0 \\ 0 & \frac{\partial}{\partial y} & -\frac{1}{a} \\ \frac{\partial}{\partial y} & \frac{\partial}{\partial x} & 0 \end{bmatrix} \begin{Bmatrix} u \\ v \\ w \end{Bmatrix} - z \begin{bmatrix} 0 & 0 & \frac{\partial^2}{\partial x^2} \\ 0 & \frac{1}{a}\frac{\partial}{\partial x} & \frac{\partial^2}{\partial y^2} \\ 0 & \frac{2}{a}\frac{\partial}{\partial x} & \frac{\partial^2}{\partial x \partial y} \end{bmatrix} \begin{Bmatrix} u \\ v \\ w \end{Bmatrix} \tag{3}$$

This equation can be written in shorthand form as

$$\{\epsilon_i\} = \left[[P] - z \, [Q] \right] \begin{Bmatrix} u \\ v \\ w \end{Bmatrix} \tag{4}$$

u, v, and w are shown in Figure 1, which defines the coordinate system.

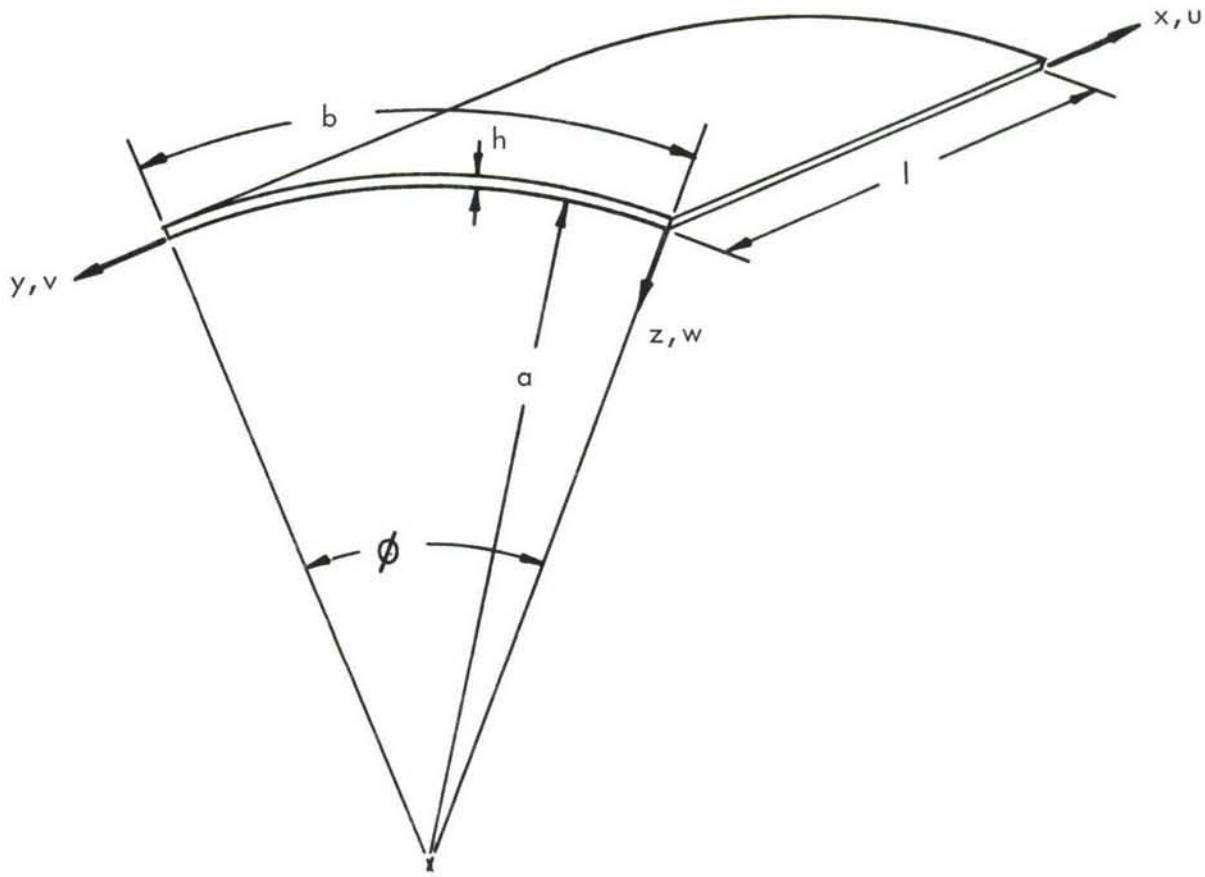

FIGURE 1. CURVED PANEL COORDINATE SYSTEM

The boundary conditions for a curved plate with clamped edges are

$$
\begin{aligned}
w(0,y) &= w(\ell,y) = w(x,0) = w(x,b) = 0 \\
w_x(0,y) &= w_x(\ell,y) = w_y(x,0) = w_y(x,b) = 0 \\
v(0,y) &= v(\ell,y) = v(x,0) = v(x,b) = 0 \\
u(0,y) &= u(\ell,y) = u(x,0) = u(x,b) = 0
\end{aligned}
$$

The geometric boundary conditions for a curved plate with simply-supported edges are

$$
\begin{aligned}
w(0,y) &= w(\ell,y) = w(x,0) = w(x,b) = 0 \\
v_y(x,0) &= v_y(x,b) = 0 \\
u_x(0,y) &= u_x(\ell,y) = 0
\end{aligned}
$$

Beam deflection functions of the form shown below satisfy both boundary conditions.

$$
\left.
\begin{aligned}
u &= \sum\sum \frac{1}{\beta_m} U_{mn} X'_m(x) Y_n(y) \\
v &= \sum\sum \frac{1}{\gamma_n} V_{mn} X_m(x) Y'_n(y) \\
w &= \sum\sum W_{mn} X_m(x) Y_n(y)
\end{aligned}
\right\} \tag{5}
$$

For clamped edges

$$
\left.
\begin{aligned}
X_m(x) &= \text{Cosh}\, \beta_m x - \text{Cos}\, \beta_m x - \alpha_m(\text{Sinh}\, \beta_m x - \text{Sin}\, \beta_m x) \\
Y_n(y) &= \text{Cosh}\, \gamma_n y - \text{Cos}\, \gamma_n y - \theta_n(\text{Sinh}\, \gamma_n y - \text{Sin}\, \gamma_n y) \\
\alpha_m &= \frac{\text{Cosh}\, \beta_m \ell - \text{Cos}\, \beta_m \ell}{\text{Sinh}\, \beta_m \ell - \text{Sin}\, \beta_m \ell} \\
\theta_n &= \frac{\text{Cosh}\, \gamma_n b - \text{Cos}\, \gamma_n b}{\text{Sinh}\, \gamma_n b - \text{Sin}\, \gamma_n b}
\end{aligned}
\right\} \tag{6}
$$

and β_m and γ_n are determined from the following relationships:

$$
\left.
\begin{aligned}
\text{Cosh}\, \beta_m \ell\, \text{Cos}\, \beta_m \ell &= 1 \\
\text{Cosh}\, \gamma_n b\, \text{Cos}\, \gamma_n b &= 1
\end{aligned}
\right\} \tag{7}
$$

The assumed deflection functions for simply-supported edges are

$$
\left.
\begin{aligned}
X_m(x) &= \text{Sin}\, \beta_m x \\
Y_n(y) &= \text{Sin}\, \gamma_n y
\end{aligned}
\right\} \tag{8}
$$

Equation (5) in matrix form is

$$\begin{Bmatrix} u \\ v \\ w \end{Bmatrix} = \begin{bmatrix} \left\lfloor \frac{1}{\beta_m} X'_m Y_n \right\rfloor & 0 & 0 \\ 0 & \left\lfloor X_m \frac{1}{\gamma_n} Y'_n \right\rfloor & 0 \\ 0 & 0 & \lfloor X_m Y_n \rfloor \end{bmatrix} \begin{Bmatrix} U_{mn} \\ V_{mn} \\ W_{mn} \end{Bmatrix} = [A] \begin{Bmatrix} U_{mn} \\ V_{mn} \\ W_{mn} \end{Bmatrix} \tag{9}$$

Substitution of (9) into (4) yields the strain-displacement relationships in terms of the mode shapes and generalized coordinates,

$$\{\varepsilon_i\} = \Big[[P] - z[Q] \Big] [A] \begin{Bmatrix} U_{mn} \\ V_{mn} \\ W_{mn} \end{Bmatrix} = \Big[[B] - z[D] \Big] \{q_r\} \tag{10}$$

The transpose of $\{\varepsilon_i\}$ is

$$\lfloor \varepsilon_i \rfloor = \lfloor q_s \rfloor \Big[[B]^T - z[D]^T \Big] \tag{11}$$

Substituting (2), (10), and (11) into (1) results in

$$U_o = \frac{1}{2} \lfloor q_s \rfloor \Big[[B]^T - z[D]^T \Big] [C] \Big[[B] - z[D] \Big] \{q_r\} \tag{12}$$

Performing the above-indicated matrix multiplications yields

$$\begin{aligned} U_o = \frac{1}{2} \lfloor q_s \rfloor \Big[& [B]^T [C][B] - z[D]^T [C][B] \\ & - z[B]^T [C][D] + z^2 [D]^T [C][D] \Big] \{q_r\} \end{aligned} \tag{13}$$

The total strain energy of the curved plate is obtained by integrating the strain energy density, U_o, over the volume of the plate. In symbolic form, the strain energy is

$$U = \int_0^b \int_0^\ell \int_{-h/2}^{h/2} U_o \, dz \, dx \, dy \tag{14}$$

Integration across the thickness gives

$$U = \frac{1}{2} \int_0^b \int_0^\ell \lfloor q_s \rfloor \Big[h[B]^T [C][B] + \frac{h^3}{12} [D]^T [C][D] \Big] \{q_r\} \, dxdy \tag{15}$$

Following through with the indicated matrix multiplications results in

$$U = \frac{1}{2} \int_0^b \int_0^\ell \lfloor q_s \rfloor \left[h\left[E\right] + \frac{h^3}{12}\left[F\right] \right] \{q_r\} \, dxdy \tag{16}$$

(Note: The terms contained in [E] are the stretching or membrane contribution to strain energy whereas [F] constitutes the bending energy.) Integrating over the surface area of the plate yields

$$U = \frac{1}{2} \lfloor q_s \rfloor \left[K\right] \{q_r\} \tag{17}$$

The kinetic energy of the vibrating plate is obtained by integrating the product of mass and one-half velocity squared over the volume of the plate:

$$T = \frac{\rho}{2} \int_0^b \int_0^\ell \int_{-h/2}^{h/2} (\dot{u}^2 + \dot{v}^2 + \dot{w}^2) dzdydx \tag{18}$$

Substituting (9) for displacements into (18) and performing the indicated time derivatives produces

$$T = \frac{\rho}{2} \int_0^b \int_0^\ell \int_{-h/2}^{h/2} \lfloor \dot{U}_{mn} \; \dot{V}_{mn} \; \dot{W}_{mn} \rfloor \left[A\right]^T \left[A\right] \begin{Bmatrix} \dot{U}_{mn} \\ \dot{V}_{mn} \\ \dot{W}_{mn} \end{Bmatrix} dz \, dx \, dy \tag{19}$$

Integration over the volume results in

$$T = \frac{\rho h}{2} \lfloor \dot{q}_s \rfloor \left[J\right] \{\dot{q}_r\} \tag{20}$$

Lagrange's equation of motion is used to obtain natural modes of vibration as follows:

$$\frac{\partial U}{\partial q_s} = \lfloor K \rfloor \{q_r\} \tag{21}$$

$$\frac{d}{dt}\left(\frac{\partial T}{\partial \dot{q}_s}\right) = \rho h \lfloor J \rfloor \{\ddot{q}_r\} \tag{22}$$

Assuming harmonic motion, (22) becomes

$$\frac{d}{dt}\left(\frac{\partial T}{\partial \dot{q}_s}\right) = -\omega^2 \rho h \lfloor J \rfloor \{q_r\} \tag{23}$$

Substituting (21) and (23) into LaGrange's equation results in an eigenvector solution:

$$\left[\left[K\right] - \omega^2 \rho h \left[J\right]\right] \{q_r\} = 0 \tag{24}$$

The intermediate manipulations required to derive the terms in the [K] and [J] matrix will not be presented for the sake of brevity. The terms in the [K] matrix can be partitioned into a 3 x 3 symmetrical matrix. The elements of this matrix are square matrices of order MN. These terms are

$$
\left.
\begin{aligned}
K_{11} &= h\left\{C_{11} A\left[\frac{{}_3M_{pm}}{\beta_p\beta_m \ell^2}\left[{}_1N_{qn}\right]\right] + \frac{C_{66}}{A}\left[\frac{{}_2M_{pm}}{\beta_p\beta_m \ell^2}\left[{}_2N_{qn}\right]\right]\right\} \\
K_{12} &= h\left\{C_{12}\left[\frac{{}_2M_{pm}}{\beta_p \ell}\left[\frac{{}_2N_{qn}}{\gamma_n b}\right]\right] + C_{66}\left[\frac{{}_2M_{pm}}{\beta_p \ell}\left[\frac{{}_2N_{qn}}{\gamma_n b}\right]\right]\right\} \\
K_{13} &= h\left\{C_{12}\varphi\left[\frac{{}_2M_{pm}}{\beta_p \ell}\left[{}_1N_{qn}\right]\right]\right\} \\
K_{22} &= h\left\{\frac{C_{22}}{A}\left(1 + \frac{\varphi^2}{12A^2t^2}\right)\left[{}_1M_{pm}\left[\frac{{}_3N_{qn}}{\gamma_q\gamma_n b^2}\right]\right]\right. \\
&\qquad \left. + C_{66} A\left(1 + \frac{\varphi^2}{3A^2t^2}\right)\left[{}_2M_{pm}\left[\frac{{}_2N_{qn}}{\gamma_q\gamma_n b^2}\right]\right]\right\} \\
K_{23} &= h\left\{C_{22}\frac{\varphi}{A}\left[{}_1M_{pm}\left[\frac{{}_2N_{qn}}{\gamma_q b}\right]\right] + \frac{C_{21}\varphi}{12At^2}\left[{}_2M_{pm}\left[\frac{{}_2N_{qn}}{\gamma_q b}\right]\right]\right. \\
&\qquad \left. + \frac{C_{22}\varphi}{12t^2A^3}\left[{}_1M_{pm}\left[\frac{{}_3N_{qn}}{\gamma_q b}\right]\right] + \frac{C_{66}\varphi}{3At^2}\left[{}_2M_{pm}\left[\frac{{}_2N_{qn}}{\gamma_q b}\right]\right]\right\} \\
K_{33} &= h\left\{C_{22}\frac{\varphi^2}{A}\left[{}_1M_{pm}\left[{}_1N_{qn}\right]\right] + \frac{C_{11}A}{12t^2}\left[{}_3M_{pm}\left[{}_1N_{qn}\right]\right]\right. \\
&\qquad \left. + \frac{C_{22}}{12t^2A^3}\left[{}_1M_{pm}\left[{}_3N_{qn}\right]\right] + (2C_{12} + 4C_{66})\frac{1}{12t^2A}\left[{}_2M_{pm}\left[{}_2N_{qn}\right]\right]\right\}
\end{aligned}
\right\} \quad (25)
$$

The [J] matrix can be shown to be

$$
\left.
\begin{aligned}
J_{11} &= \left[\frac{{}_2M_{pm}}{\beta_p\beta_m \ell}\left[b\ {}_1N_{qn}\right]\right] = \ell b\left[\frac{{}_2M_{pm}}{\beta_p\beta_m \ell^2}\left[{}_1N_{qn}\right]\right] \\
J_{22} &= \left[\ell\ {}_1M_{pm}\left[\frac{{}_2N_{qn}}{\gamma_q\gamma_n b}\right]\right] = \ell b\left[{}_1M_{pm}\left[\frac{{}_2N_{qn}}{\gamma_q\gamma_n b^2}\right]\right] \\
J_{33} &= \left[\ell\ {}_1M_{pm}\left[b\ {}_1N_{qn}\right]\right] = \ell b\left[{}_1M_{pm}\left[{}_1N_{qn}\right]\right]
\end{aligned}
\right\} \quad (26)
$$

The non-dimensional parameters $A = b/\ell$, $\varphi = b/a$, and $t = \ell/h$ were used in equations (25) and (26).

Since the matrix notion $\left[Mpm\left[Nqn\right]\right]$ is unconventional the following definition is given:

$$[M] = \begin{bmatrix} m_{11} & m_{12} \\ m_{21} & m_{22} \end{bmatrix} \qquad [N] = \begin{bmatrix} n_{11} & n_{12} \\ n_{21} & n_{22} \end{bmatrix}$$

$$[M'] = \begin{bmatrix} m_{11}[I] & m_{12}[I] \\ m_{21}[I] & m_{22}[I] \end{bmatrix} \qquad [N'] = \begin{bmatrix} [N] & 0 \\ 0 & [N] \end{bmatrix}$$

$[I]$ is the identity matrix of the same order as $[N]$

$$\left[M[N]\right] = [M'] \; [N'] = \begin{bmatrix} m_{11}[N] & m_{12}[N] \\ m_{21}[N] & m_{22}[N] \end{bmatrix}$$

Integrations of the clamped mode functions over the surface which were used to derive (25) and (26) are (Reference 3)

$$\left.\begin{aligned}
&\int_0^{\ell} X_p X_m \, dx = \delta_{pm} \ell && = \ell \; {}_1M_{pm} \\
&\int_0^{\ell} X'_p X'_m \, dx = \delta_{pm} \alpha_m \beta_m (\alpha_m \beta_m \ell - 2) \\
&\qquad + (1 - \delta_{pm}) \frac{4\beta_p^2 \beta_m^2 (\alpha_m \beta_m - \alpha_p \beta_p)}{\beta_m^4 - \beta_p^4} \left[1 + (-1)^{m+p}\right] && = \frac{{}_2M_{pm}}{\ell} \\
&\int_0^{\ell} X''_p X''_m \, dx = \delta_{pm} \beta_m^4 \ell && = \frac{{}_3M_{pm}}{\ell^3} \\
&\int_0^{\ell} X''_p X_m \, dx = \int_0^{\ell} X_p X''_m \, dx && = -\frac{{}_2M_{pm}}{\ell} \\
&\int_0^{b} Y_q Y_n \, dy = \delta_{qn} b && = b \; {}_1N_{qn}
\end{aligned}\right\} \quad (27)$$

$$\left.\begin{aligned}
\int_0^b Y_q' Y_n' \, dy &= \delta_{qn} \theta_n \gamma_n (\theta_n \gamma_n b - 2) \\
&\quad + (1 - \delta_{qn}) \frac{4\gamma_q^2 \gamma_n^2 (\theta_q \gamma_q - \theta_n \gamma_n)}{\gamma_n^4 - \gamma_q^4} \left[1 + (-1)^{q+n}\right] = \frac{2N_{qn}}{b} \\
\int_0^b Y_q'' Y_n'' \, dy &= \delta_{qn} \gamma_n^4 b \qquad = \frac{3N_{qn}}{b^3} \\
\int_0^b Y_q Y_n'' \, dy &= \int_0^b Y_q'' Y_n \, dy \qquad = -\frac{2N_{qn}}{b}
\end{aligned}\right\} \begin{matrix}(27)\\ \text{(cont'd)}\end{matrix}$$

where δ_{ij} is the Kroneker delta:

$$\delta_{ij} = \begin{Bmatrix} 1 & i = j \\ 0 & i \neq j \end{Bmatrix}$$

Table 1 is a tabulation of the non-dimensional values ${}_2M_{ij} = {}_2N_{ij}$. These values are taken from Young (Reference 4).

TABLE 1

VALUES OF ${}_2M_{ij} = {}_2N_{ij}$

i/j	1	2	3	4	5	6
1	12.30262	0	-9.73079	0	-7.61544	0
2	0	46.05012	0	-17.12892	0	-15.19457
3	-9.73079	0	98.90480	0	-24.34987	0
4	0	-17.12892	0	171.58566	0	-31.27645
5	-7.61544	0	-24.34987	0	263.99798	0
6	0	-15.19457	0	-31.27645	0	376.15008

Table 2 is a listing of the non-dimensional quantities $\beta_i \ell = \gamma_i b$ taken from results published by Young and Felgar (Reference 5).

TABLE 2

VALUES OF $\beta_i \ell = \gamma_i b$ FOR CLAMPED BOUNDARIES

i	$B_i \ell = \gamma_i b$	$(B_i \ell)^4 = (\gamma_i b)^4$
1	4.7300408	500.5639
2	7.85320046	3,800.5370
3	10.9956078	14,617.6299
4	14.1371655	39,943.7991
5	17.2787596	89,135.4065
6	20.4203522	173,881.316

Clamped Boundaries: $i > 6$; $\beta_i \ell = \gamma_i b = (2i + 1) \frac{\pi}{2}$

Simply Supported Boundaries: $i = 1, 2, \ldots \infty$;
$\beta_i \ell = \gamma_i b = i\pi$

The values of the integrals of the assumed mode functions over the plate surface for simply-supported edge conditions are

$$\left.\begin{aligned}
\int_0^\ell X_p X_m \, dx &= \delta_{pm} \frac{\ell}{2} &&= \ell \, {}_1M_{pm} \\
\int_0^\ell X'_p X'_m \, dx &= \delta_{pm} \beta_m^2 \frac{\ell}{2} &&= \frac{{}_2M_{pm}}{\ell} \\
\int_0^\ell X''_p X''_m \, dx &= \delta_{pm} \beta_m^4 \frac{\ell}{2} &&= \frac{{}_3M_{pm}}{\ell^3} \\
\int_0^\ell X''_p X_m \, dx &= \int_0^\ell X_p X''_m \, dx &&= -\frac{{}_2M_{pm}}{\ell} \\
\int_0^b Y_q Y_n \, dy &= \delta_{qn} \frac{b}{2} &&= b \, {}_1N_{qn} \\
\int_0^b Y'_q Y'_n \, dy &= \delta_{qn} \frac{\gamma_n^2 b}{2} &&= \frac{{}_2N_{qn}}{b}
\end{aligned}\right\} \qquad (28)$$

$$\left.\begin{aligned}
\int_0^b Y_q'' Y_n'' \, dy &= \delta_{qn} \frac{\gamma_n^4 b}{2} = \frac{3^N{}_{qn}}{b^3} \\
\int_0^b Y_q'' Y_n \, dy &= \int_0^b Y_q Y_n'' \, dy = -\frac{2^N{}_{qn}}{b}
\end{aligned}\right\} \qquad \begin{matrix}(28)\\ \text{(cont'd)}\end{matrix}$$

For an orthotropic elastic, thin plate, the elastic coefficient matrix reduces to

$$\left.\begin{aligned}
[C] &= \begin{bmatrix} C_{11} & C_{12} & 0 \\ C_{21} & C_{22} & 0 \\ 0 & 0 & C_{66} \end{bmatrix} \\
\text{where} \quad C_{11} &= \frac{E_x}{1 - \upsilon_x \upsilon_y} \\
C_{12} &= \frac{\upsilon_x E_y}{1 - \upsilon_x \upsilon_y} \\
C_{21} &= \frac{\upsilon_y E_x}{1 - \upsilon_x \upsilon_y} \\
C_{22} &= \frac{E_y}{1 - \upsilon_x \upsilon_y} \\
C_{66} &= G_{xy}
\end{aligned}\right\} \qquad (29)$$

and the relationship $\upsilon_x E_y = \upsilon_y E_x$ is necessary for orthotropic media, and the elastic coefficient matrix must be symmetric (Reference 7).

This concludes the frequency analysis for orthotropic curved panels; however, there are several important points which need to be discussed. These are

a. Referring to equation (27), the integrals of $X_p' X_m'$, $X_p'' X_m$ and $X_p X_m''$ for clamped edge conditions are non-zero when p is not equal to m. Thus the analysis doesn't display the desired orthogonality between the modes. A numerical analysis for one of the test panels used in this program compared with a numerical analysis which assumed orthogonality shows insignificant differences; however, a complete investigation of the effects of including this non-orthogonality relationship has not been evaluated because of computer time requirements. In order to obtain the first 25 (through 5,5 mode) panel modes from (24) for clamped edges, it is necessary to solve a 75 x 75 eigenvalue matrix. Computer time required for this analysis precluded parameter studies.

b. Examination of (28) reveals that the integrals of the mode shapes are orthogonal for simply-supported edges, since sine functions were chosen.

c. A simplification of considerable interest to the orthotropic curved panel frequency analysis occurs provided the modal integrations are taken to be orthogonal and the material is isotropic. In this case $[{}_1M_{pm}]$, $[{}_2M_{pm}]$, $[{}_3M_{pm}]$, $[{}_1N_{qn}]$, $[{}_2N_{qn}]$ and $[{}_3N_{qn}]$ become diagonal matrices and the modes are uncoupled. Also, the elastic matrix reduces to

$$C_{11} = C_{22} = \frac{E}{1 - \upsilon^2}$$

$$C_{12} = C_{21} = \frac{\upsilon E}{1 - \upsilon^2}$$

$$C_{66} = G = \frac{E}{2(1 + \upsilon)}$$

Also, it is assumed that

$$\frac{h^2}{a^2} << 1$$

Incorporation of these parameters into the eigenvalue problem results in a 3 x 3 matrix for determining the m n^{th} natural frequency. The determinant of coefficients is

$$\left| [G] - \lambda^2 [L] \right| = 0$$

where

$$[K] = \frac{Eh^3}{\ell^2(1 - \upsilon^2)} [G]$$

$$[J] = \ell b [L]$$

and

$$\lambda^2 = \frac{\rho \ell^3 b(1 - \upsilon^2)}{Eh^2} \omega^2$$

The terms in the G matrix are

$$\left.\begin{aligned} G_{11} &= At^2 \frac{M_3(m)N_1(n)}{(\beta_m \ell)^2} + \frac{t^2}{A}\left(\frac{1 - \upsilon}{2}\right) \frac{M_2(m)N_2(n)}{(\beta_m \ell)^2} \\ G_{12} &= t^2 \left(\frac{1 + \upsilon}{2}\right) \frac{M_2(m)N_2(n)}{(\beta_m \ell)(\gamma_n b)} \end{aligned}\right\} \qquad (30)$$

$$G_{13} = \varphi t^2 \upsilon \frac{M_2(m) N_1(n)}{\beta_m \ell}$$

$$G_{22} = \frac{t^2}{A} M_1(m) \frac{N_3(n)}{(\gamma_n b)^2} + A t^2 \left(\frac{1-\upsilon}{2}\right) M_2(m) \frac{N_2(n)}{(\gamma_n b)^2}$$

$$G_{23} = \frac{\varphi t^2}{A} M_1(m) \frac{N_2(n)}{\gamma_n b} + \frac{\varphi}{A}\left(\frac{2-\upsilon}{12}\right) M_2(m) \frac{N_2(n)}{\gamma_n b} + \frac{\varphi}{12A^3} M_1(m) \frac{N_3(n)}{\gamma_n b}$$

$$G_{33} = \frac{\varphi^2 t^2}{A} M_1(m) N_1(n) + \frac{A}{12} M_3(m) N_1(n) + \frac{1}{12A^3} M_1(m) N_3(n) + \frac{1}{6A} M_2(m) N_2(n)$$

The terms in the $[L]$ matrix are

$$L_{11} = \frac{M_2(m)\, N_1(n)}{(\beta_m \ell)^2}$$

$$L_{22} = M_1(m) \frac{N_2(n)}{(\gamma_n b)^2}$$

$$L_{33} = M_1(m)\, N_1(n)$$

(30) (cont'd)

This form of the frequency theory reduces to an analysis performed by Sewell (Reference 6).

Table 3 contains a tabulation of M_i and N_i for both clamped and simply-supported edges.

TABLE 3

VALUES OF M_i AND N_i

	Clamped	Simply-Supported
$M_1(m)$	1	1/2
$M_2(m)$	$\alpha_m \beta_m \ell(\alpha_m \beta_m \ell - 2)$	$(\beta_m \ell)^2/2$
$M_3(m)$	$(\beta_m \ell)^4$	$(\beta_m \ell)^4/2$
$N_1(n)$	1	1/2
$N_2(n)$	$\theta_n \gamma_n b(\theta_n \gamma_n b - 2)$	$(\gamma_n b)^2/2$
$N_3(n)$	$(\gamma_n b)^4$	$(\gamma_n b)^4/2$

d. Finally, if $a = \infty$ (flat plate, $\varphi = 0$) then the 3 x 3 matrix reduces to a 2 x 2 and one equation in terms of λ^2 in the 3,3 position. The equation resulting from the 3,3 element yields the flat plate flexural modes, whereas the 2 x 2 matrix gives the in-plane or longitudinal vibration modes.

3. Response to Acoustical Excitations

The analytical procedure used for evaluating panel response to an arbitrary acoustic excitation is a modal analysis derived from LaGrange's equations having the form (Reference 8):

$$\frac{d}{dt}\left(\frac{\partial T}{\partial \dot{q}_i}\right) - \frac{\partial T}{\partial q_i} + \frac{\partial U}{\partial q_i} + \frac{\partial R}{\partial \dot{q}_i} = Q_i \tag{31}$$

where R is the dissipation function defined as

$$R = 2\beta T \quad , \quad \beta = (c/c_c)\omega_i \tag{32}$$

and it is necessary to determine $\partial T/\partial \dot{q}_i$, $\partial T/\partial q_i$, and $\partial U/\partial q_i$.

Although the modes do not display orthogonality between some of the terms (see (27)), orthogonality will be assumed for the response calculation. From (22),

$$\frac{\partial T}{\partial \dot{q}_i} = \rho h \lfloor J \rfloor_i \{\dot{q}_i\} \tag{33}$$

However, since $[J]$ is diagonal,

$$\begin{aligned} \frac{\partial T}{\partial \dot{q}_i} &= \rho h\, J_i\, \dot{q}_i = M_i\, \dot{q}_i \\ \frac{\partial T}{\partial q_i} &= 0 \end{aligned} \tag{34}$$

also

$$\frac{\partial U}{\partial q_i} = \lfloor K \rfloor_i \{q_i\} \tag{35}$$

If the system is vibrating in the ith natural mode, with zero damping and harmonic motion, (31) becomes

$$\frac{\partial U}{\partial q_i} + \frac{d}{dt}\left(\frac{\partial T}{\partial \dot{q}_i}\right) = \left[\lfloor K \rfloor_i - \omega_i^2\, \rho h \lfloor J \rfloor_i\right] \{q_i\} \tag{36}$$

For arbitrary values of q_i,

$$\lfloor K \rfloor_i = \omega_i^2\, \rho h \lfloor J \rfloor_i = \omega_i^2\, M_i \tag{37}$$

Substituting (32), (34), and (37) into (31) produces

$$M_i \ddot{q}_i + \frac{c}{c_c} \omega_i M_i \dot{q}_i + \omega_i^2 M_i q_i = Q_i \tag{38}$$

For a distributed acoustical pressure, Q_i has the following form:

$$Q_i = \int_0^b \int_0^\ell p(x,y,t)(X(x)Y(y))_i \, dxdy \tag{39}$$

$p(x,y,t)$ is the acoustic pressure distribution.

For the mn^{th} mode, using the results of (30), (38) reduces to

$$M_{mn}\ddot{W}_{mn} + \frac{c}{c_c}\omega_{mn}M_{mn}\dot{W}_{mn} + \omega_{mn}^2 M_{mn}W_{mn} = \int_0^b \int_0^\ell p(x,y,t)X_m(x)Y_n(y)dxdy \tag{40}$$

where M_{mn} and ω_{mn} are the generalized mass and natural frequency associated with resonance in the radial direction (i.e., transverse vibration).

The solution of (40), assuming harmonic motion, is

$$\left.\begin{aligned}
W_{mn} &= \frac{Q_{mn}}{M_{mn}\,\omega_{mn}^2}\left[\left(1 - \frac{\omega}{\omega_{mn}}\right)^2 + \left(2\zeta_{mn}\frac{\omega}{\omega_{mn}}\right)^2\right]^{-1/2} \operatorname{Sin}(\omega t + \varphi_{mn}) \\
\varphi_{mn} &= \tan^{-1}\left[\frac{2\,\zeta_{mn}\,(\omega/\omega_{mn})}{1 - (\omega/\omega_{mn})^2}\right] \\
Q_{mn} &= \int_0^b \int_0^\ell p(x,y,t)X_m(x)Y_n(y)dxdy
\end{aligned}\right\} \tag{41}$$

For uniform pressure distribution, Q_{mn} reduces to

$$\left.\begin{aligned}
Q_{mn} &= 4p\,\frac{\alpha_m\,\theta_n}{\beta_m\,\gamma_n}\left[1 - (-1)^m\right]\left[1 - (-1)^n\right] \\
&\text{for clamped edges and} \\
Q_{mn} &= \frac{p}{\beta_m\,\gamma_n}\left[1 - (-1)^m\right]\left[1 - (-1)^n\right] \\
&\text{for simply supported edges.}
\end{aligned}\right\} \tag{42}$$

The generalized mass associated with radial vibration is

$$M_{mn} = \rho h \ell b \text{ for clamped edges}$$
$$M_{mn} = \frac{\rho h \ell b}{4} \text{ for simply supported edges} \tag{43}$$

Upon definition of W_{mn} and ω_{mn}, U_{mn} and V_{mn} can be determined from (30).

A procedure is now available for determinating the absolute magnitude of U_{mn}, V_{mn} and W_{mn}. The displacements u, v, and w, can be determined using (5).

The surface stresses for a thin cylindrical shell are (Reference 9)

$$\left.\begin{aligned}
\sigma_x &= \frac{E}{1-\upsilon^2}\left\{\frac{\partial u}{\partial x} + \upsilon\left(\frac{\partial v}{\partial y} - \frac{w}{a}\right) + z\left[\frac{\partial^2 w}{\partial x^2} + \upsilon\left(\frac{1}{a}\frac{\partial v}{\partial y} + \frac{\partial^2 w}{\partial x^2}\right)\right]\right\} \\
\sigma_y &= \frac{E}{1-\upsilon^2}\left\{\frac{\partial v}{\partial y} - \frac{w}{a} + \upsilon\frac{\partial u}{\partial x} + z\left[\frac{1}{a}\frac{\partial v}{\partial y} + \frac{\partial^2 w}{\partial y^2} + \upsilon\frac{\partial^2 w}{\partial x^2}\right]\right\} \\
\tau_{xy} &= \frac{E}{2(1+\upsilon)}\left\{\frac{\partial u}{\partial y} + \frac{\partial v}{\partial x} + 2z\left(\frac{1}{a}\frac{\partial v}{\partial x} + \frac{\partial^2 w}{\partial x \partial y}\right)\right\}
\end{aligned}\right\} \tag{44}$$

In the evaluation of the effects of curvature upon natural frequencies, stress response and ultimately fatigue life, it is desirable to arrange the theory to yield frequency ratio and stress ratio.

Some important simplifications can be made in the frequency theory if the angle which the panel subtends is small. For angles, φ, less than 0.2 radians, the frequency of flexural vibration can be approximated by

$$\lambda^2 = K_{33}/J_{33} \tag{45}$$

With all edges clamped, this reduces to

$$\lambda^2 = 41.7A + \frac{25.2}{A} + \frac{41.7}{A^3} + \frac{t^2\varphi^2}{A} \tag{46}$$

Equations (44) for maximum stress on the straight edge reduces to

$$\sigma_y = \frac{E}{1-\upsilon^2}\left[\frac{\partial v}{\partial y} - \frac{h}{2}\frac{\partial^2 w}{\partial y^2}\right] \tag{47}$$

Substituting the mode shape at the center of the straight edge gives

$$\sigma_y = \frac{E}{1-\upsilon^2}\gamma_n^2 X_m(\ell/2)hW_{mn}\left\{\frac{2K}{\gamma_n h} - 1\right\} \tag{48}$$

K is the ratio of the generalized coordinates V_{mn}/W_{mn} and is expressed by expanding the first two equations which make up the frequency determinant, (30).

$$V_{mn} = \frac{\left[K_{21} K_{13} - K_{23}(K_{11} - \lambda_{mn}^2 J_{11})\right] W_{mn}}{(K_{11} - \lambda_{mn} J_{11})(K_{22} - \lambda_{mn}^2 J_{22}) - K_{21} K_{12}} = K W_{mn} \tag{49}$$

For thin panels, $\lambda^2 J_{11} \ll K_{11}$ and $\lambda^2 J_{22} \ll K_{22}$. Using this approximation

$$\frac{2K}{\gamma_n h} \approx - D \left[\frac{A^2 + 0.108}{A^4 + 9.62A^2 + 1} \right] At\varphi \tag{50}$$

The theoretical first mode value of D is 0.445 for a panel with clamped edges.

The ratio of curved panel stress to flat panel stress at resonance reduces to, using results of (48) and (41),

$$\frac{\sigma_{yc}}{\sigma_{y\infty}} = \left(\frac{\omega_{mn\infty}}{\omega_{mnc}}\right)^2 \left\{1 - \frac{2K}{\gamma_n h}\right\} \tag{51}$$

From (46),

$$\left(\frac{\omega_{11c}}{\omega_{11\infty}}\right)^2 = 1 + \frac{C(At\varphi)^2}{A^4 + 0.61A^2 + 1} \tag{52}$$

The theoretical value of C is 0.024 for clamped edges. Combining the results of (50), (51) and (52) gives

$$\frac{\sigma_{yc}}{\sigma_{y\infty}} = \left[1 + \frac{C(At\varphi)^2}{A^4 + 0.61A^2 + 1}\right]^{-1} \left[1 + D\left(\frac{A^2 + 0.108}{A^4 + 9.62A^2 + 1}\right)At\varphi\right] \tag{53}$$

A design nomograph which solves (53) is included in Appendix I. This nomogram is to be used in conjunction with existing design charts for flat rib-skin structure. The constants C and D were determined from the experimental test results discussed in Section II.B.

B. Experimental

1. Introduction

This experimental investigation was designed to determine the effect of curvature on structural response and acoustical fatigue and the effect of thermal cycling on acoustical fatigue. Broad-band high intensity sound tests on simple panels were made to evaluate these effects.

To determine the effect of curvature, simple unstiffened panels were used. The panel thickness and size were held constant within manufacturing tolerances and the radius of curvature was varied to encompass a forseeable range for present and future flight vehicles. Flat panels made of heat resistant materials were used to evaluate the thermal cycling effects.

A description of the test facility, data collection and data reduction system, test procedures, and test results is contained in subsequent sections.

2. Laboratory Test Facilities

The High Intensity Sound System, designed by Ling-Altec, Inc., is an electronically controlled system which can produce random, sinusoidal, or a taped output as desired. The system has the capability of producing an overall sound pressure level output of 163 decibels when operating in the random mode. The useful frequency range in the random mode is 50 to 2000 cps. Random mode operation is adjustable in octave band widths. Air for the system is supplied from plant compressors and is used up to 50 psig. The air flow is modulated by an electrical signal to the four transducers in the system to produce the desired acoustical noise output. The sound passes through exponential horns to the progressive wave test section where it impinges on test specimens with grazing incidence. The test section is one-foot wide and can accommodate test specimens 4 feet by 10 feet in size. Figure 2 is a photograph which shows the general arrangement of the system.

The complete complement of sound generating system controls, data collection, and data reduction system is shown schematically in Figure 3. Specifically, transducer (microphones, accelerometers, and strain gage) outputs are displayed on meters and/or oscilloscopes and recorded on a fourteen-track Ampex FM magnetic tape recorder. Data processing equipment includes an Ampex tape loop system with data analyses performed using a Technical Products Corporation Wave Analyzer system with a filter having a nominal bandwidth of one cps. A Bruel and Kjaer one-third octave band analyzer and plotter is used mostly to reduce acoustical noise data.

3. Ambient Temperature Tests

The simple test specimen response and fatigue tests were conducted at ambient temperature to minimize the variables. A description of the test specimens, test procedure, and test results is given below:

a. Test Specimen. For reasons related to stress, linearity, and time to failure, two panel configurations were tested. The first configuration had flat pattern overall dimensions of 11" x 13" x 0.051" with arbitrarily chosen radii of curvature of 48", 72", 96", and infinity. The second configuration was the same as the first except for an 0.032" thickness. Both configurations were 7075-T6 clad aluminum alloy.

   Only a few of the 0.051" test specimens were tested because the time required to fatigue the panels with the 48" radius was unreasonable. Consequently, the 0.051" panels were discarded in lieu of the 0.032" panels.

   Figure 4 is a drawing which gives the details of the 0.032" test specimens.

b. Test Procedure. In conducting the fatigue tests the following procedure was employed.

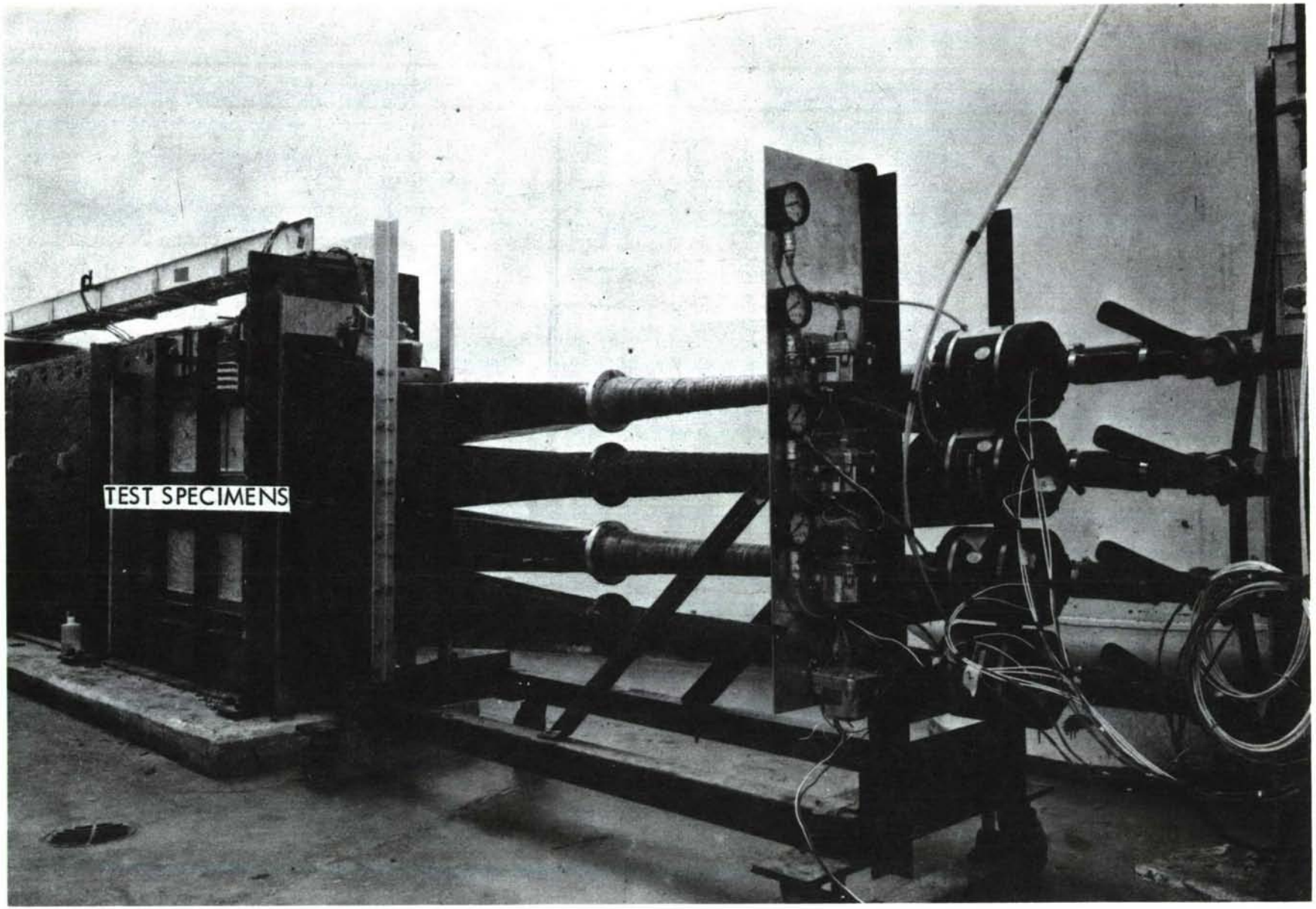

FIGURE 2. GENERAL VIEW OF HIGH INTENSITY SOUND SYSTEM

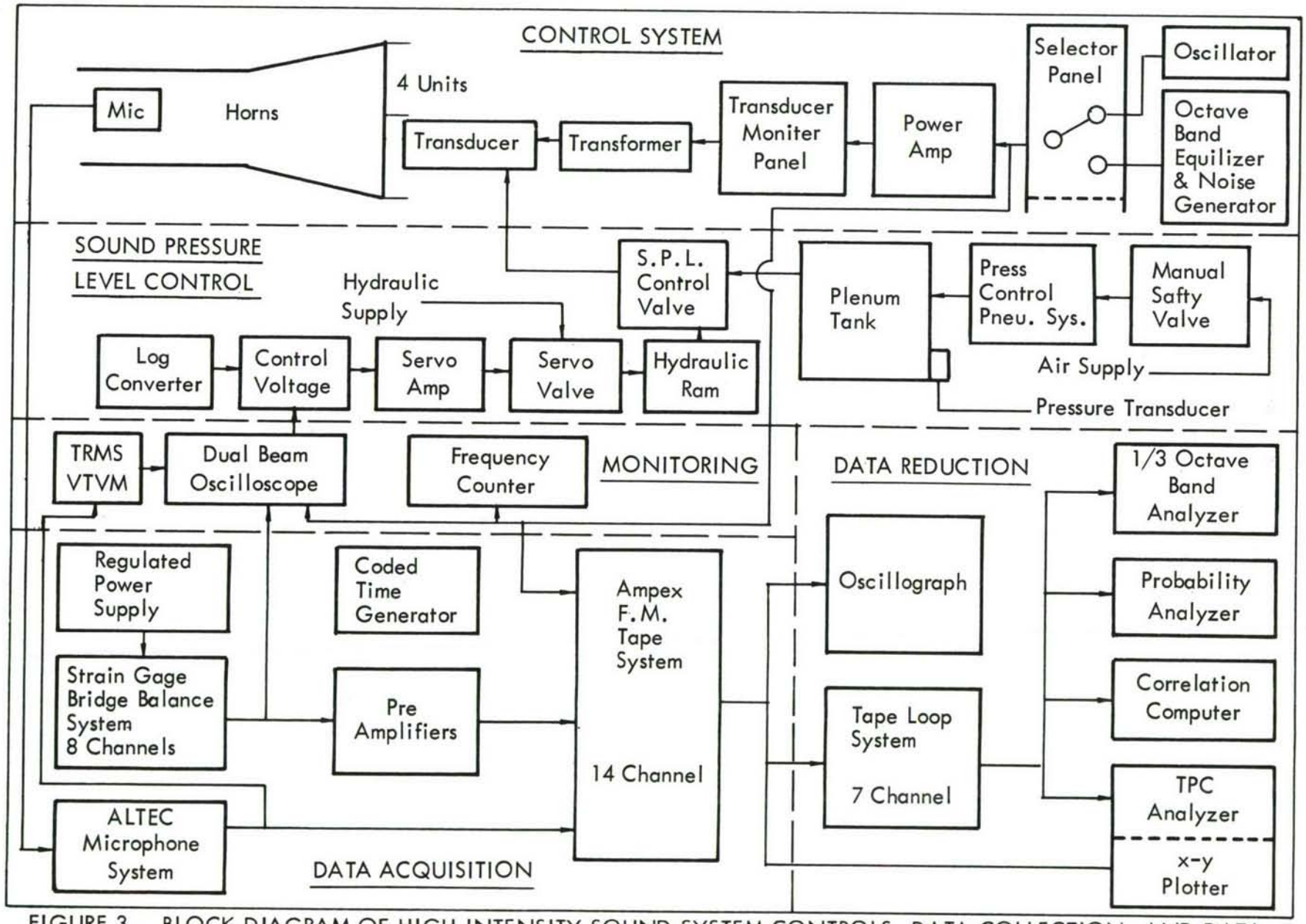

FIGURE 3. BLOCK DIAGRAM OF HIGH INTENSITY SOUND SYSTEM CONTROLS, DATA COLLECTION, AND DATA AND DATA REDUCTION SYSTEM

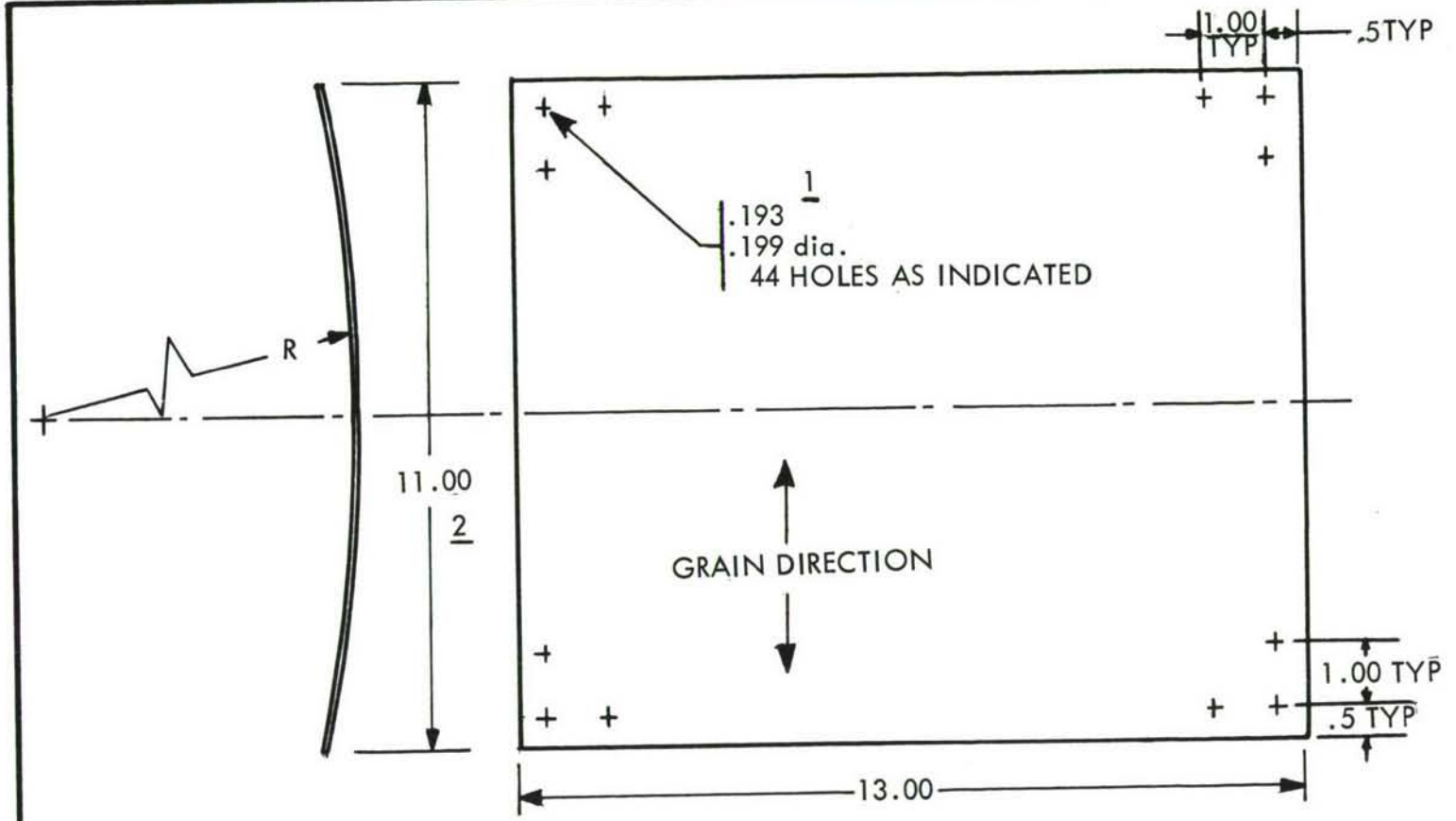

NOTE: 2 FLAT PATTERN DIMENSIONS
1 HOLES TO BE DRILLED AT ASS'Y

NUMBER	MATL.	SIZE	RADIUS
-4	7075-T6	11 x 13 x .032	48
-3	7075-T6	11 x 13 x .032	72
-2	7075-T6	11 x 13 x .032	96
-1	7075-T6	11 x 13 x .032	INFINITE

FIGURE 4. SIMPLE TEST SPECIMEN DESIGN DETAILS

First, mode shapes for each panel configuration were determined. The panels were fastened in a picture frame mounting fixture of the type shown in Figure 5. They were mounted one at a time over a loudspeaker. The modes were excited and the Chladni patterns were photographed, when possible, through the (5,5) mode. After a study of the mode shapes and panel response characteristics, it was decided that strain gages should be placed in the four locations shown in Figure 6 on one panel of each configuration. Frequency sweeps were then made at various discrete frequency sound pressure levels to determine the characteristics of each panel response, damping ratios, and the range of linear response.

Strain gaged specimens, mounted as shown in Figure 7, were next excited by low-level broad-band acoustical noise having a flat spectrum to determine the most active strain gages and the significant modes of response. The data obtained from the sinusoidal frequency sweeps and the low-level broad-band excitation were used to establish the most active strain gages to be used for monitoring purposes during the fatigue tests and to shape the broad-band acoustical noise spectra.

Last, fatigue tests were conducted using the broad-band spectra shaped from frequency sweep and low level broad-band excitation data. The tests were conducted for periods of time ranging from five-minute segments at the beginning of a run to 20-minute segments after one hour of exposure.

c. Test Sound Pressure Levels. Test sound pressure levels were chosen such that the computed minimum time-to-failure would be approximately one hour for the shortest time and ten hours the maximum time. The upper time limit was varied when necessary to keep non-linearities at a minimum.

The spectra were shaped for fatigue tests to concentrate the acoustical energy in a desired range of frequencies. It was determined from Reference 10 that the bandwidth for testing should be a minimum of three times the bandwidth of response in order for the structure to be excited with broad-band noise relative to the response bandwidth.

d. Test Results. Results of the ambient temperature tests will be described beginning with mode studies and progressing systematically through the fatigue tests.

- Mode Shapes. Mode shapes (Chladni patterns) for each panel configuration were determined through the (5,5) mode for both the 0.051 and 0.032-inch thick test specimens. Figures 8 through 10 are photographs of the mode shapes for an 0.051" panel with 48-inch radius, an 0.032" panel with 48-inch radius, and an 0.032" flat panel. Figure 8 should be compared to Figure 10 to get the effect of panel thickness on frequency. Figure 9 should be compared to Figure 10 to get the effect of radius of curvature on frequency.

  The mode shape studies were also used to obtain a rigidly controlled check on the frequency theory derived in Section II.A.

- Frequency Sweeps. Frequency sweeps were made at various sound pressure levels to determine response characteristics, damping ratio, and range of linear response. Figures 11 through 14 are typical plots of strain response for sinusoidal frequency sweep excitation at 130 decibels. Frequency was swept from 50 cps to 2000 cps but only the 50 cps to 600 cps range is shown because the response of each test specimen was negligible at frequencies above 600 cps.

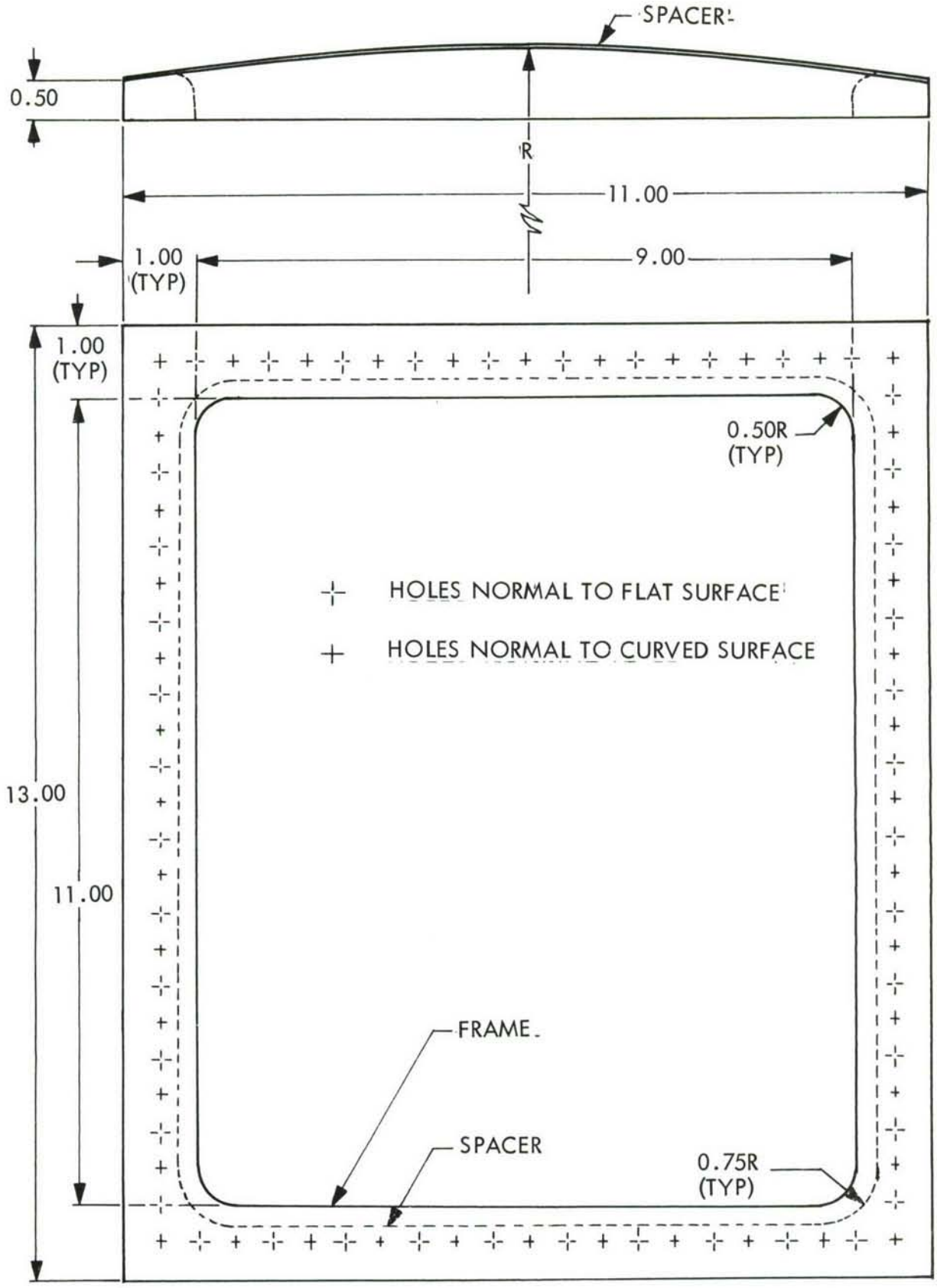

FIGURE 5. SIMPLE PANEL TEST MOUNTING FRAME

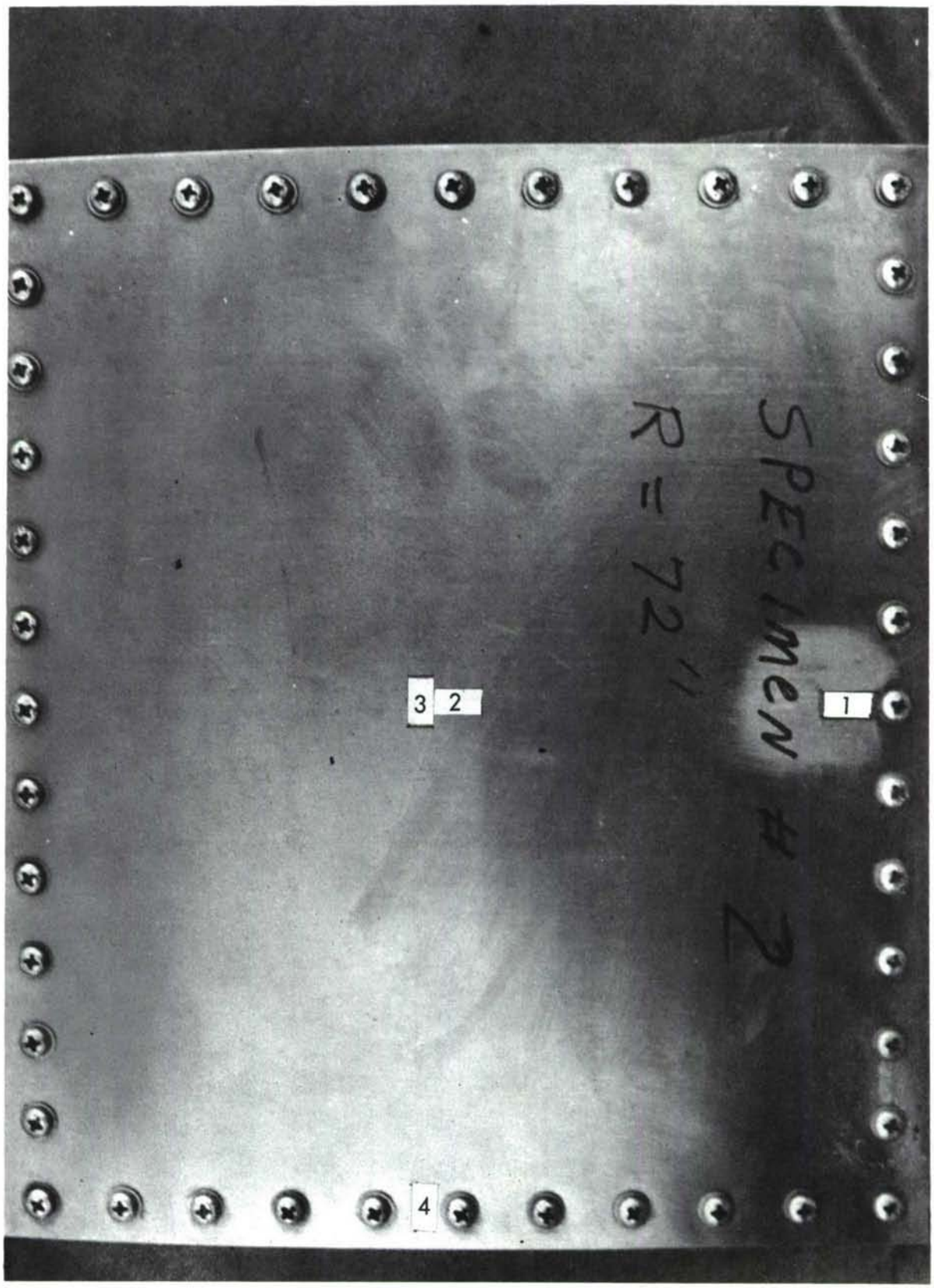

FIGURE 6. TYPICAL STRAIN GAGE LOCATIONS FOR DETERMINING PANEL RESPONSE

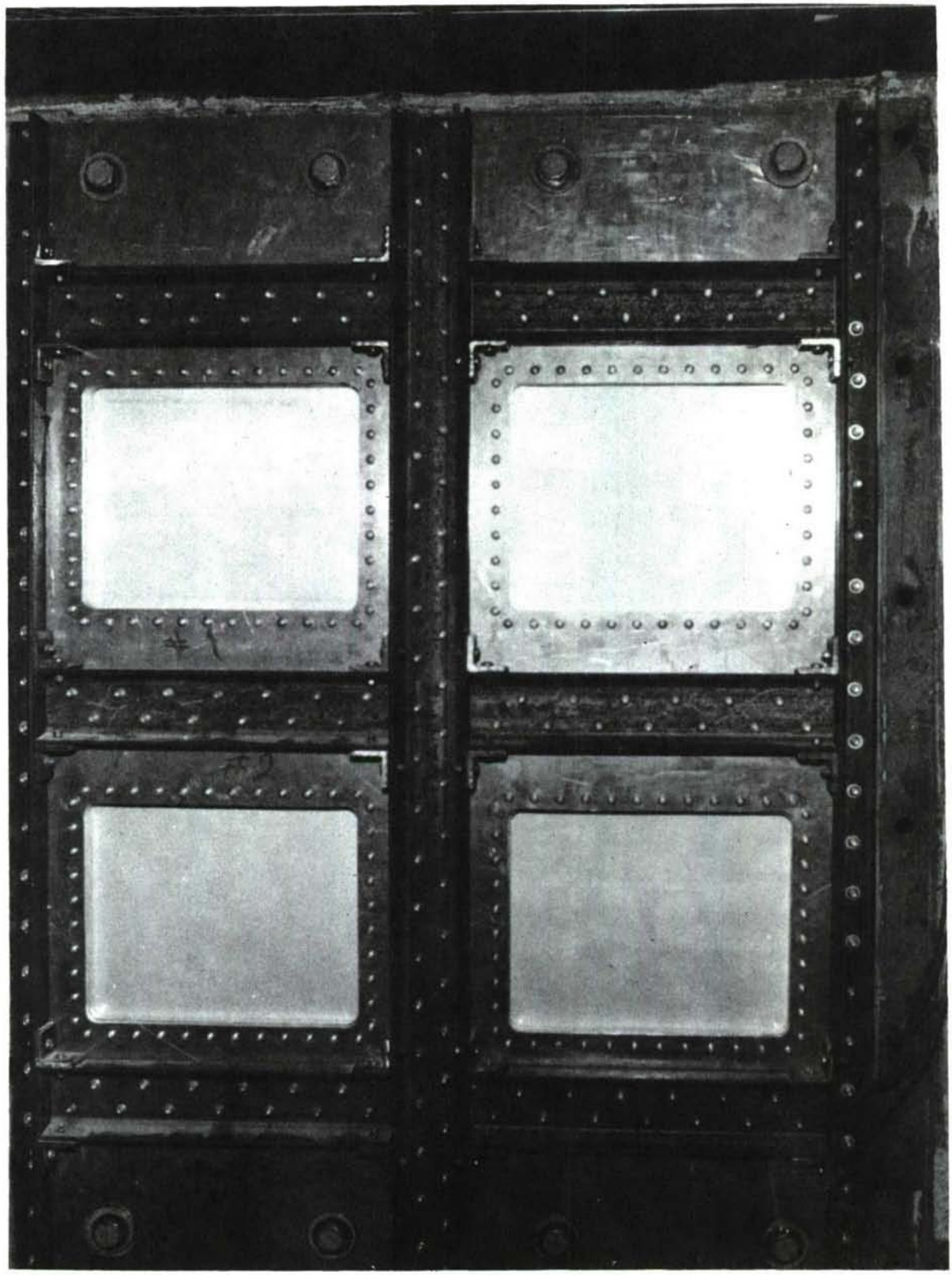

FIGURE 7. SIMPLE PANEL TEST FIXTURE AND TEST SPECIMENS INSTALLED FOR TEST

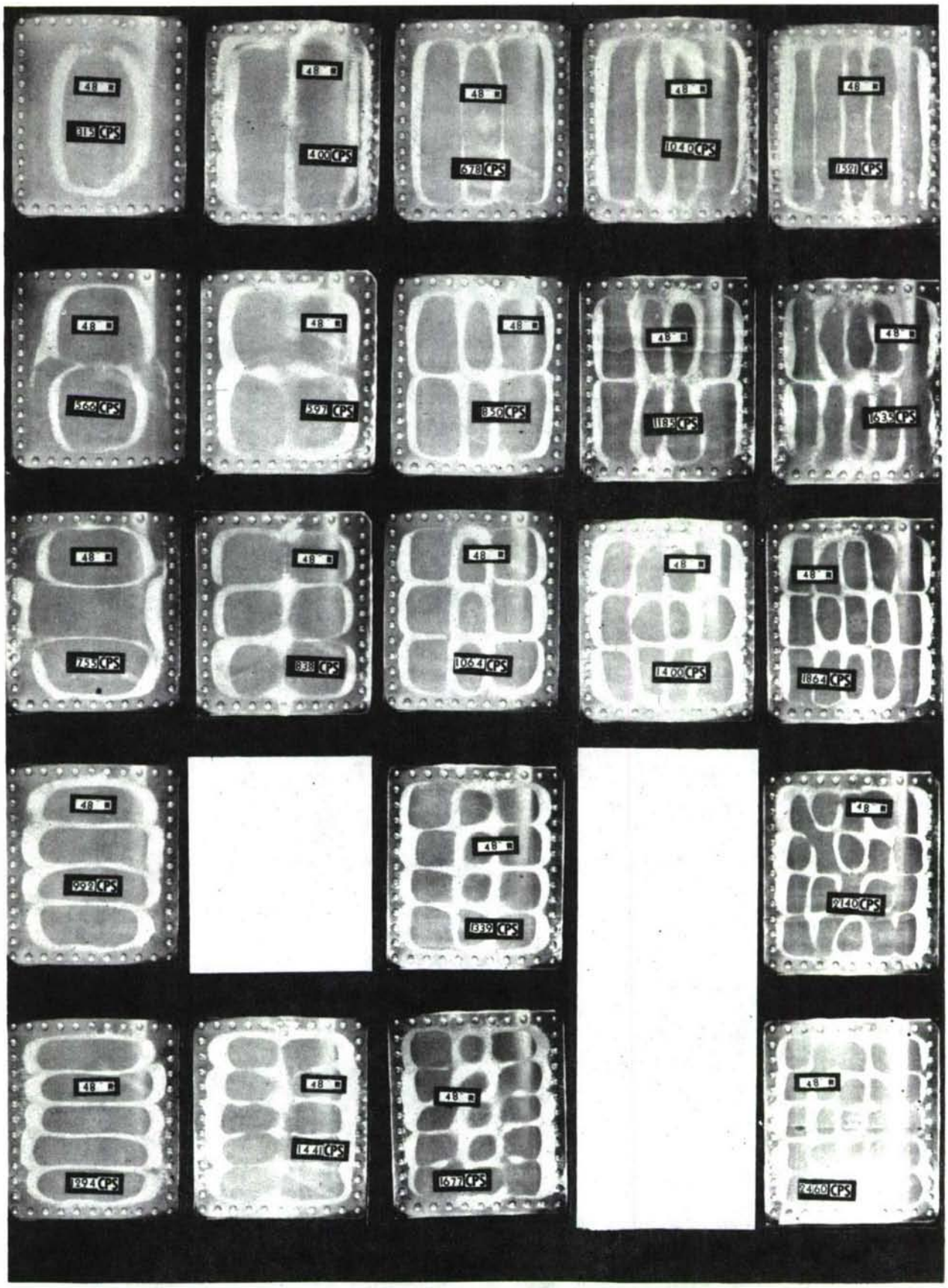

FIGURE 8. MODE SHAPES FOR 0.051 PANEL WITH 48-INCH RADIUS

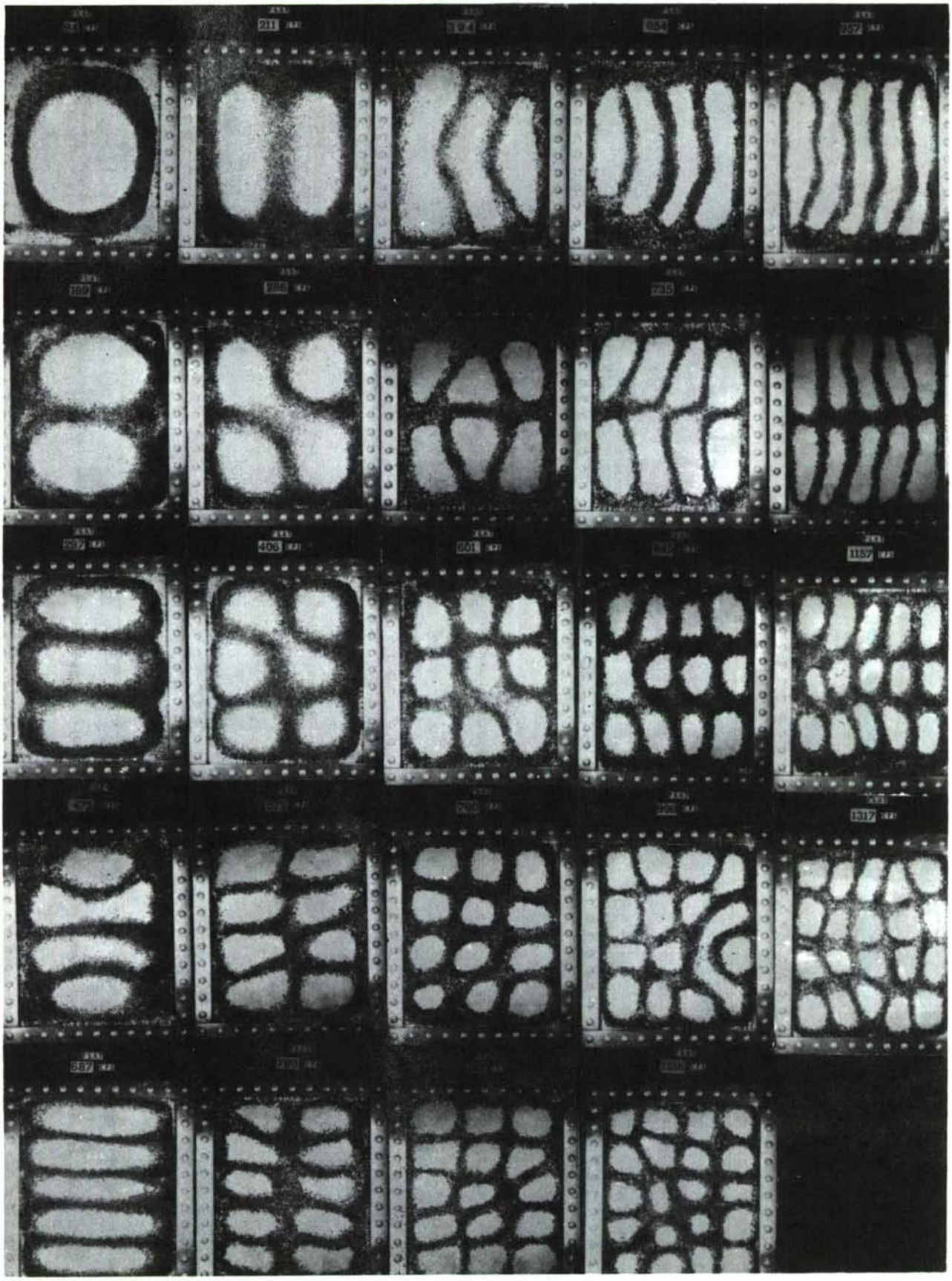

FIGURE 9. MODE SHAPES FOR 0.032 FLAT PANEL

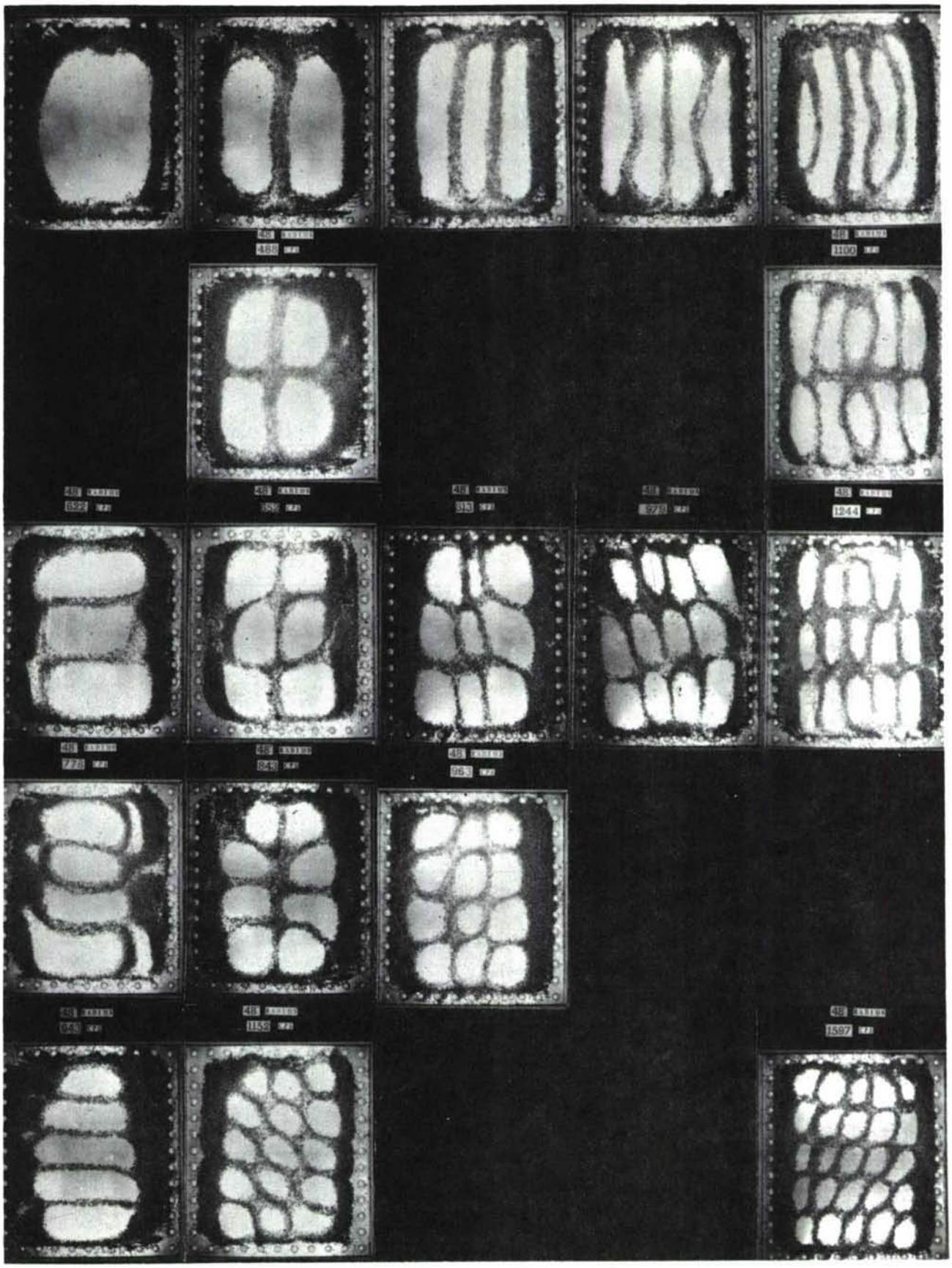

FIGURE 10. MODE SHAPES FOR 0.032 PANEL WITH 48-INCH RADIUS

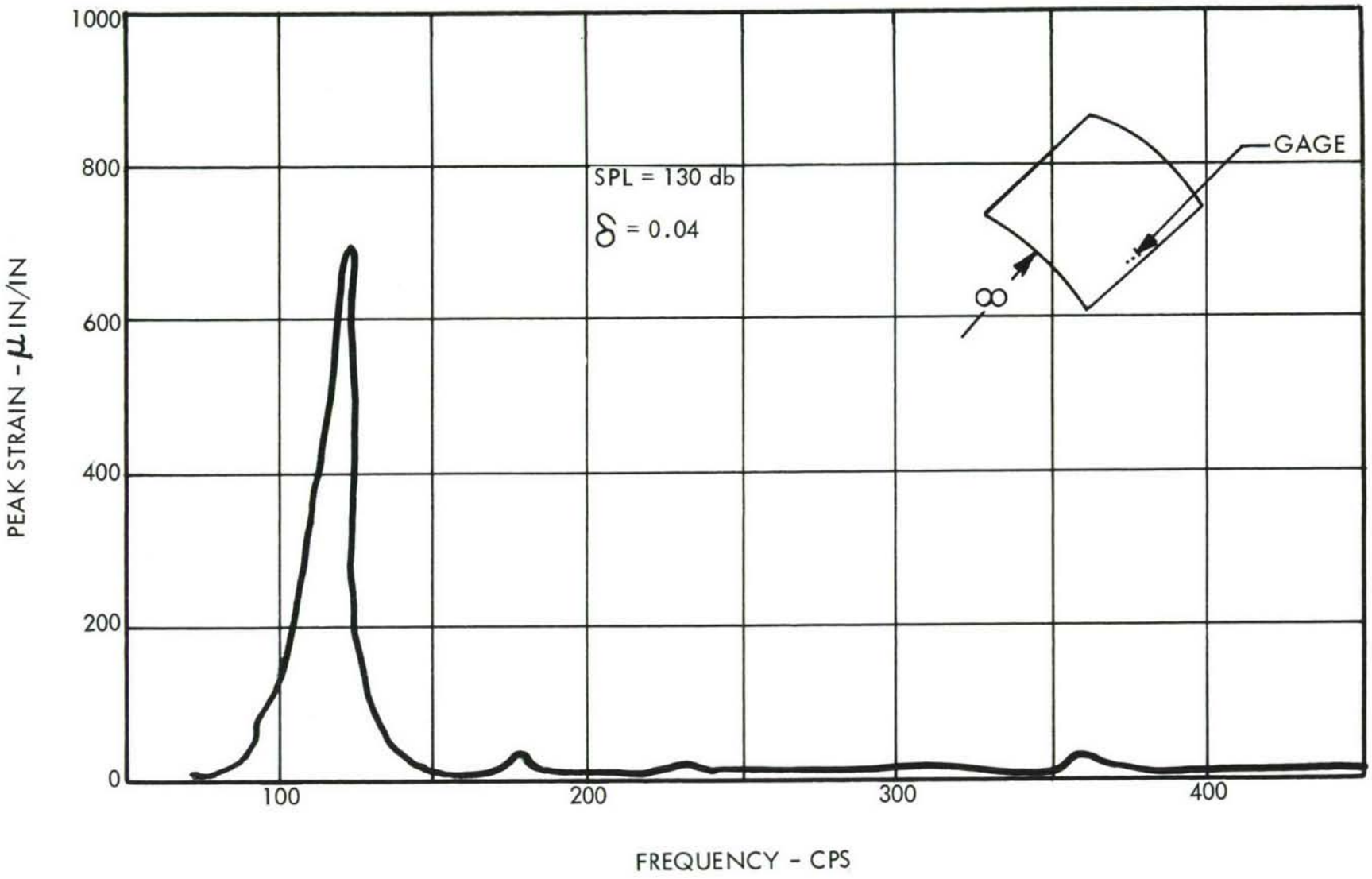

FIGURE 11. SINE SWEEP EXCITATION - FLAT PANEL

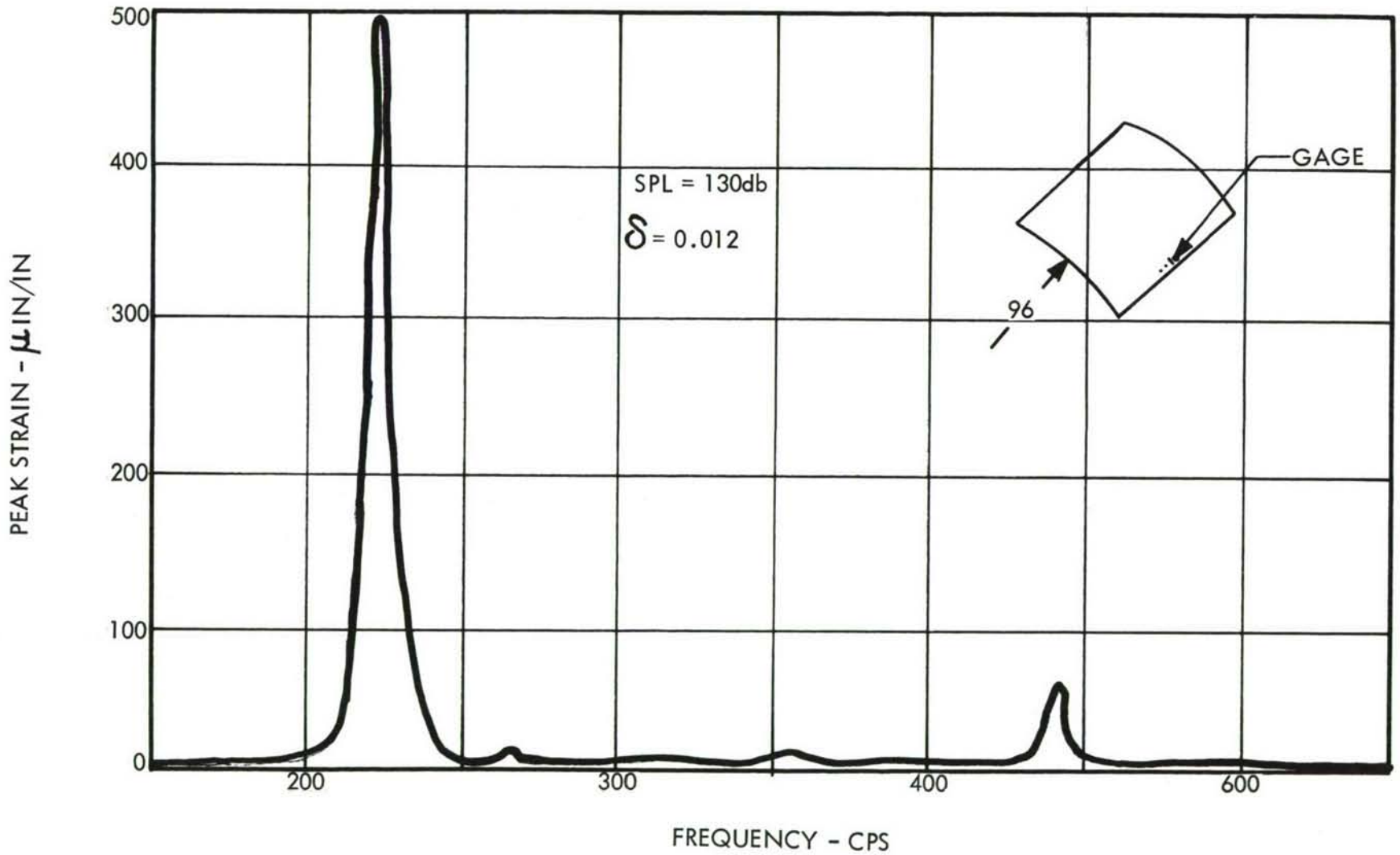

FIGURE 12. SINE SWEEP EXCITATION - 96" R

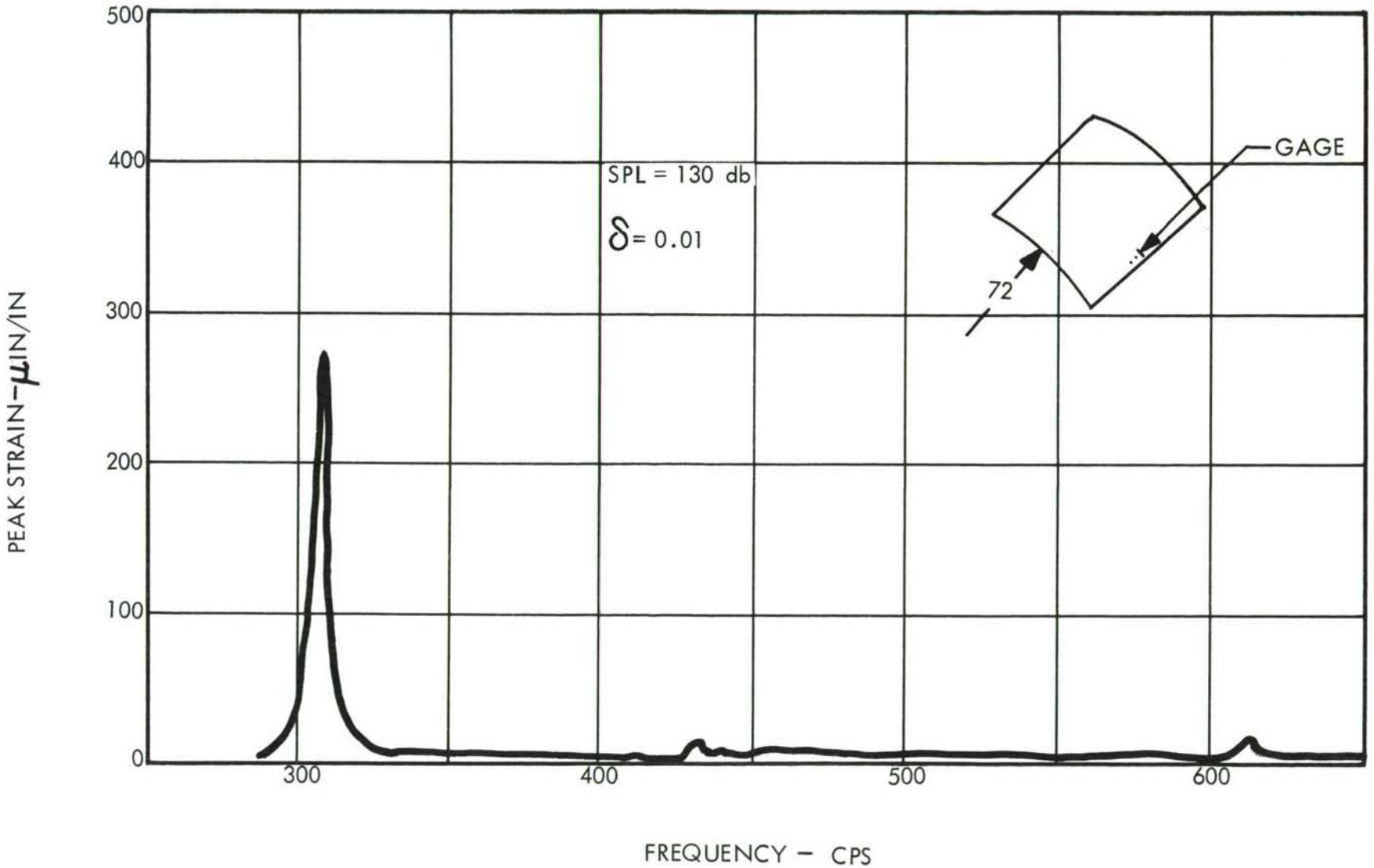

FIGURE 13 SINE SWEEP EXCITATION-72" R

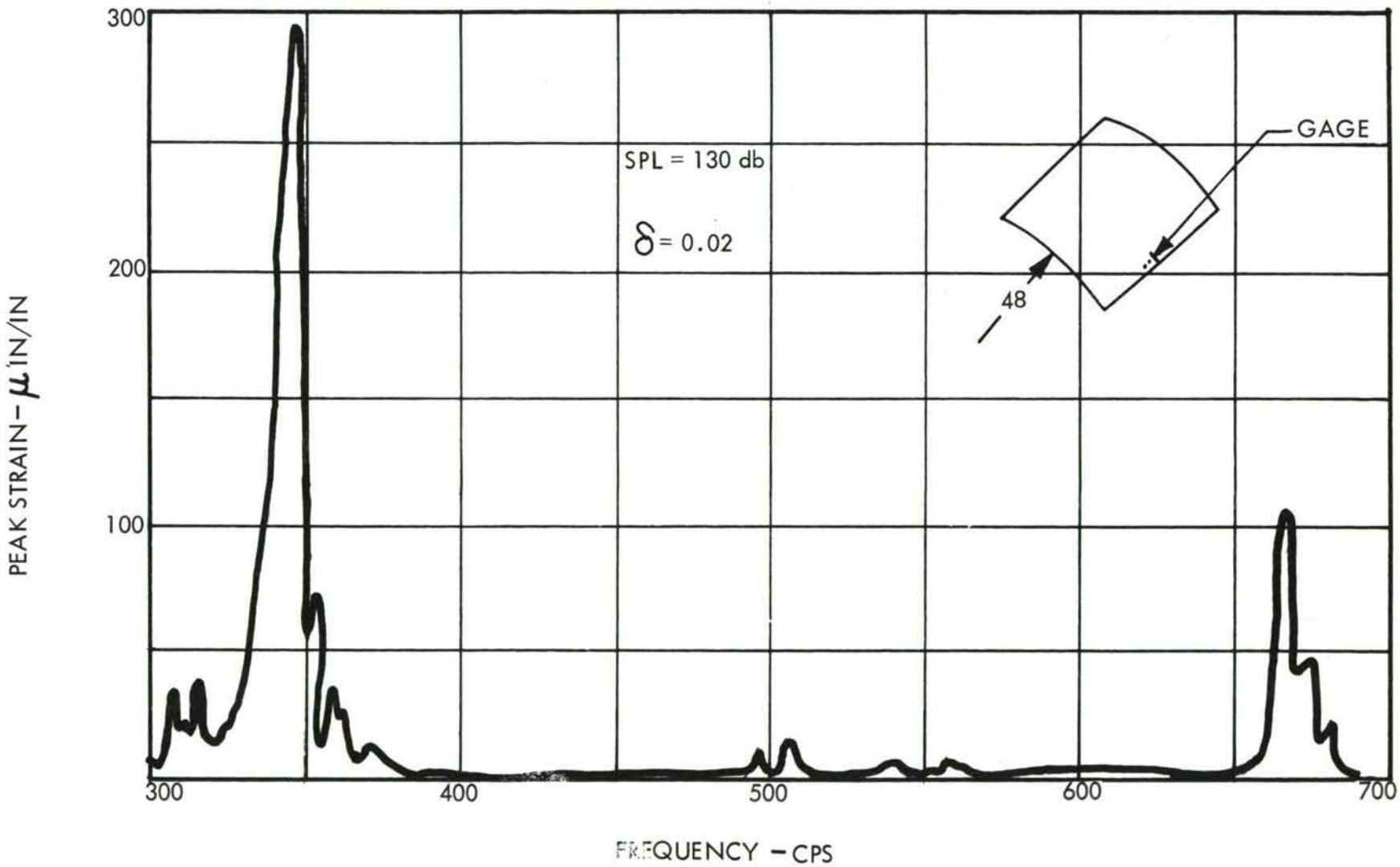

FIGURE 14. SINE SWEEP EXCITATION -48" R

The damping ratio, δ, was determined for each test specimen configuration using the bandwidth method and the log-decrement method. Both methods produced damping ratios which compared reasonably well. The values of the damping ratios ranged from 1% to 4%. These lie within the range of damping ratios for simple panels published in Reference 11.

- Broad-Band Excitation. Each configuration of curved panel was exposed to broad-band noise having a flat spectrum from 50 to 2,000 cps. Dynamic strain measurements were made of the most active gage (gage #1) for each configuration. The strain data were recorded on magnetic tape and later analyzed by a narrow-band (1 cps) analyzer to compare the sinusoidal frequency sweep responses with the flat spectrum, broad-band excitation responses. Figures 15 through 18 are nominal one-cps bandwidth analyses of strain responses resulting from flat spectrum, broad-band noise excitation at an overall sound pressure level of 151 decibels.

- Broad-Band Acoustical Noise Spectra. In a previous section it was pointed out that a shaped spectrum can be used for broad-band testing provided the bandwidth of the excitation is at least three times the bandwidth of the response. The acoustical noise spectra for the fatigue tests were shaped accordingly and are shown in Figure 19. Two spectra were required to satisfactorily encompass the significant response peaks (1,1 mode) of the four panel configurations. The spectrum of Figure 19 drawn with a dashed line was used to test the flat panels and those with the 48-inch radius. The spectrum drawn with a solid line was used to test the panels with the 72-inch radius and the 96-inch radius. These spectra were raised or lowered to obtain a desired test level. There was no noticeable change in spectrum shape when the test levels were raised or lowered as required for the fatigue tests.

- Fatigue Tests. Twenty-four test specimens of the designs shown in Figure 4 were tested to failure at the test spectrum levels shown in the following table.

TABLE 4

SIMPLE SPECIMEN TEST SUMMARY

Configuration	Replicates	Test Spectrum Level, db (re. 0.0002 Microbar)
Flat	2	134
Flat	2	137
Flat	2	140
96"R	2	136
96"R	2	139
96"R	2	142
72"R	2	135.5
72"R	2	138.5
72"R	2	141.5
48"R	2	136
48"R	2	139
48"R	2	142

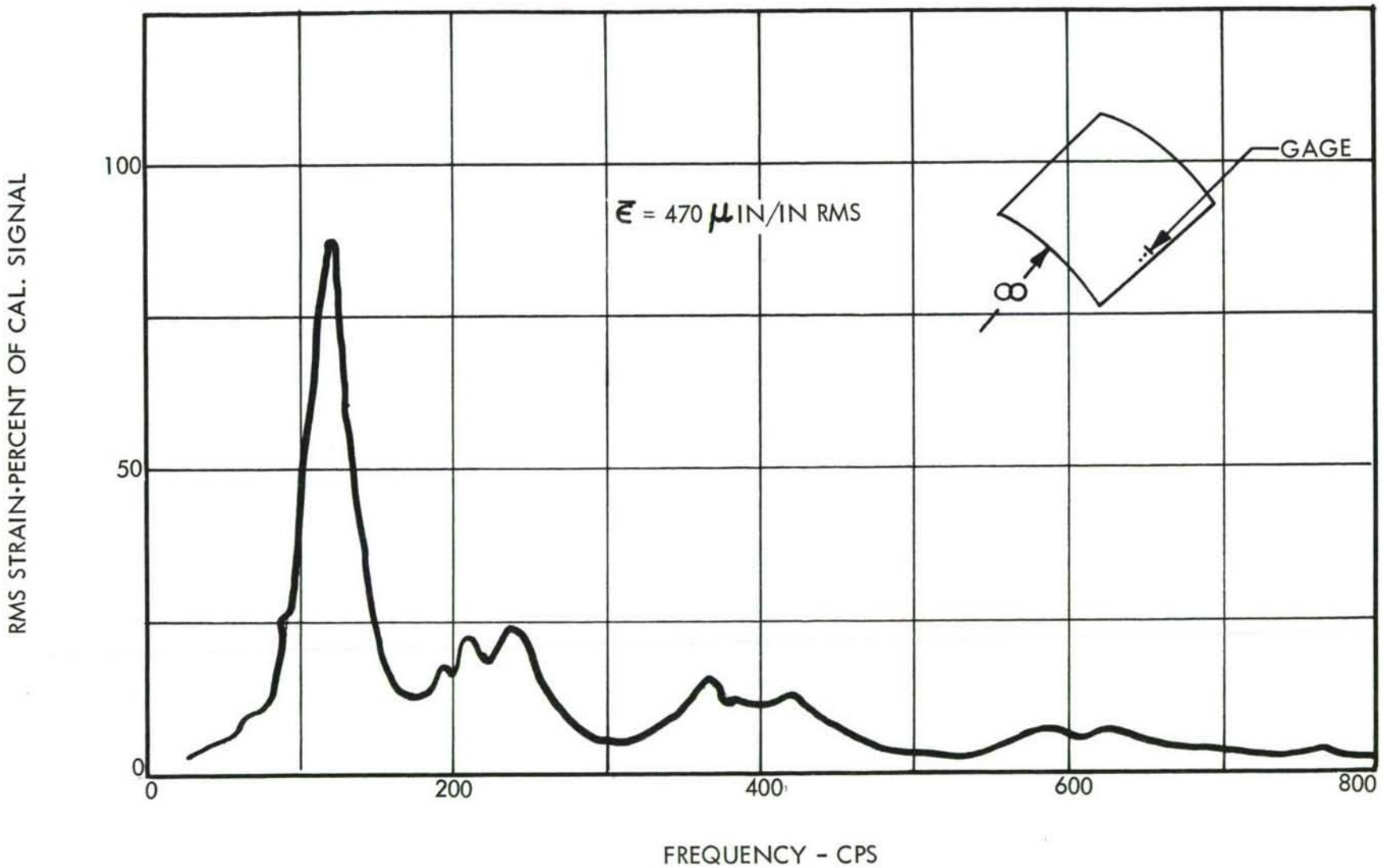

FIGURE 15. BROAD-BAND NOISE EXCITATION, 151 DB - FLAT PANEL

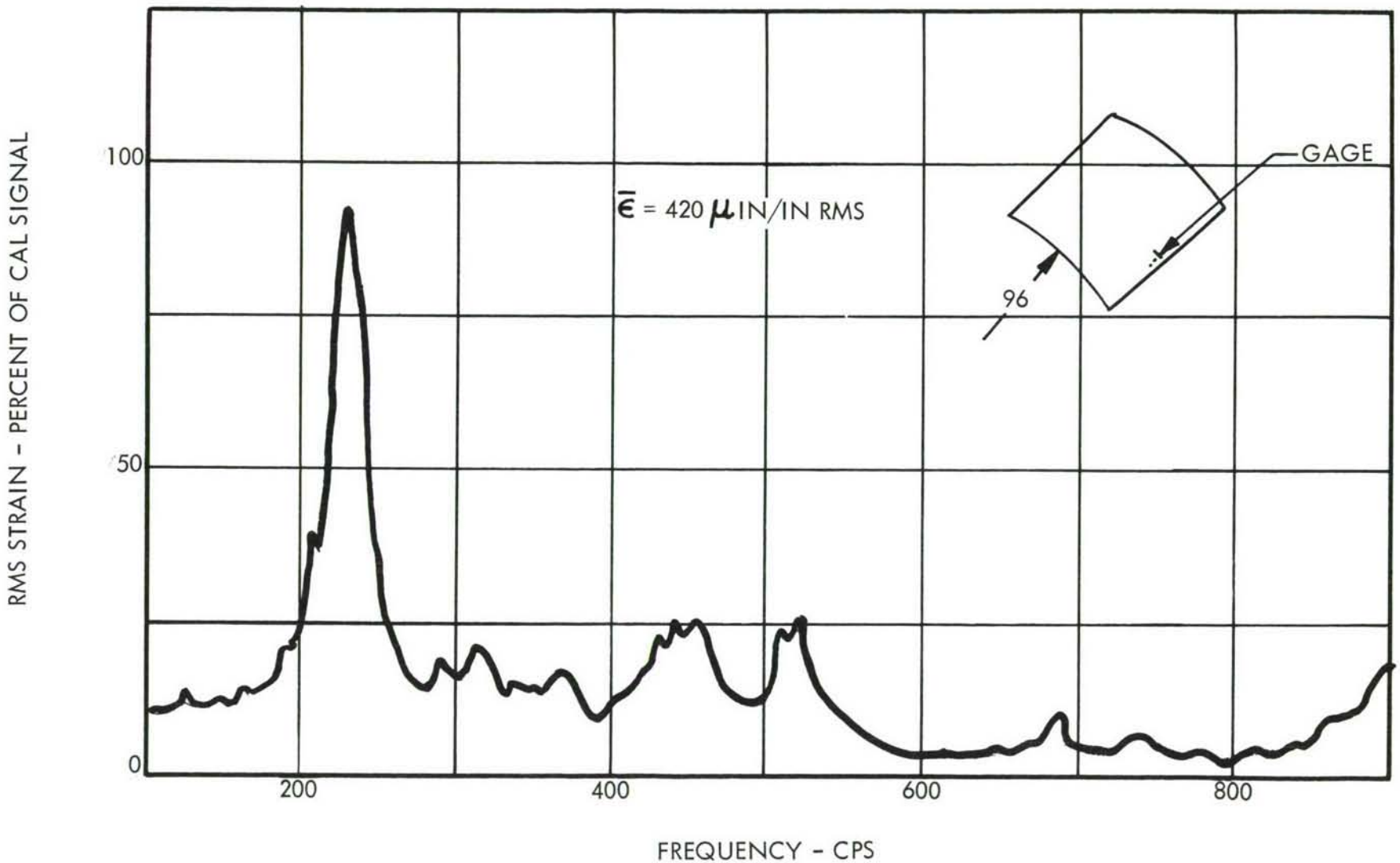

FIGURE 16. BROAD-BAND NOISE EXCITATION, 151 DB - 96" R

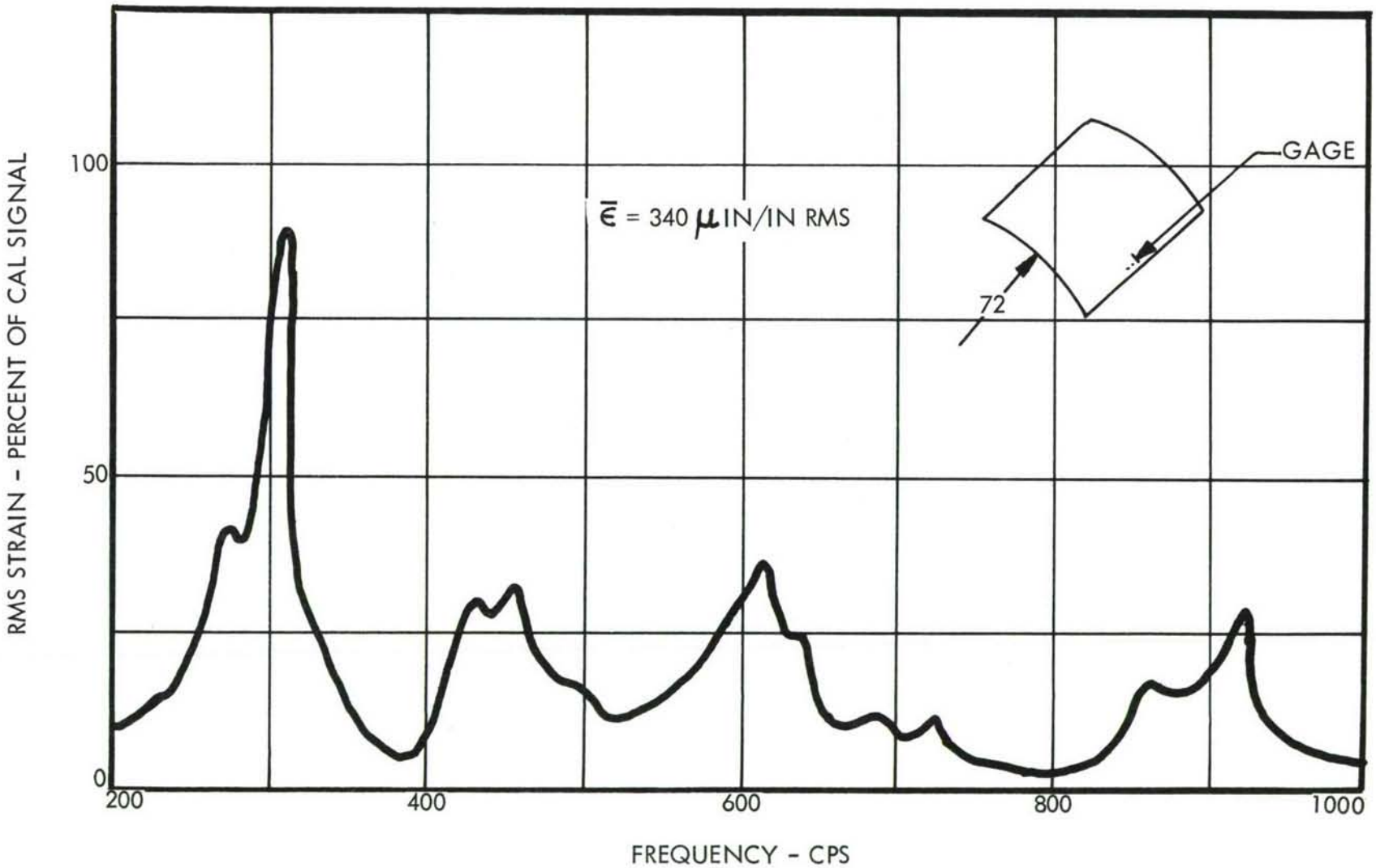

FIGURE 17. BROAD-BAND NOISE EXCITATION, 151 DB - 72" R

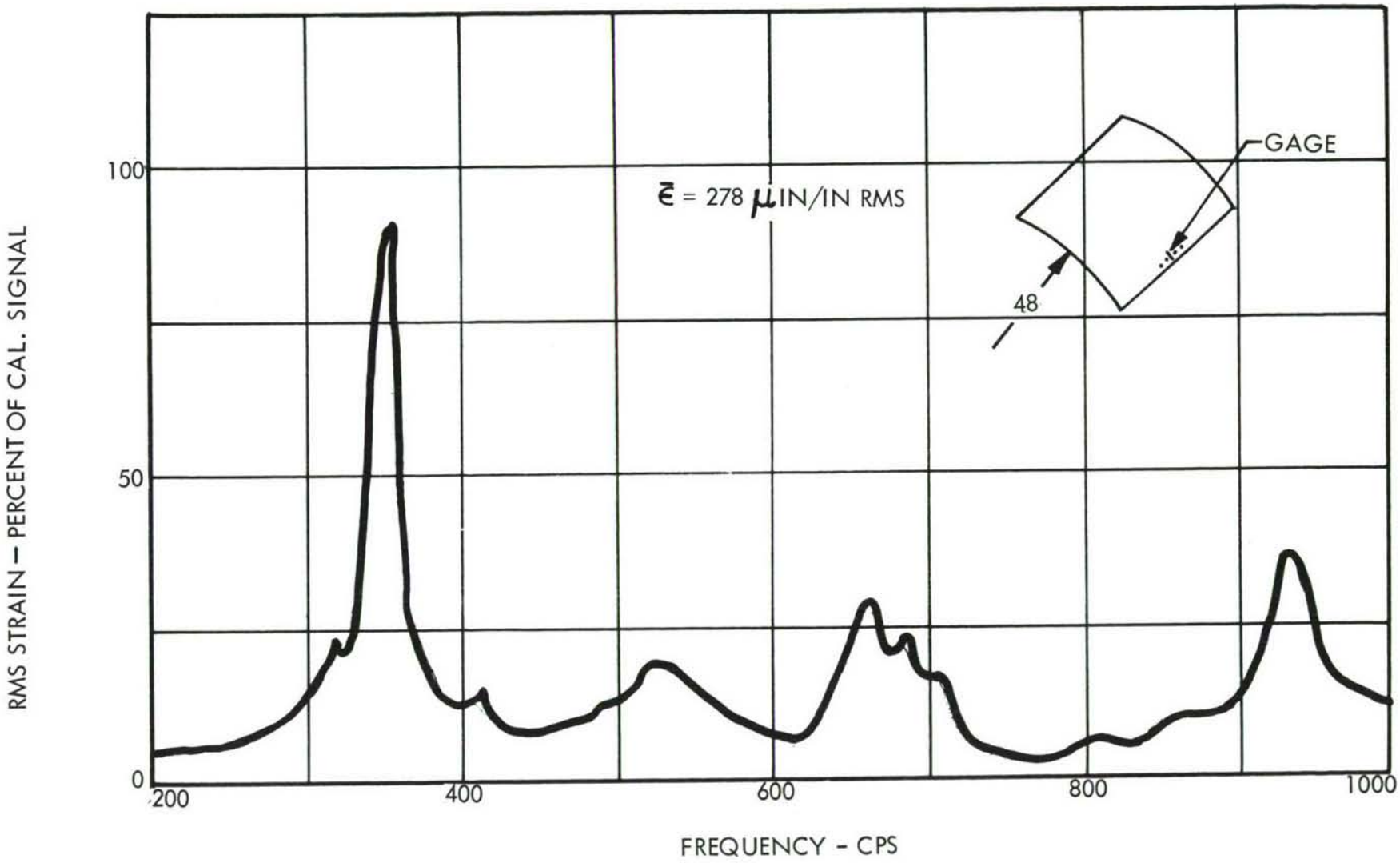

FIGURE 18. BROAD-BAND NOISE EXCITATION, 151 DB - 48" R

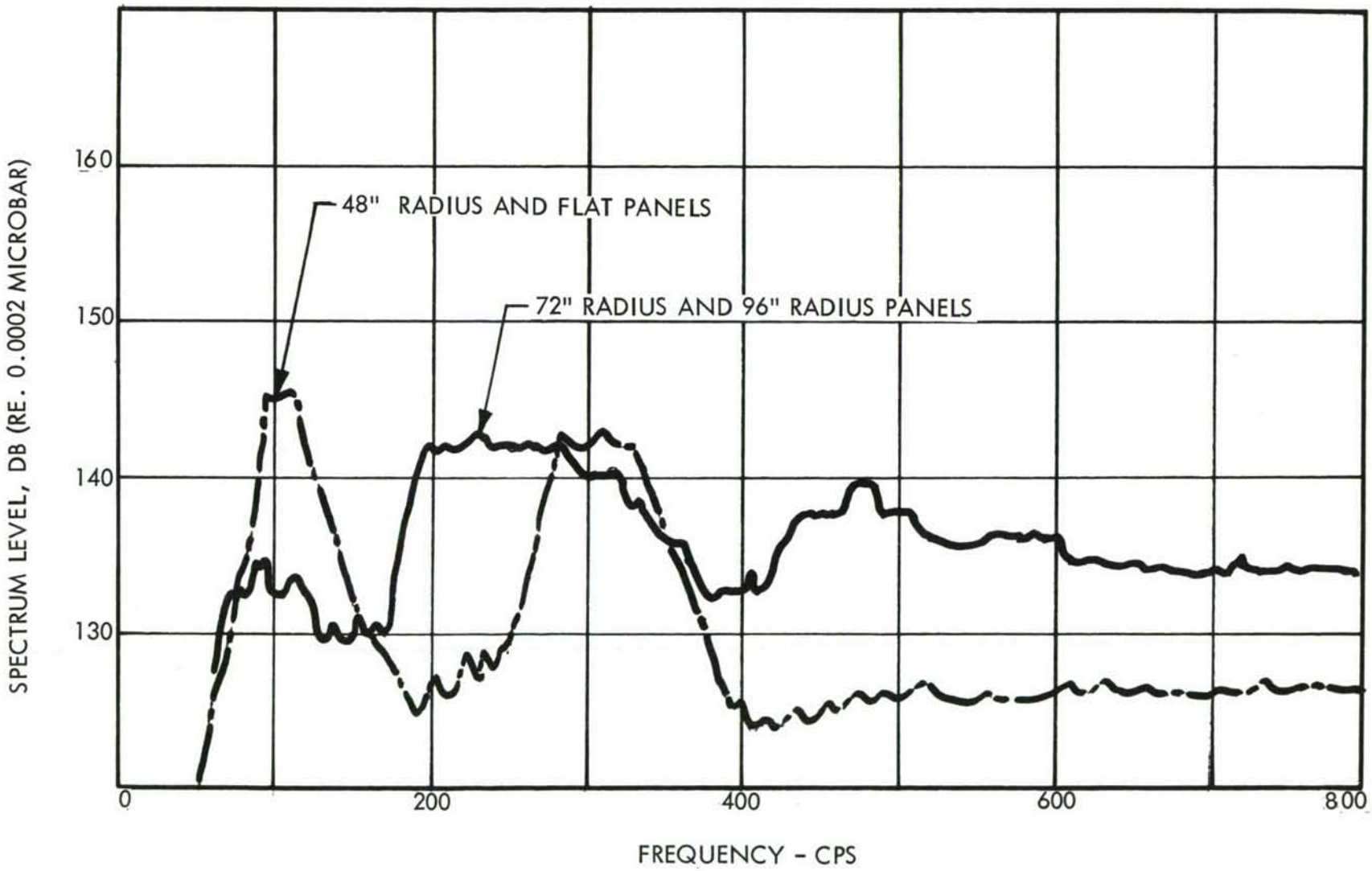

FIGURE 19. BROAD-BAND NOISE SPECTRA FOR FATIGUE TESTS

The results of the fatigue tests are presented in the form of fatigue curves, Figure 20. The fatigue curves were plotted using spectrum level, db, as the ordinate and mean cycles-to-failure as the abscissa. (Cycles-to-failure were determined as the product of time-to-failure and critical response frequency.)

Figure 21 is presented to show the relationship between maximum root-mean-square (rms) panel strain versus cycles-to-failure. As expected, these $\overline{\epsilon}$ - N curves have the same general appearance as the curves of Figure 20.

Magnetic tape recordings of strain which produced response spectra of the type shown in Figures 15 through 18 were analyzed to determine the nature of their statistical properties. A 30-second sample of the maximum strain response from each of the four test specimen configurations was analyzed by a probability analyzer to determine probability distribution of strain peaks. The strain data analyzed were those obtained at the highest test spectrum level. Figure 22 is a plot of the probability distribution of the strain peaks for the four configurations.

4. Elevated Temperature Tests

The object of this phase of the simple specimen experimental investigation was to determine the relative fatigue damage resulting from alternate application of heat and acoustical excitation and simultaneous application of heat and acoustical excitation.

A description of the test specimens, test setup, test procedure, and test results will follow in that order.

a. Test Specimen. The test specimens were flat with overall dimensions of 11.0" x 13.0" x 0.032". Four of the specimens were 8Al-1Mo-1V titanium and four were 17-7 PH stainless steel. Holes for 3/16-inch diameter bolts were drilled around the perimeter of each specimen as shown on the drawing of the test specimen, Figure 4.

b. Test Setup. Each test specimen was attached to a picture frame mounting fixture of the type shown in Figure 5. A torque of 45-55 inch-pounds was applied to each bolt to keep the edge fixity uniform for all specimens.

Two of the mounting fixtures were bolted to each side of the progressive wave test section of the High Intensity Sound System as shown in Figure 23. This photograph shows that a removable side of the test section has been opened for access. Also, three monitor microphones are located along the vertical centerline of the test specimens and one located forward at the mouth of the horn.

Quartz lamp tubes were used to supply the heat for the test specimens. Figure 24 is a photograph of these heaters moved away from two test specimens to facilitate inspection for fatigue cracks and permanent thermal buckling.

Each test specimen was instrumented with thermocouples to determine the temperature distribution during elevated temperature tests. Test specimen thermocouple locations are shown in Figure 25. The thermocouples were held to the surface of each test specimen by aluminized tape.

High temperature strain gages were mounted on the test specimens in the pattern shown in Figure 26.

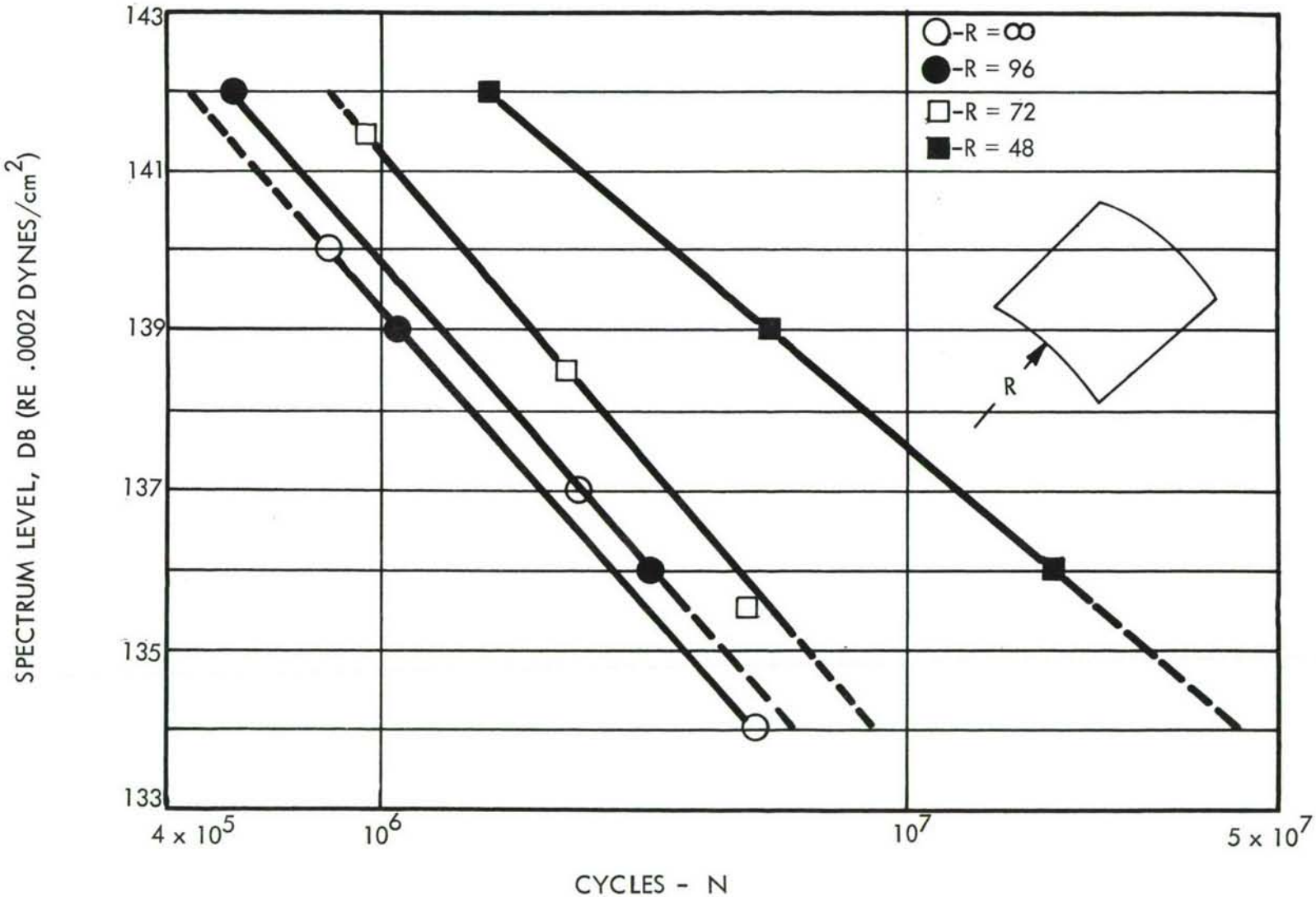

FIGURE 20. SPECTRUM LEVEL VERSUS MEAN CYCLES-TO-FAILURE

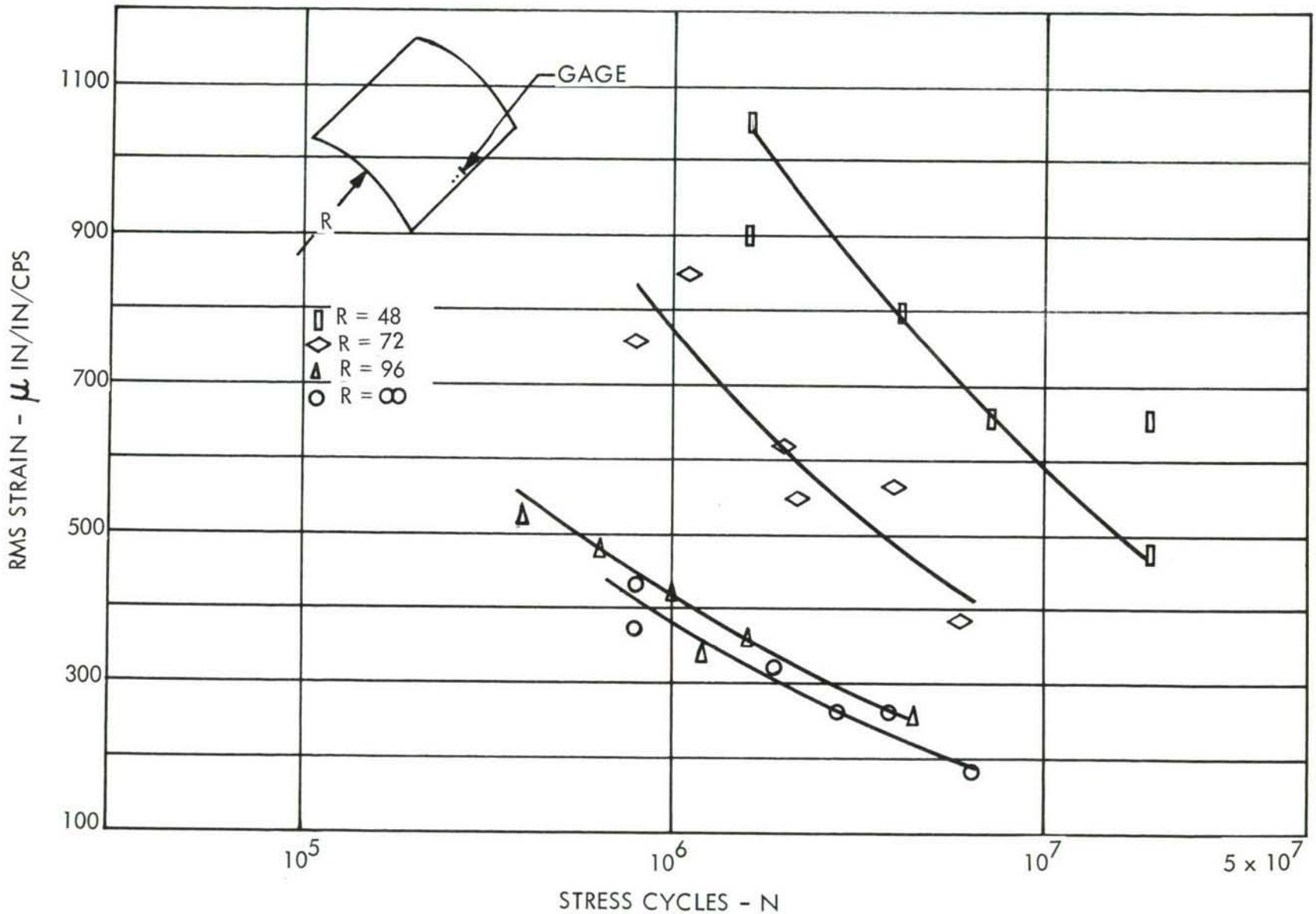

FIGURE 21. $\bar{\epsilon}$ -N CURVES FOR SIMPLE CURVED PANELS

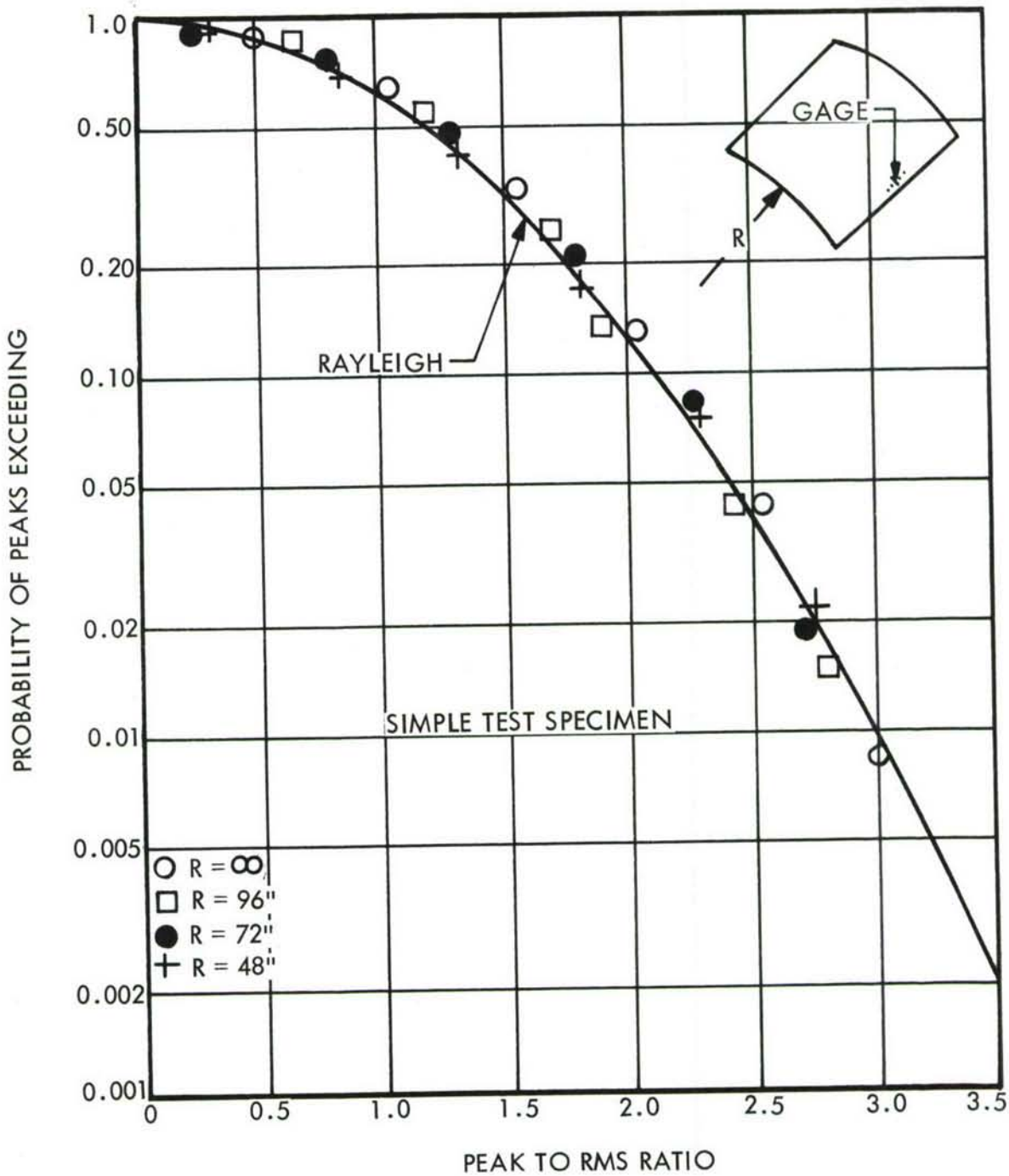

FIGURE 22. PROBABILITY DISTRIBUTION OF STRAIN PEAKS

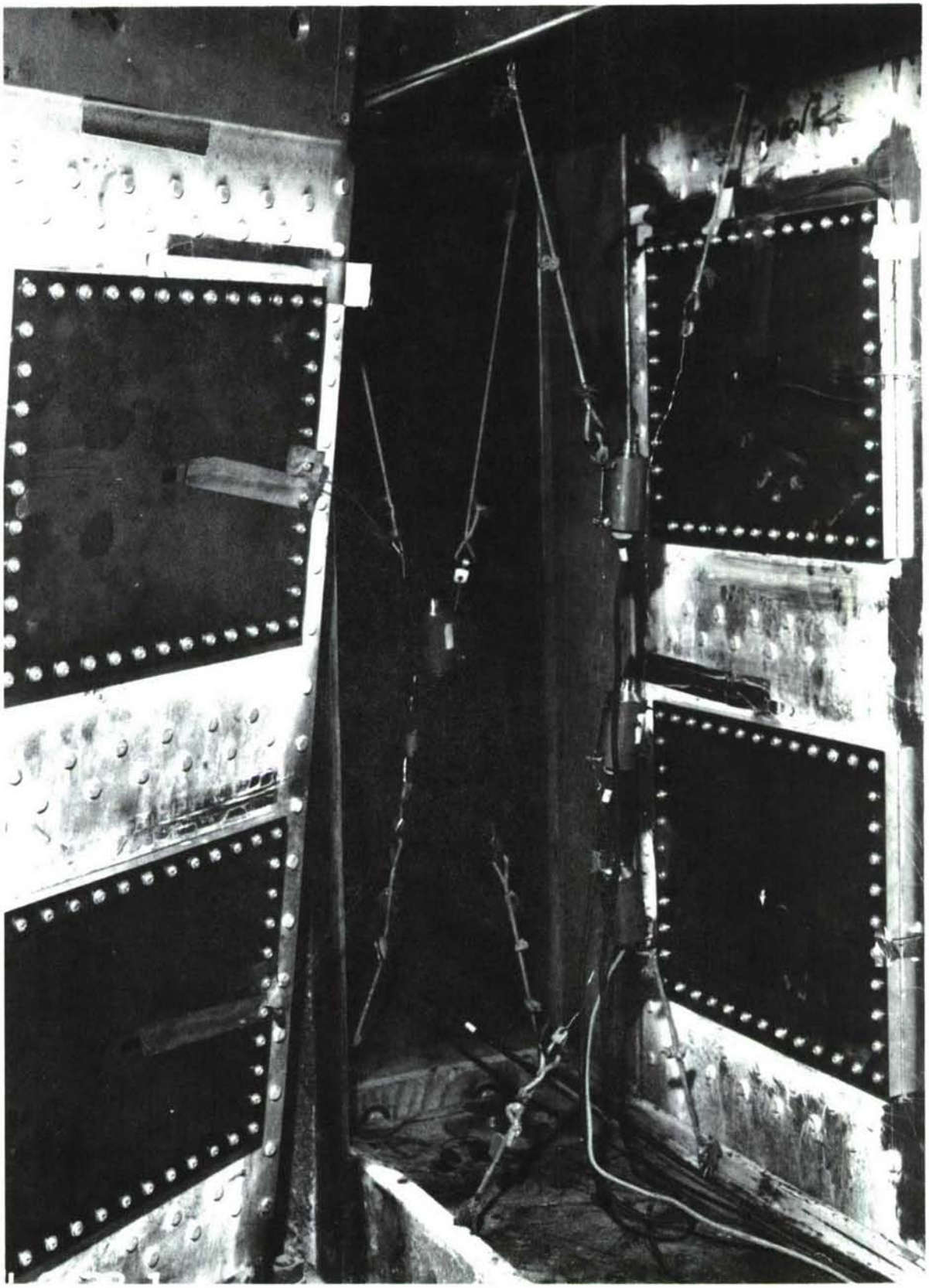

FIGURE 23. VIEW OF TEST SPECIMENS MOUNTED IN TEST SECTION (A REMOVABLE SIDE HAS BEEN OPENED FOR ACCESS)

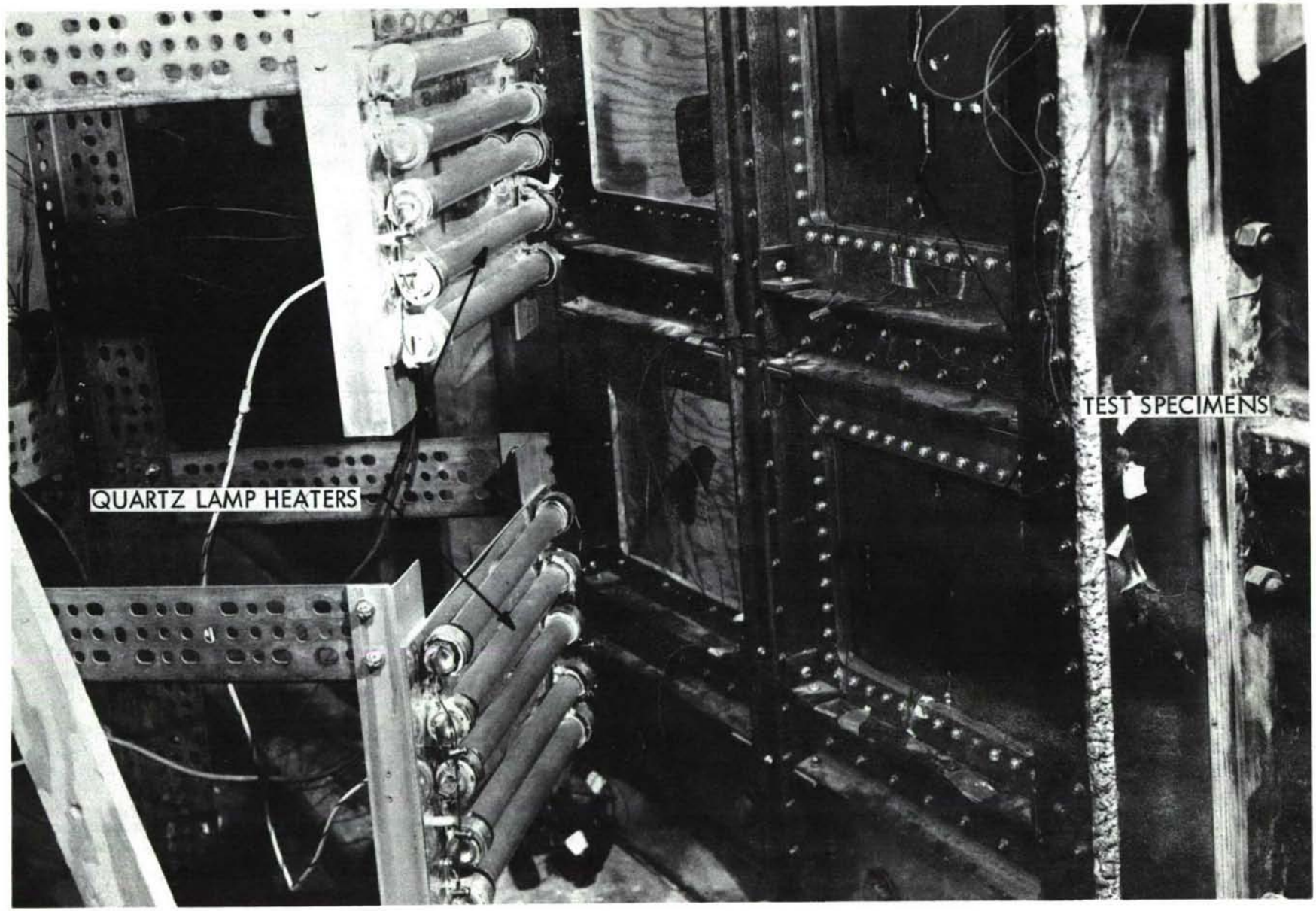

FIGURE 24. QUARTZ LAMP HEATERS FOR ELEVATED TEMPERATURE TESTS

17-7PH STAINLESS STEEL

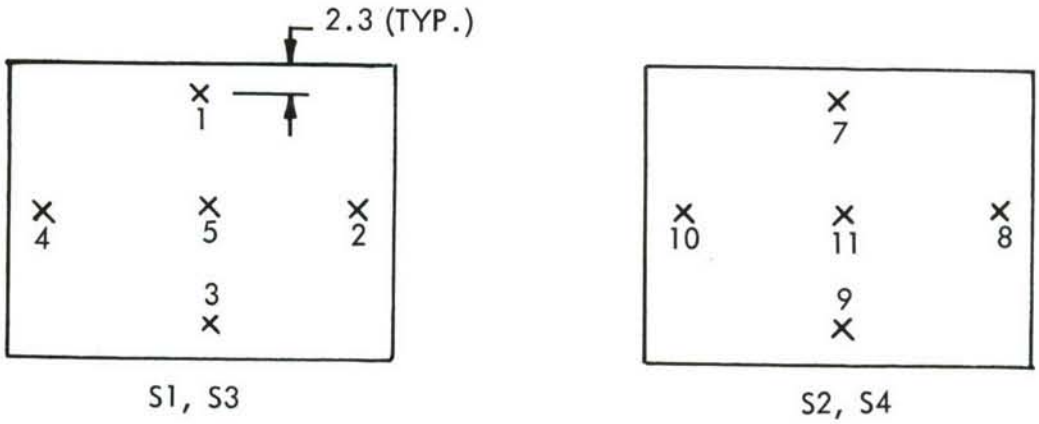

8Al-1Mo-1V TITANIUM

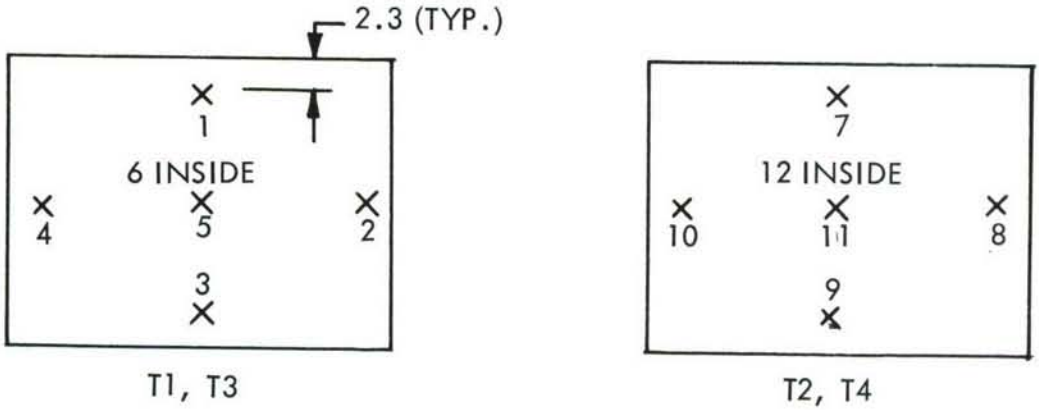

FIGURE 25. THERMOCOUPLE LOCATIONS

17-7 PH STAINLESS STEEL

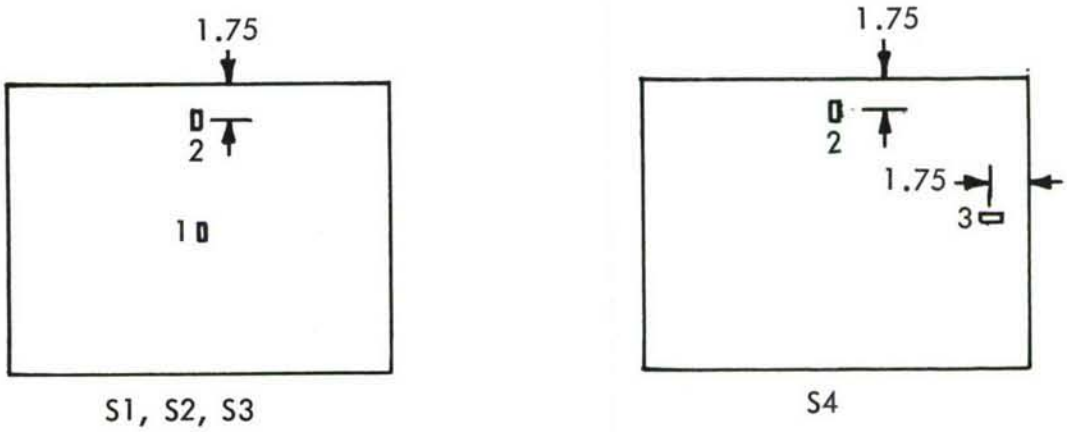

8Al-1Mo-1V TITANIUM

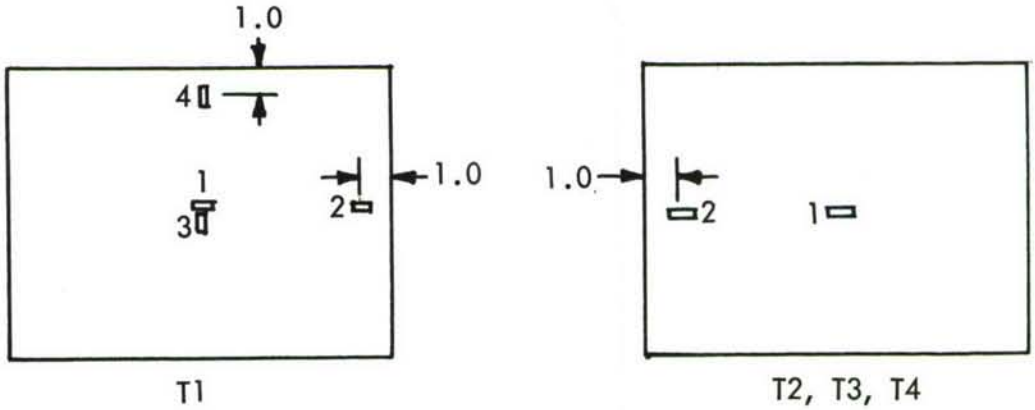

FIGURE 26. STRAIN GAGE LOCATIONS - ELEVATED TEMPERATURE TESTS

c. Test Procedure. Frequency sweeps were made at a number of discrete frequency sound pressure levels to determine the response characteristics of the two configurations. These frequency sweeps were made at ambient temperature and test temperature of 450° F.

The frequency sweeps were used to shape broad-band sound pressure test spectra for the fatigue tests. Results of the ambient temperature tests reported in Section II.B.3 showed similar test specimen response characteristics for broad-band excitation and discrete frequency excitation. Consequently, the low-intensity, broad-band tests were omitted for this phase of the simple test specimen investigation.

The procedure for the fatigue test on one set of four specimens was as follows: Two specimens, say 1 and 2, were exposed to heat generated by quartz lamps. Shortly after reaching thermal equilibrium, the sound generators were started and the sound pressure level brought up to the test level on all four specimens. The two specimens, 3 and 4, mounted on the opposite side of the test section were excited acoustically at ambient temperature. After a predetermined time of exposure the acoustical excitation and heat were removed. The heaters were then moved to specimens 3 and 4. They were heated to the same temperature and for the same length of time as specimens 1 and 2, but without acoustical excitation. This completed one cycle of the fatigue test. The specimens were dye-penetrant checked for fatigue cracks after each acoustical excitation. When a crack was discovered its location and length were recorded versus test time until the panels were removed from the test chamber.

d. Test Results. Results of the elevated temperature tests will be described. The description will begin with the frequency sweeps and end with the fatigue tests of the titanium and stainless steel specimens.

- Frequency Sweeps. Figures 27 through 29 are plots of strain response for sinusoidal frequency sweep excitation at 130 decibels. Frequency sweeps for the titanium and stainless steel specimen were made of 450° F and ambient temperature.

  Damping was determined for each panel configuration and test condition. Damping ratios determined by the bandwidth method range from 1.3% to 2.1%. The damping ratios at elevated temperatures were less than ambient temperature ratios.

- Broad-Band Acoustical Noise Spectra. It was necessary to shape the test spectrum so that fatigue failures could be produced in a reasonable length of time. Figure 30(b) is a typical test spectrum for the elevated and room temperature tests of the titanium specimens. Figure 30(a) is a typical test spectrum for the elevated and room temperature tests of the stainless steel specimens. The spectrum for the stainless steel specimens had two lobes. One lobe was required to excite specimen response at ambient temperature whereas the other lobe was needed to excite specimen response at elevated temperature.

- Temperature. A table of typical temperature distribution over the specimen surfaces during frequency sweeps and fatigue tests is shown below.

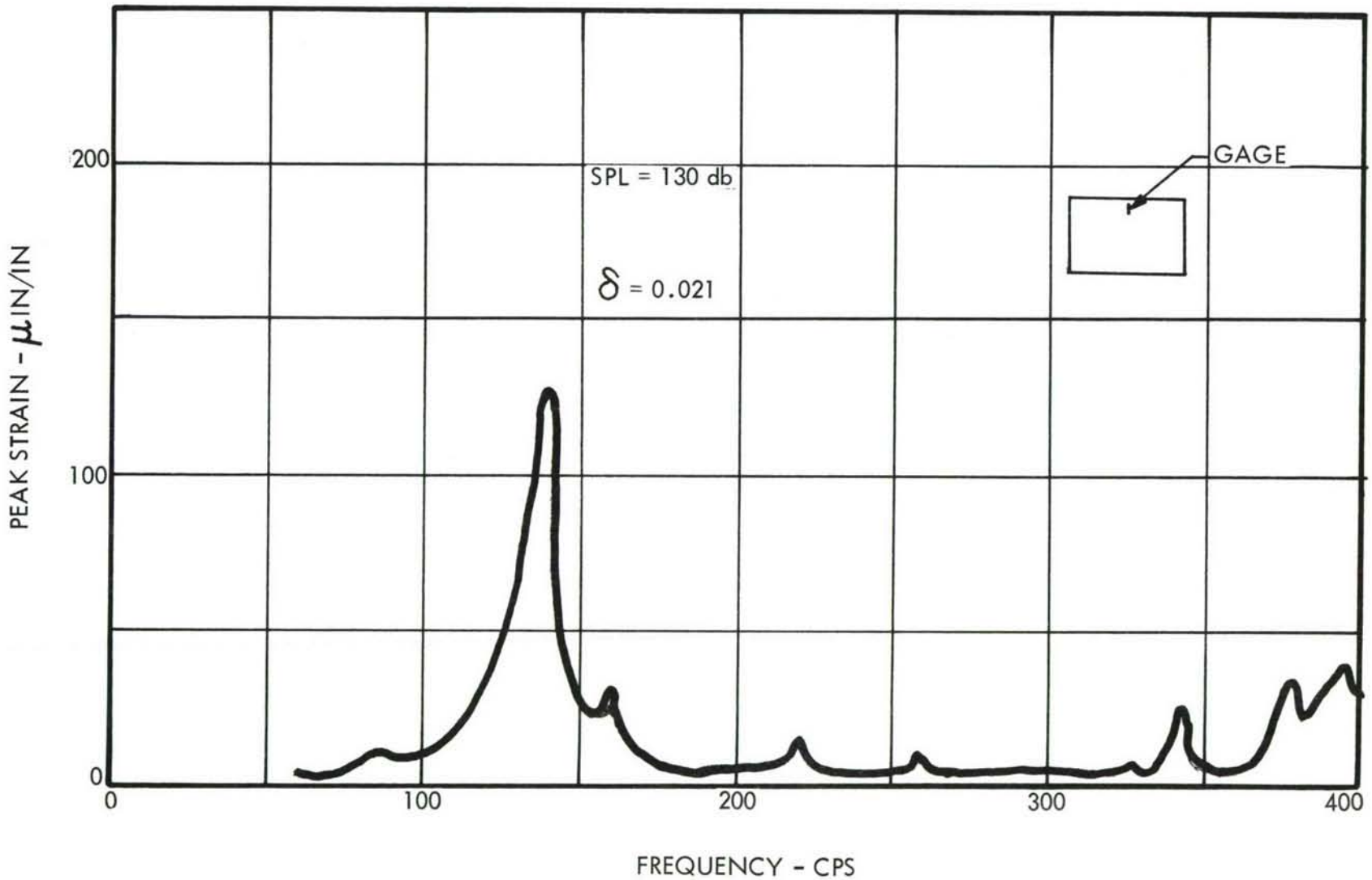

FIGURE 27. SINE SWEEP EXCITATION, AMBIENT TEMPERATURE–TITANIUM

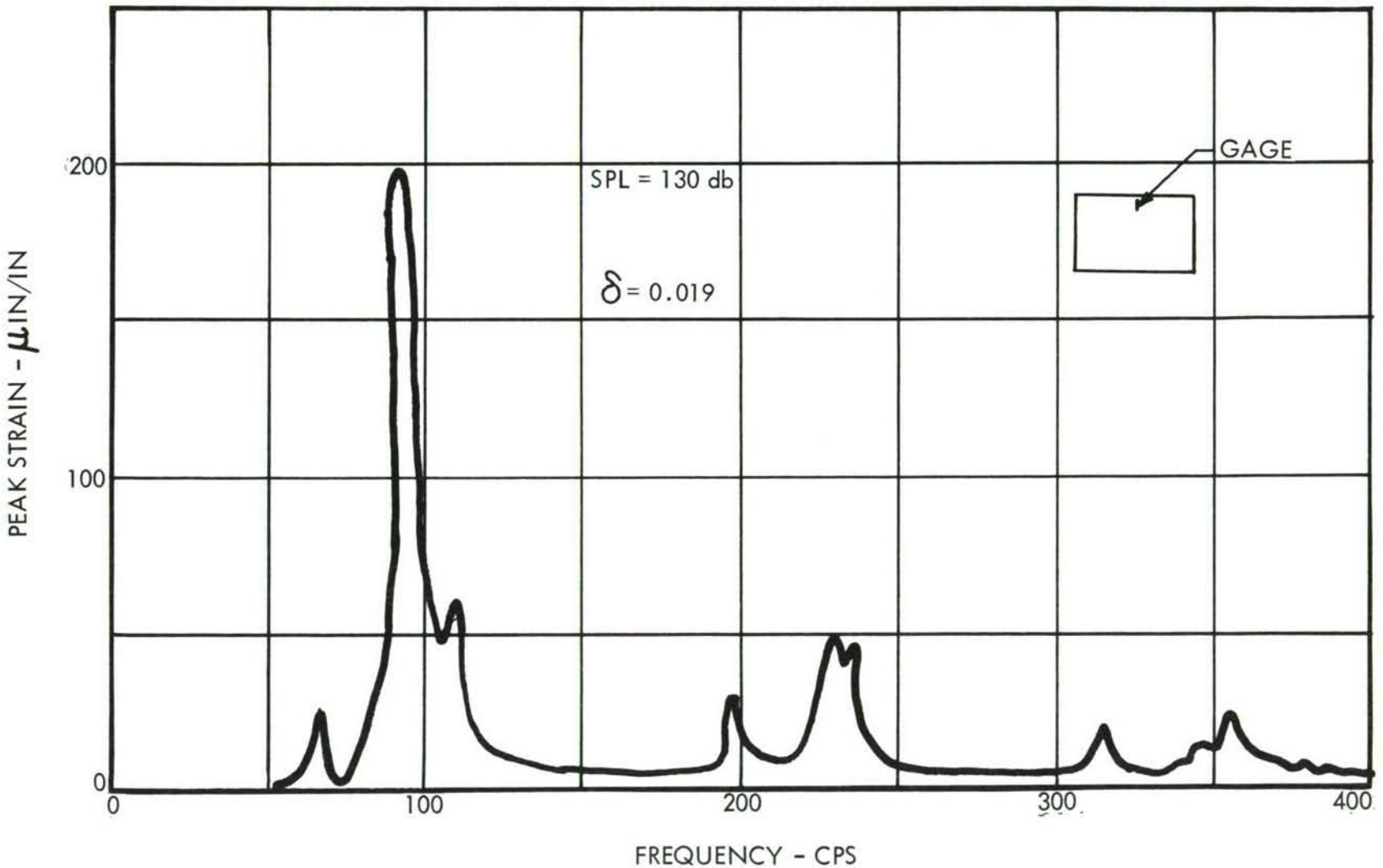

FIGURE 28. SINE SWEEP EXCITATION, 450° F - TITANIUM

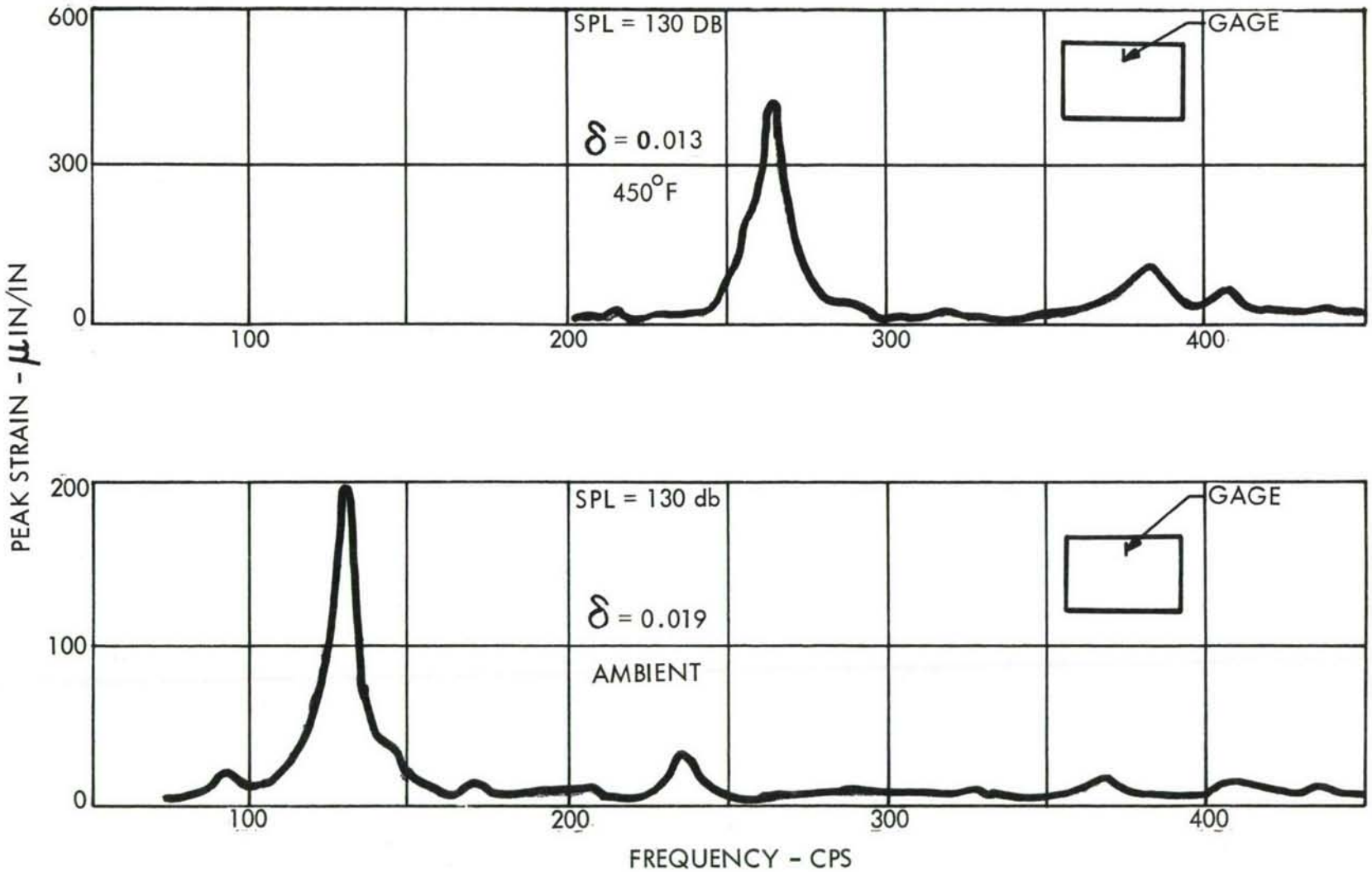

FIGURE 29. SINE SWEEP EXCITATION, AMBIENT AND 450° F - STAINLESS STEEL

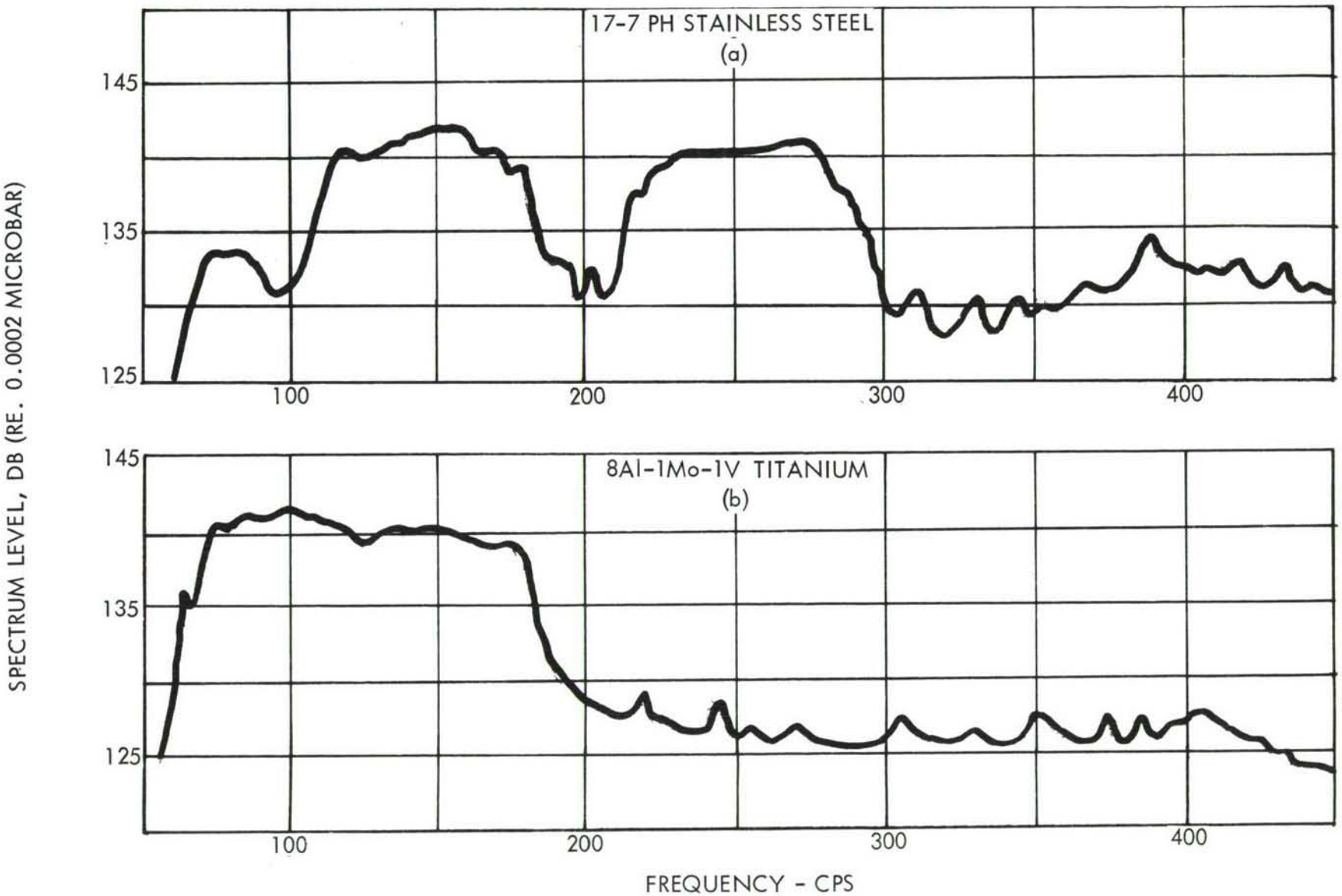

FIGURE 30. BROAD-BAND NOISE SPECTRA FOR ELEVATED TEMPERATURE TESTS

TABLE 5

TYPICAL FAHRENHEIT TEMPERATURE DISTRIBUTION

Thermocouple No. (See Figure 25)	Ti-8Al-1Mo-1V		17-7PH Stainless Steel	
	Frequency Sweeps	Fatigue Tests	Frequency Sweeps	Fatigue Tests
1	430	420	410	460
2	420	460	420	470
3	490	460	490	420
4	420	390	460	460
5	450	470	470	520
6	430	430	-	-
7	450	460	-	480
8	-	450	-	440
9	470	440	-	390
10	420	420	420	490
11	480	470	420	470
12	440	490	-	-

- Fatigue Tests. Four titanium and four stainless steel test specimens were tested to failure at a spectrum level of 141 db using the test procedure described previously. The results of these tests are contained in Tables 6 and 7. Sketches of crack location and tabulated crack propagation are also included.

C. Comparison of Theoretical and Experimental Results

Natural frequencies for one of the test panels described in Section II.B were determined experimentally to assess the accuracy of the theoretical frequency analysis. The edge conditions of the test setup described in Section II.B could be classified as being somewhere between clamped and simply-supported. In an effort to make the edges consistent with theory the frame shown in Figure 5 was reinforced with a 1/2" thick aluminum picture frame type member bolted to the outer surface of the panel. Extra fasteners were added to increase the clamping effects.

The mode shapes and frequencies were determined as follows: First, two loudspeakers which could be freely positioned, were used to acoustically excite the different modes. One of the speakers was equipped with a phase reversal switch in the line because even modes were most easily excited with the speakers out-of-phase.

Table 8 shows calculated values of natural frequency for both clamped and simply-supported edge conditions along with the experimental values for a 9" x 11" aluminum panel having a 96" radius of curvature and 0.048" thickness. The comparison is quite good except for the (1,1) through (1,4) modes. This difference probably lies in the matching of boundary conditions between theory and experiment.

TABLE 6

FAILURE SUMMARY: TITANIUM SPECIMENS

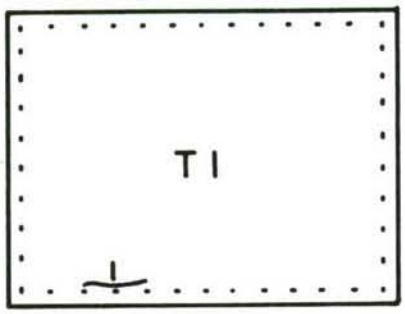

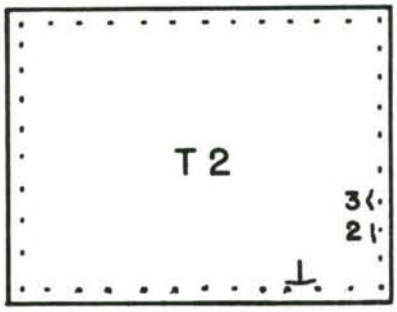

HEAT AND SOUND SIMULTANEOUSLY

TEST TIME MIN.	CRACK NUMBER	CRACK LENGTH INCHES
120	1	1.3
—	—	—
—	—	—

TEST TIME MIN.	CRACK NUMBER			CRACK LENGTH INCHES		
20	1	2	3	1.8	0.6	–
30	1	2	3	2.5	0.8	0.6
45	1	2	3	3.0	3.0	3.0

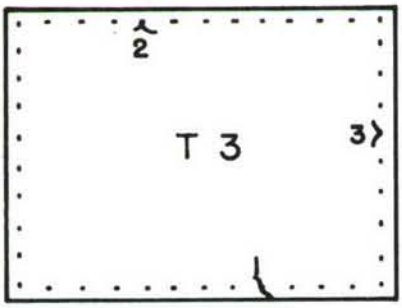

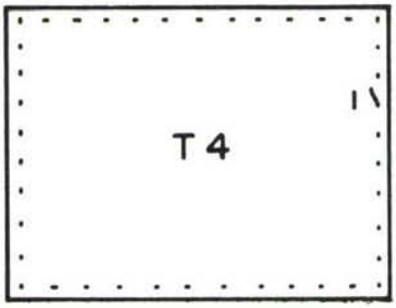

HEAT AND SOUND ALTERNATELY

TEST TIME MIN.	CRACK NUMBER			CRACK LENGTH INCHES		
420	1	2	3	0.1	0.2	–
540	1	2	3	–	0.2	–
645	1	2	3	3.0	0.3	1.0

TEST TIME MIN.	CRACK NUMBER	CRACK LENGTH INCHES
645	1	0.1
—	—	—
—	—	—

TABLE 7

FAILURE SUMMARY: STAINLESS STEEL SPECIMENS

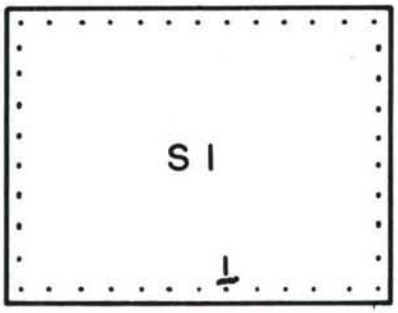

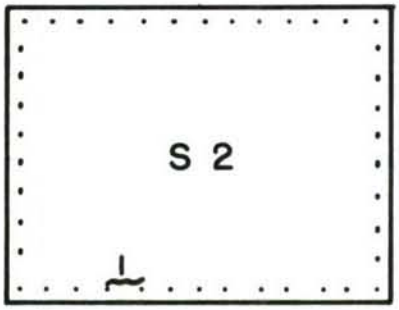

HEAT AND SOUND SIMULTANEOUSLY

TEST TIME MIN.	CRACK NUMBER	CRACK LENGTH INCHES
30	1	0.03
60	1	0.75
90	1	1.75

TEST TIME MIN.	CRACK NUMBER	CRACK LENGTH INCHES
90	1	1.50
—	—	—
—	—	—

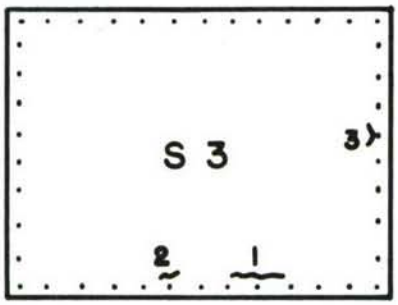

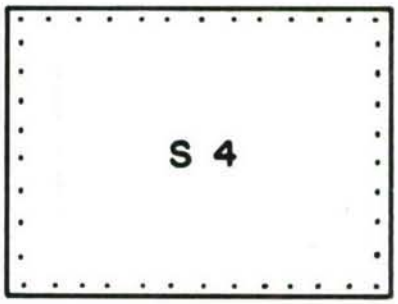

HEAT AND SOUND ALTERNATELY

TEST TIME MIN.	CRACK NUMBER	CRACK LENGTH INCHES
200	1	3.0
200	2	0.75
200	3	0.10

TEST TIME MIN.	CRACK NUMBER	CRACK LENGTH INCHES
NO FAILURES TEST STOPPED AFTER 330 MIN. TEST TIME		

TABLE 8

FREQUENCY STUDIES ON CURVED PANEL WITH 96" RADIUS

m^n	1	2	3	4	5	
1	346	471	778	1225	1795	Clamped-Theory
	231	385	696	1128	1746	Experimental
	165	273	557	960	1478	Simply Supported Theory
2	440	590	900	1347	1917	Clamped-Theory
	436	561	861	1283	1815	Experimental
	323	407	677	1077	1594	Simply Supported Theory
3	628	794	1104	1548	2117	Clamped-Theory
	636	793	1077	1492	2025	Experimental
	496	611	876	1272	1788	Simply Supported Theory
4	909	1085	1393	1832	2397	Clamped-Theory
	899	1093	1371	1775	2297	Experimental
	741	882	1149	1544	2059	Simply Supported Theory
5	1278	1458	1765	2199	2759	Clamped-Theory
	1245	1441	1728	2125	--	Experimental
	1069	1224	1498	1893	2407	Simply Supported Theory

D. Discussion of Results

1. Non-Dimensional Frequency Charts

The frequency analysis for isotropic curved panels with no coupled mode terms (equation (30)) has been programmed in Fortran language for solution on the IBM 7094. The equations are non-dimensionalized in terms of three independent variables, A, φ, and t, and the dependent variable which is non-dimensional frequency.

Based upon information related to practical aircraft structure, a range of the aforementioned variables was selected as follows:

$$0 \leq b/a = \varphi \leq 3.14$$

$$20 \leq \ell/h = t \leq 1000$$

$$0.5 \leq b/\ell = A \leq 2.0$$

Values, including the limits, of each of the above parameters were selected and frequency was calculated for all combinations for both simply supported and clamped edges.

For particular values of aspect ratio, A, non-dimensional frequency is plotted for six modes and six values of φ for variation of length-to-thickness ratio. Figures 31 to 35 are for simply supported edges and Figures 36 to 40 give clamped edge frequencies.

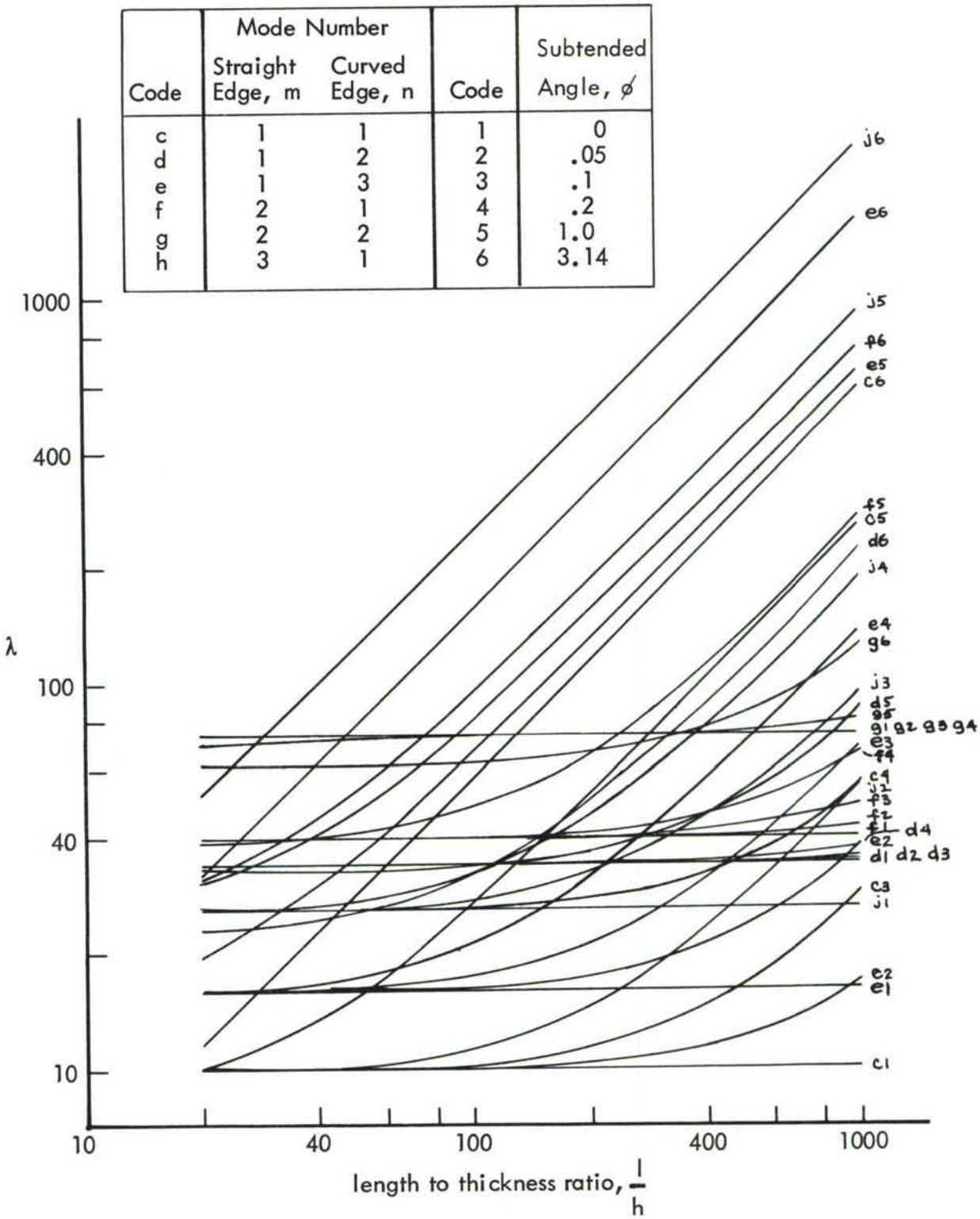

Code	Mode Number Straight Edge, m	Mode Number Curved Edge, n	Code	Subtended Angle, ϕ
c	1	1	1	0
d	1	2	2	.05
e	1	3	3	.1
f	2	1	4	.2
g	2	2	5	1.0
h	3	1	6	3.14

FIGURE 31. NON-DIMENSIONAL FREQUENCY SOLUTIONS SIMPLY-SUPPORTED EDGES, A = 0.50

Code	Mode Number Straight Edge, m	Mode Number Curved Edge, n	Code	Subtended Angle, ϕ
c	1	1	1	0
d	1	2	2	.05
e	1	3	3	.1
f	2	1	4	.2
g	2	2	5	1.0
h	3	1	6	3.14

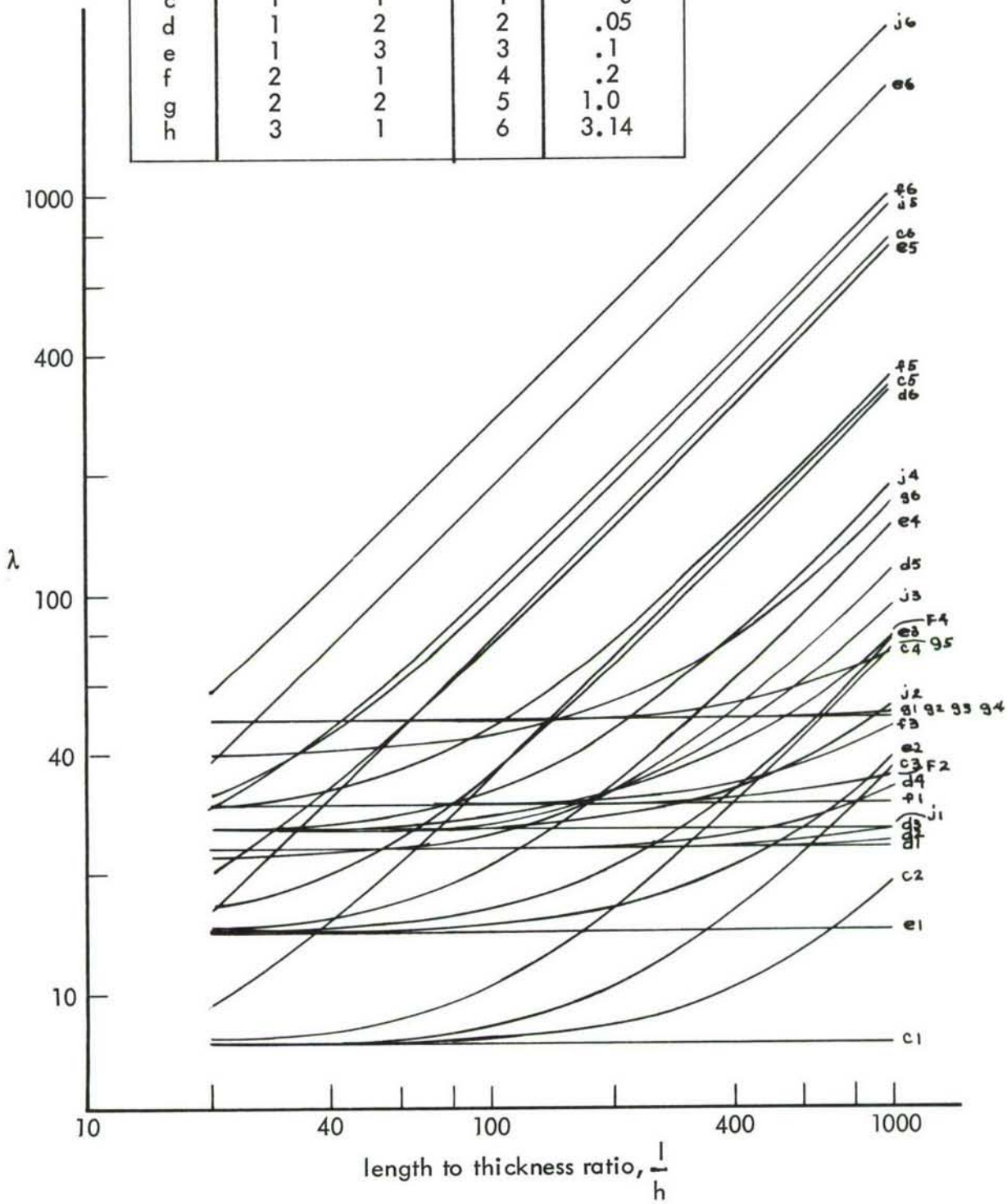

FIGURE 32. NON-DIMENSIONAL FREQUENCY SOLUTIONS SIMPLY-SUPPORTED EDGES, A = 0.67

Code	Mode Number Straight Edge, m	Mode Number Curved Edge, n	Code	Subtended Angle, ø
c	1	1	1	0
d	1	2	2	.05
e	1	3	3	.1
f	2	1	4	.2
g	2	2	5	1.0
h	3	1	6	3.14

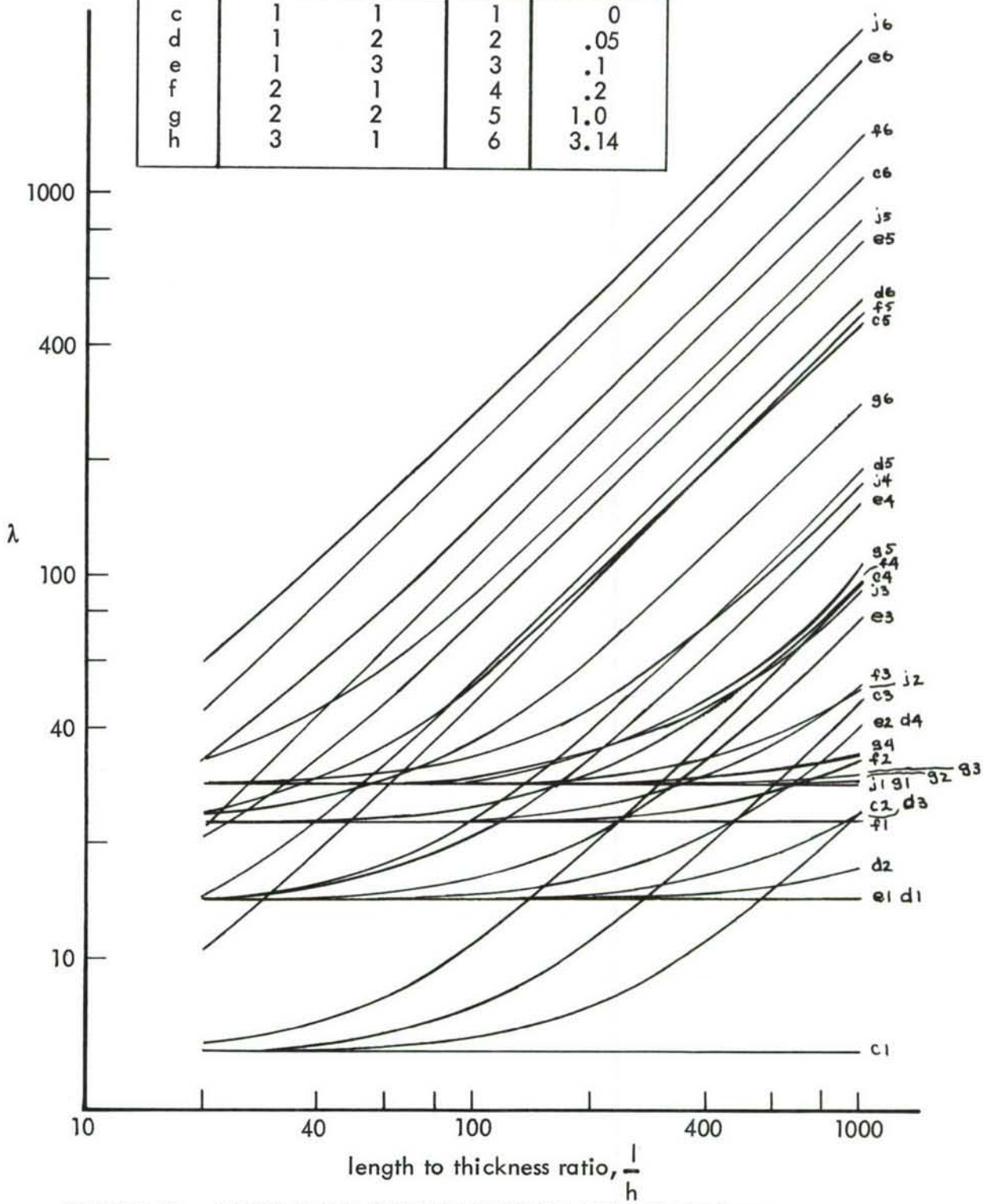

FIGURE 33. NON-DIMENSIONAL FREQUENCY SOLUTIONS SIMPLY-SUPPORTED EDGES, A = 1.00

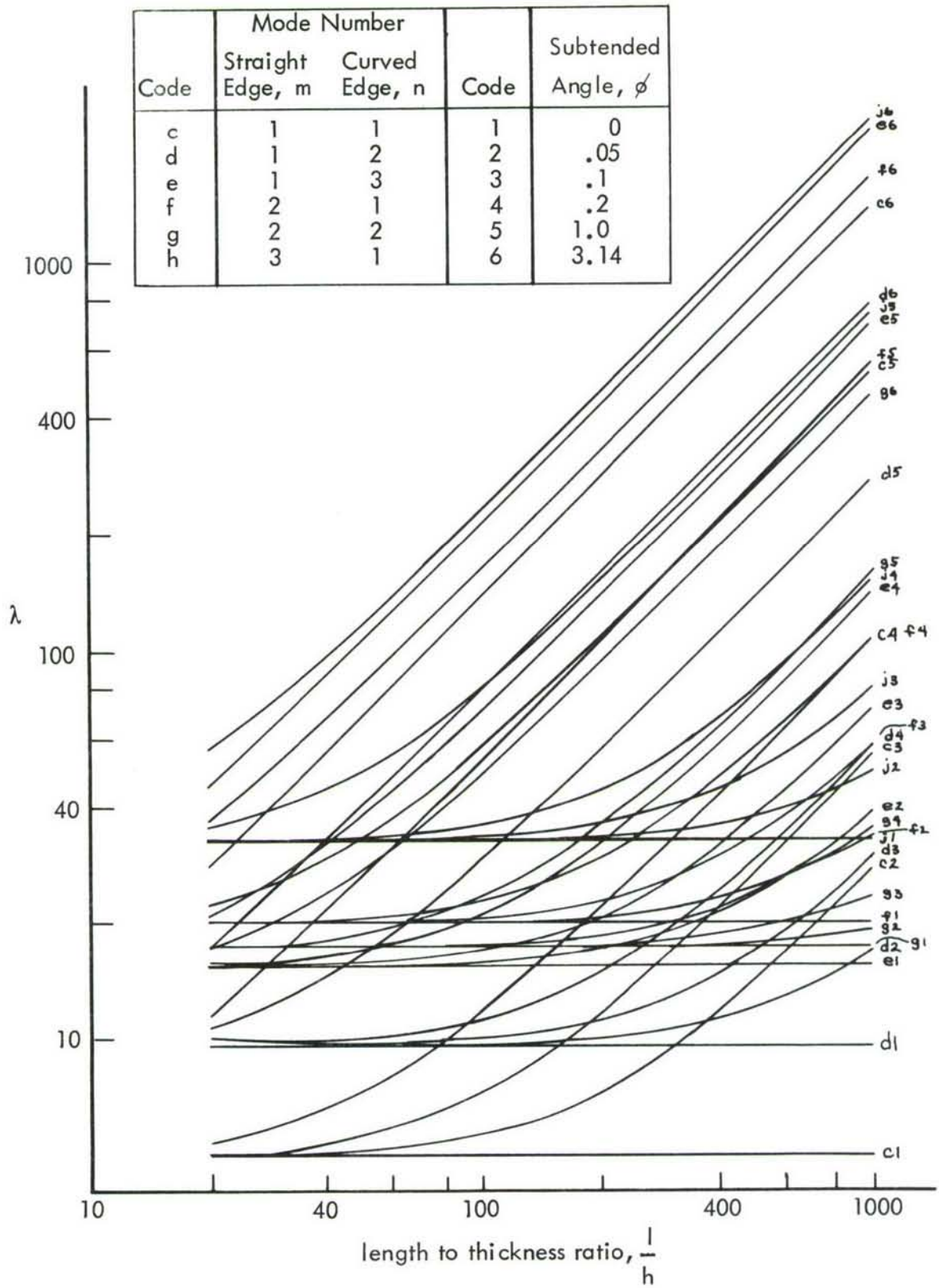

Code	Mode Number Straight Edge, m	Mode Number Curved Edge, n	Code	Subtended Angle, ø
c	1	1	1	0
d	1	2	2	.05
e	1	3	3	.1
f	2	1	4	.2
g	2	2	5	1.0
h	3	1	6	3.14

FIGURE 34. NON-DIMENSIONAL FREQUENCY SOLUTIONS SIMPLY-SUPPORTED EDGES, A = 1.50

Code	Mode Number Straight Edge, m	Mode Number Curved Edge, n	Code	Subtended Angle, ϕ
c	1	1	1	0
d	1	2	2	.05
e	1	3	3	.1
f	2	1	4	.2
g	2	2	5	1.0
h	3	1	6	3.14

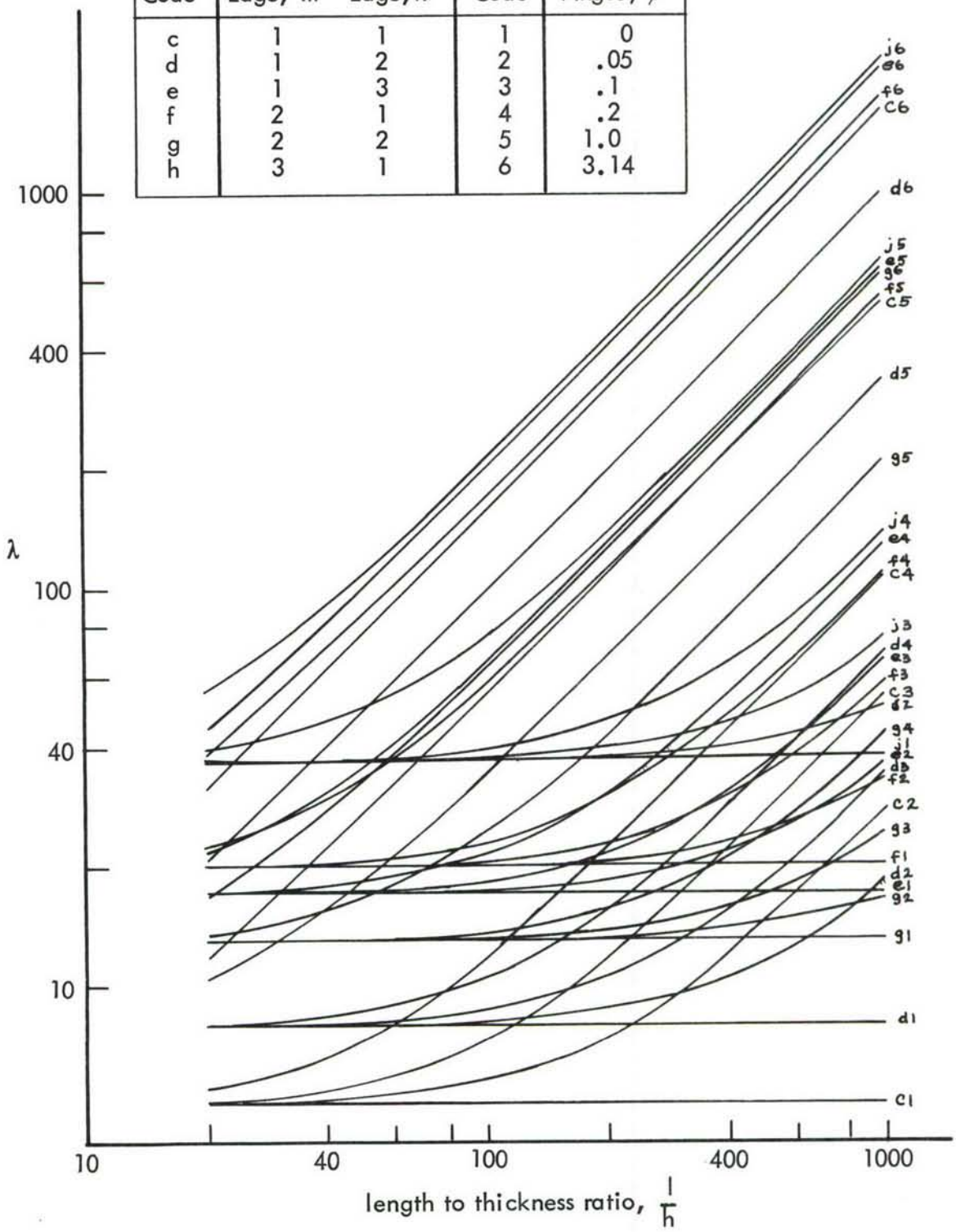

FIGURE 35. NON-DIMENSIONAL FREQUENCY SOLUTIONS SIMPLY-SUPPORTED EDGES, A = 2.00

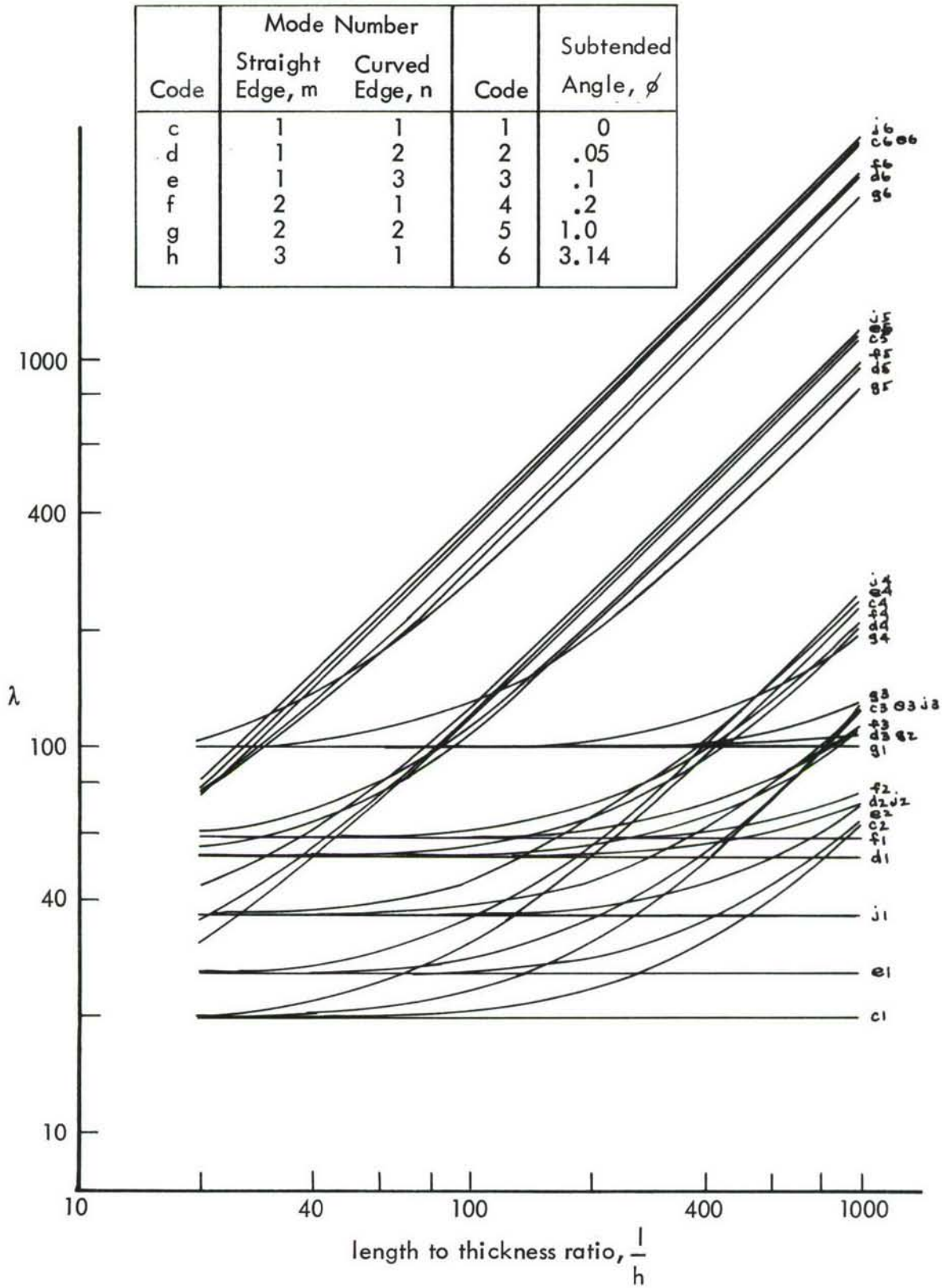

FIGURE 36. NON-DIMENSIONAL FREQUENCY SOLUTIONS
CLAMPED EDGES, A = 0.50

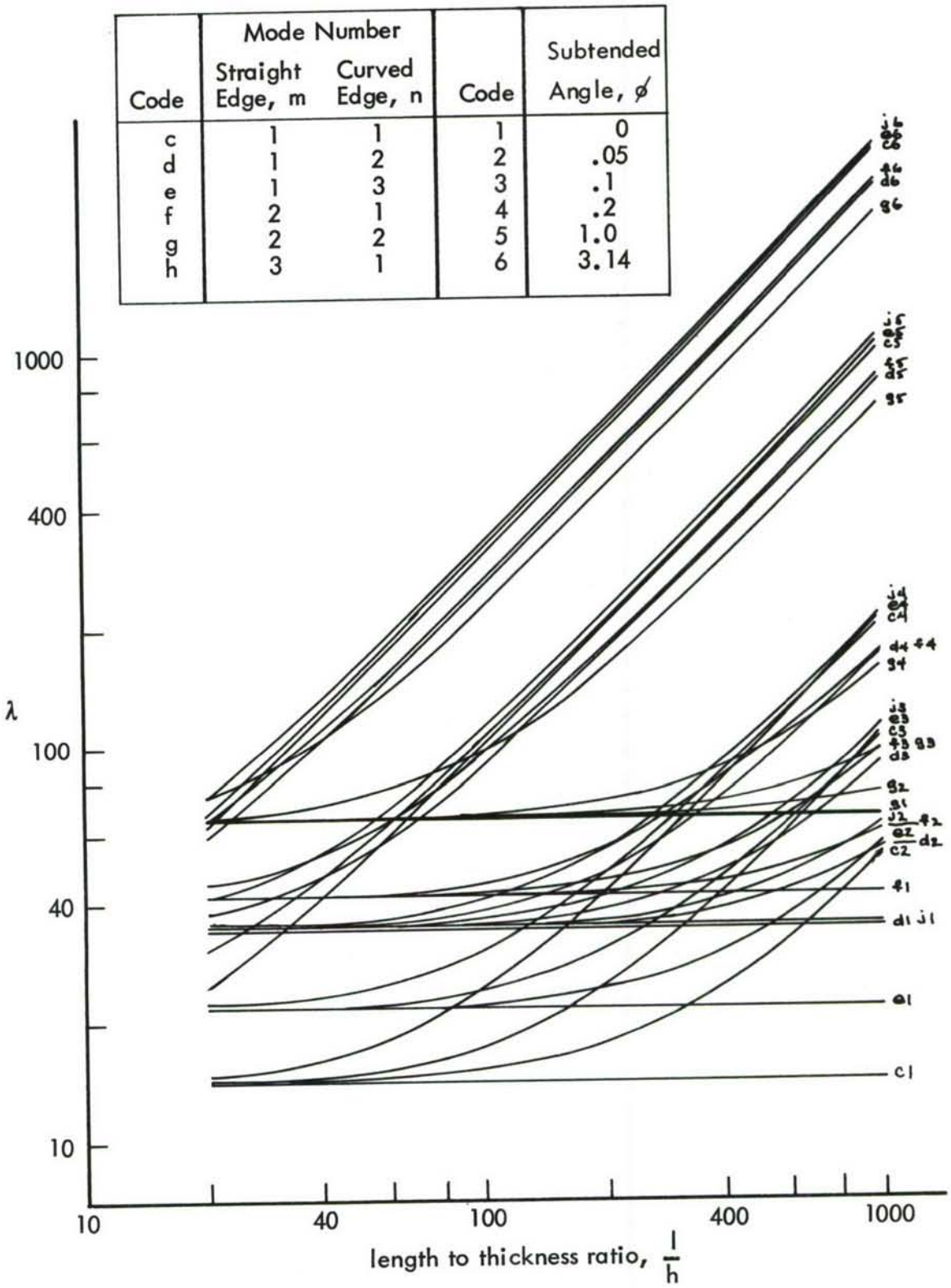

Code	Mode Number Straight Edge, m	Mode Number Curved Edge, n	Code	Subtended Angle, ø
c	1	1	1	0
d	1	2	2	.05
e	1	3	3	.1
f	2	1	4	.2
g	2	2	5	1.0
h	3	1	6	3.14

FIGURE 37. NON-DIMENSIONAL FREQUENCY SOLUTIONS CLAMPED EDGES, A = 0.67

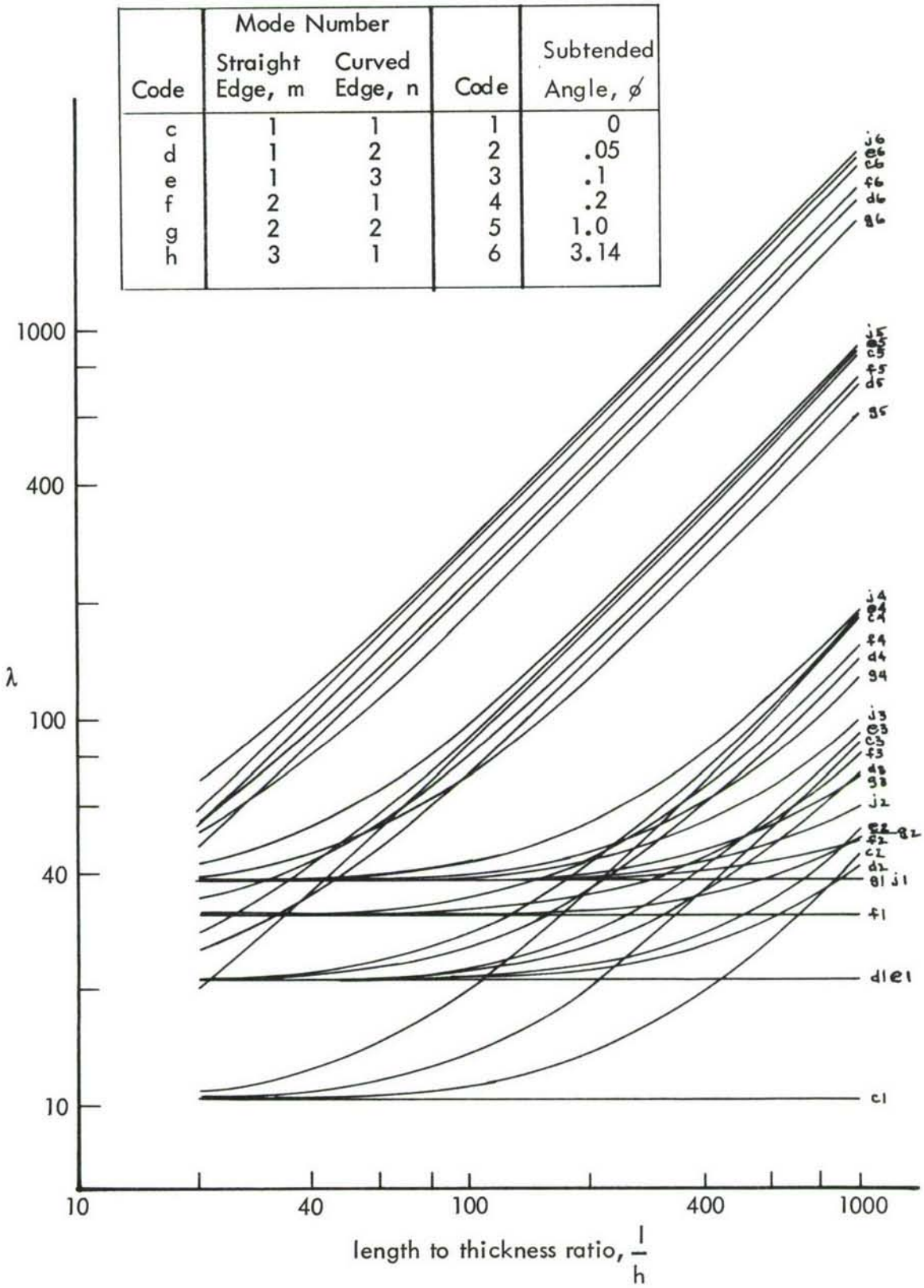

Code	Mode Number Straight Edge, m	Mode Number Curved Edge, n	Code	Subtended Angle, ϕ
c	1	1	1	0
d	1	2	2	.05
e	1	3	3	.1
f	2	1	4	.2
g	2	2	5	1.0
h	3	1	6	3.14

FIGURE 38. NON-DIMENSIONAL FREQUENCY SOLUTIONS CLAMPED EDGES, A = 1.00

Code	Mode Number Straight Edge, m	Mode Number Curved Edge, n	Code	Subtended Angle, ø
c	1	1	1	0
d	1	2	2	.05
e	1	3	3	.1
f	2	1	4	.2
g	2	2	5	1.0
h	3	1	6	3.14

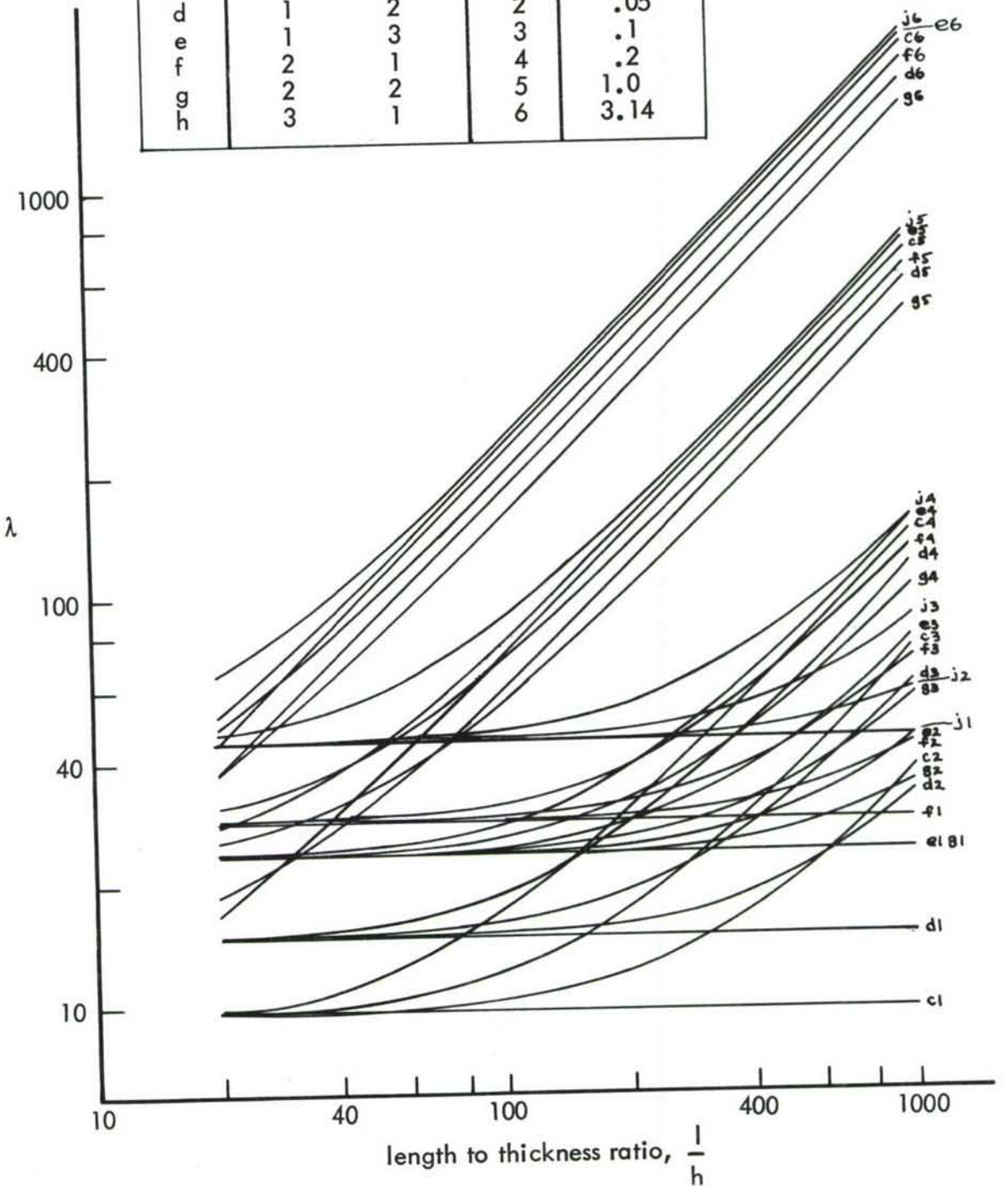

FIGURE 39. NON-DIMENSIONAL FREQUENCY SOLUTIONS CLAMPED EDGES, A = 1.50

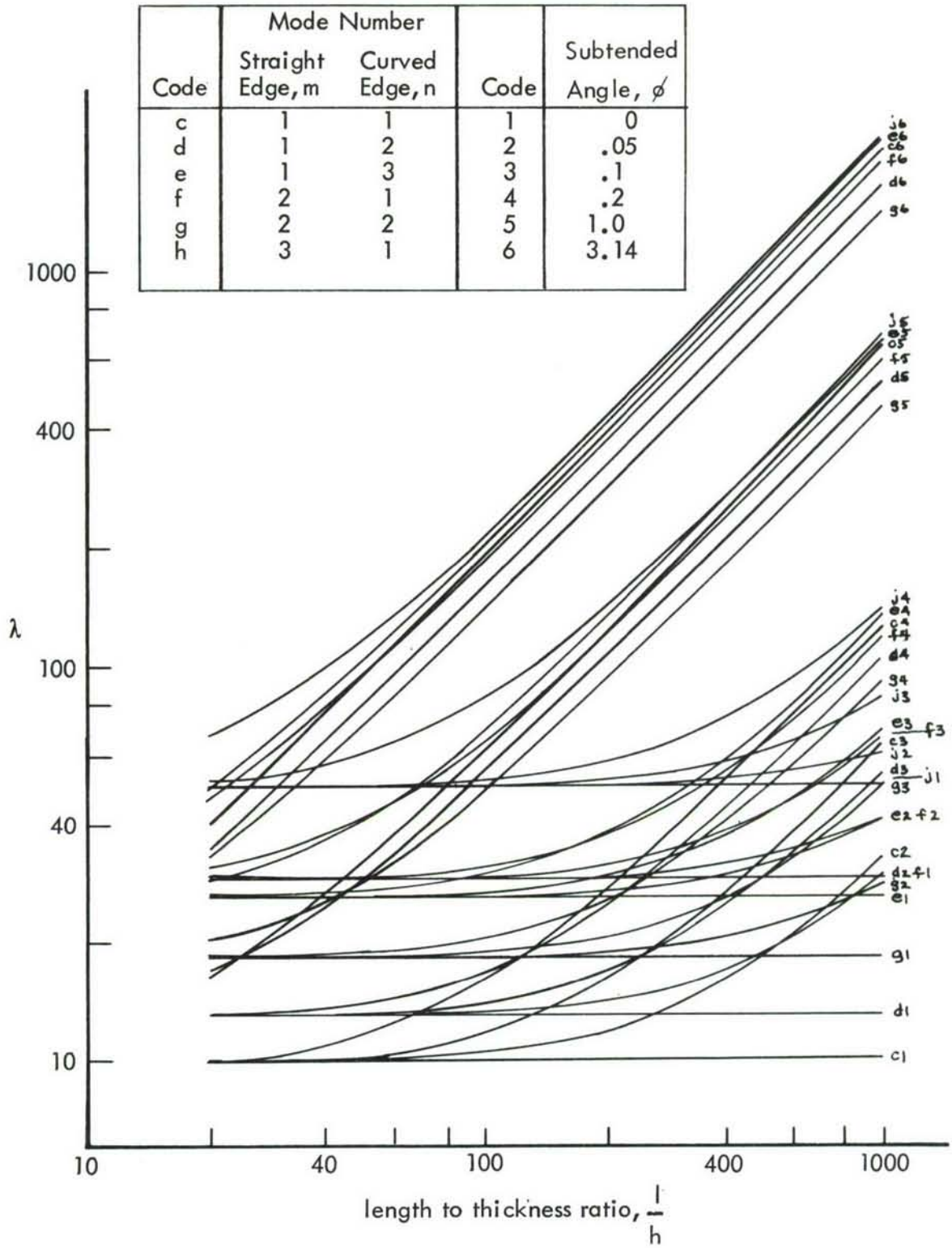

Code	Mode Number Straight Edge, m	Mode Number Curved Edge, n	Code	Subtended Angle, ϕ
c	1	1	1	0
d	1	2	2	.05
e	1	3	3	.1
f	2	1	4	.2
g	2	2	5	1.0
h	3	1	6	3.14

FIGURE 40. NON-DIMENSIONAL FREQUENCY SOLUTIONS
CLAMPED EDGES, A = 2.00

Once non-dimensional frequency is found then actual frequency can be determined from the nomogram (Figure 41).

For example, calculate the natural frequencies of a clamped, curved panel having the following dimensions:

radius, a = 100"
arc length, b = 10"
length, ℓ = 20"
thickness, h = 0.05"

The non-dimensional ratios are:

$$A = 0.5$$
$$\varphi = 0.1$$
$$t = 400$$

Table 9 shows values of λ for the different combinations of mode number. These values were taken from Figure 36 for $A = 0.5$. Frequency converted through the use of the nomogram is also displayed in Table 9.

TABLE 9

NATURAL FREQUENCIES FOR EXAMPLE PROBLEM

m	n	λ	f
1	1	51	300
1	2	65	382
1	3	101	594
2	1	54	318
2	2	71	418
3	1	61	359

2. Experimental

a. Ambient Temperature Tests.

- Mode Shapes. Some of the modes could not be excited. From Figure 8 it can be seen that the (4,2), (4,4), and (5,4) modes were unresponsive. Also, the (5,5) mode was unresponsive for the 0.032-inch flat panel as shown in Figure 9. Figure 10 shows that seven modes, (2,1), (2,3), (2,4), (4,4), (4,5), (5,3), and (5,4) did not readily respond. The lack of response is attributed to high damping and low excitation.

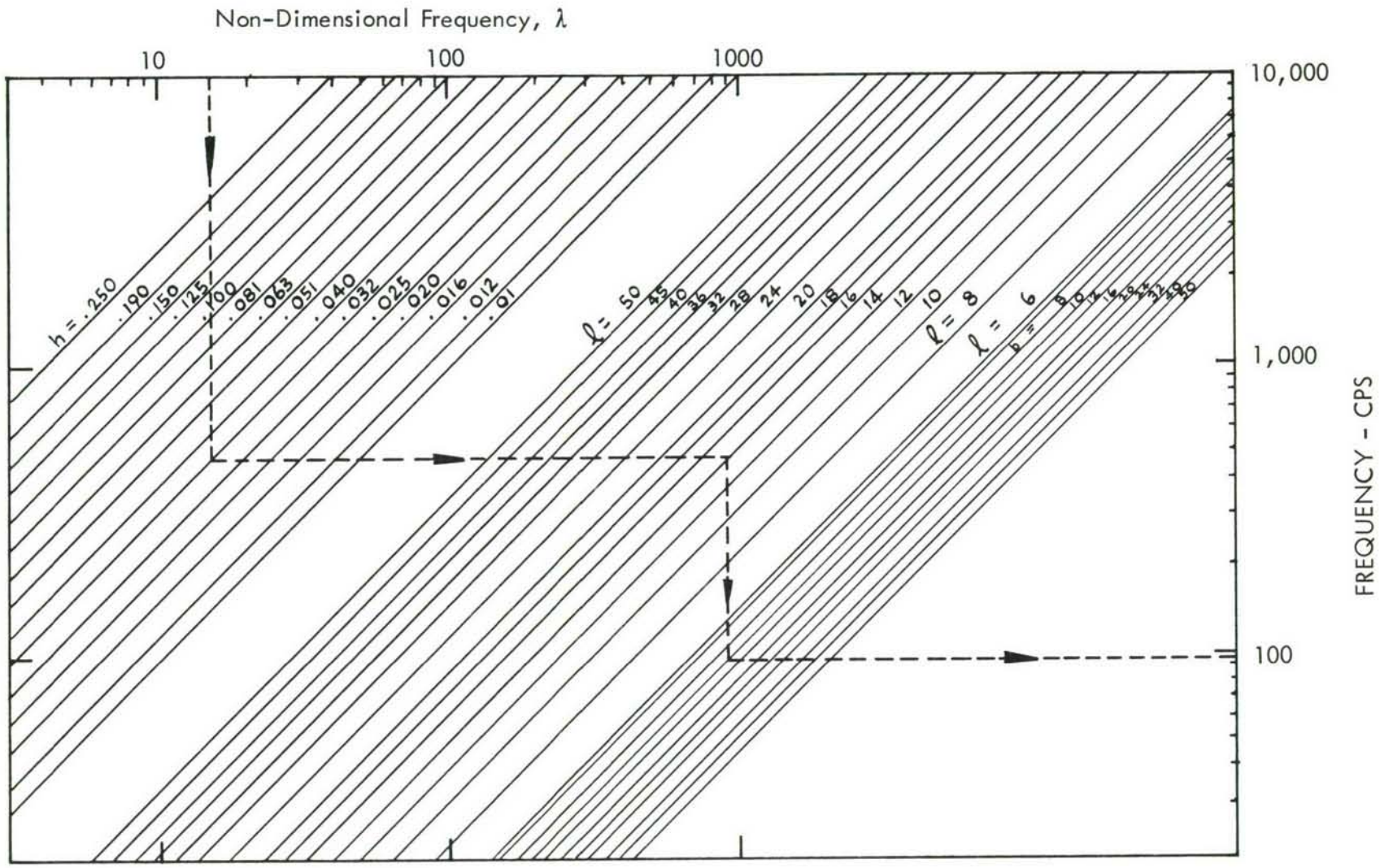

FIGURE 41. NOMOGRAM FOR CONVERTING NON-DIMENSIONAL FREQUENCY TO ACTUAL FREQUENCY

Cross-over effects, (1,2) mode having lower frequency than the (1,1) mode, were observed for each of the curved panels with 0.032-inch thickness.

- Frequency Sweeps. Strain activity above the first mode of response was negligible for all specimen configurations except the panel with the 48-inch radius. It showed some activity at 665 cps which is the (1,3) mode. The strain associated with this higher mode was approximately 30 percent of the strain at the fundamental frequency.

  Unlike the mode shape studies, cross-over effects were not observed during the frequency sweeps, Figure 12 through 14. Out-of-phase speakers were required to excite the (1,2) mode during the mode shape studies. Therefore, it is possible that the acoustical excitation and test specimen did not have the required phase relationship to excite the (1,2) mode when the sinusoidal frequency sweeps were made.

  Significant frequencies determined from the mode shape studies did not compare with those determined from the frequency sweeps. This lack of correlation is attributed to dissimilar edge fixities and ambient temperatures.

  Sub-harmonics of the type described by Rucker in Reference 12 were not observed at any time.

- Broad-Band Excitation. Strain spectra resulting from broad-band acoustical excitation, Figures 15 through 18, had the same general shape as the sinusoidal frequency sweeps in the vicinity of the (1,1) mode, but were more active at the higher frequencies. This activity in the higher modes was considered insignificant relative to fatigue damage because, with the exception being the 72" radius, the higher mode strain magnitudes were less than 30 percent of the strain response of the (1,1) mode.

  Cross-over effects were observed when the curved panels were exposed to broad-band excitation. Evidence of this effect is present in Figures 16 through 18 where, in each case, a small crinkle in the response curve precedes the maximum response peak. This crinkle is indicative of the (1,2) mode response.

- Fatigue Tests. It can be seen from Figure 21 that curvature had a pronounced effect on fatigue resistance with the degree depending on the radius of curvature. The test specimens with a 96-inch radius of curvature showed only a slight advantage over the flat test specimens. The test specimens with the 72-inch radius and the 48-inch radius demonstrated considerably more fatigue resistance than the flat test specimens. At a spectrum level of 139 db, the average cycles-to-failure advantage of the test specimens having radii of curvature of 96 inches, 72 inches, and 48 inches over the flat test specimen was determined from Figure 20 to be 1.2, 1.7, and 5 times respectively.

  The slopes of the fatigue curves, Figure 20, for the test specimens having radii of infinity, 96, and 72 inches were the same for practical purposes. The flatter slope for the test specimen with the 48-inch radius can be attributed to data scatter.

  The $\overline{\varepsilon}$ - N curves of Figure 21 show that tests specimen fatigue resistance increases inversely as the radius of curvature.

  Cross-plots of rms versus 1/R, R being the radius of curvature in feet, and 1/R versus mean cycles-to-failure are shown in Figures 42 and 43. The curves of

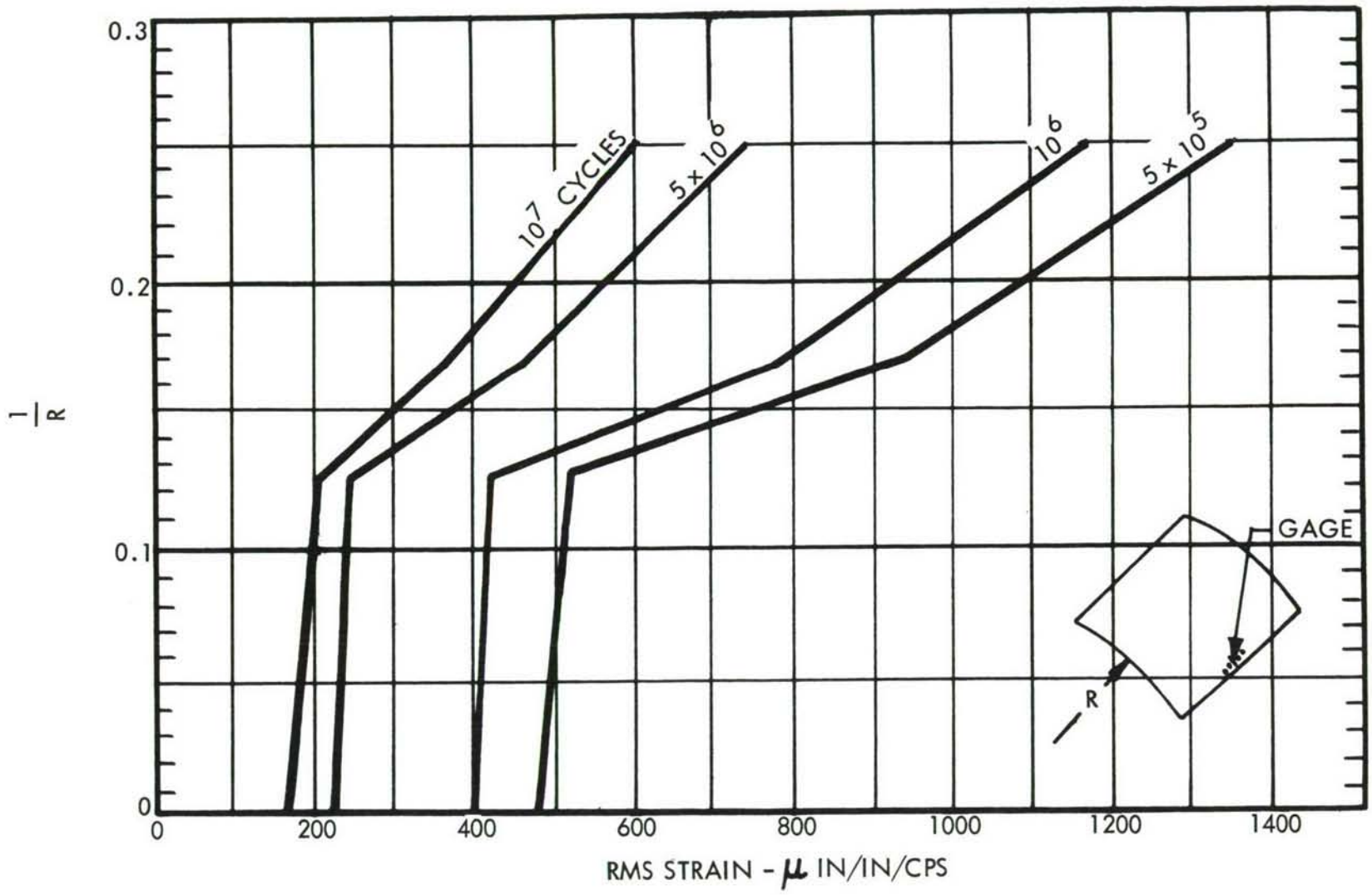

FIGURE 42. 1/R VERSUS RMS STRAIN

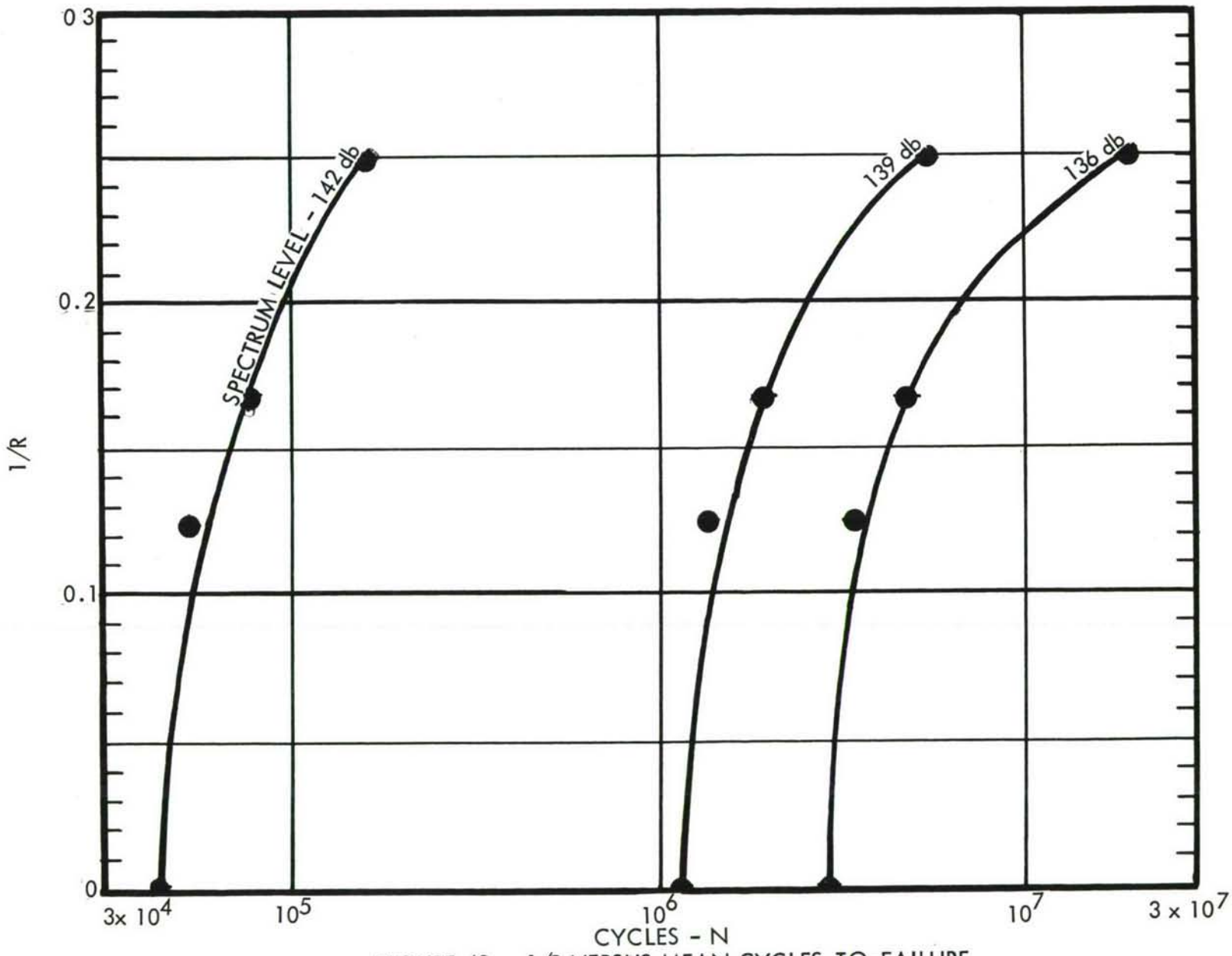

FIGURE 43. 1/R VERSUS MEAN CYCLES-TO-FAILURE

Figure 43, fatigue life of the test specimens as a function of curvature, clearly show that the most significant increase in fatigue life is the increase of radius from 72 inches to 48 inches. This does not agree with the conclusions drawn from discrete frequency tests of curved panels reported in Reference 13. A possible explanation of the difference in results of Reference 13 and this investigation is the nature of the failures experienced in each case. In Reference 13, it was stated that the flat panels failed near the bolt heads whereas the curved panels generally failed along the long side near the edge of the supporting frame. In this investigation, the nature of failure for both the flat panels and the curved panels was the same. Fatigue cracks formed in every case along the fastener row as shown in Figure 44. The supporting frame had rounded edges to prevent cracks from forming there.

The experimentally determined probability distribution of strain peaks for each panel configuration as shown in Figure 22 lies very close to the Rayleigh distribution line for peak-to-rms ratios up to three. The probability distribution of strain peaks will deviate appreciably from the Rayleigh distribution if the response is nonlinear and multiple-modal. Therefore, data plotted on Figure 22 show that the response of each test specimen configuration was essentially unimodal and linear.

- Strain Measurements. Response of the test specimens to the acoustical excitation was determined through the use of electrical strain gages attached to the specimen at points of high strain. The strain magnitudes thus measured can only be used qualitatively because the placement and orientation of a strain gage permits sensing the strain only at one small area and only in the direction in which the gage is sensitive. Only if the gage is placed where failure ultimately occurs and if the gage direction is the principal strain direction for the dominant mode at this point is the measured strain magnitude quantitatively meaningful. Therefore, strain magnitudes shown in this report are nominal values only.

b. Elevated Temperature Tests.

- Frequency Sweeps. Sinusoidal frequency sweeps for the titanium test specimens at ambient and elevated temperatures, Figure 27 and 28, show negligible response above the (1,1) mode. The frequency of the (1,1) mode at ambient temperature was 140 cps whereas the frequency of this mode shifted downward to 95 cps at 450° F. Also, the strain magnitude at 450° F was 60 percent greater than the strain response at ambient temperatures. It is believed that the heated titanium panel strain response was strongly influenced by the first thermal buckling mode. This mode is characterized by a general bowing of the panel in one direction. When heat was applied, the titanium panels were observed to have a buckling pattern similar to that of the first thermal buckling mode.

  Frequency sweeps for the stainless steel panels were similar to those for titanium. At ambient temperature there was negligible activity above the (1,1) mode, Figure 29, which occurred at 130 cps. At 450° F the maximum response appeared at 265 cps as shown in Figure 29. The strain at this frequency was two times greater than the maximum strain response at ambient temperature. There was some response at 385 cps but it was considered insignificant relative to its contribution to fatigue damage.

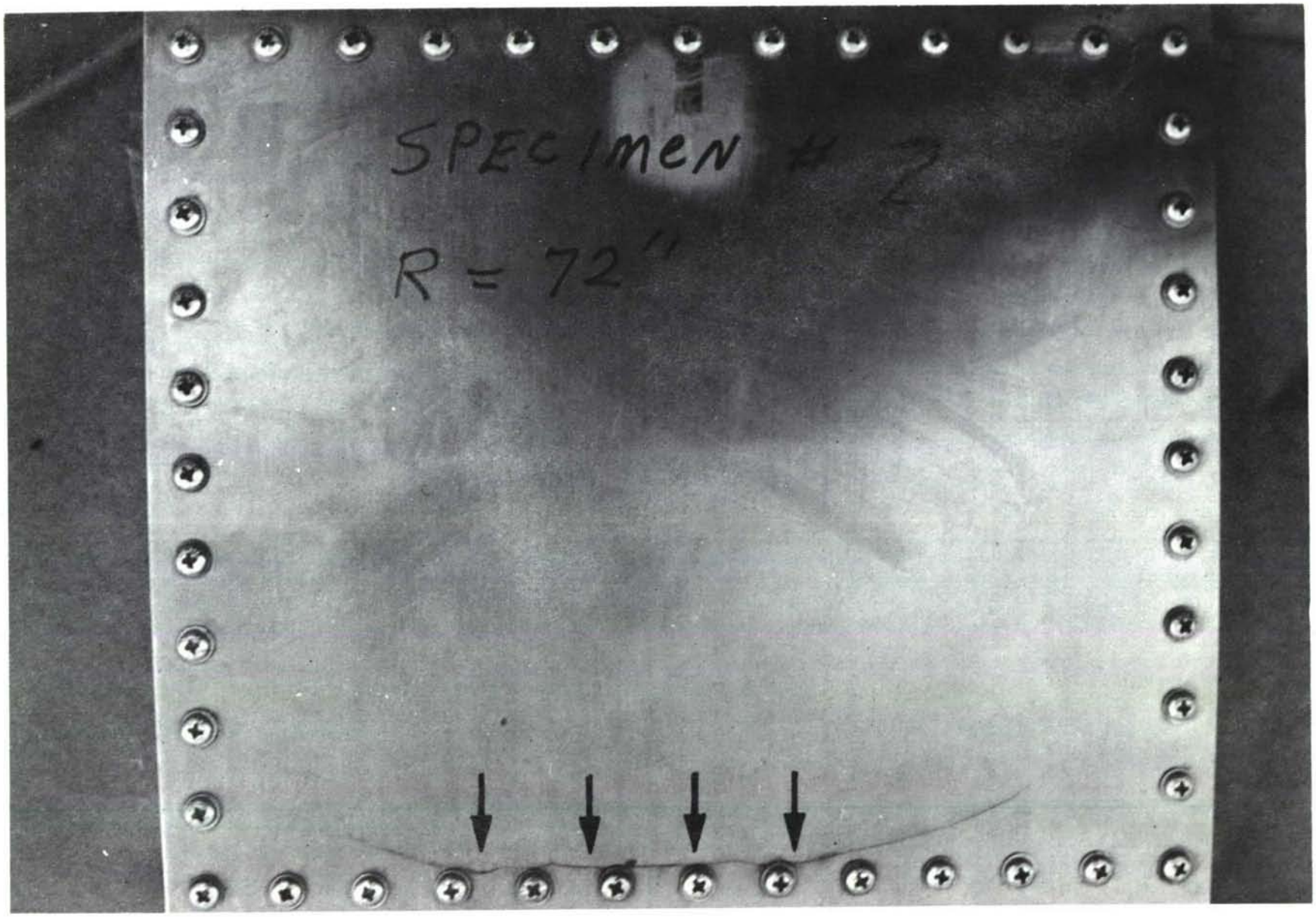

FIGURE 44. TYPICAL FATIGUE CRACK FOR CURVED TEST SPECIMENS

The elevated temperature response of the stainless steel test specimen was not the same mode as that of the titanium. The maximum response frequency shifted upward from 130 cps to 265 cps. This upward shift in frequency was probably caused by second-mode thermal buckling rather than first-mode buckling.

- Temperatures. Considerable difficulty was encountered in obtaining uniform temperature over the surface of the test specimens. This was due primarily to three things: The area of the test specimens was small, the mounting frame was a heat sink in spite of the thin phenolic spacer placed between the frame and the test specimen, and the air flow in the test section, necessary in the sound generation, caused uneven convection heat losses over the test specimen surface. A one-inch width of heat-resistant black paint was applied to the edges of the test specimen to increase the temperature around the periphery where the heat loss was the greatest.

- Fatigue Tests. A comparison of the time to first failure for the specimens exposed to heat and sound simultaneously to that of the specimens exposed to heat and sound alternately revealed that the former was considerably more severe than the latter. This is true for both titanium and stainless steel.

  Based upon the data contained in Tables 6 and 7, the fatigue life of the titanium specimens exposed to heat and sound simultaneously was about one-eighth the fatigue life of the specimens exposed to heat and sound alternately. The ratio for the stainless steel specimens was about one-fourth.

  Crack propagation was also greater for the combined environmental condition.

  Figures 45a and 45b are typical strain spectra for the titanium and stainless steel specimens during the combined heat and acoustical excitation tests. Figure 45a shows the titanium panel responded in the first thermal buckling mode with very little activity at higher frequencies. The stainless steel panel experienced its maximum response at the second thermal buckling mode, Figure 45b, with insignificant response at other frequencies.

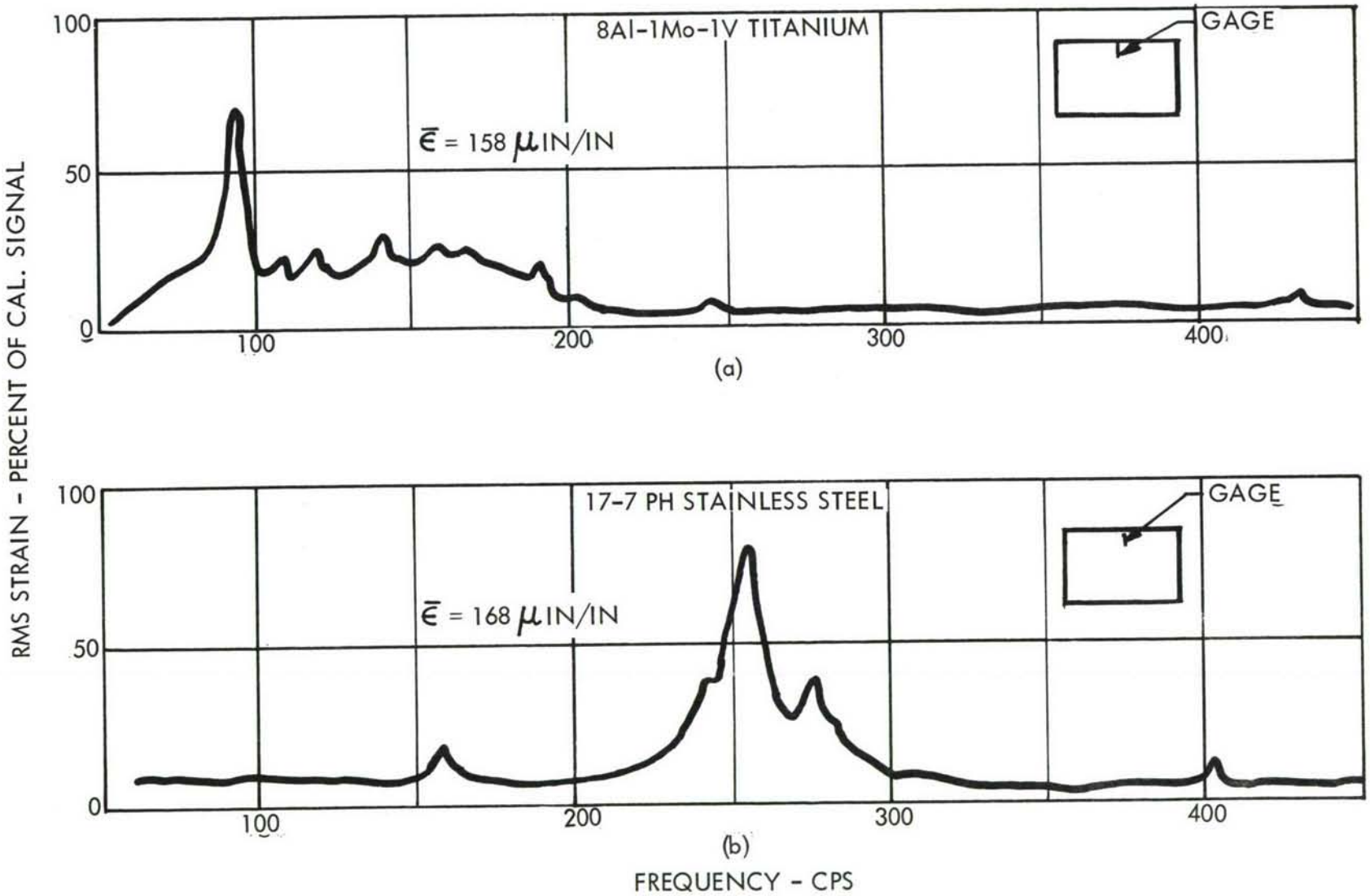

FIGURE 45. BROAD-BAND NOISE EXCITATION, 162 DB - 450° F

III

COMPLEX SPECIMEN INVESTIGATION

A. Theoretical and Analytical

1. Introduction

Honeycomb sandwich structure has been used in the construction of aerospace vehicles for the past decade. This type of construction is generally used because environmental problems will not permit usage of conventional aircraft structure due to weight penalties. Honeycomb sandwich is the best structure, weight-wise, for high intensity noise environments because of its resistance to acoustical fatigue.

Most honeycomb sandwich structures are in the elemental form of panels. These panels may be either flat or curved. In general, the design of these panels has evolved from that of a uniform thickness to the more efficient, lighter weight structure typical of that shown in Figure 49. This design consists of a core bonded to two thin facing sheets, which may be of different thickness. The core gradually tapers to zero thickness near the edge and the inner skin stresses are transmitted to the edge through a bonded doubler and "wet-layup" fiberglass edge member.

In previous vibration analyses of honeycomb sandwich panels, uniform thickness of the core and face sheets has been assumed (References 14 and 15). In these analyses, the boundaries are simply supported.

The analysis to be presented in this section includes the effects of the tapered edge on natural modes of vibration. The theoretical model chosen to represent the edge is shown in Figure 46. This model is compared with the actual edge geometry. Although the taper is reduced to a step-discontinuity in thickness, it is felt that this effect on the theory will be negligible.

The frequency analysis which follows will be based upon a Rayleigh-Ritz energy analysis. Mode shapes are assumed which satisfy the geometric boundary conditions.

2. Honeycomb Panel Frequency Analysis

The strain energy density of an elastic body is

$$U_o = \frac{1}{2} \lfloor \sigma_i \rfloor \{\epsilon_i\} \tag{1}$$

In the notation introduced by Love (Reference 2), $\sigma_1 = \sigma_x$, $\sigma_2 = \sigma_y$, $\sigma_3 = \sigma_z$, $\sigma_4 = \sigma_{yz}$, $\sigma_5 = \sigma_{zx}$, $\sigma_6 = \sigma_{xy}$. The notation is identical for strains.

The Hooke's law relationship between stress and strain is then expressed as

$$\lfloor \sigma_i \rfloor = \lfloor \epsilon_i \rfloor \quad C_{ij} \tag{2}$$

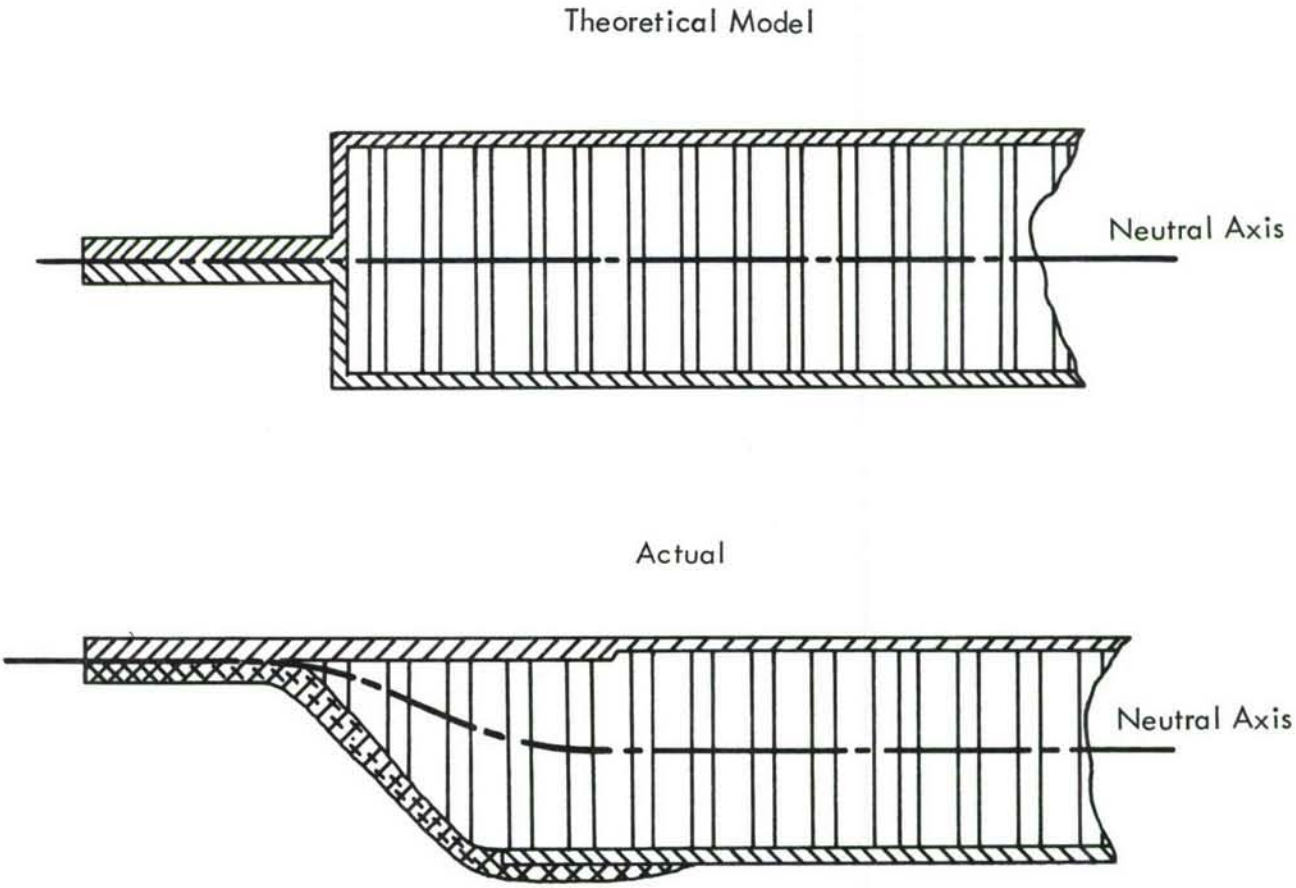

FIGURE 46. THEORETICAL AND ACTUAL MODELS OF TAPERED EDGE GEOMETRY

For an orthotropic linear elastic solid the elastic coefficient matrix, $[C_{ij}]$, is symmetric and has the following form:

$$C_{ij} = \begin{bmatrix} C_{11} & C_{12} & C_{13} & 0 & 0 & 0 \\ C_{21} & C_{22} & C_{23} & 0 & 0 & 0 \\ C_{31} & C_{32} & C_{33} & 0 & 0 & 0 \\ 0 & 0 & 0 & C_{44} & 0 & 0 \\ 0 & 0 & 0 & 0 & C_{55} & 0 \\ 0 & 0 & 0 & 0 & 0 & C_{66} \end{bmatrix} \qquad \begin{matrix} C_{12} = C_{21} \\ C_{13} = C_{31} \\ C_{23} = C_{32} \end{matrix} \tag{3}$$

Using these relationships, the strain energy density becomes

$$U_o = \frac{1}{2} \lfloor \epsilon_i \rfloor \left[C_{ij} \right] \{\epsilon_j\} \tag{4}$$

In expressing strain in terms of displacement, the core will be treated as a thick shell; however, in order to reduce the complexity of the analysis the facing sheets will be considered as thin membranes.

In considering the facings as membranes, it is implicitly assumed that no transverse shear strain occurs (i.e., $\varphi = \psi = 0$). To make this assumption since there are minor transverse shear stresses, the elastic coefficients for transverse shear, C_{44} and C_{55}, are assumed to be infinite. Because of this assumption, C_{44} and C_{55} must be omitted from the elastic coefficient matrix. This assumption is not detrimental to the analysis since facing sheets are usually an order of magnitude thinner than the core.

Assuming no variation of displacement through the thickness the exact strain displacement relationships for thick circular cylindrical shells are

$$\{\epsilon_i\} = \left[\begin{array}{c|c|c|c|c} \frac{\partial}{\partial x} & 0 & 0 & z\frac{\partial}{\partial x} & 0 \\ \hline 0 & \frac{R}{R+z}\frac{\partial}{\partial y} & \frac{1}{R+z} & 0 & \frac{zR}{R+z}\frac{\partial}{\partial y} \\ \hline 0 & 0 & 0 & 0 & 0 \\ \hline 0 & -\frac{1}{R+z} & \frac{R}{R+z}\frac{\partial}{\partial y} & 0 & \frac{R}{R+z} \\ \hline 0 & 0 & \frac{\partial}{\partial x} & 0 & 0 \\ \hline \frac{R}{R+z}\frac{\partial}{\partial y} & \frac{\partial}{\partial x} & 0 & \frac{zR}{R+z}\frac{\partial}{\partial y} & z\frac{\partial}{\partial x} \end{array}\right] \left\{\begin{array}{c} u \\ \hline v \\ \hline w \\ \hline \psi \\ \hline \varphi \end{array}\right\} = \left[A_{ik}\right] \{u_k\} \tag{5}$$

where $u_1 = u$, $u_2 = v$, etc.

The displacements and rotations are defined in Figure 47, which shows the coordinate system. The configuration of the panel is shown in Figure 48. Referring to this figure,

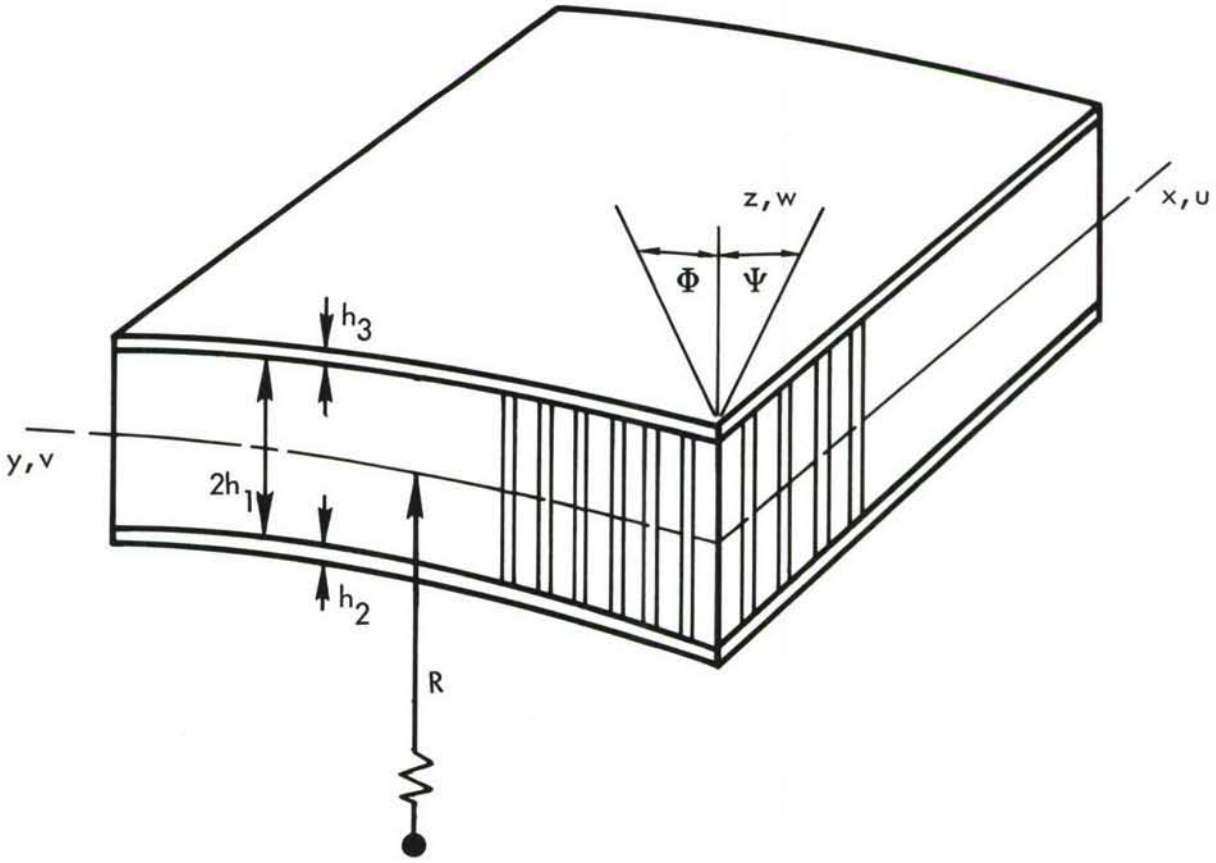

FIGURE 47. HONEYCOMB SANDWICH PANEL COORDINATE SYSTEM

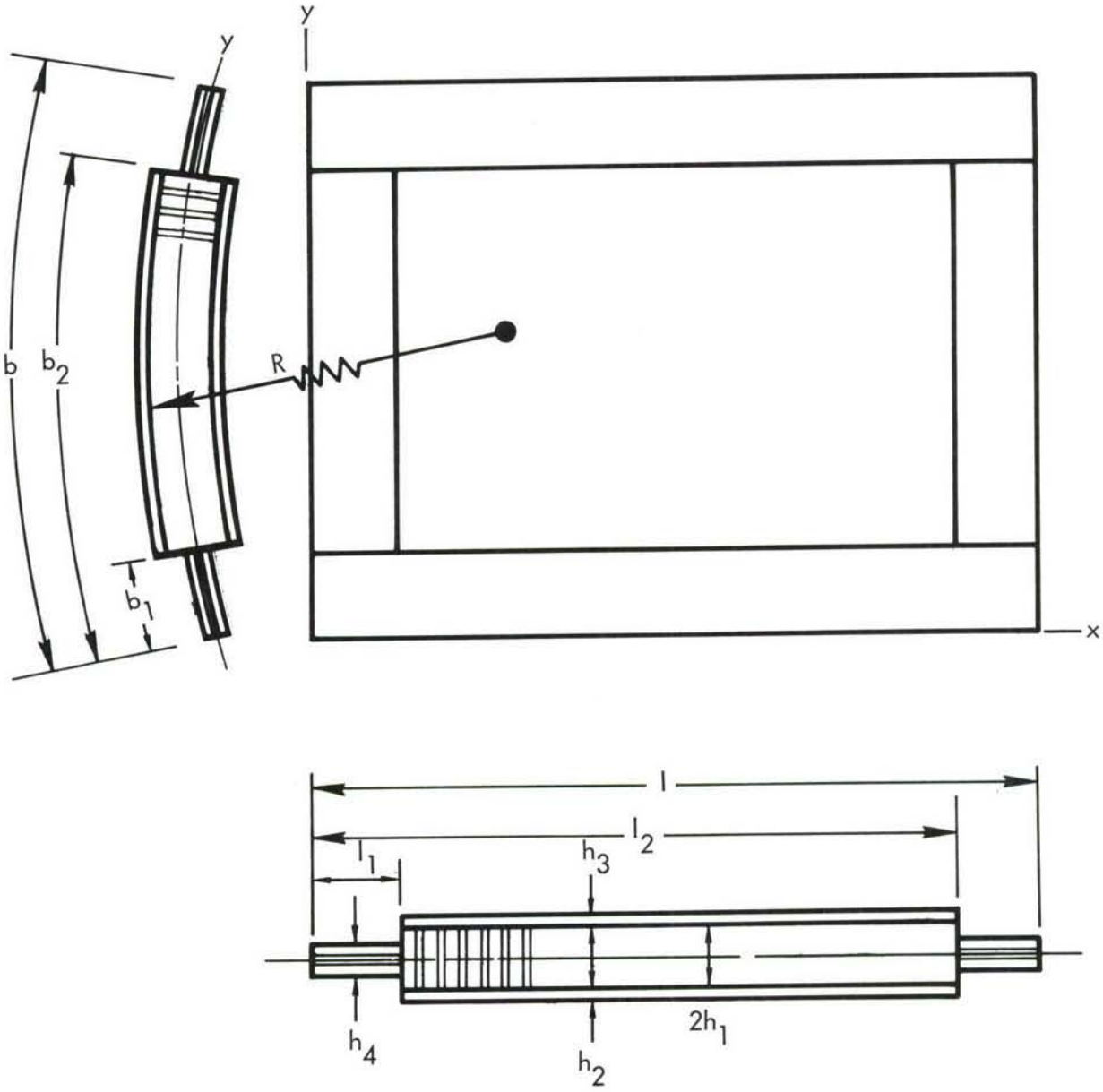

FIGURE 48. HONEYCOMB SANDWICH PANEL CONFIGURATION AND DIMENSIONS

the panel is assumed to be composed of four individual layers of material. These are: layer 1 - the core, layer 2 - the inner skin (inner refers to layer closest to origin of curvature), layer 3 – the outer skin, and layer 4 - the edge attachment or "tabs." In the energy analysis a presubscript, r, will be incorporated to indicate the layer. This notation will be necessary for the strain energy, the elastic coefficient matrix and the strains.

The boundary conditions for simply supported edges are assumed to be

$$@\, x = 0 \;\&\; x = \ell: \quad w = 0,\ \frac{\partial \psi}{\partial x} = 0,\ \frac{\partial u}{\partial x} = 0$$

$$@\, y = 0 \;\&\; y = b: \quad w = 0,\ \frac{\partial \varphi}{\partial y} = 0,\ \frac{\partial v}{\partial y} = 0$$

The constraint on w is a pure geometric constraint; however, the conditions on u, v, ψ, and φ are necessary to satisfy both compatibility relationships and geometric relationships. The $\partial u/\partial x = 0$ is a constraint on the direct strain in the x direction and satisfies the moment requirements at the edge.

Sinusoidal mode functions are chosen as the assumed mode shapes. They are

$$\left.\begin{aligned}
u &= \sum_{m=1} \sum_{n=1} U_{mn} \cos\beta_m x \sin\gamma_n y \\
v &= \sum_{m=1} \sum_{n-1} V_{mn} \sin\beta_m x \cos\gamma_n y \\
w &= \sum_{m=1} \sum_{n=1} W_{mn} \sin\beta_m x \sin\gamma_n y \\
\psi &= \sum_{m=1} \sum_{n=1} \Psi_{mn} \cos\beta_m x \sin\gamma_n y \\
\varphi &= \sum_{m=1} \sum_{n=1} \Phi_{mn} \sin\beta_m x \cos\gamma_n y
\end{aligned}\right\} \tag{6}$$

In matrix form,

$$\{u_k\} = [B]\,\{q^k_{mn}\} \tag{7}$$

$$B = \begin{bmatrix} \lfloor X'_m Y_n \rfloor & 0 & 0 & 0 & 0 \\ 0 & \lfloor X_m Y'_n \rfloor & 0 & 0 & 0 \\ 0 & 0 & \lfloor X_m Y_n \rfloor & 0 & 0 \\ 0 & 0 & 0 & \lfloor X'_m Y_n \rfloor & 0 \\ 0 & 0 & 0 & 0 & \lfloor X_m Y'_n \rfloor \end{bmatrix} \qquad \text{(7 cont'd)}$$

The case of clamped boundaries will also be considered, provided the tapered edge is not present. The clamped edge boundary conditions are

$$\begin{aligned} w(0,y) &= w(\ell,y) = w(x,0) = w(x,b) = 0 \\ w_x(0,y) &= w_x(\ell,y) = w_y(x,0) = w_y(x,b) = 0 \\ v(x,0) &= v(x,b) = 0 \\ \varphi(x,0) &= \varphi(x,b) = 0 \\ \psi(0,y) &= \psi(\ell,y) = 0 \\ u(0,y) &= u(\ell,y) = 0 \end{aligned}$$

The clamped edge beam functions will be used. These functions are defined in Section II.A.2, equation (6). The assumed mode functions satisfy the notation utilized in (7).

Now, substitution of (7) into (5) gives

$$\{\varepsilon_i\} = [A]\ [B]\ \{q^k_{mn}\} = [D]\ \{q^k_{mn}\} \tag{8}$$

and substitution of (8) into (4) results in

$${}_rU_o = \frac{1}{2} \lfloor q^\ell_{pq} \rfloor\ [{}_rD]^T\ [{}_rC][{}_rD]\ \{q^k_{mn}\} = \frac{1}{2} \lfloor q^\ell_{pq} \rfloor\ [{}_rE]\{q^k_{mn}\} \tag{9}$$

where the presubscript r denotes the layer.

The strain energy of the vibrating plate is

$$U = \sum_{r=1}^{4} \int_{vol.} {}_rU_o\, dV \tag{10}$$

Integration is first performed with respect to z and then with respect to x and y.

The integration with respect to z is represented as follows:

$$U = \frac{1}{2}\int_{\ell_1}^{\ell_2}\int_{b_1}^{b_2}\left[\int_{-h_1}^{h_1} \lfloor q_{pq}^{\ell}\rfloor [{}_1E]\{q_{mn}^{k}\}dz + \int_{-h_1-h_2}^{-h_1} \lfloor q_{pq}^{\ell}\rfloor [{}_2E]\{q_{mn}^{k}\}dz\right.$$

$$\left. + \int_{h_1}^{h_1+h_3} \lfloor q_{pq}^{\ell}\rfloor [{}_3E]\{q_{mn}^{k}\}dz\right] dydx$$

$$+ \frac{1}{2}\int_0^{\ell}\int_0^{b_1}\int_{-h_4/2}^{h_4/2} \lfloor q_{pq}^{\ell}\rfloor [{}_4E]\{q_{mn}^{k}\}dzdydx + \frac{1}{2}\int_0^{\ell}\int_{b_2}^{b}\int_{-h_4/2}^{h_4/2} \lfloor q_{pq}^{\ell}\rfloor [{}_4E]\{q_{mn}^{k}\}dzdydx$$

$$+ \frac{1}{2}\int_0^{\ell_1}\int_{b_1}^{b_2}\int_{-h_4/2}^{h_4/2} \lfloor q_{pq}^{\ell}\rfloor [{}_4E]\{q_{mn}^{k}\}dzdydx + \frac{1}{2}\int_{\ell_2}^{\ell}\int_{b_1}^{b_2}\int_{-h_4/2}^{h_4/2} \lfloor q_{pq}^{\ell}\rfloor [{}_4E]\{q_{mn}^{k}\}dzdydx$$

$$= U_1 + U_2 + U_3 + U_4 + U_5 \tag{11}$$

The first three terms, symbolized by U_1, contain the strain energy of the core and face sheets, whereas the last four terms represent the energy of the tabs.

The types of integration with respect to z which appear in ${}_1E$ are

$$\left.\begin{aligned}
\int_{-h_1}^{h_1} \frac{dz}{R+z} &= \ln\left(\frac{R+h_1}{R-h_1}\right) \approx \frac{2h_1}{R}\left(1 + \frac{h_1^2}{3R^2}\right) = \frac{2h_1}{R} H_1 \\
\int_{-h_1}^{h_1} \frac{zdz}{R+z} &= 2h_1 - R\ln\left(\frac{R+h_1}{R-h_1}\right) \approx -\frac{2}{3}\frac{h_1^3}{R^2} \\
\int_{-h_1}^{h_1} \frac{z^2dz}{R+z} &= -2Rh_1 - R^2\ln\left(\frac{R+h_1}{R-h_1}\right) \approx \frac{2}{3}\frac{h_1^3}{R} \\
\int_{-h_1}^{h_1} \frac{dz}{(R+z)^2} &= -\frac{1}{R+h_1} - \frac{1}{R-h_1} \approx \frac{2h_1}{R^2}\left(1 - \frac{h_1^2}{R^2}\right) = \frac{2h_1}{R^2} H_3
\end{aligned}\right\} \tag{12}$$

$$\left.\begin{aligned}
\int_{-h_1}^{h_1} \frac{zdz}{(R+z)^2} &= \frac{R}{R+h_1} - \frac{R}{R-h_1} - \ln\left(\frac{R+h_1}{R-h_1}\right) \approx -\frac{4}{3}\frac{h_1^3}{R^3} \\
\int_{-h_1}^{h_1} \frac{z^2dz}{(R+z)^2} &= 2h_1 - \frac{R^2}{R+h_1} + \frac{R^2}{R-h_1} - 2R\ln\left(\frac{R+h_1}{R-h_1}\right) \approx \frac{2}{3}\frac{h_1^3}{R^2}
\end{aligned}\right\} \quad \text{(12 cont'd)}$$

The required integrations in ${}_2E$ are

$$\left.\begin{aligned}
\int_{-h_1-h_2}^{-h_1} \frac{dz}{R+z} &\approx \frac{h_2}{R}\left(1 - \frac{2h_1+h_2}{2R} + \frac{3h_1^2+3h_1h_2+h_2^2}{3R^2}\right) = \frac{h_2}{R}H_5 \\
\int_{-h_1-h_2}^{-h_1} \frac{dz}{(R+z)^2} &\approx \frac{h_2}{R^2}\left(1 - \frac{2h_1+h_2}{R} + \frac{3h_1^2+3h_1h_2+h_2^2}{R^2}\right) = \frac{h_2}{R^2}H_6
\end{aligned}\right\} \quad (13)$$

Integrations appearing in ${}_3E$ are

$$\left.\begin{aligned}
\int_{h_1}^{h_1+h_3} \frac{dz}{R+z} &\approx \frac{h_3}{R}\left(1 - \frac{2h_1+h_3}{2R} + \frac{3h_1^2+3h_1h_3+h_3^2}{3R^2}\right) = \frac{h_3}{R}H_8 \\
\int_{h_1}^{h_1+h_3} \frac{dz}{R+z} &\approx \frac{h_3}{R^2}\left(1 - \frac{2h_1+h_3}{R} + \frac{3h_1^2+3h_1h_3+h_3^2}{R^2}\right) = \frac{h_3}{R^2}H_{10}
\end{aligned}\right\} \quad (14)$$

The indicated integrations over the surface of the sandwich portion are now required. The following integrals must be evaluated to write the E matrices.

$$
\left.
\begin{aligned}
\int_{\ell_1}^{\ell_2} X_p X_m dx &= (1-\delta_{pm})\left[\frac{\sin(\beta_p-\beta_m)\ell_2}{2(\beta_p-\beta_m)} - \frac{\sin(\beta_p+\beta_m)\ell_2}{2(\beta_p+\beta_m)} + \right. \\
&\quad \left. - \frac{\sin(\beta_p-\beta_m)\ell_1}{2(\beta_p-\beta_m)} + \frac{\sin(\beta_p+\beta_m)\ell_1}{2(\beta_p+\beta_m)}\right] + \\
&\quad + \delta_{pm}\left[\frac{\ell_2-\ell_1}{2} - \frac{\sin\beta_m\ell_2\cos\beta_m\ell_2}{2\beta_m} + \frac{\sin\beta_m\ell_1\cos\beta_m\ell_1}{2\beta_m}\right] \\
&= {}_1M_{pm} \\
\int_{\ell_1}^{\ell_2} X'_p X'_m dx &= (1-\delta_{pm})\left[\frac{\sin(\beta_p-\beta_m)\ell_2}{2(\beta_p-\beta_m)} + \frac{\sin(\beta_p+\beta_m)\ell_2}{2(\beta_p+\beta_m)} + \right. \\
&\quad \left. - \frac{\sin(\beta_p-\beta_m)\ell_1}{2(\beta_p-\beta_m)} - \frac{\sin(\beta_p+\beta_m)\ell_1}{2(\beta_p+\beta_m)}\right] + \\
&\quad + \delta_{pm}\beta_m^2\left[\frac{\ell_2-\ell_1}{2} + \frac{\sin\beta_m\ell_2\cos\beta_m\ell_2}{2\beta_m} - \frac{\sin\beta_m\ell_1\cos\beta_m\ell_1}{2\beta_m}\right] \\
&= {}_2M_{pm} \\
\int_{\ell_1}^{\ell_2} X''_p X_m dx &= -\beta_p^2\, {}_1M_{pm} \\
\int_{\ell_1}^{\ell_2} X_p X''_m dx &= -\beta_m^2\, {}_1M_{pm} \\
\int_{\ell_1}^{\ell_2} X''_p X''_m dx &= \beta_p^2\beta_m^2\, {}_1M_{pm}
\end{aligned}
\right\} (15)
$$

Similarly,

$$
\left.
\begin{aligned}
\int_{b_1}^{b_2} Y_q Y_n dy &= (1 - \delta_{qn}) \left[\frac{\sin(\gamma_q - \gamma_n)b_2}{2(\gamma_q - \gamma_n)} - \frac{\sin(\gamma_q + \gamma_n)b_2}{2(\gamma_q + \gamma_n)} + \right. \\
&\quad \left. - \frac{\sin(\gamma_q - \gamma_n)b_1}{2(\gamma_q - \gamma_n)} + \frac{\sin(\gamma_q + \gamma_n)b_1}{2(\gamma_q + \gamma_n)} \right] + \\
&\quad + \delta_{qn} \left[\frac{b_2 - b_1}{2} + \frac{\sin\gamma_n b_2 \cos\gamma_n b_2}{2\gamma_n} + \frac{\sin\gamma_n b_1 \cos\gamma_n b_1}{2\gamma_n} \right] \\
&= {}_1N_{qn} \\
\int_{b_1}^{b_2} Y'_q Y'_n dy &= (1 - \delta_{qn})\gamma_q\gamma_n \left[\frac{\sin(\gamma_q - \gamma_n)b_2}{2(\gamma_q - \gamma_n)} + \frac{\sin(\gamma_q + \gamma_n)b_2}{2(\gamma_q + \gamma_n)} + \right. \\
&\quad \left. - \frac{\sin(\gamma_q - \gamma_n)b_1}{2(\gamma_q - \gamma_n)} - \frac{\sin(\gamma_q + \gamma_n)b_1}{2(\gamma_q + \gamma_n)} \right] + \\
&\quad + \delta_{qn}\gamma_n^2 \left[\frac{b_2 - b_1}{2} + \frac{\sin\gamma_n b_2 \cos\gamma_n b_2}{2\gamma_n} - \frac{\sin\gamma_n b_1 \cos\gamma_n b_1}{2\gamma_n} \right] \\
&= {}_2N_{qn} \\
\int_{b_1}^{b_2} Y''_q Y_n dy &= -\gamma_q^2 \, {}_1N_{qn} \\
\int_{b_1}^{b_2} Y_q Y''_n dy &= -\gamma_n^2 \, {}_1N_{qn} \\
\int_{b_1}^{b_2} Y''_q Y''_n dy &= \gamma_q^2 \, {}_1N_{qn}
\end{aligned}
\right\} \quad (16)
$$

In the case where $b_1 = 0$, $b_2 = b$ and $\ell_1 = 0$, $\ell_2 = \ell$, the above integrals for simply-supported edges and similar integrals for clamped edges can be easily written. For the case of the constant thickness panel, the notation of (27) and (28) in Section II.A.2 should be used. This problem has been individually solved and a report is being prepared (Reference 16).

After summing the first three integrals in (11) and performing the integrations over the surface, the integral is represented as follows:

$$U_1 = \frac{1}{2}\int_{\ell_1}^{\ell_2}\int_{b_1}^{b_2} \lfloor q^{\ell}_{pq} \rfloor \left({}_1F + {}_2F + {}_3F\right)\{q^k_{mn}\}dydx = \lfloor q^{\ell}_{pq} \rfloor \left[{}_1K\right]\{q^k_{mn}\} \qquad (17)$$

where K is a generalized stiffness matrix.

The terms in the ${}_1K$ matrix are given in Appendix II.

Now, the edge numbers will be treated differently, since instead of being thick, as in the core, they can be considered thin. Therefore, the analysis for the "tabs" will follow that of the curved plate in Section II.A.2. The analysis is identical up to the point where integration over the surface is required.

Therefore, the strain energy of the edges, prior to integration over the surface, is of the form of equation (16), Section II.A.2. Integrating over the surface of the edges, using terminology of equation (16) Section II, gives

$$\left.\begin{aligned}
U_2 &= \frac{1}{2}\int_0^{\ell}\int_0^{b_1} \lfloor q^{\ell}_{pq} \rfloor \left[h_4[E] + \frac{h_4^3}{12}[F]\right]\{q^k_{mn}\}dydx = \lfloor q^{\ell}_{pq} \rfloor \left[{}_2K\right]\{q^k_{mn}\} \\
U_3 &= \frac{1}{2}\int_0^{\ell}\int_{b_2}^{b} \lfloor q^{\ell}_{pq} \rfloor \left[h_4[E] + \frac{h_4^3}{12}[F]\right]\{q^k_{mn}\}dydx = \lfloor q^{\ell}_{pq} \rfloor \left[{}_3K\right]\{q^k_{mn}\} \\
U_4 &= \frac{1}{2}\int_0^{\ell_1}\int_{b_1}^{b_2} \lfloor q^{\ell}_{pq} \rfloor \left[h_4[E] + \frac{h_4^3}{12}[F]\right]\{q^k_{mn}\}dydx = \lfloor q^{\ell}_{pq} \rfloor \left[{}_4K\right]\{q^k_{mn}\} \\
U_5 &= \frac{1}{2}\int_{\ell_2}^{\ell}\int_{b_1}^{b_2} \lfloor q^{\ell}_{pq} \rfloor \left[h_4[E] + \frac{h_4^3}{12}[F]\right]\{q^k_{mn}\}dydx = \lfloor q^{\ell}_{pq} \rfloor \left[{}_5K\right]\{q^k_{mn}\}
\end{aligned}\right\} \qquad (18)$$

The matrix of coefficients for the terms in ${}_2K$, ${}_3K$, ${}_4K$, and ${}_5K$ is listed in Appendix II. Integrations of the mode functions over the surface are identical to the terms in (15) and (16) except for a change in limits. Symbols used for the integrals are listed below.

Limits for X Integrations

Integral	ℓ_1 to ℓ_2	0 to ℓ_1	ℓ_2 to ℓ	0 to ℓ
$\int X_p X_m dx =$	${}_1M_{pm}$	${}_3M_{pm}$	${}_5M_{pm}$	${}_7M_{pm}$
$\int X'_p X'_m dx =$	${}_2M_{pm}$	${}_4M_{pm}$	${}_6M_{pm}$	${}_8M_{pm}$
$\int X''_p X_m dx =$	$-\beta_p^2\, {}_1M_{pm}$	$-\beta_p^2\, {}_3M_{pm}$	$-\beta_p^2\, {}_5M_{pm}$	$-\beta_p^2\, {}_7M_{pm}$
$\int X_p X''_m dx =$	$-\beta_m^2\, {}_1M_{pm}$	$-\beta_m^2\, {}_3M_{pm}$	$-\beta_m^2\, {}_5M_{pm}$	$-\beta_m^2\, {}_7M_{pm}$
$\int X''_p X''_m dx =$	$\beta_p^2 \beta_m^2\, {}_1M_{pm}$	$\beta_p^2 \beta_m^2\, {}_3M_{pm}$	$\beta_p^2 \beta_m^2\, {}_5M_{pm}$	$\beta_p^2 \beta_m^2\, {}_7M_{pm}$

Limits for Y Integrations

Integral	b_1 to b_2	0 to b_1	b_2 to b
$\int Y_q Y_n dy =$	${}_1N_{qn}$	${}_3N_{qn}$	${}_5N_{qn}$
$\int Y'_q Y'_n dy =$	${}_2N_{qn}$	${}_4N_{qn}$	${}_6N_{qn}$
$\int Y''_q Y_n dy =$	$-\beta_q^2\, {}_1N_{qn}$	$-\beta_q^2\, {}_3N_{qn}$	$-\beta_q^2\, {}_5N_{qn}$
$\int Y_q Y''_n dy =$	$-\beta_n^2\, N_{qn}$	$-\beta_n^2\, {}_3N_{qn}$	$-\beta_n^2\, {}_5N_{qn}$
$\int Y''_q Y''_n dy =$	$\beta_q^2 \beta_m^2\, {}_1N_{qn}$	$\beta_q^2 \beta_n^2\, {}_3N_{qn}$	$\beta_q^2 \beta_n^2\, {}_5N_{qn}$

For example, the integral $\int_0^{b_1} Y_q Y_n dy$ is of the same form as (16), except that in (16) b_2 is replaced by b_1 and b_1 is replaced by 0.

The integrals tabulated above could also be evaluated for clamped edges; however, the size of the task was prohibitive for this investigation. If the beam functions are used,

each of the above integrals would contain 16 terms to be evaluated at both the upper and lower limits.

The kinetic energy of an elastic multilayered shell is

$$T = \sum_{r} \int_{vol.} \left\{ \frac{1}{2} \rho_r (\dot{u}_r^2 + \dot{v}_r^2 + \dot{w}_r^2) \right\} dv \tag{19}$$

where r indicates the layer and the $\dot{u}_r$, $\dot{v}_r$, and $\dot{w}_r$ are total velocities of a point (x,y,z) in the shell. The total velocities, defined in terms of mid-plane velocity, are

$$\left.\begin{aligned} u_1 &= u + z\psi \;, & v_1 &= v + z\varphi \;, & w_1 &= w \\ u_2 &= u - h_1\psi \;, & v_2 &= v - h_1\varphi \;, & w_2 &= w \\ u_3 &= u + h_1\psi \;, & v_3 &= v + h_1\varphi \;, & w_3 &= w \\ u_4 &= u \;, & v_4 &= v \;, & w_4 &= w \end{aligned}\right\} \tag{20}$$

Upon introducing the actual limits of integration, (19) becomes

$$\begin{aligned} T = \frac{1}{2} \int_{\ell_1}^{\ell_2} \int_{b_1}^{b_2} \Big\{ \rho_1 \int_{-h_1}^{h_1} & (\dot{u}^2 + 2z\dot{u}\dot{\psi} + z^2\dot{\psi}^2 + \dot{v}^2 + 2z\dot{v}\dot{\varphi} + z^2\dot{\varphi}^2 + \dot{w}^2) dz + \\ + \rho_2 \int_{-(h_1+h_2)}^{-h_1} & (\dot{u}^2 - 2h_1\dot{u}\dot{\psi} + h_1^2\dot{\psi}^2 + \dot{v}^2 - 2h_1\dot{v}\dot{\varphi} + h_1^2\dot{\varphi}^2 + \dot{w}^2) dz + \\ + \rho_3 \int_{h_1}^{h_1+h_3} & (\dot{u}^2 + 2h_1\dot{u}\dot{\psi} + h_1^2\dot{\psi}^2 + \dot{v}^2 + 2h_1\dot{v}\dot{\varphi} + h_1^2\dot{\varphi}^2 + \dot{w}^2) dz \Big\} dydx + \\ + \frac{1}{2}\rho_4 \int_0^{\ell} \int_0^{b_1} \int_{-h_4}^{h_4} & (\dot{u}^2 + \dot{v}^2 + \dot{w}^2) dzdydx + \frac{1}{2}\rho_4 \int_0^{\ell} \int_{b_2}^{b} \int_{-h_4}^{h_4} (\dot{u}^2 + \dot{v}^2 + \dot{w}^2) dzdydx + \\ + \frac{1}{2}\rho_4 \int_0^{\ell_1} \int_{b_1}^{b_2} \int_{-h_4}^{h_4} & (\dot{u}^2 + \dot{v}^2 + \dot{w}^2) dzdydx + \frac{1}{2}\rho_4 \int_{\ell_2}^{\ell} \int_{b_1}^{b_2} \int_{-h_4}^{h_4} (\dot{u}^2 + \dot{v}^2 + \dot{w}^2) dzdydx \end{aligned} \tag{21}$$

Integrating through the thickness, introducing the assumed mode shapes, and integrating over the surface yields the kinetic energy in terms of generalized coordinates.

$$T = \sum_{i=1}^{5} \frac{1}{2} \lfloor q_{pq}^{\ell} \rfloor \, [{}_iM] \, \{q_{mn}^{k}\} \tag{22}$$

The ${}_iM$'s are associated with the different surface areas. ${}_1M$ denotes the generalized mass matrix for the honeycomb sandwich center sections and ${}_2M$ to ${}_5M$ are the generalized mass matrices of the edges. The terms in the M matrices appear in Appendix II.

It is of interest to note that in the honeycomb sandwich analysis the generalized mass matrix is not diagonal due to coupling between in-plane velocity and shear rotational velocity.

To obtain natural frequencies and mode shpaes, harmonic motion is assumed and Lagrange's equation for conservative systems is utilized. This step yields

$$\left[\left[\sum_{i=1}^{5} {}_iK \right] - \omega^2 \left[\sum_{i=1}^{5} {}_iM \right] \right] \{q_{mn}^{k}\} = 0 \tag{23}$$

This is the form of the eigenvalue problem.

In applying this analysis to the calculation of natural frequencies and mode shapes of typical structure, it is necessary to define the elastic coefficient matrices. For a honeycomb core, the elastic coefficients are

$${}_1C_{11} = {}_1C_{12} = {}_1C_{21} = {}_1C_{22} = 0$$

The assumption that $\partial w/\partial z = 0$ obviates the need of defining ${}_1C_{13}$, ${}_1C_{23}$, ${}_1C_{31}$, ${}_1C_{32}$, and ${}_1C_{33}$ since they do not appear in the analysis. In actuality $\partial w/\partial z = 0$ is based on the assumption that the core is inelastic through the thickness (the C's are infinite).

$$\left.\begin{aligned} {}_1C_{44} &= {}_1G_{yz} \\ {}_1C_{55} &= {}_1G_{xz} \\ {}_1C_{66} &= {}_1G_{xy} \end{aligned}\right\} \tag{24}$$

The facing sheets and tabs are normally constructed from isotropic materials. The elasticity coefficients are

$$\left.\begin{aligned} {}_2C_{11} &= \frac{E_2}{1-\upsilon_2^2} & {}_3C_{11} &= \frac{E_3}{1-\upsilon_3^2} & {}_4C_{11} &= \frac{E_4}{1-\upsilon_4^2} \\ {}_2C_{12} = {}_2C_{21} &= \frac{\upsilon_2 E_2}{1-\upsilon_2^2} & {}_3C_{12} = {}_3C_{21} &= \frac{\upsilon_3 E_3}{1-\upsilon_3^2} & {}_4C_{12} = {}_4C_{21} &= \frac{\upsilon_4 E_4}{1-\upsilon_4^2} \\ {}_2C_{22} &= \frac{E_2}{1-\upsilon_2^2} & {}_3C_{22} &= \frac{E_3}{1-\upsilon_3^2} & {}_4C_{22} &= \frac{E_4}{1-\upsilon_4^2} \end{aligned}\right\} \tag{25}$$

$$_2C_{66} = \frac{E_2}{2(1+\upsilon_2)} \quad _3C_{66} = \frac{E_3}{2(1+\upsilon_3)} \quad _4C_{66} = \frac{E_4}{2(1+\upsilon_4)}$$

(25 cont'd)

When this theory is applied to practical aircraft structures, the following simplifications can be made

$$H_1 = H_3 \approx 1$$

and $(h/R)^2 = 0$ when compared to 1 in the same expression. When used separately, this term represents the contribution of bending and cannot be neglected.

B. Experimental

1. Introduction

This section covers the experimental investigations conducted to extend the analytical and experimental results from the simple panel investigation to more complex flight vehicle structure. It was designed to determine the effects of dynamic loads and heat on complex structure, and combined the environments of

a. Low-frequency vibration of the type encountered during taxi or high speed buffet.

b. Aerodynamic heating typical of future high performance aircraft.

c. Curvature representation of typical flight vehicle fuselage structure.

d. Acoustic excitation from broad-band noise source typical of present and future power plants.

Titanium honeycomb sandwich panels were selected for this investigation due to a high strength-to-weight ratio and good physical properties in the temperature region involved. A test temperature of 450° F was selected to correspond to surface temperatures expected on future high performance vehicles.

The curved honeycomb sandwich specimens were tested under a combination of environment as follows:

a. Broad-band acoustical noise.

b. Broad-band acoustical noise and heat.

c. Broad-band acoustical noise and low frequency vibration.

d. Broad-band acoustical noise, heat, and low frequency vibration.

The objectives of this phase of the experimental investigation were:

a. To determine the separate and combined effects of low frequency vibratory loading, heat, curvature, and high intensity random noise on the fatigue life of titanium honeycomb sandwich structure.

b. To establish design criteria for sonic fatigue in combined environment.

c. To advance the state-of-the-art for sonic fatigue testing and life prediction.

2. Test Specimen Design

The test specimens were fabricated of titanium faced honeycomb sandwich to meet the requirements of the thermal environment and application to advanced flight vehicle structure with minimum weight and fabrication cost. Sonic fatigue design criteria from Reference 17 were used, compensating for the effects of curvature and elevated temperature. The panels were designed for a test life of approximately seven hours at an overall SPL of 156 db, five hours at an overall SPL of 160 db, and one hour at an overall SPL of 164 db, giving due consideration to fatigue data scatter, etc.

Two titanium honeycomb sandwich configurations were designed. The details are shown in the following table.

TABLE 10

TITANIUM HONEYCOMB SANDWICH PANEL DETAILS

Item	Pilot Model	Test Specimen
Facing Sheets (Ti, 6Al-4V)	0.010 in.	0.008 in.
Doubler (Ti, 6Al-4V)	0.016 in.	0.008 in.*
Honeycomb Core (Polyester)	3.5 lb./ft^3	3.5 lb./ft^3
Core Thickness	0.25 in.	0.25 in.
Adhesive System	HT 424	HT 424
Close-out Member (181 Fiberglass)	2 Ply	2 Ply
Radius of Curvature	84 in.	84 in.
Flat Pattern Size	24 x 30 in.	24 x 30 in.
Weight/Surface Area	-	0.60 lb./ft^2

* 0.020-inch sheet stock chem-milled to 0.016-inch in the doubler area and 0.008-inch in the skin area, resulting in an integral skin-doubler arrangement.

A "pilot model" test specimen was designed and built to evaluate the design prior to fabrication of the fatigue test articles. This panel was tested in the Lockheed High Intensity Sound Facility for approximately 30 hours of broad-band acoustical noise excitation at 160 db overall with no significant failures. Using the results of this test, the final specimen design was determined to be that which is shown in Table 10 and Figure 49. This design has facing sheet thicknesses which are considered to be about minimum from the fabrication point-of-view.

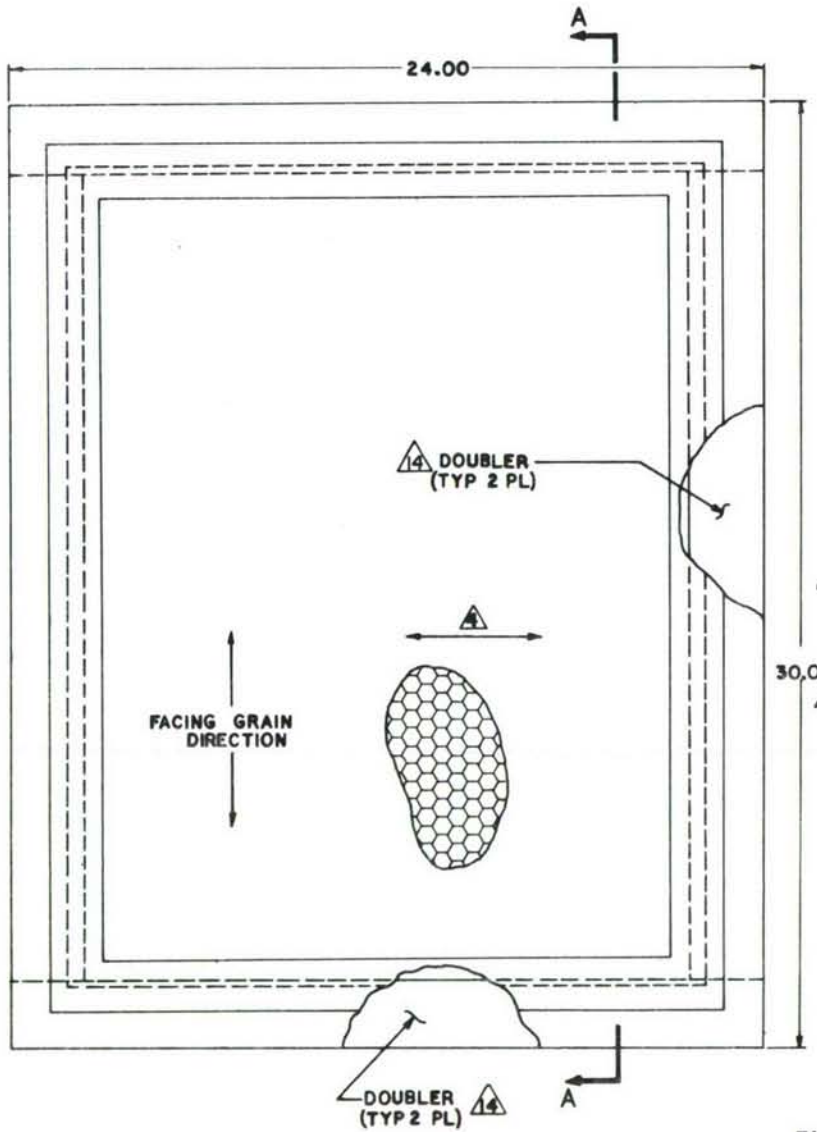

(-1) PLAN VIEW
PANEL ASS'Y

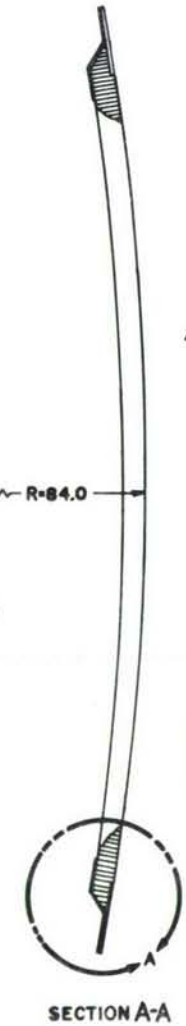

SECTION A-A

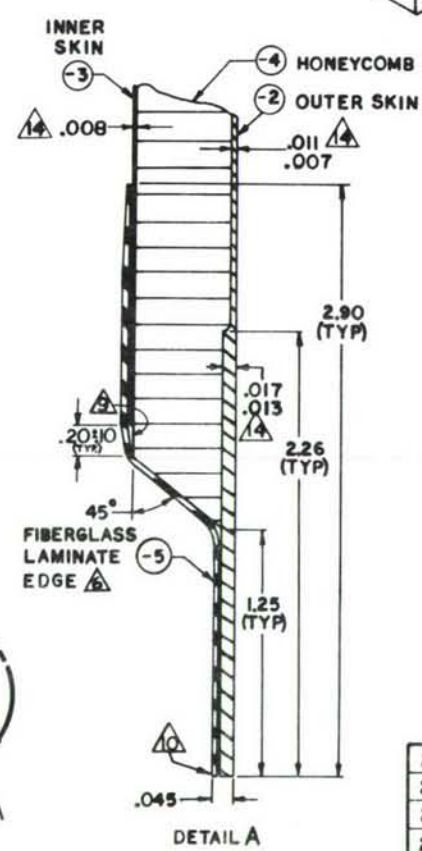

DETAIL A

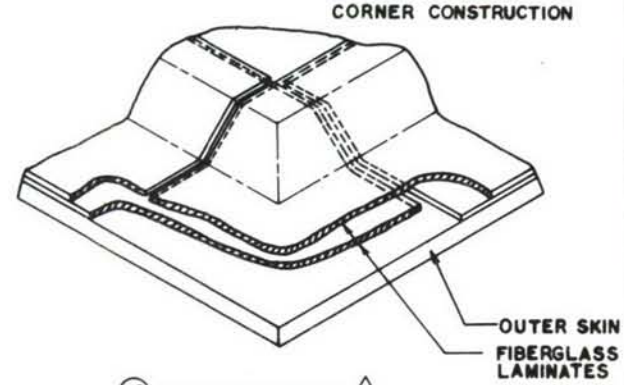

14 CHEM MILL TO DIM. SHOWN
13 CURVED DIMENSION
12 IMPRESSION STAMPING NOT PERMITTED
10 DETAILS OF FRP EDGE PER LAC G-529, AM.2, PAGE 4, FIGURE 2B.
9 THIS AREA MUST BE FILLED WITH FIBERGLASS LAMINATE.
8. APPLY STRIPPABLE PROTECTIVE COATING PER LAC 659.
7 HRP-1/4-6F11-3.5 CORE (.250±.006 THICK).
6 EPOXY PREPREG BP 908-181 VOLAN "A" (PER MIL-R-9300, TYPE II), 2 PLY LAMINATE, BLOOMINGDALE RUBBER CO., ABERDEEN, MD., OR EQUAL.
5 BOND PER LAC 2009. USE HT 424 ADHESIVE SYSTEM.
4 INDICATES CORE RIBBON DIRECTION.
2. MACHINE PER LAC 0701.
1. FABRICATE PER LAC 1241.

NOTES

-1	PART NO	DESC.	MAT'L	MAT'L SIZE	MAT'L SPEC
24	-5	FIBERGLASS EDGE MBER	6	—	6
24	-4	CORE	7	.25 x 2.5 x 27.5	7
24	-3	INNER SKIN	6Al-4V TITANIUM	.008×240 ×300	—
24	-2	OUTER SKIN	6Al-4V TITANIUM	.008×240 ×300	—
—	-1	PANEL ASS'Y	—	—	—

FIGURE 49.
TITANIUM HONEYCOMB SANDWICH
TEST SPECIMEN

3. Test Fixture Design

Test fixtures were designed to provide peripheral support for the test specimens representative of actual flight vehicle installation. The design required the capability of providing support for the specimen while both fixture and test specimen were subjected to low frequency vibration, noise, and heat environment. Each fixture was designed to support four test specimens in order to reduce overall test time and cost. A limited amount of fixture flexibility was required to introduce shear loads into the specimen when the low frequency vibratory load was applied. A detailed stress analysis of each critical component in the fixture was made following standard aircraft procedure with allowable stresses obtained from Reference 18. Each part was designed to withstand an ultimate alternating load of 30,000 pounds and sound pressure levels of 170 decibels. A typical analysis was comprised of

a. Analysis of loads.

b. Determination of section properties.

c. Tension and/or column analysis.

d. Fastener analysis.

e. Margin of safety for all stresses.

f. Fatigue life at all stresses.

The fixtures which are shown in Figures 50 through 52 were capable of supporting four test specimens simultaneously in a manner representative of actual flight vehicle installation. The upper two specimens on each fixture were subjected to elevated temperatures produced by seven quartz lamps arranged around the periphery of the specimen as shown in Figure 53. Low frequency vibratory loads were produced by an electro-hydraulic force system. Test specimens were installed with the concave side toward the acoustical noise field, or reversed to normal flight vehicle installation, to protect the heat lamps from the high intensity sound.

4. Test Results

a. Preliminary Tests. Three preliminary tests were made prior to the fatigue tests conducted at Wright-Patterson Air Force Base, Ohio. These tests were designed to accomplish three things. First, a "pilot model" test was used to evaluate the fatigue life of the titanium honeycomb sandwich design prior to fabrication of the fatigue test articles. Next, tests conducted at the TF-33P-7 engine test stand were designed to check out test fixture rigidity, instrumentation, and quartz lamp heating system. Last, a near-field acoustical noise survey was made to initially set the position of each test fixture in its desired acoustical noise environment.

A brief description of each preliminary test is described in the following sections.

- "Pilot Model" Test. The "pilot" specimen described in Table 10 was tested in the Lockheed-Georgia High Intensity Sound Facility prior to fabrication of the fatigue test specimens used for this investigation. This test specimen was instrumented with eight uniaxial strain gages strategically located to define the panel response. A series of sine-sweeps from 100 cps to 700 cps were made to determine significant frequencies, damping, etc. A plot of typical panel strain response is shown in Figure 54.

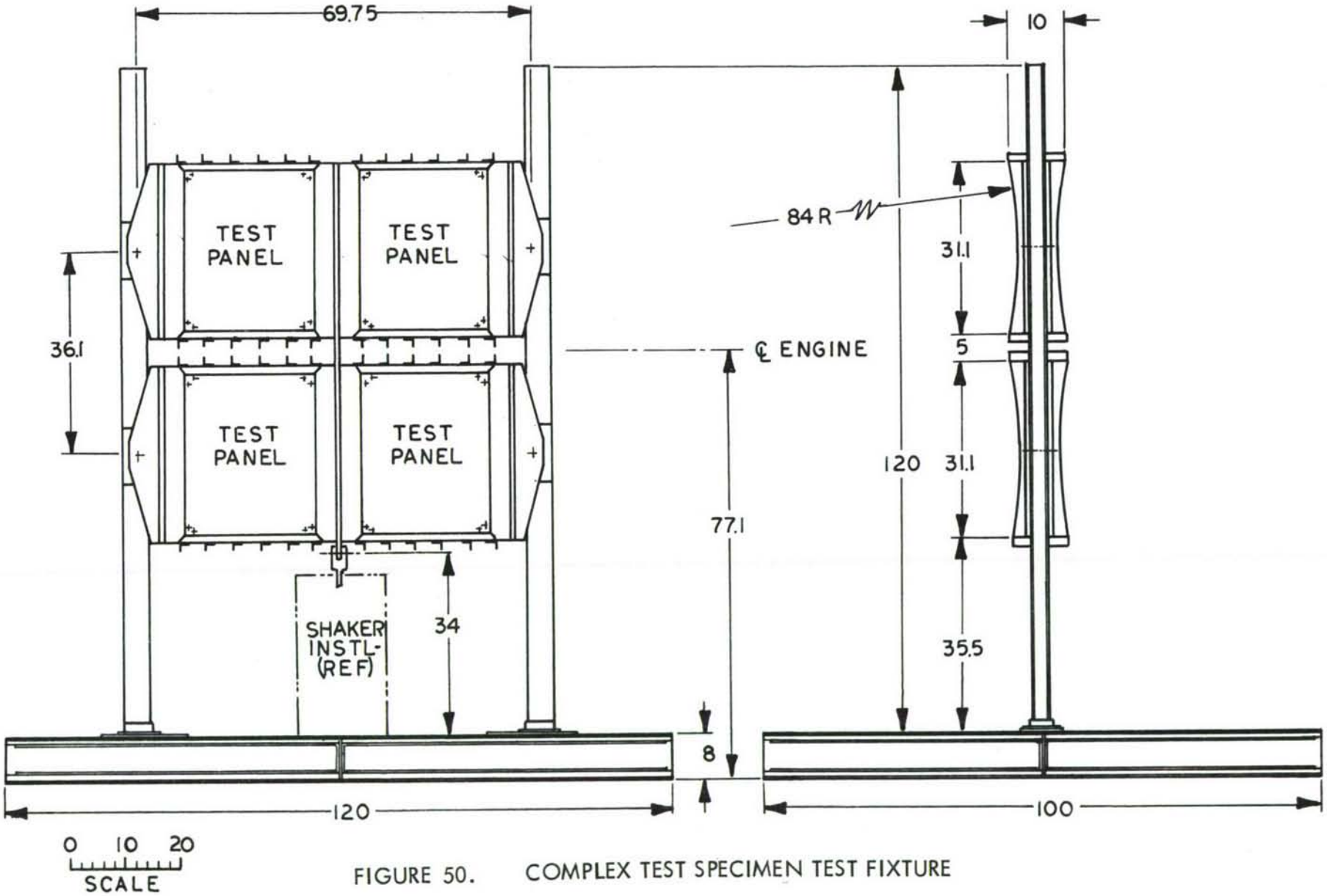

FIGURE 50. COMPLEX TEST SPECIMEN TEST FIXTURE

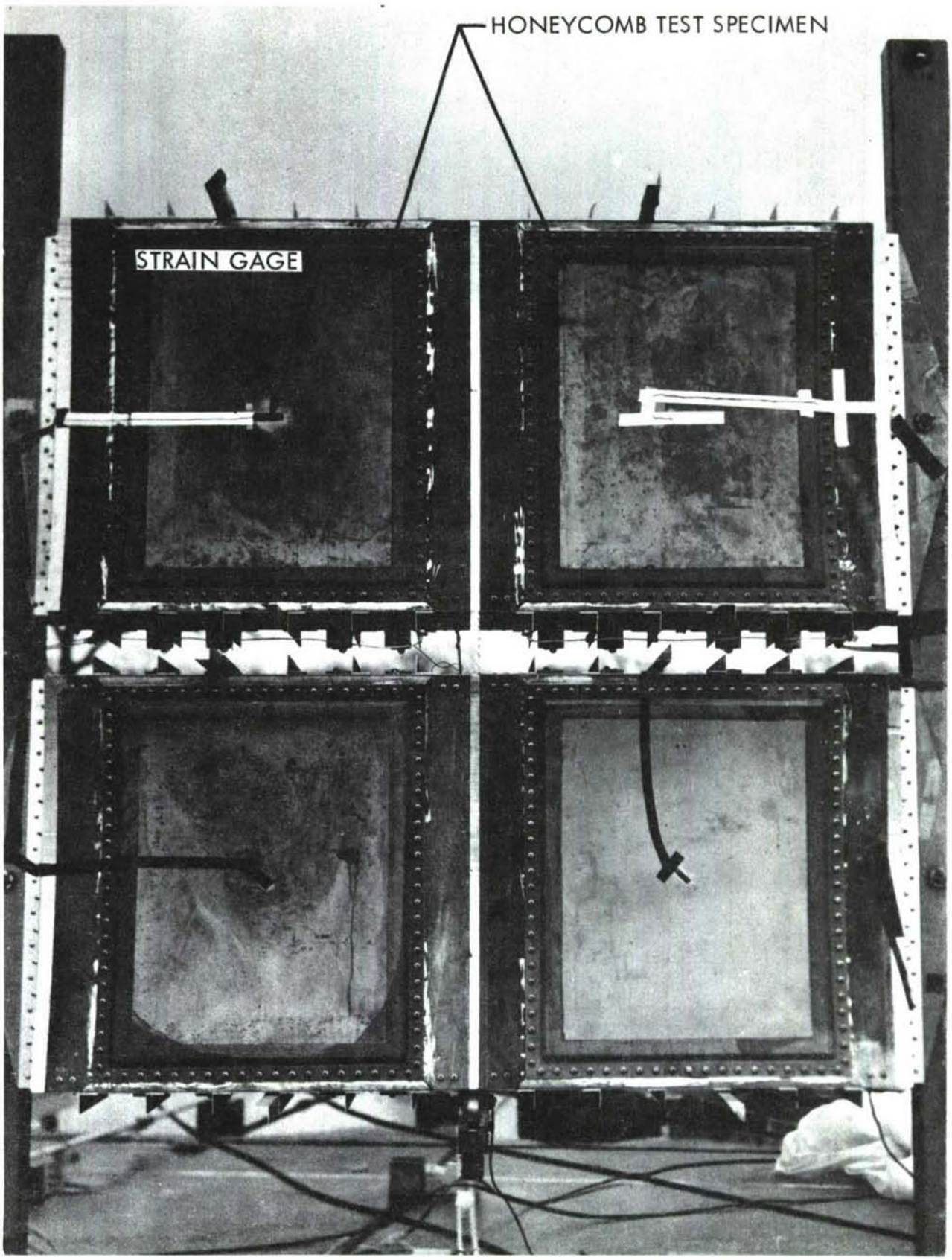

FIGURE 51. FRONT VIEW - TEST FIXTURE

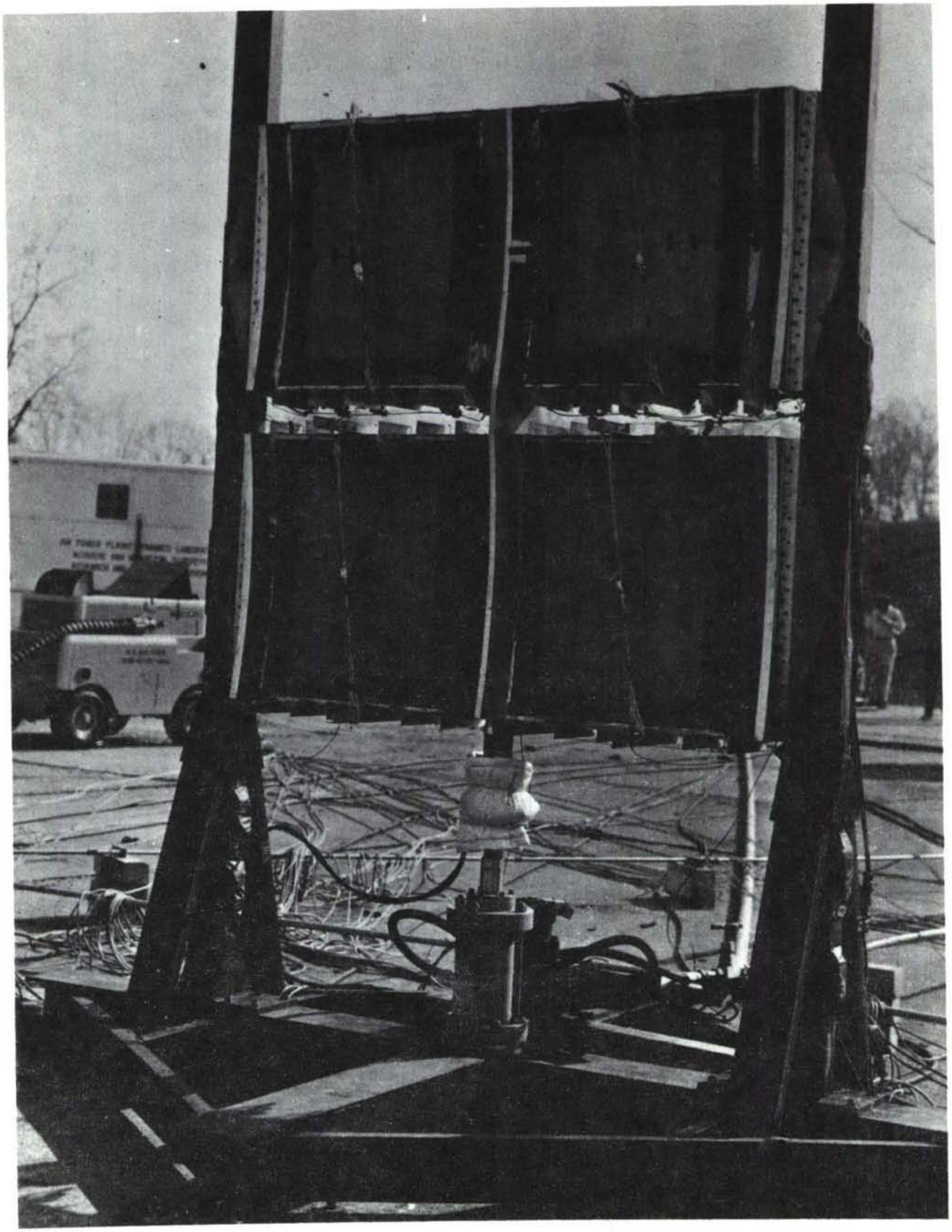

FIGURE 52. FRONT VIEW - TEST FIXTURE WITH HYDRAULIC ACTUATOR

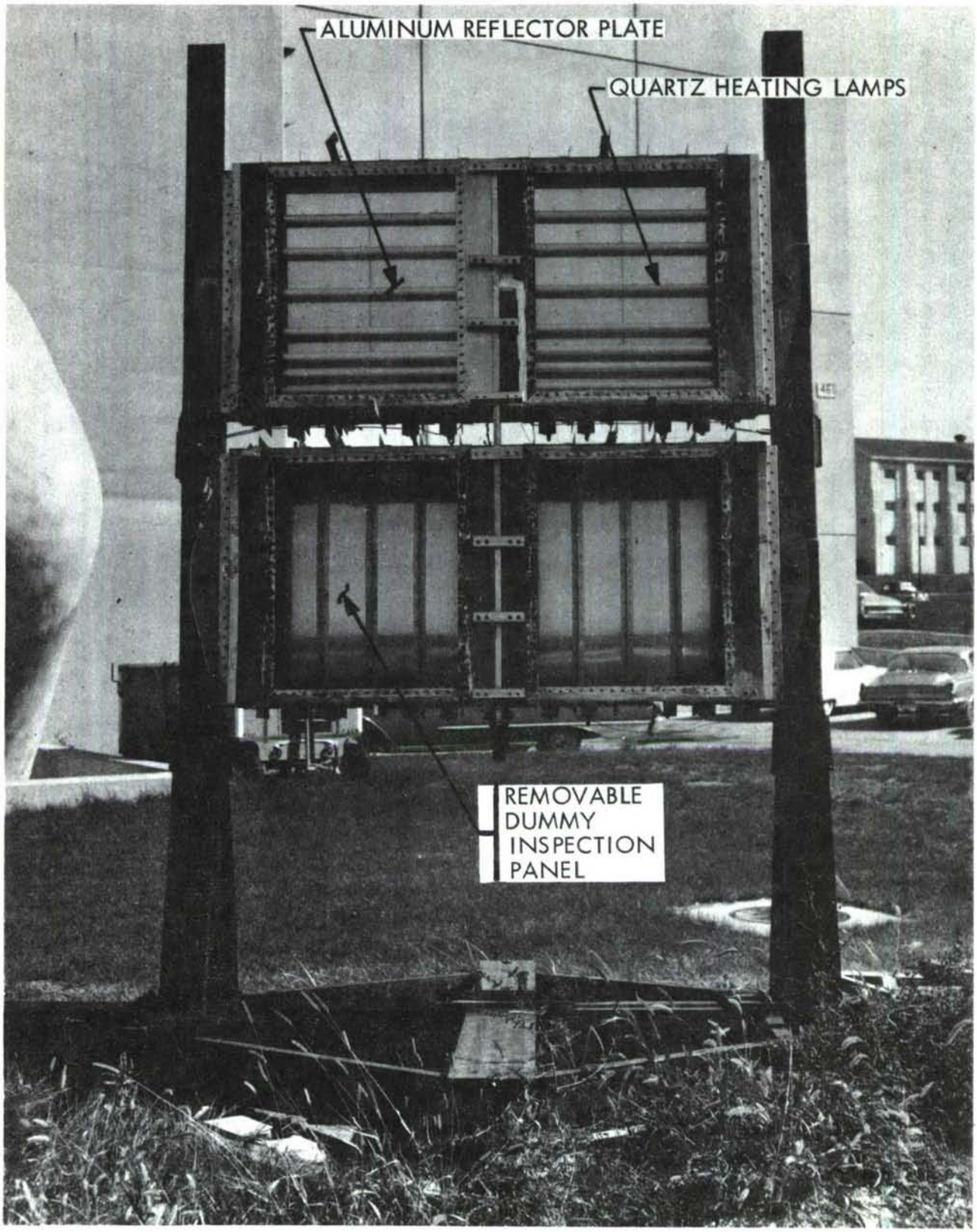

FIGURE 53. FRONT VIEW - TEST FIXTURE WITH TEST PANELS REMOVED

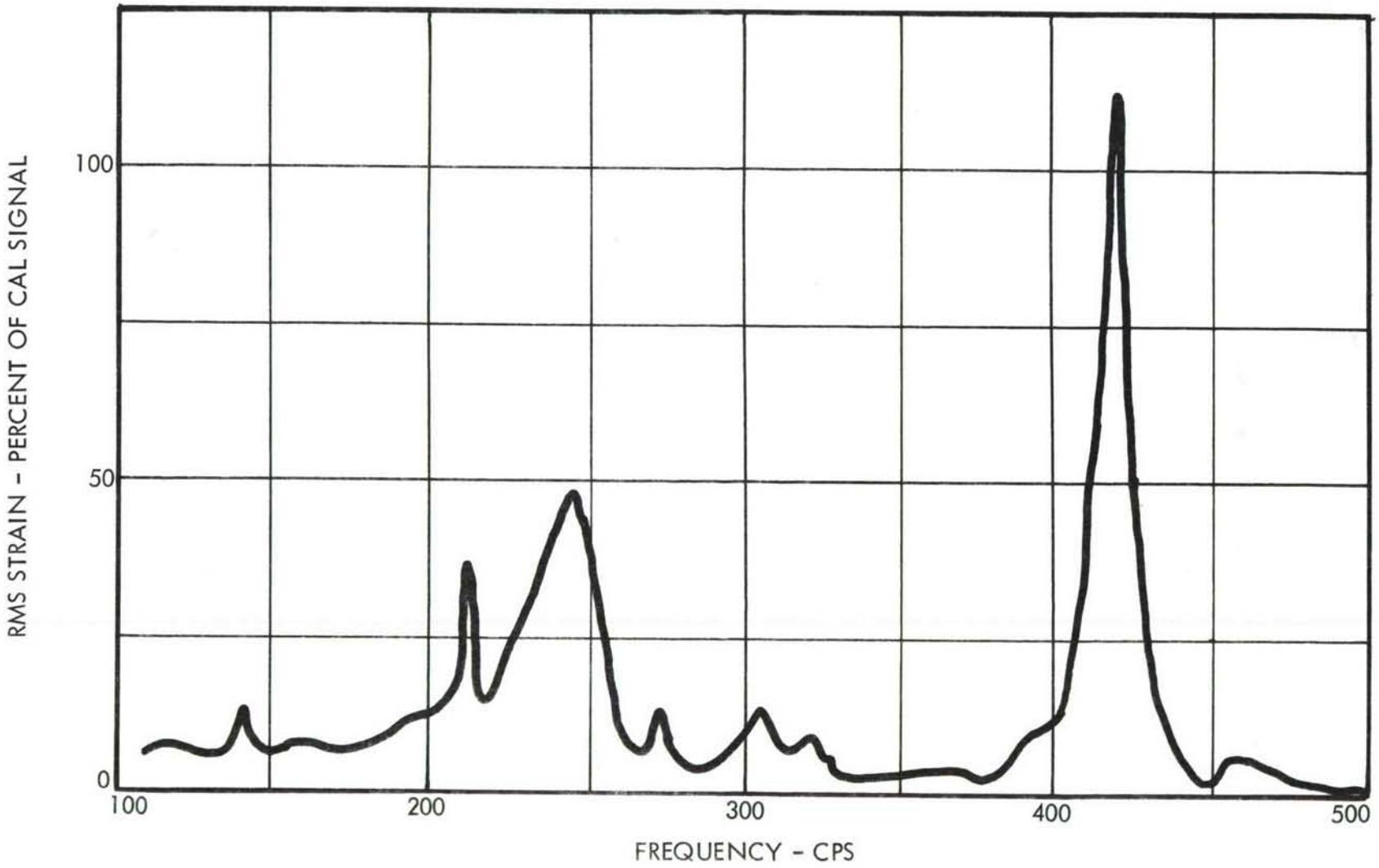

FIGURE 54. TYPICAL "PILOT MODEL" RESPONSE

TABLE 11

NEAR-FIELD NOISE SURVEY, J57-P21 AT MAX A/B

Microphone Position	Distance from Engine		Overall SPL - db	1/3-OBL db (160 cps*)	1/3-OBL db (200 cps*)	1/3-OBL db (250 cps*)	1/3-OBL db (315 cps*)
	X/D	Y/D					
1	2	0.85	164.5	152.5	153	153.5	153
2	3	1.03	163	146.5	147	148.5	148.5
3	4	1.20	164	147	147	148	148
4	2	1.56	160	147	147	148.5	149
5	8	1.91	159	147	147	148	149
6	12	2.61	155.5	145.5	146	144	145
7	16	3.32	150	138	139	138.5	135
8	0	2	142	121	122.5	124	125.5
9	2	2	151	131.5	132.5	134.5	135
10	4	2	161	142.5	142.5	144	145.5
11	4	3	147.5	133	133.5	134	137
12	6	3	155.5	141.5	143.5	143.5	147
13	8	3	159	145.5	147	146	148.5
14	10	3	157	145	147	146	148
15	2	4	144	128	128.5	126.5	128.5
16	4	4	151	134	135	134	136.5
17	6	4	154.5	139	142.5	142	143
18	8	4	155	141.5	145	144	144.5
19	10	4	156.5	144	147.5	147.5	146.5
20	12	4	156	144	148.5	149	147.5
21	5	5	512	135	138	137.5	138
22	10	5	154	141	146	147	143.5
23	15	5	151.5	139.5	142	144	142
24	0	10	138	116.5	117	120.5	123.5
25	5	10	144.5	120.5	124	128.5	131
26	10	10	151	128.5	129	135.5	142
27	15	10	148	133	130.5	135	139

*Center frequency of 1/3 octave band filter.

Upon completion of the frequency sweeps, a broad-band noise fatigue test was made at an overall sound pressure level of 160 db with no thermal or low frequency vibration input. Thirty hours of testing at 160 db overall were accumulated and only a small delamination of the edge member was the result. Data obtained during this test were used to establish the final design of the test specimen.

- Engine Test Stand Checkout. One complete test fixture comprising an electro-hydraulic force system, heating lamps, and test specimens was checked for specimen and fixture response in the acoustical noise field of a TF-33P-7 jet engine. This test served as a proving ground for the high temperature strain gages, thermocouples, and adhesives used in the 450° F fatigue test thermal environment.

- Near-Field Acoustical Noise Survey. Prior to positioning the fixtures at the test site, a free-field survey of the acoustic output of the J57-P21 jet engine was made. Sound pressure levels were sampled at 62 positions, 27 of which are shown in Figure 55. The results of this survey are tabulated in Table 11. Measurements made near the boundary of the jet efflux were used to position the four test fixtures in the desired acoustical noise environment.

b. Fatigue Tests at Wright Field. The four test fixtures were placed behind the J57-P21 turbo-jet engine at the RTD facility, Wright Field, as shown in Figures 56 and 57. Titanium honeycomb sandwich specimens 1 through 16 were tested during the first part of the test. Heat was applied to each of the upper test specimens. Low frequency vibration loads were applied to Fixture 2 and 3.

The tests were divided into segments as shown in Table 12. Each specimen was thoroughly inspected after each segment.

TABLE 12

COMPLEX SPECIMEN TEST RUNS

Specimen No.	Segment No.	Run Time	Accumulated Time Hr-Min.
1-16	1-6	5	00:30
1-16	7-9	10	01:00
1-16	10-17	15	03:00
1-16	18-23	20	05:00
9-24	24-51	20	14:20

The J57-P21 turbo-jet engine was operated at afterburner power during each test segment. It developed an average thrust of 15,000 pounds at this power setting. The quartz lamp heating system maintained an average temperature of 400° F on the internal, exposed surface of each heated test specimen. The electro-hydraulic force system delivered an average force of 6000 lbs RMS, random

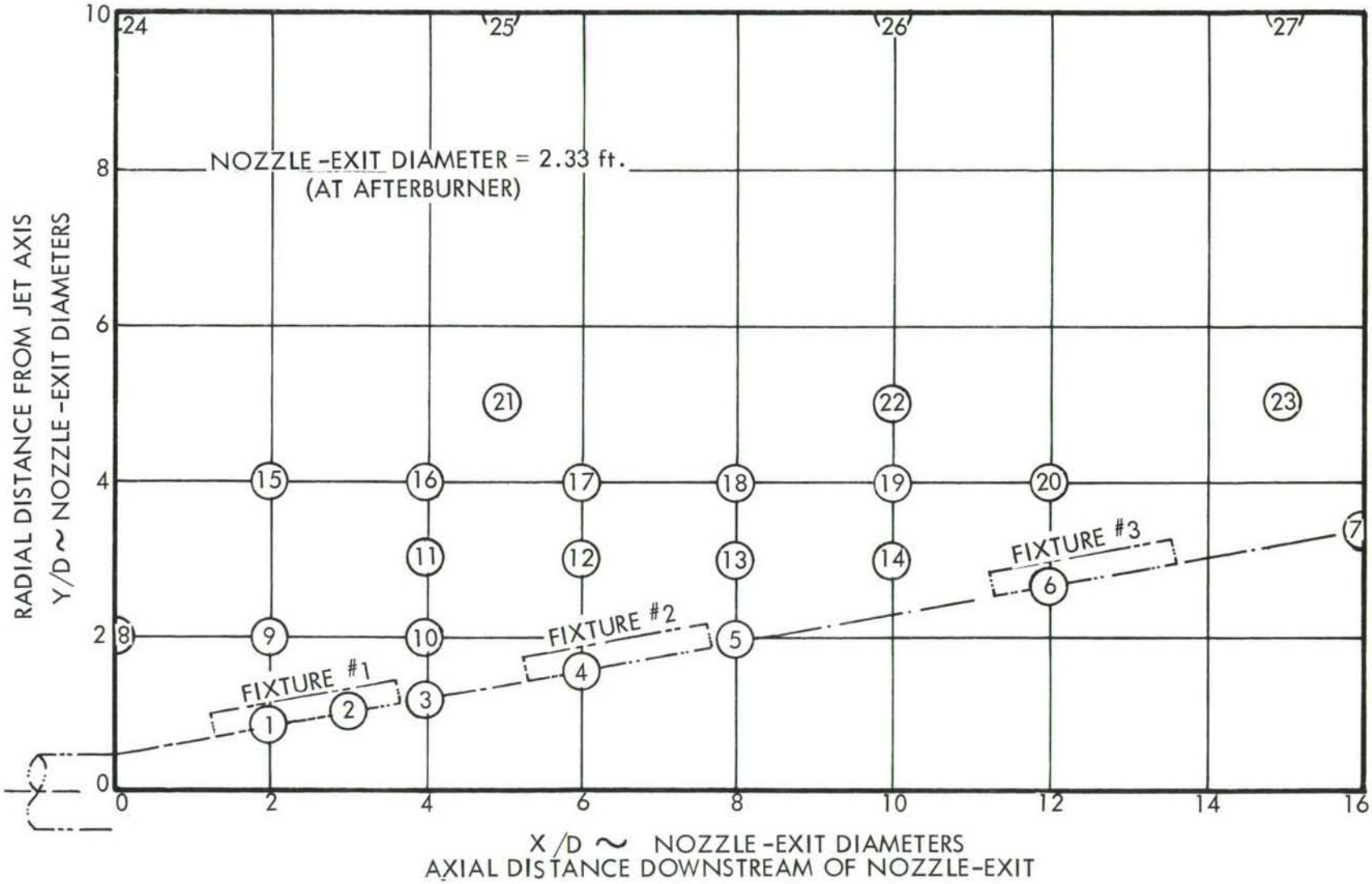

FIGURE 55. NEAR FIELD NOISE SURVEY-MICROPHONE LOCATIONS

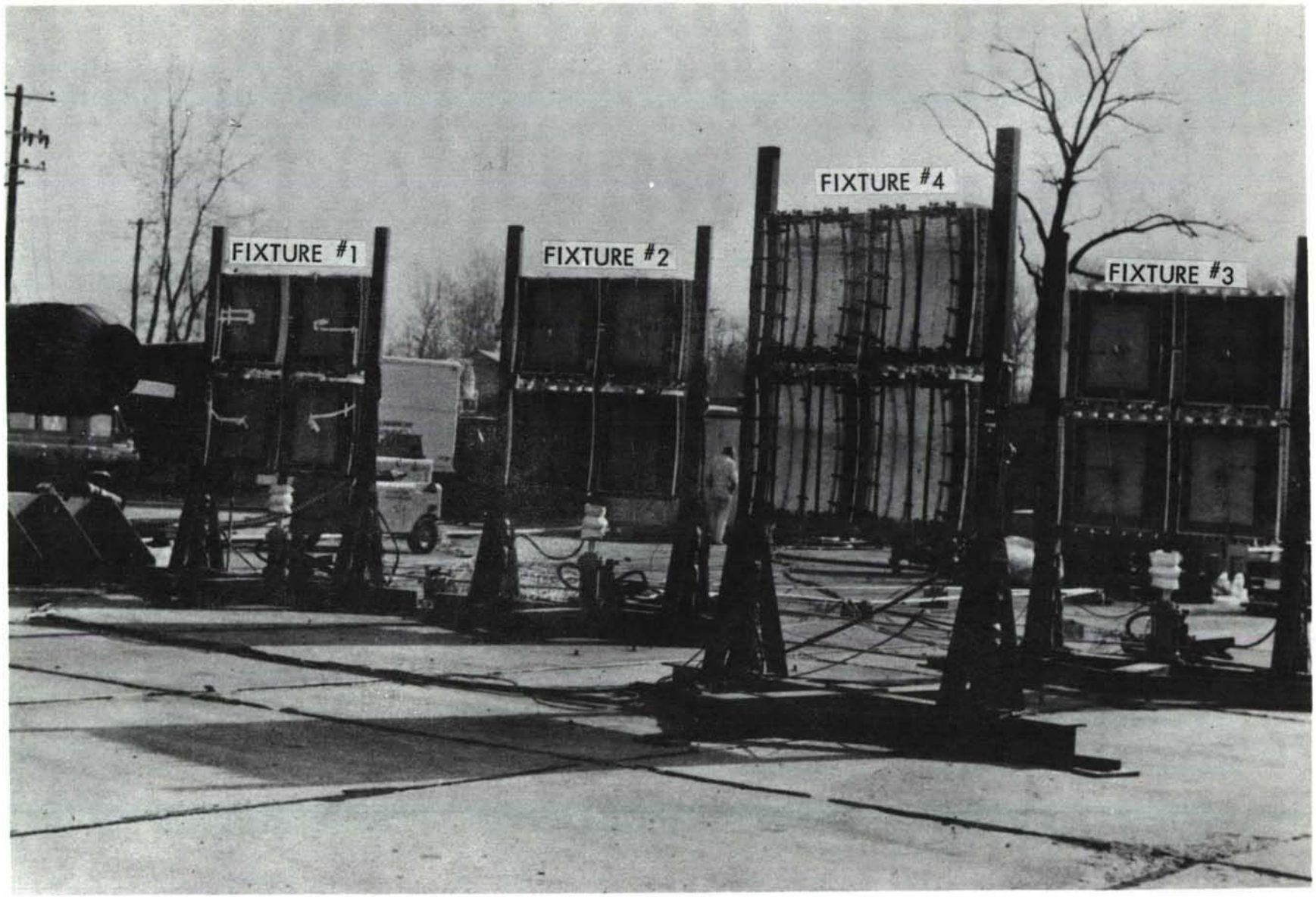

FIGURE 56. OVERALL VIEW OF TEST ARRANGEMENT

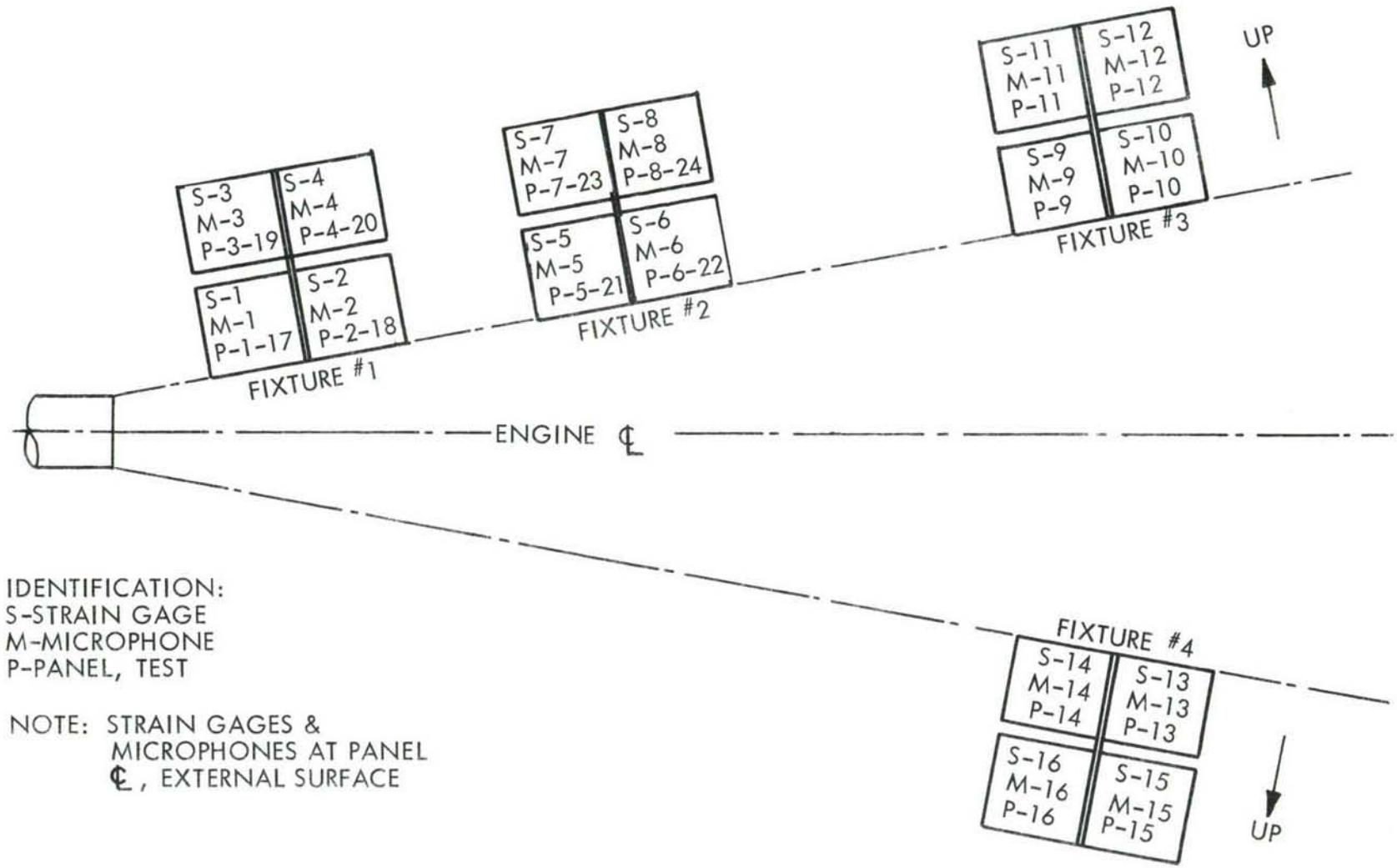

FIGURE 57. TEST SET-UP

amplitude load at a frequency of approximately 12 cps. Strain and microphone data were recorded on magnetic tape during each run, with the strain from the gages mounted at the center of the test specimen as shown in Figure 51 recorded continuously. Microphone data and strain from the remaining gages were recorded periodically throughout the entire test.

Only one major fatigue failure was experienced during run segments 1-24. This failure occurred at five hours of test time. It was a delamination of the inner face sheet from the core on specimen 5, Figure 58, after 215 minutes of afterburner time. The delmaination was deduced to be the result of a void in the core-to-face sheet bond, as no other similar failure was experienced subsequently. Specimens 3 and 9 experienced delamination of the edge member around the attachment holes as shown in Figures 59 and 60. Specimen numbers 17 through 24 were then installed on Fixture 1 and 2 in place of specimens 1 through 8. The low frequency vibratory load was transferred from Fixture 2 to Fixture 1 and testing was resumed with 20 minute time segments.

Testing was discontinued after accumulation of 14 hours and 20 minutes of afterburner time with only nine major failures. The most significant failure occurred on specimen number 24, Figure 61, during the first 20 minute run. It was caused by heat and a void in the bond between the face sheet and honeycomb core.

The test specimens were removed from the fixtures and dye-checked for incipient cracks at the completion of the test program. Six panels had skin cracks in the inner face sheet at the attachment holes. Figure 62 is a group of sketches which show the location of each crack and the accumulated time at the end of the test program.

Microphone and strain gage data recorded during the test were analyzed as follows:

1. Microphone data
   - Overall sound pressure level
   - 1/3-octave band sound pressure level
2. Strain gage data
   - Root-mean-square strain
   - Narrow band 10 cps filter bandwidth (10-second sample)
   - Probability density

Typical 1/3-octave band sound pressure levels are presented in Figures 63 through 65 for specimens 1 through 5 and 10. These 1/3-octave band analyses of the turbo-jet noise show the frequency at which the peak sound energy occurs decreases with increasing distance from the exhaust nozzle.

Typical narrow-band strain response analyses for the various combinations of environment are shown in Figures 66 through 69. Tables 13 and 14 are summaries of the measured sound pressure and strain magnitudes from each test specimen, as well as total test time.

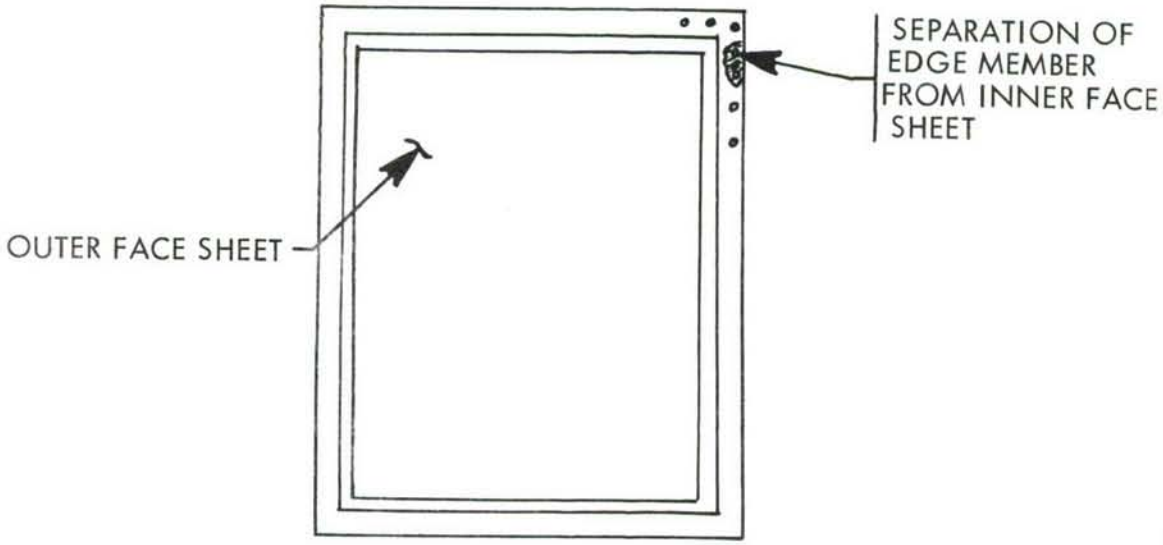

FIGURE 58. PANEL #3 (FRONT VIEW) TIME TO FAILURE - 165 MINUTES

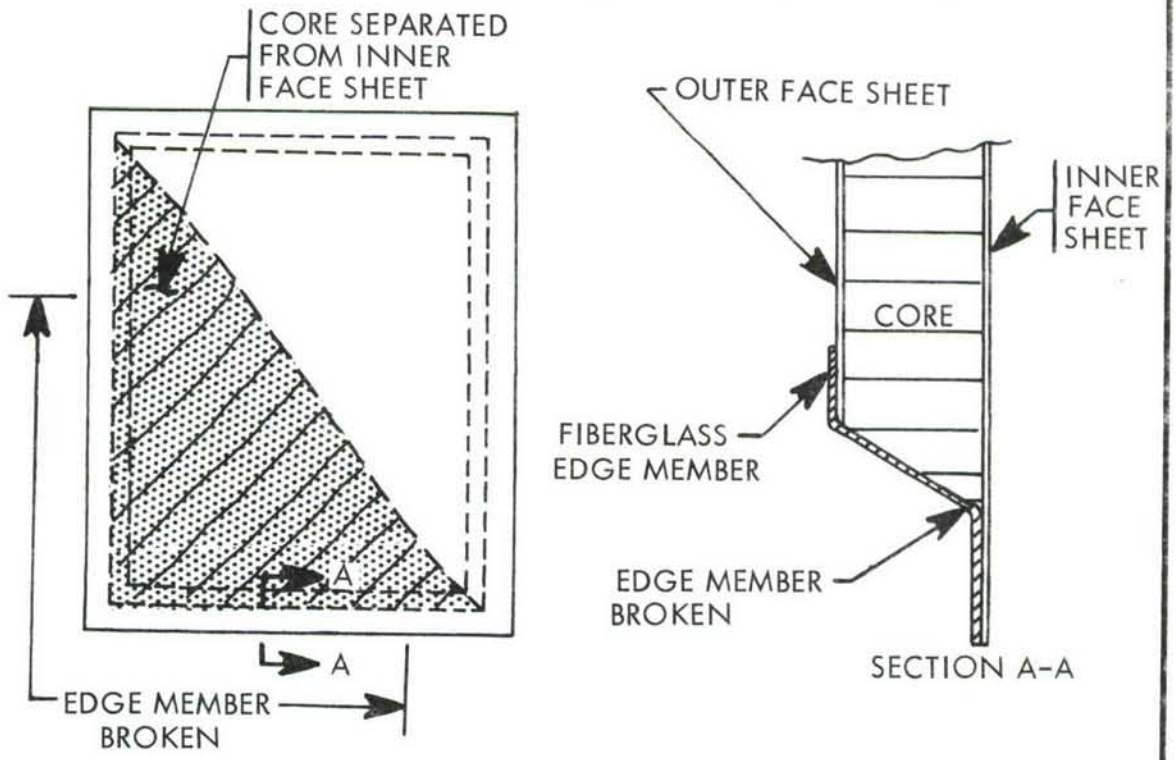

FIGURE 59. PANEL # 5 (BACK VIEW) TIME TO FAILURE - 215 MINUTES

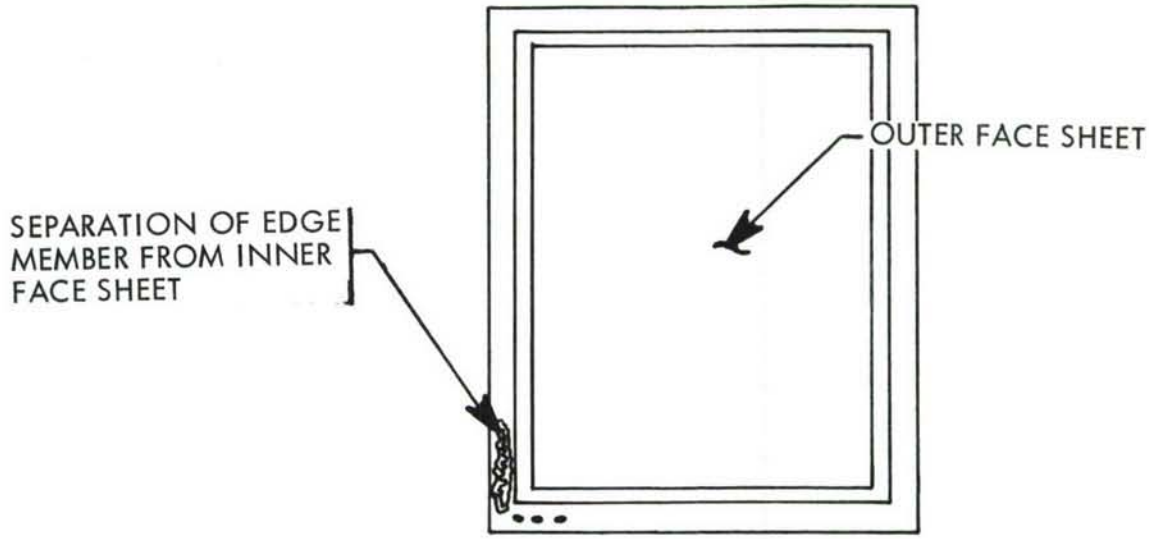

FIGURE 60. PANEL #9 (FRONT VIEW) TIME TO FAILURE - 180 MINUTES

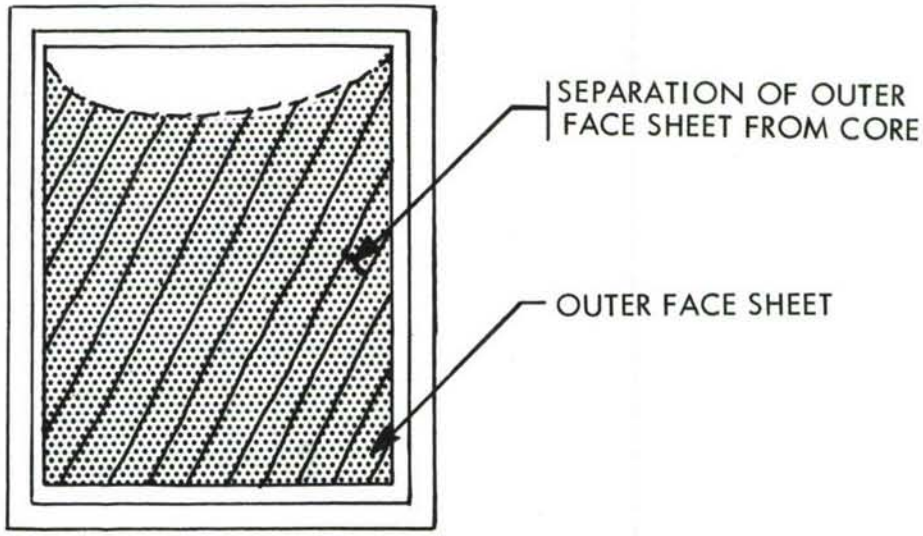

FIGURE 61. PANEL # 24 (FRONT VIEW) TIME TO FAILURE - 20 MINUTES

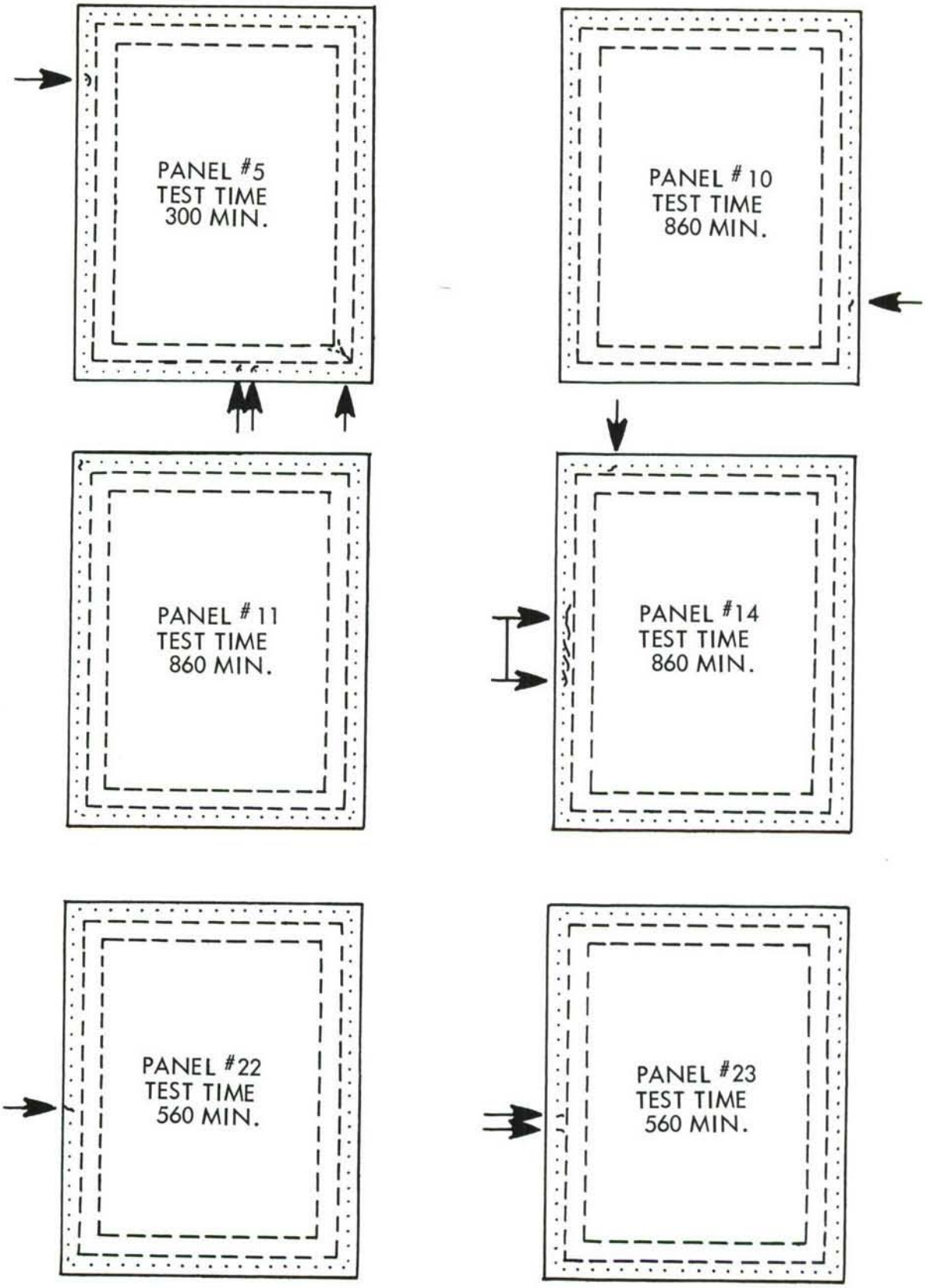

FIGURE 62. TEST PANEL SKIN CRACKS

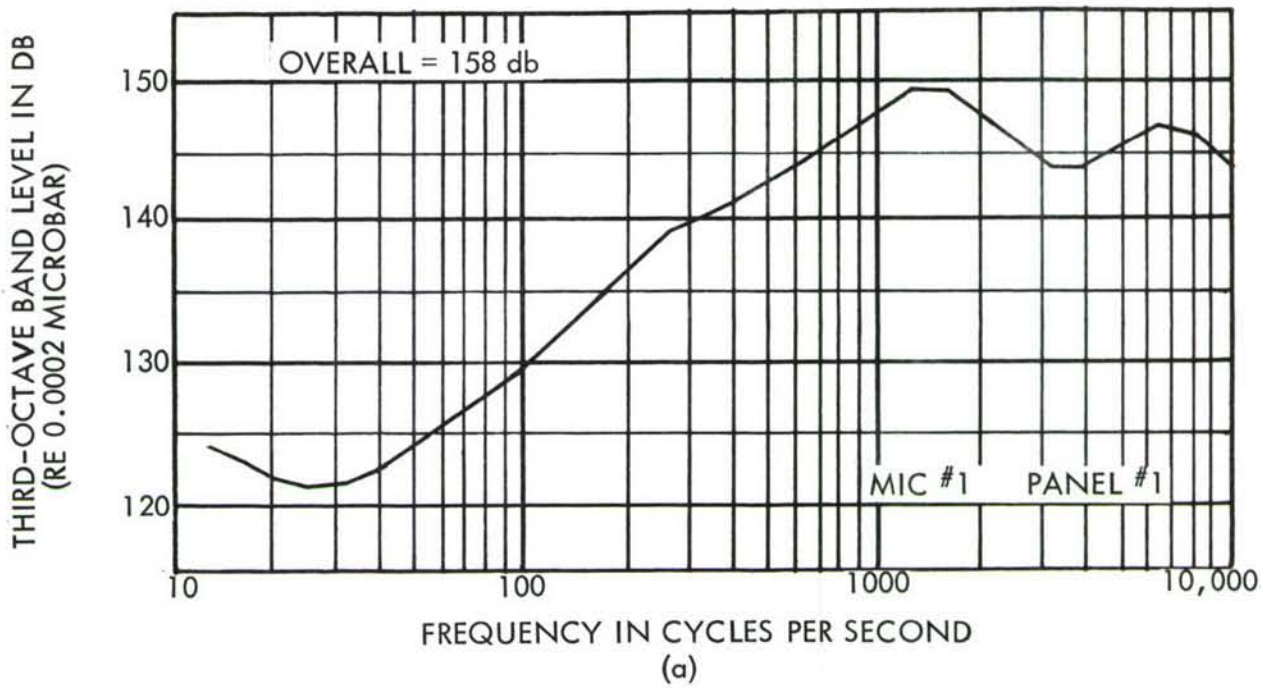

(a)

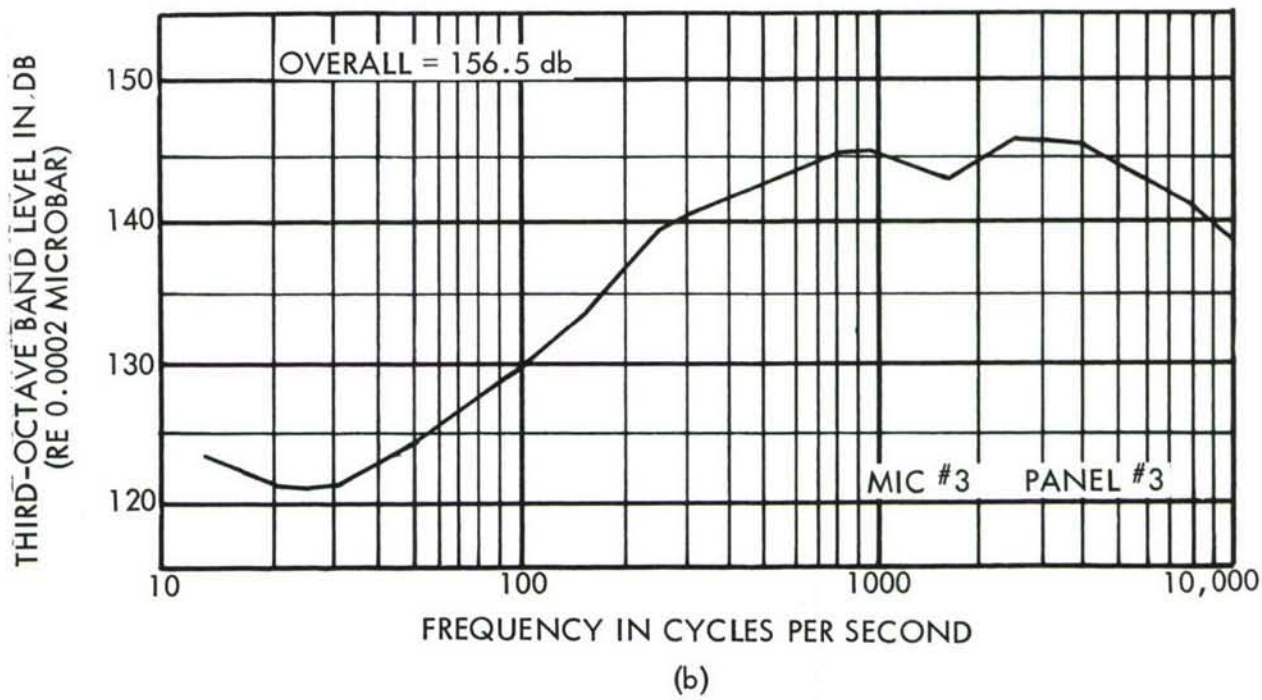

(b)

FIGURE 63. MICROPHONE DATA - 1/3 OCTAVE BAND LEVELS

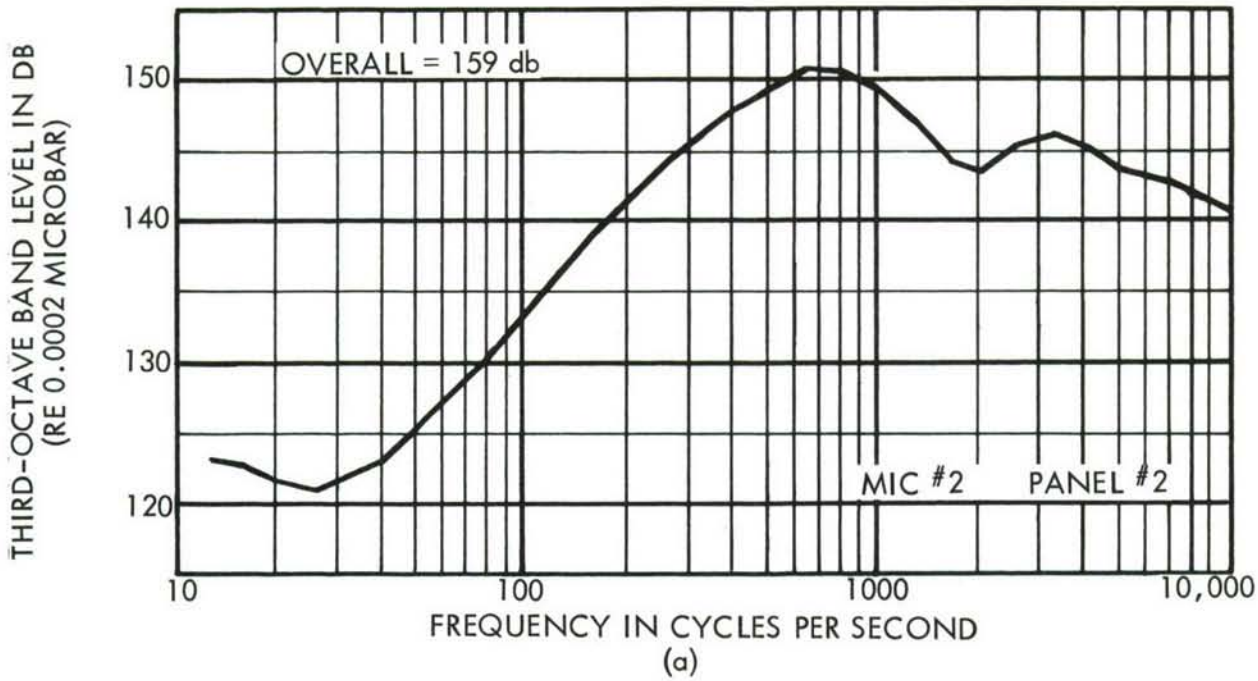

(a)

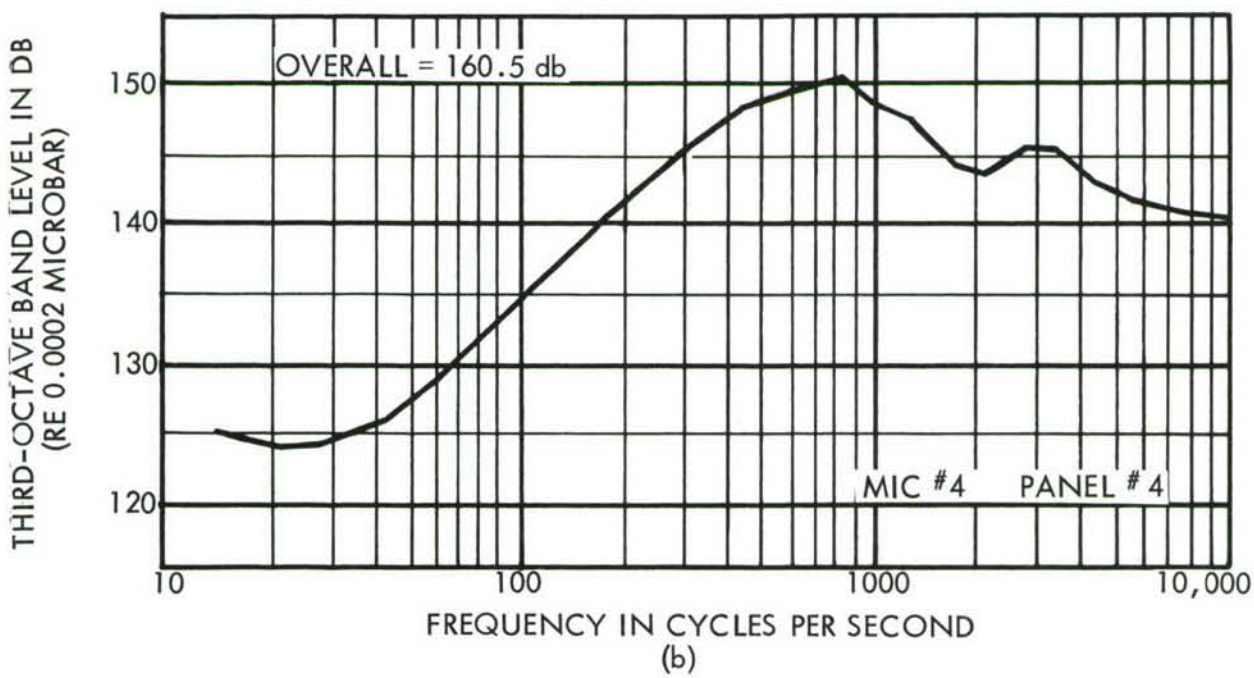

(b)

FIGURE 64. MICROPHONE DATA - 1/3 OCTAVE BAND LEVELS

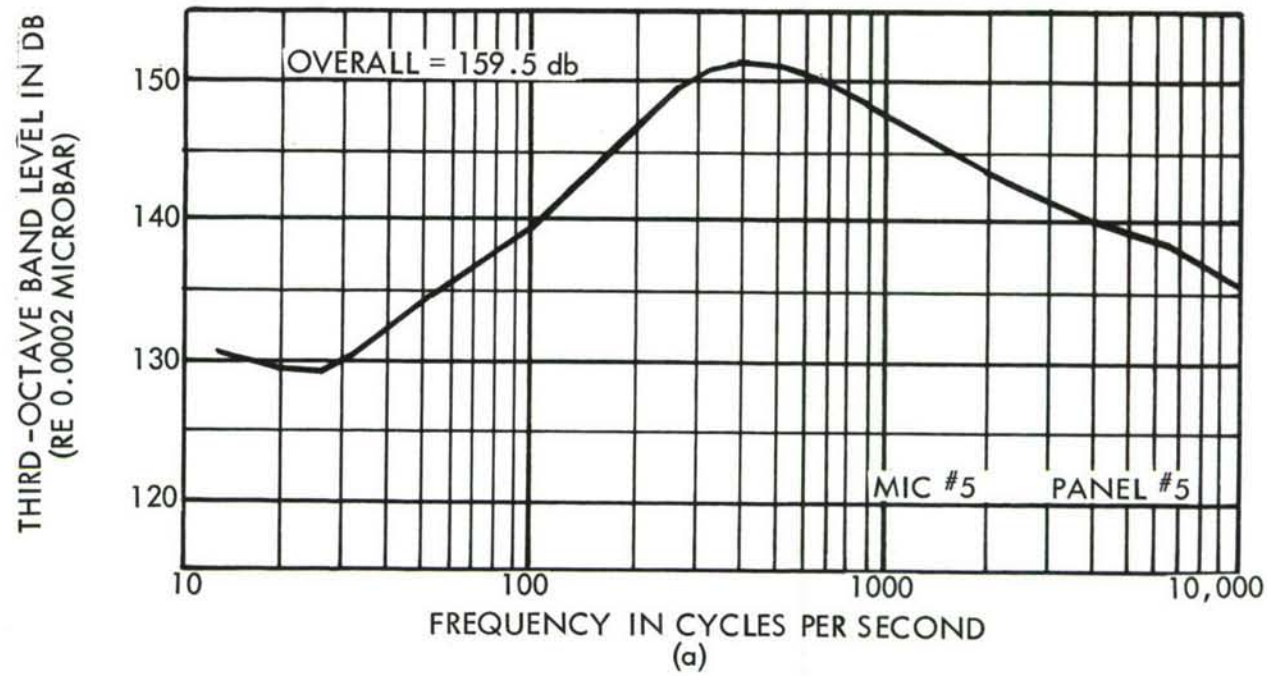

(a)

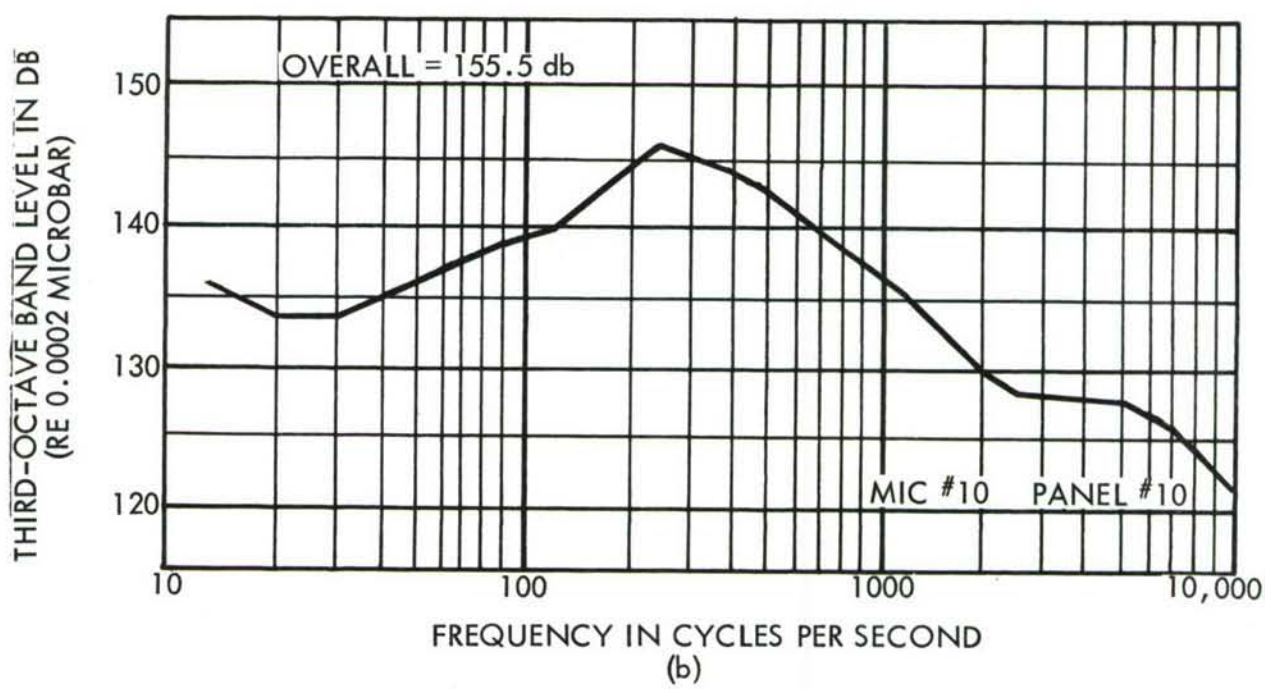

(b)

FIGURE 65. MICROPHONE DATA - 1/3 OCTAVE BAND LEVELS

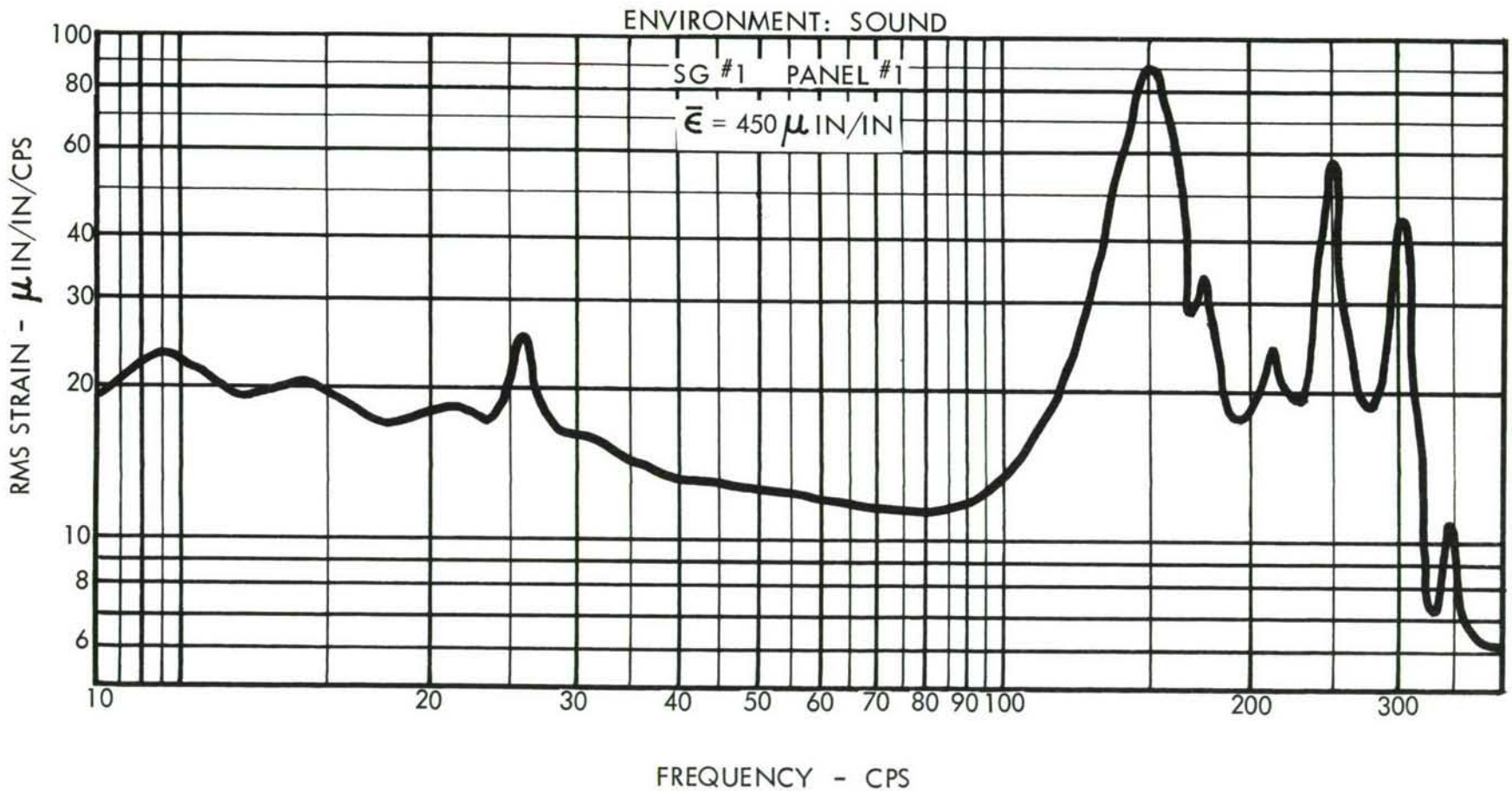

FIGURE 66. COMPLEX TEST SPECIMEN RESPONSE

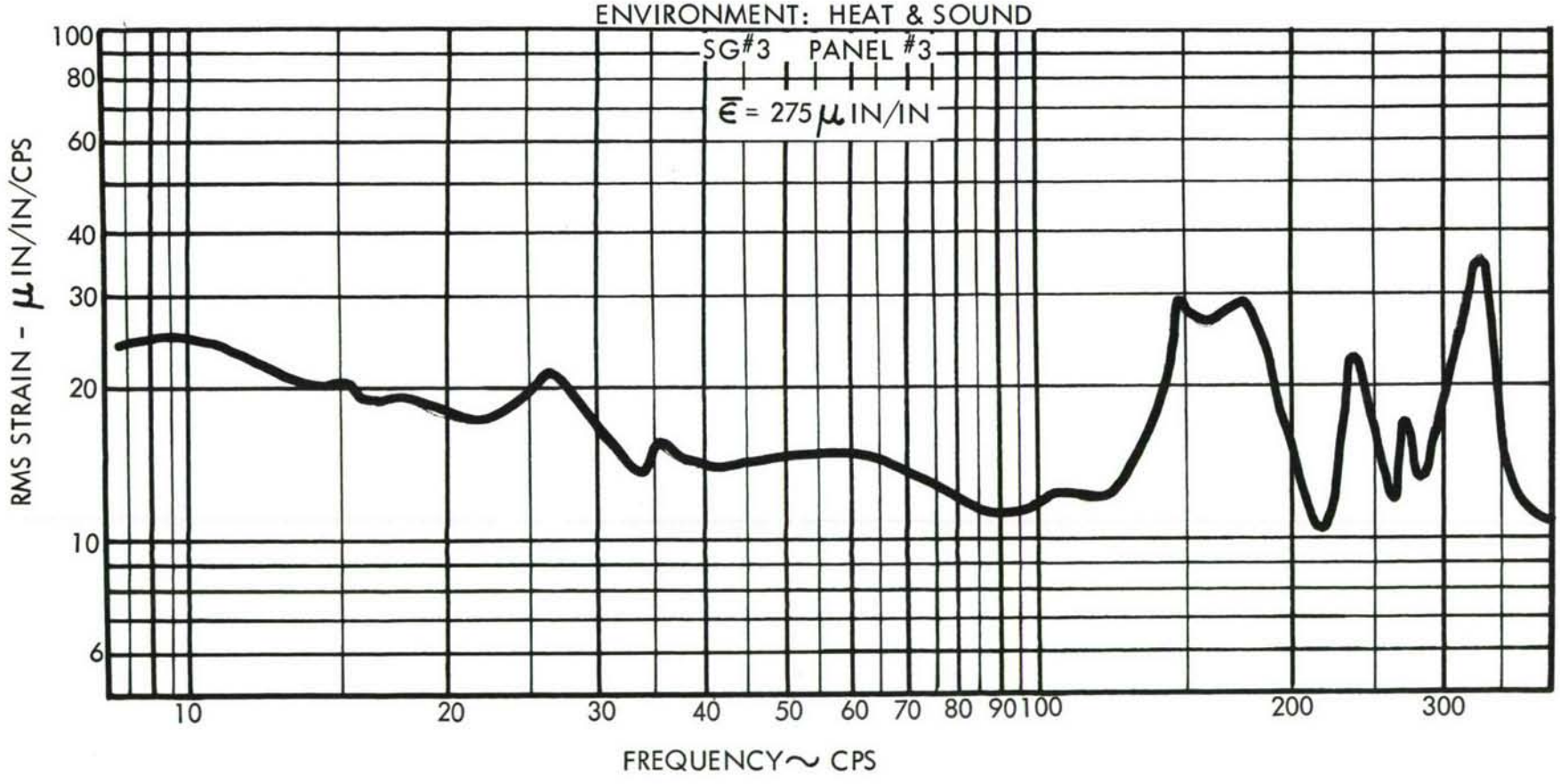

FIGURE 67. COMPLEX TEST SPECIMEN RESPONSE

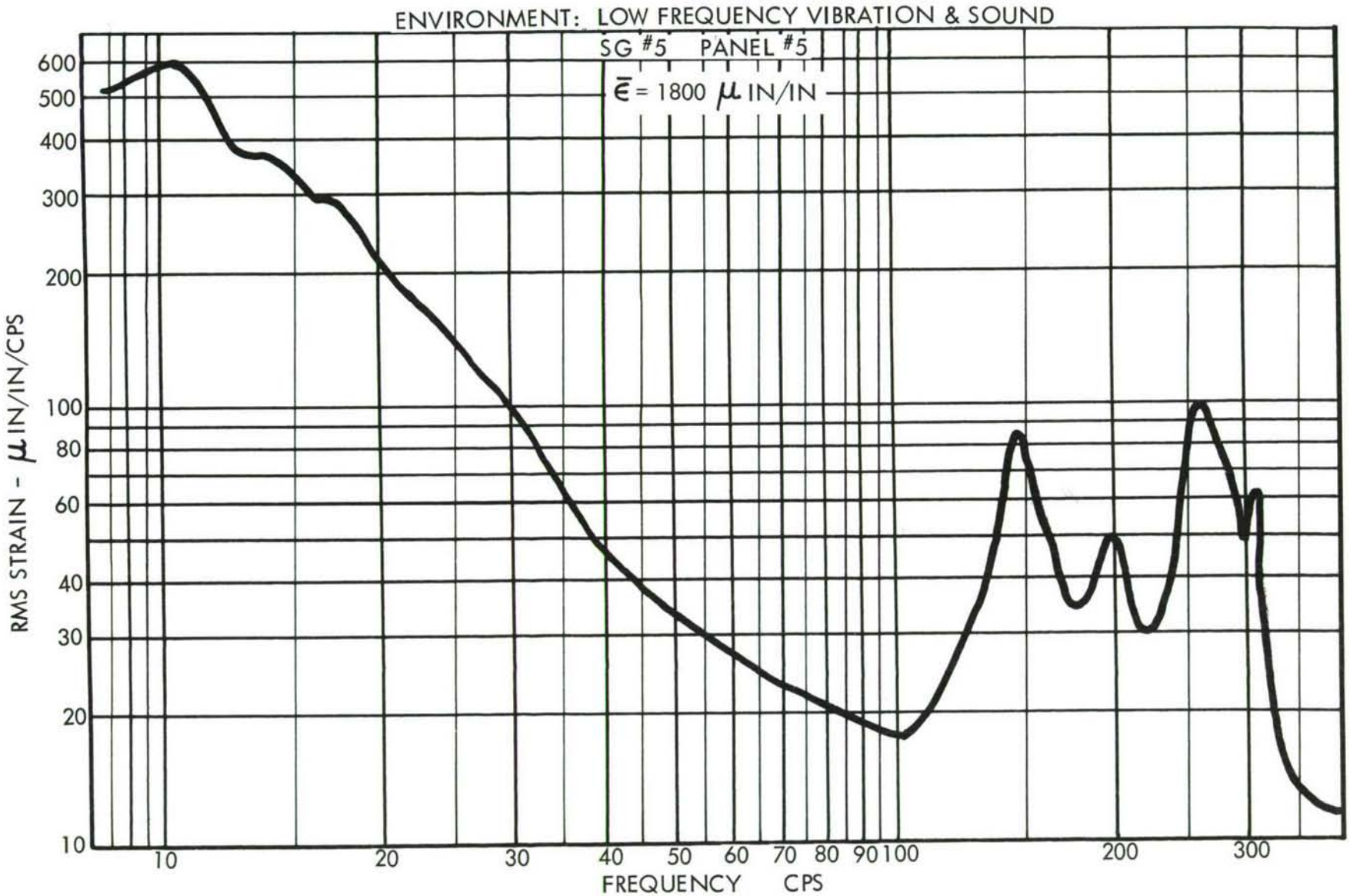

FIGURE 68. COMPLEX TEST SPECIMEN RESPONSE

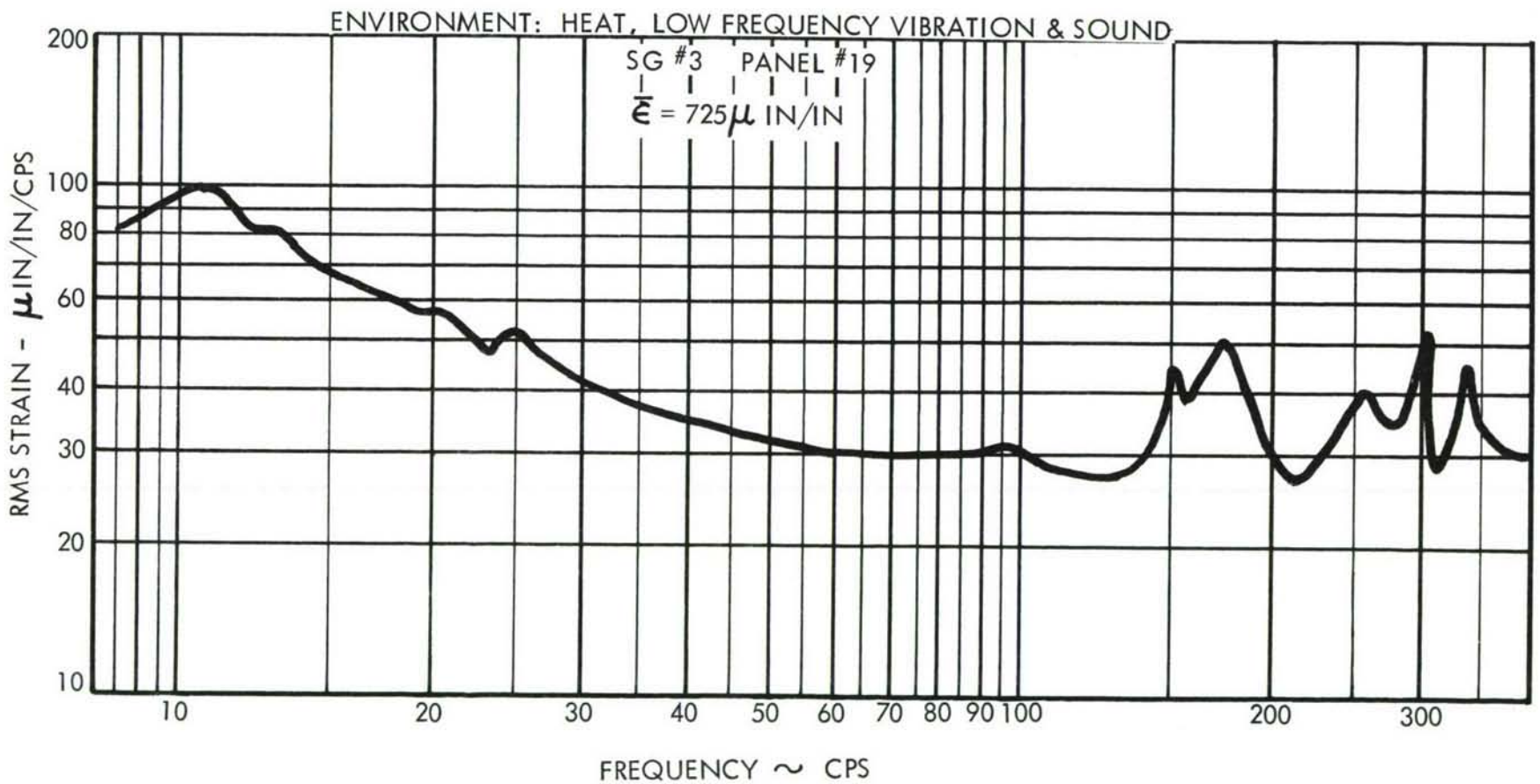

FIGURE 69. COMPLEX TEST SPECIMEN RESPONSE

TABLE 13

SPL MEASURED AT PANEL CENTERLINE

Specimen	*Environment	Overall SPL db	Maximum Value		Total Time at A/B min.	Total Time at 80% Pwr. & Above min.	Remarks
			1/3-OBL db	Frequency cps			
1	A	158	149	1600	300	360.5	
2	A	159	151	630	300	360.5	
3	B	156	146	2500	300	360.5	Separation of edge member at 165 min.
4	B	161	150.5	630	300	360.5	
5	C	158.5	150	315	300	360.5	Back face sheet separated from core at 215 min. Small cracks at 300 min.
6	C	155	152	400	300	360.5	
7	D	159	151	400	300	360.5	
8	D	158	147.5	400	300	360.5	
9	C	156.5	147	400	860	980	Separation of edge member at 180 min.
10	C	155.5	146	250	860	980	Small crack from bolt hole at final inspection.
11	D	155.5	145	160	860	980	Small crack from bolt hole at final inspection.
12	D	157	148	200	860	980	
13	A	157	147.5	250	860	980	
14	A	-	-	-	860	980	Cracks around bolts at final inspection.
15	B	154	145	160	860	980	
16	B	-	-	-	860	980	
17	C	158	149	1600	560	619.5	
18	C	159	151.5	630	560	619.5	
19	D	157	147	3150	560	619.5	
20	D	-	-	-	560	619.5	
21	A	164.5	154	500	560	619.5	
22	A	154	147	400	560	619.5	Small crack from bolt hole at final inspection.
23	B	160.5	153	400	560	619.5	Small cracks from bolt hole at final inspection.
24	B	156.5	148.5	315	560	619.5	Front sheet separated from core at 20 min.

*Note: A - Sound
B - Sound, Heat
C - Sound, Low-Frequency Vibration
D - Sound, Heat, Low-Frequency Vibration

TABLE 14

STRAIN MEASURED AT CENTERLINE OF CURVED HONEYCOMB SANDWICH PANELS

Specimen No.	*Environment	RMS Strain μ in/in/cps	Strain at Significant Frequencies					
			RMS Strain μ in/in/cps	Frequency cps	RMS Strain μ in/in/cps	Frequency cps	RMS Strain μ in/in/cps	Frequency cps
1	A	450	--	--	90	150	62	250
2	A	200	--	--	30	140	32	255
3	B	275	--	--	30	160	30	240
4	B	400	--	--	36	155	24	240
5	C	1800	600	11	90	145	100	260
6	C	1500	470	11	45	140	190	260
7	D	1300	80	11	250	165	120	240
8	D	--	--	--	--	--	--	--
9	C	1600	540	11	18	160	82	270
10	C	1250	500	11	24	170	90	260
11	D	--	--	--	--	--	--	--
12	D	--	--	--	--	--	--	--
13	A	--	--	--	--	--	--	--
14	A	750	--	--	38	150	32	250
15	B	--	--	--	--	--	--	--
16	B	--	--	--	--	--	--	--
17	C	1900	600	11	68	150	55	260
18	C	2110	750	11	70	160	110	270
19	D	725	100	11	50	175	40	250
20	D	825	150	11	42	160	50	250
21	A	1125	--	--	140	150	260	260
22	A	--	--	--	--	--	--	--
23	B	1000	--	--	100	160	52	250
24	B	--	--	--	--	--	--	--

*Note: A - Sound
B - Sound, Heat
C - Sound, Low Frequency Vibration
D - Sound, Heat, Low Frequency Vibration

Figures 70 through 73 show the probability distribution of strain peaks for the various combinations of environment. It can be seen that the distribution is essentially Rayleigh because the points determined from experimental data lie near the Rayleigh distribution line for peak-to-rms ratios up to three.

C. Comparison of Theoretical and Experimental Results

As a means of confirming the theoreitcal frequency analysis for tapered edge sandwich panels, one of the titanium panels used in the tests described in Section III.B was tested to determine natural frequencies.

The method adopted for experimentally determining natural frequencies was visual observation of Chladni (nodal) patterns of the panel when excited acoustically. An aluminum frame with overall dimensions of 24" x 30" and a cross-section of 1" x 4" was used to clamp the edges of the panel. This frame-panel combination made up the front wall (grill-cloth side) of a dual speaker enclosure. The surface of the panel was four inches from the two 15" Altec 605A loudspeakers. The speakers were electrically connected so that the phasing could be reversed. This allowed determination of some of the even modes.

The edge frame was rigid enough to stabilize the panel; however, it did not produce clamped edge boundaries.

The experimental edge condition was probably closer to simply-supported than clamped as verified by the test comparison.

Panel dimensions, physical constants, and elastic constants were

$$\ell_1 = 0.75", \ \ell_2 = 22.00", \ \ell = 22.75"$$

$$b_1 = 0.75", \ b_2 = 28.00", \ b = 28.75",$$

$$h_1 = 0.100", \ h_2 = 0.008", \ h_3 = 0.008", \ h_4 = 0.020"$$

$$\rho_1 = 5.25 \times 10^{-6} \ \#\text{-sec}^2/\text{in}^4, \ \rho_2 = \rho_3 = \rho_4 = 4.15 \times 10^{-4} \ \#\text{-sec}^2/\text{in}^4$$

$${}_1G_{xz} = 11{,}000 \text{ psi}, \ {}_1G_{yz} = 21{,}500 \text{ psi}$$

$$E_2 = E_3 = E_4 = 1.6 \times 10^7 \text{ psi}, \ \nu_2 = \nu_3 = \nu_4 = 0.322$$

The facing sheets were 6Al-4V titanium and the core was polyester honeycomb. The edge member was a laminate of 6Al-4V titanium and fiberglass. For calculation purposes, it was considered to be titanium alone because the fiberglass does not contribute significantly to the total stiffness.

The following table shows calculated and measured natural frequencies.

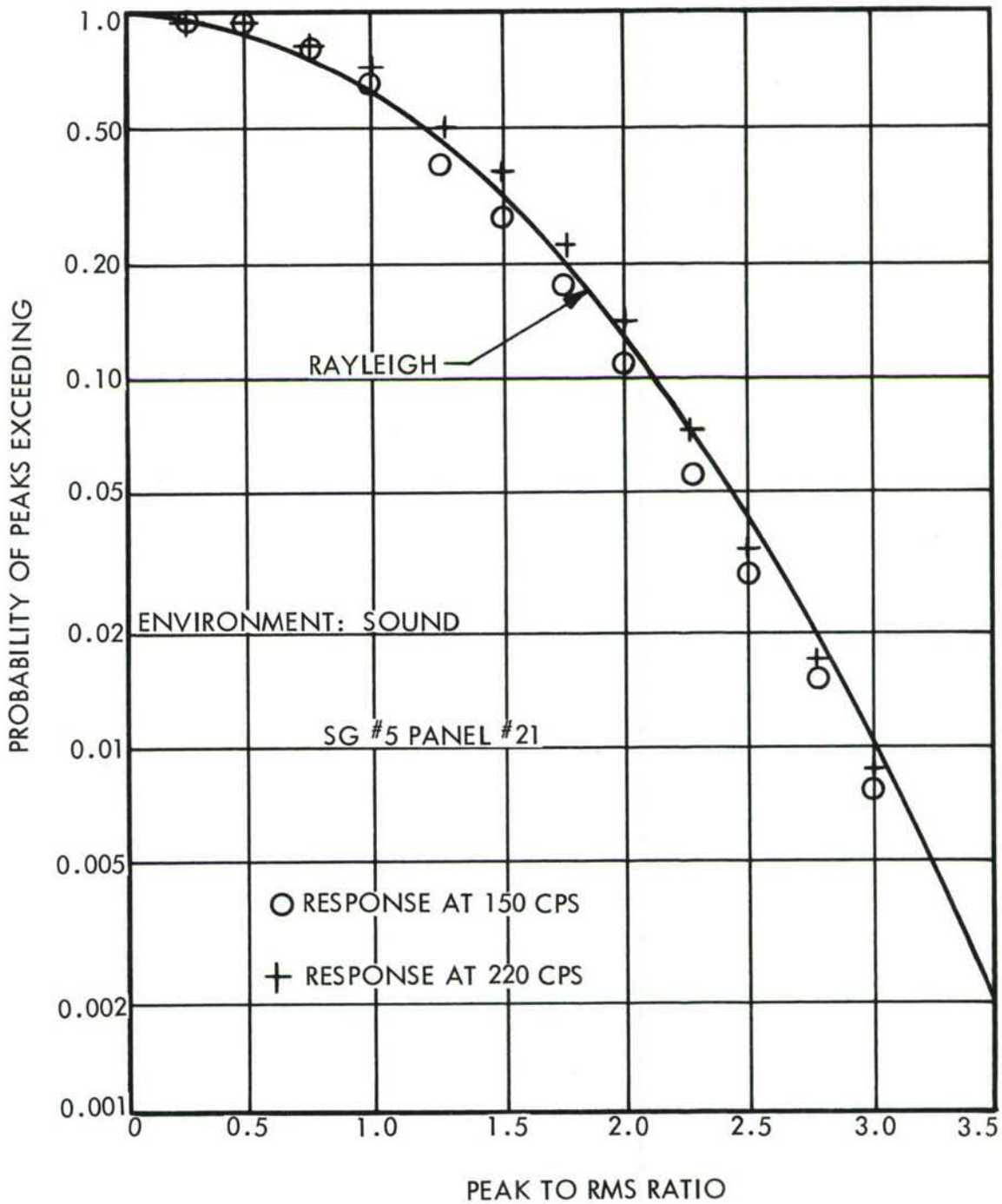

FIGURE 70. PROBABILITY DISTRIBUTION OF STRAIN PEAKS

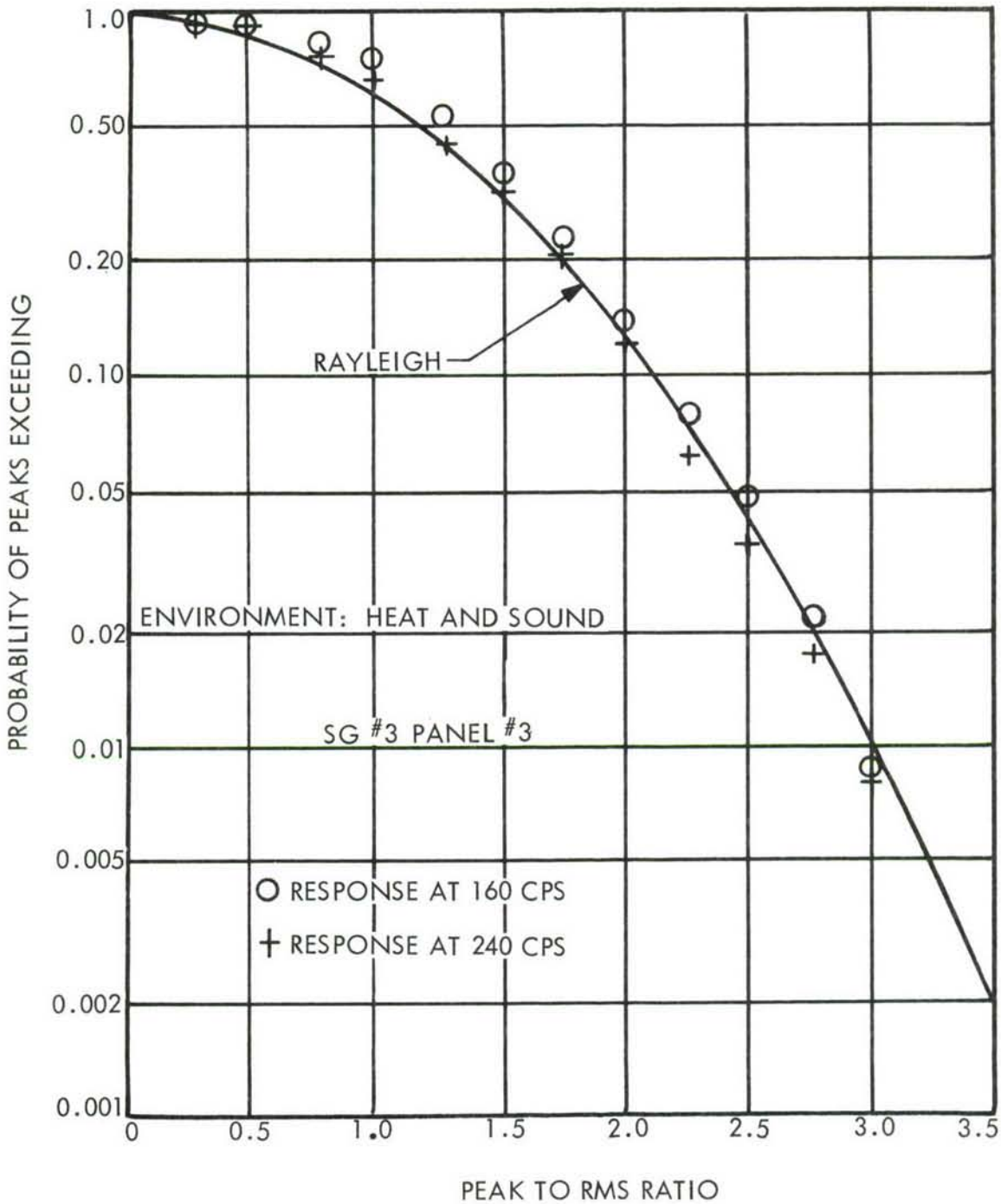

FIGURE 71. PROBABILITY DISTRIBUTION OF STRAIN PEAKS

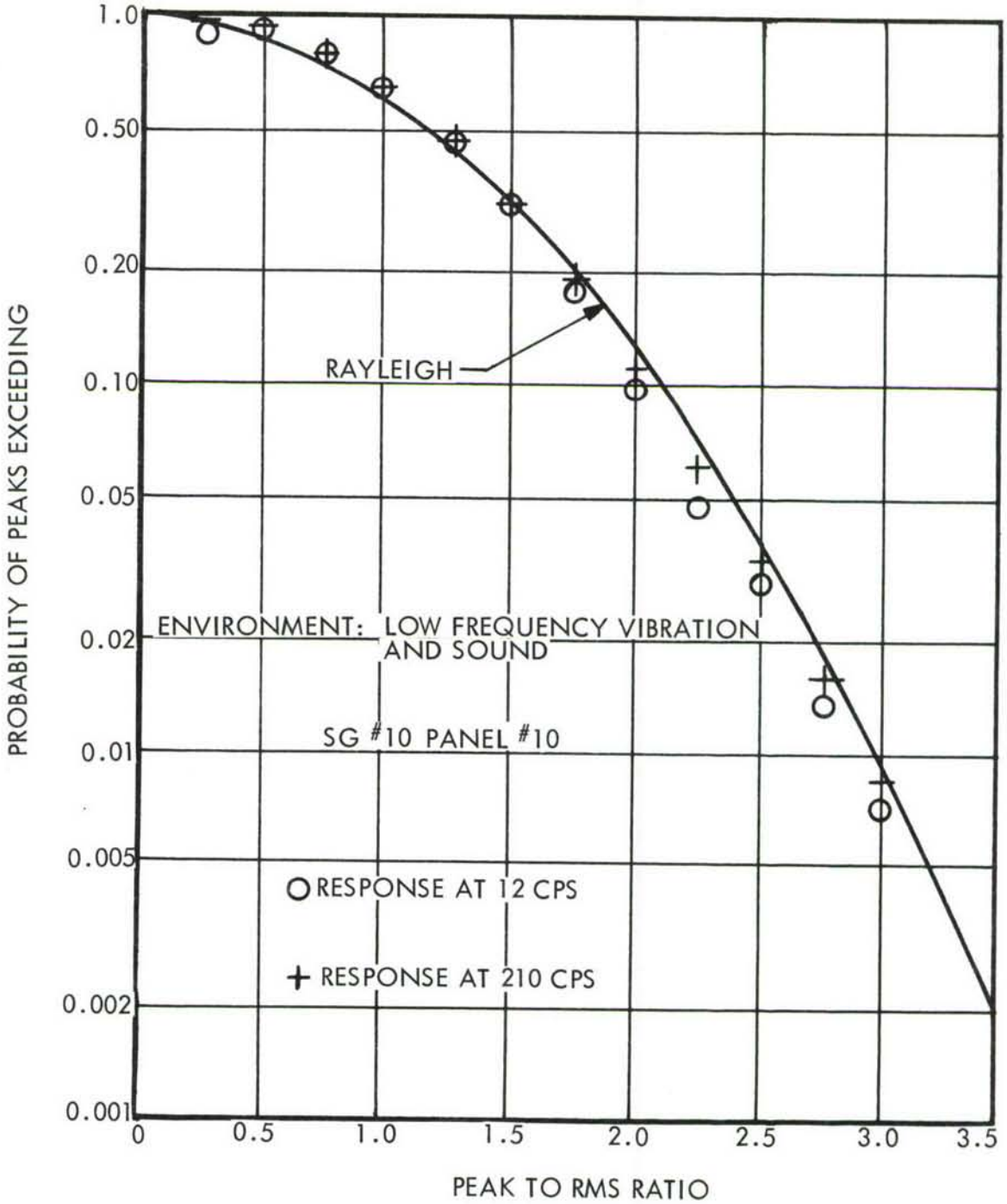

FIGURE 72. PROBABILITY DISTRIBUTION OF STRAIN PEAKS

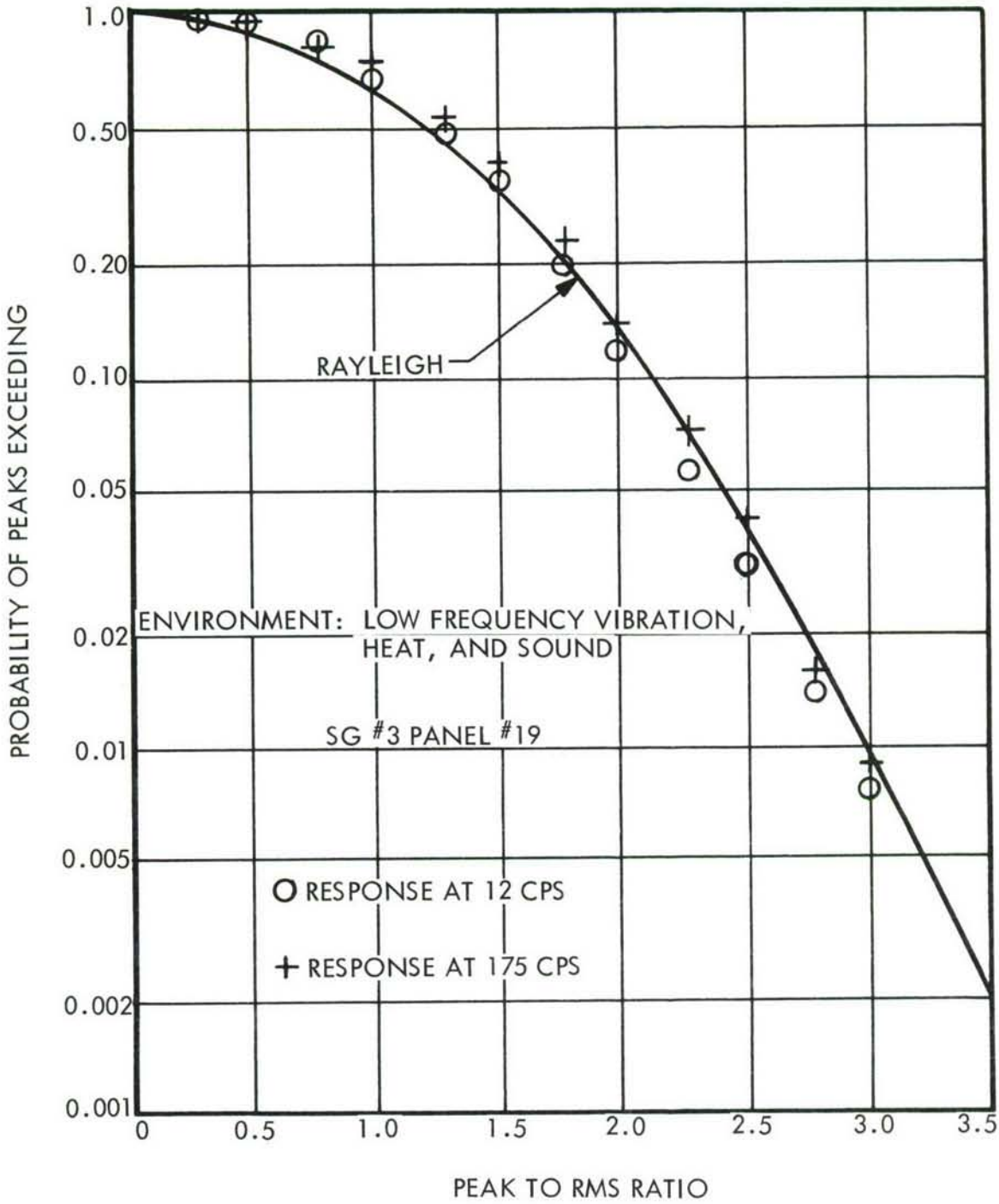

FIGURE 73. PROBABILITY DISTRIBUTION OF STRAIN PEAKS

TABLE 15

NATURAL FREQUENCIES OF TITANIUM SANDWICH PANEL

n	m	1	2	3	
1		246.0 204	399.0 347	593.1 617	Calculated Experimental
2		219.0 219	412.6 -	642.6 627	Calculated Experimental
3		364.5 369	521.4 484	750.9 -	Calculated Experimental

Although the theory-experimental agreement is good for a majority of the modes, it is believed that differences in the higher modes are due to inaccuracies in the transverse shear moduli for the honeycomb core. In the next section, the effect of transverse shear modulus on natural frequency is shown.

Also, as stated earlier, the actual boundary conditions of the test panel were not the same as the boundary conditions of the theory. This is the most probable cause of the differences between theoretical and experimental values in the lower modes.

D. Discussion of Results

1. Theoretical Results

A number of parameter variation studies were made to assess the importance and the effects of individual parameters on the natural frequencies. To keep the studies simple, only one parameter was varied for each study. All variations were made around the basic panel design used for comparison of theory and experiment. Some parameters such as core thickness and radius are extremely influential in the determination of frequency, whereas others such as tab width have only secondary effects. The effect of these parameters on natural frequency will be discussed in the following section.

a. Core Transverse Shear Modulus of Elasticity. In general, experimental values of transverse shear modulus have not been very reliable. It is probably the most difficult parameter to accurately measure of all the parameters associated with a honeycomb sandwich design. For this reason, the effects of this parameter are considered to be very important.

Two parametric studies were made in assessing the effects of shear modulus. In one case, the two shear moduli, G_{xz} and G_{yz}, were set equal and varied over the range of 100 to 1,000,000 psi. The variation of modal frequency with shear modulus is shown in Figure 74.

One very important conclusion gained from this investigation is that core shear modulus has only a minor effect on the natural frequency of the first mode. It

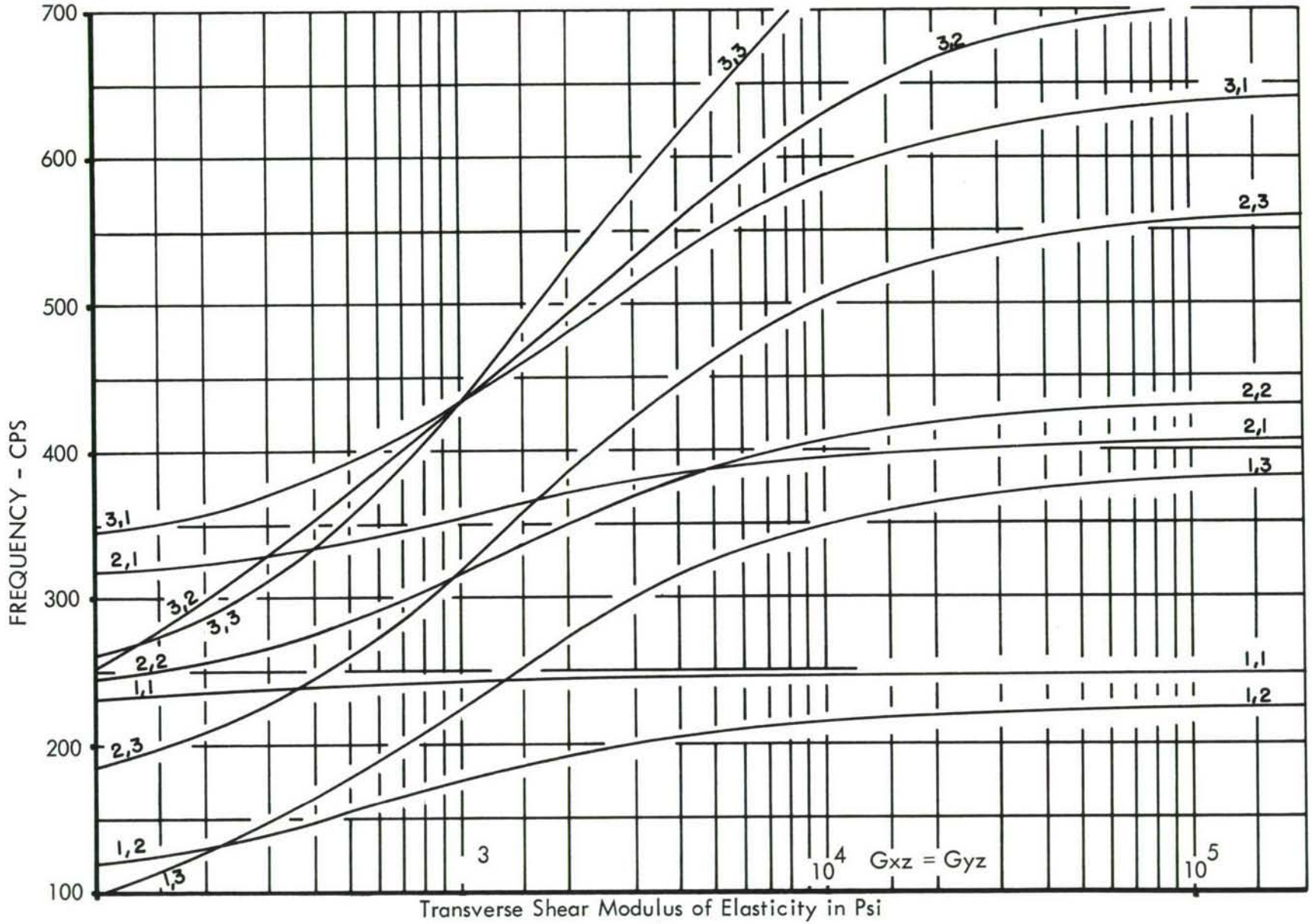

FIGURE 74. EFFECT OF VARIATION OF TRANSVERSE SHEAR MODULUS

serves only as a means to separate the two facing sheets. This implies, that for practical purposes, theories which define first resonance, neglecting transverse core shear, will give acceptable results. This is substantiated for flat panels by Sweers (Reference 19).

The effect of transverse shear modulus on high frequency modes is appreciable. In this case, low values of transverse shear modulus tend to cause a decrease in resonant frequencies. The frequencies are considerably lower than those calculated by a theory which neglects the transverse shear modulus. In Reference 19, the following simple equation for calculating natural frequency is given:

$$f_n = \frac{\pi}{2}\sqrt{\frac{D}{\rho}}\left[\left(\frac{n}{b}\right)^2 + \left(\frac{m}{\ell}\right)^2\right]$$

where

$$D = \frac{(2h_1 + h_2)^2 h_2 E}{2(1 - \nu^2)}$$

Higher mode frequencies for values of transverse shear modulus above 100,000 psi could be calculated using the simple frequency analysis shown above. In instances where the core has a weak transverse shear modulus the theory needs refining.

Reduction of the basic curved design used in these parameter studies to a flat panel gives a calculated 1,1 mode of 92.6 cps and 721 cps for the 3,3 mode frequency. The simple theory gives 106 cps for the 1,1 mode and 954 for the 3,3 mode. Although this is a relatively thin panel with high shear modulus, the effect can still be observed. The ratio of simple theory to complex theory for the 1st mode is 1.15 while it increased to 1.32 for the 3,3 mode. If, instead of the high strength fiberglass core, a core with shear modulus of 1,000 psi had been used, the above comparison would show an error factor of approximately two.

Another interesting effect is observed by holding G_{xz} constant at 11,000 psi (the basic design value) and varying G_{yz} from 2000 to 500,000 psi, Figure 75. The results are similar to Figure 74. The investigation emphasizes the importance of core weakness and shows that a core which is weak along one transverse axis will have lower natural frequencies in the higher modes than an isotropic core.

b. Effect of Curvature. Curvature is the most significant parameter from the standpoint of its effect on frequency. In Figure 76, the radius is varied over a broad range about the basic panel design radius of 84 inches, at a radius of 9 inches and an arc length of 27.25 inches, the basic panel design will subtend an angle of 180 degrees. The radius-to-thickness ratio in this case is greater than 40; therefore, the approximation of plane sections remaining plane after deformation is valid.

At a radius of 1,000", the panel is flat for all practical purposes. As expected, the lowest frequency mode is the 1,1 or fundamental. At the basic panel design radius of 84 inches, the 1,2 mode has the lowest frequency with the fundamental modal frequency being slightly higher. This "cross-over" effect was noted by Arnold and Warburton in a theoretical study of the natural frequencies of thin

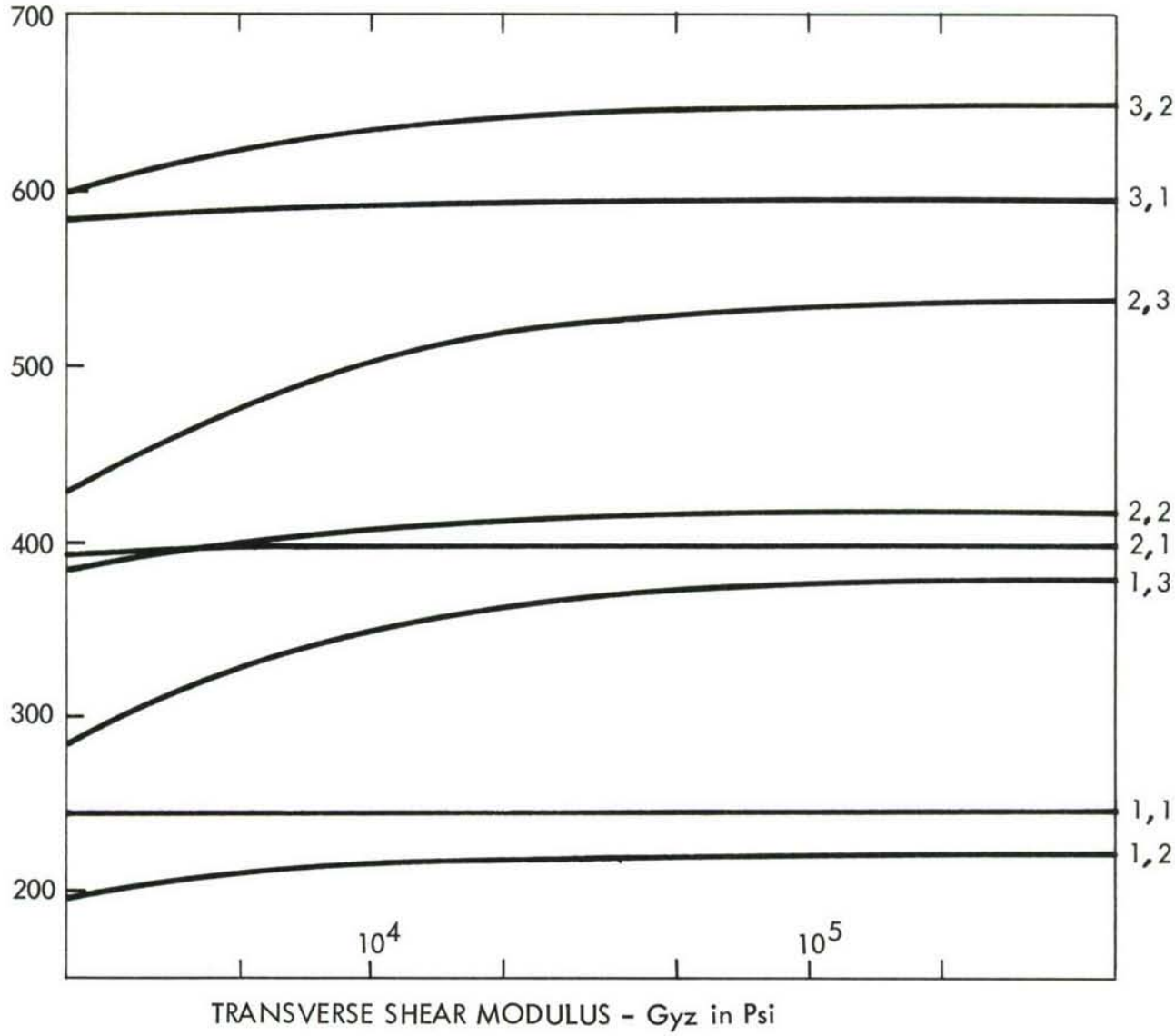

FIGURE 75. EFFECT OF ONE-DIMENSIONAL VARIATION OF TRANSVERSE SHEAR MODULUS

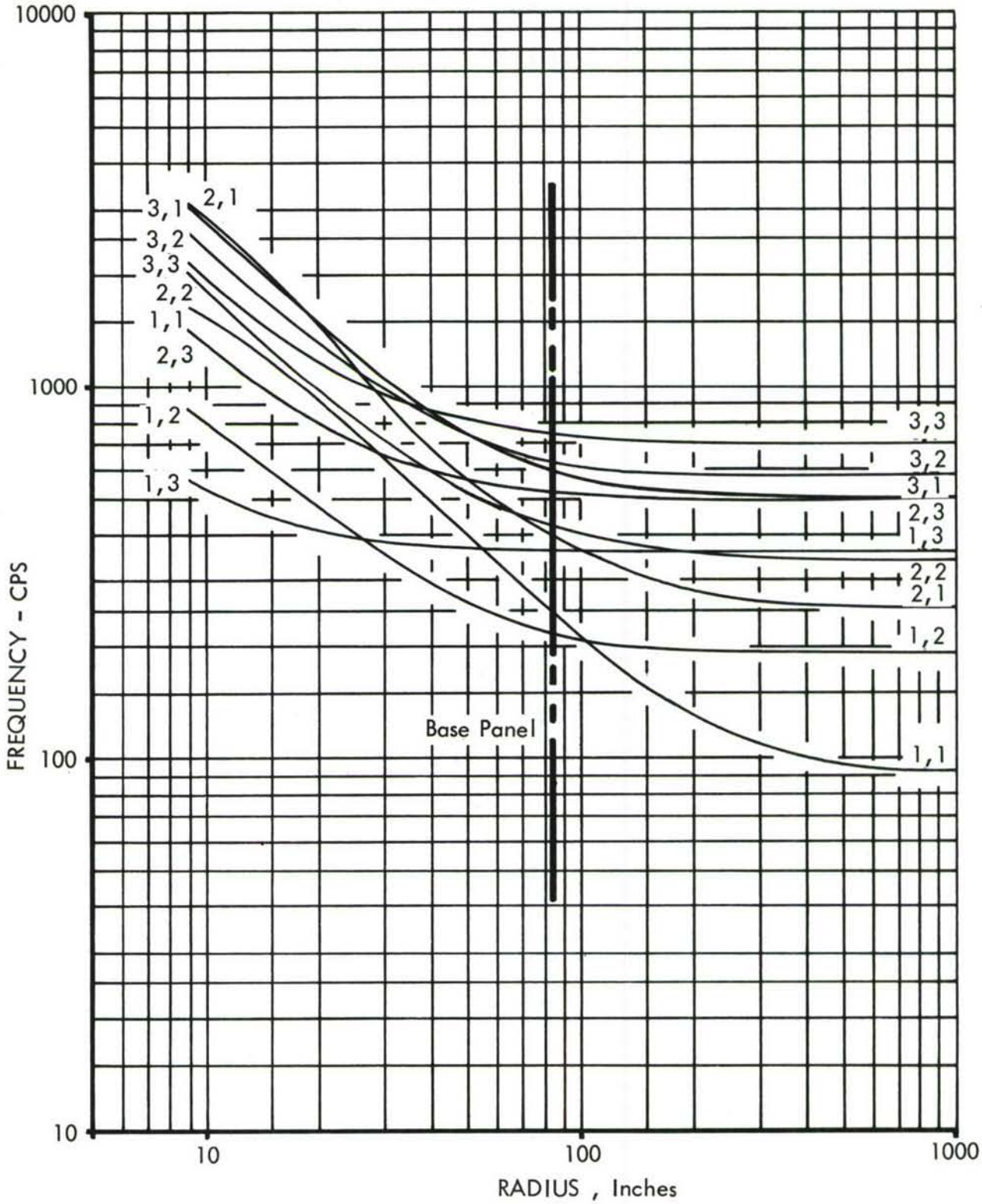

FIGURE 76. EFFECT OF CURVATURE

cylinder (Reference 20). The experimental results do not demonstrate the "cross-over" predicted by theory. The 1,1 mode was measured at 204 cps and the 1,2 mode was 219 cps so the trend to cross-over is evident in the results.

Examination of the curves in Figure 76 reveals that modal frequencies which have node lines parallel to the straight edges of the panel (1,2 and 1,3) are insensitive to a change in radius as compared to modal frequencies with node lines parallel to the curved edges (2,1 and 3,1).

c. Effect of Core Thickness. The simple theory for flat panels included in the discussion of shear modulus is of the following form, provided core thickness is the only variable:

$$f_n = C_n(2h_1 + h_2)$$

This relationship is plotted in Figure 77 for the first mode frequency. The constant C was determined using the base panel first modal frequency. In comparing this simple relationship to the thickness effects calculated with the theory of Section III.A, it is seen that the above equation does not provide a first order approximation of the actual results for the lower order modes. The slope of the higher modes does approach that of the linear approximation for an intermediate range of core thickness.

Actually, the first mode frequency variation shown in Figure 77 should probably be attributed to curvature rather than thickness for thickness less than 0.3".

This phenomenon has also been noted in frequency calculations of thin shells where it was observed that the "cross-over" was more predominate for thinner shells.

It is interesting to note that higher modes, which were not affected by curvature, for instance the 1,3 mode, have approximated the same slope as that of the linear relationship. The slope at higher thickness is attributed to transverse shear effects.

d. Effect of Skin Thickness. The express purpose of the core in a honeycomb sandwich is to stabilize the facing sheets in creating a rigid, light-weight structure. In designing the honeycomb sandwich panel it is desirable to create the greatest stiffness-to-weight ratio possible in order to decrease the bending stresses. Therefore, an item for assessing a honeycomb panel design is its stiffness-to-weight ratio. In the simple flat honeycomb panel theory, the natural frequency is proportional to $\sqrt{D/\rho}$. For very thin faces, where the core controls panel weight, the frequency varies approximately as the square root of face thickness. In the mid-range, the frequency is nearly independent of face thickness and when skin thickness approaches the order of magnitude of core thickness, the frequency approaches a linear variation.

The effects described above are somewhat different for the curved honeycomb sandwich panel. Examination of the curves in Figure 78 shows that frequency at first increases with skin thickness, then peaks and subsequently decreases for increases in facing thickness. It is the peak in frequency that is of significance in structural design. The peak in frequency represents the most efficient structure from the standpoint of rigidity.

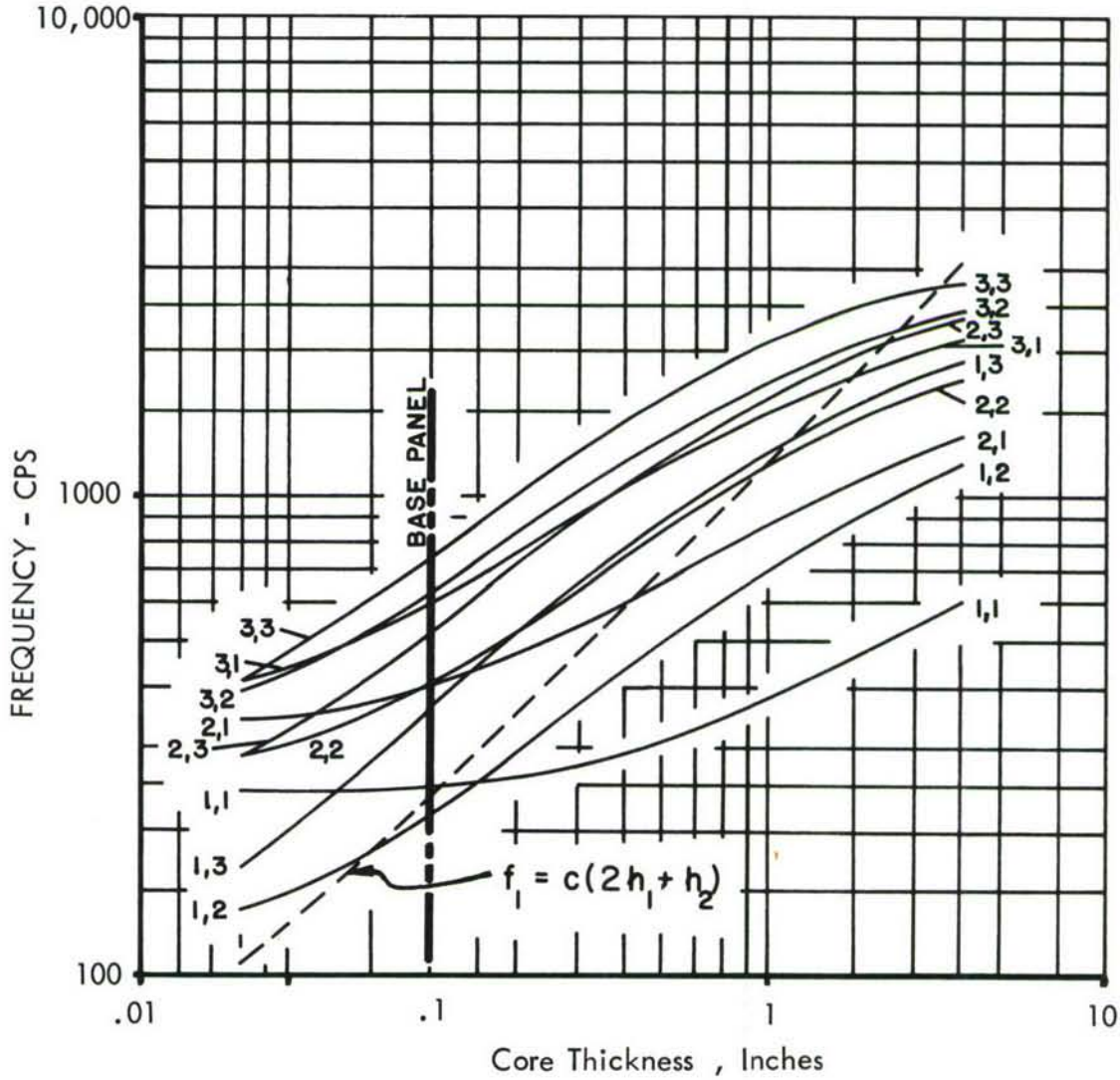

FIGURE 77. EFFECT OF CORE THICKNESS

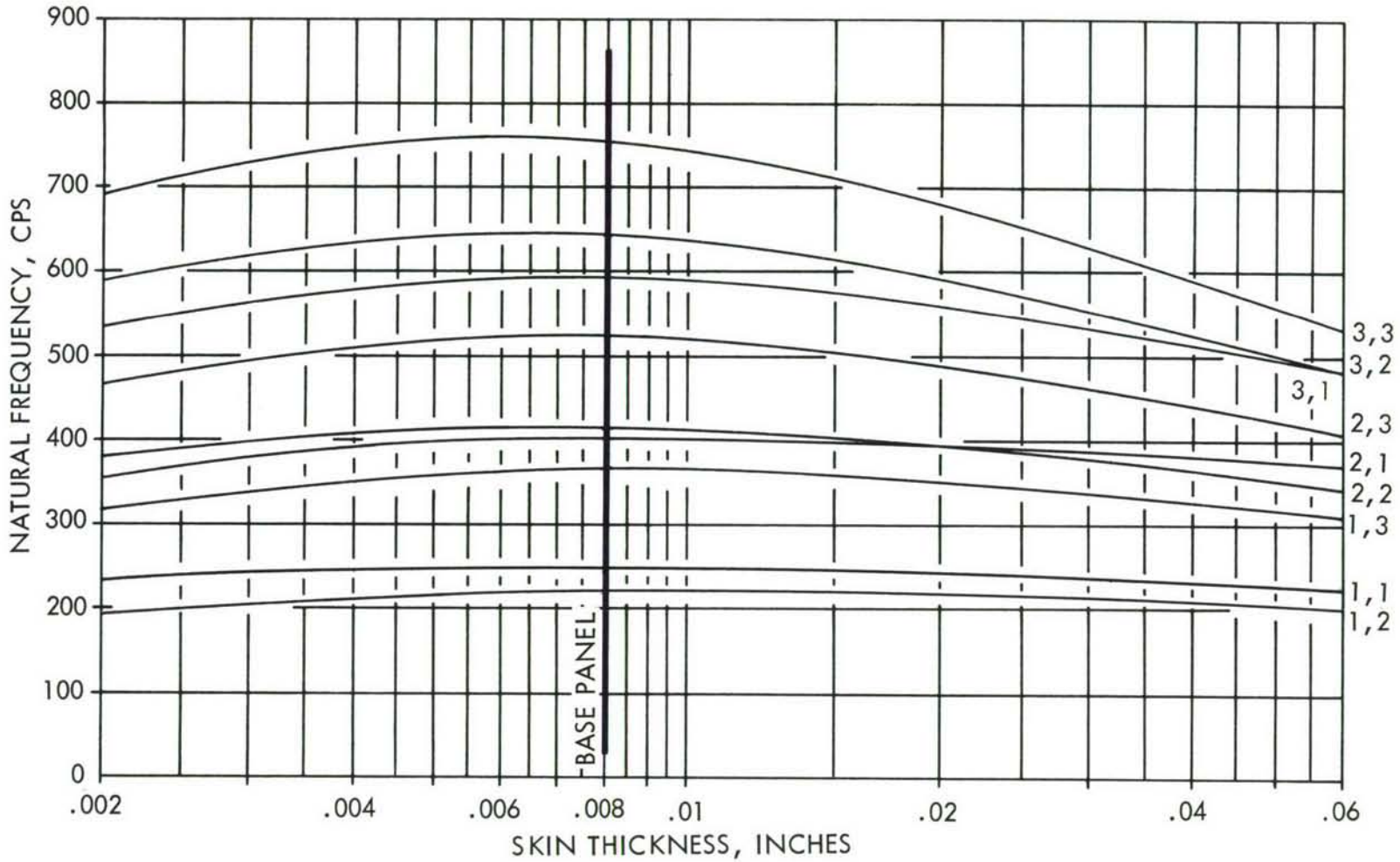

FIGURE 78. EFFECT OF SKIN THICKNESS

Another interesting aspect of the effect of face thickness is concerned with the ratio of inner skin to outer skin thickness. In Figure 79, it is seen that if both skins are of approximately the same thickness the natural frequencies are highest indicating the highest "dynamic stiffness." This is also indicative of efficiency in design.

2. Experimental Results

a. Test Specimen. The test specimen for the complex specimen investigation was designed using an engineering approach. State-of-the-art design criteria were taken from Reference 17 to initially set the dimensions. The design nomographs from Reference 17 were modified as described in Appendix I to account for curvature effects and the effect of elevated temperature on fatigue life. Extrapolation of the nomograph of Reference 17 was necessary to obtain a design.

A "pilot model" of the design was made and tested in the High Intensity Sound System Facility to experimentally determine the fatigue life of the design. It was exposed to 30 hours of broad-band acoustical noise at an overall sound pressure level of 160 decibels without a significant failure. The "pilot model" design was too strong so it was weakened using the strain data, etc., from the test to scale it down. As a result, the facing sheets were reduced from 0.01" to 0.008" and the edge doubler was also reduced from 0.01" to 0.008". The total metal thickness at the edge was 0.016". From the production point of view, most of the design details were minimal. The test specimen had an average surface weight of 0.6 pound per square foot, which is less than most structural components designed to withstand environmental conditions comparable to those of this test.

b. Test Fixture. The test fixtures were designed to provide peripheral support for the test specimens representative of flight vehicle installation. In addition, fixture flexibility was necessary to transmit bending and shear loads produced by the electro-hydraulic shaker to the honeycomb sandwich panels. The test fixtures were designed to hold four specimens at one time so that each environmental condition could be evaluated simultaneously to minimize the test time and cost.

During the fatigue tests at Wright Field, Ohio, a few of the fixture test specimen support structures experienced fatigue cracks. These support members were replaced with a like part and the tests were continued. Stop drilling was also used but only as a temporary measure. The cracks are believed to have been caused by a horizontal component of the low-frequency vibratory force resulting from lateral vibration of the test fixtures. This lateral vibration was produced by jet efflux buffet and was not accounted for in the stress analysis.

c. Acoustical Noise Environment. Figures 63 through 65 show the 1/3-octave band sound pressure levels in the range of significant test specimen response was about 140 decibels. The maximum acoustical energy, in most cases, appeared at frequencies above 315 cps. This is well above the frequencies demonstrating the greatest test specimen strain response. Downstream from the engine nozzle, Fixtures 3 and 4 positions, the acoustical energy peaked at lower frequencies, 250 cps. Jet efflux buffet of the fixture was an undesirable feature of these locations, however.

A comparison of the sound pressure levels from the near-field noise survey contained in Table 11 with those made at the surface of the test specimens, Table

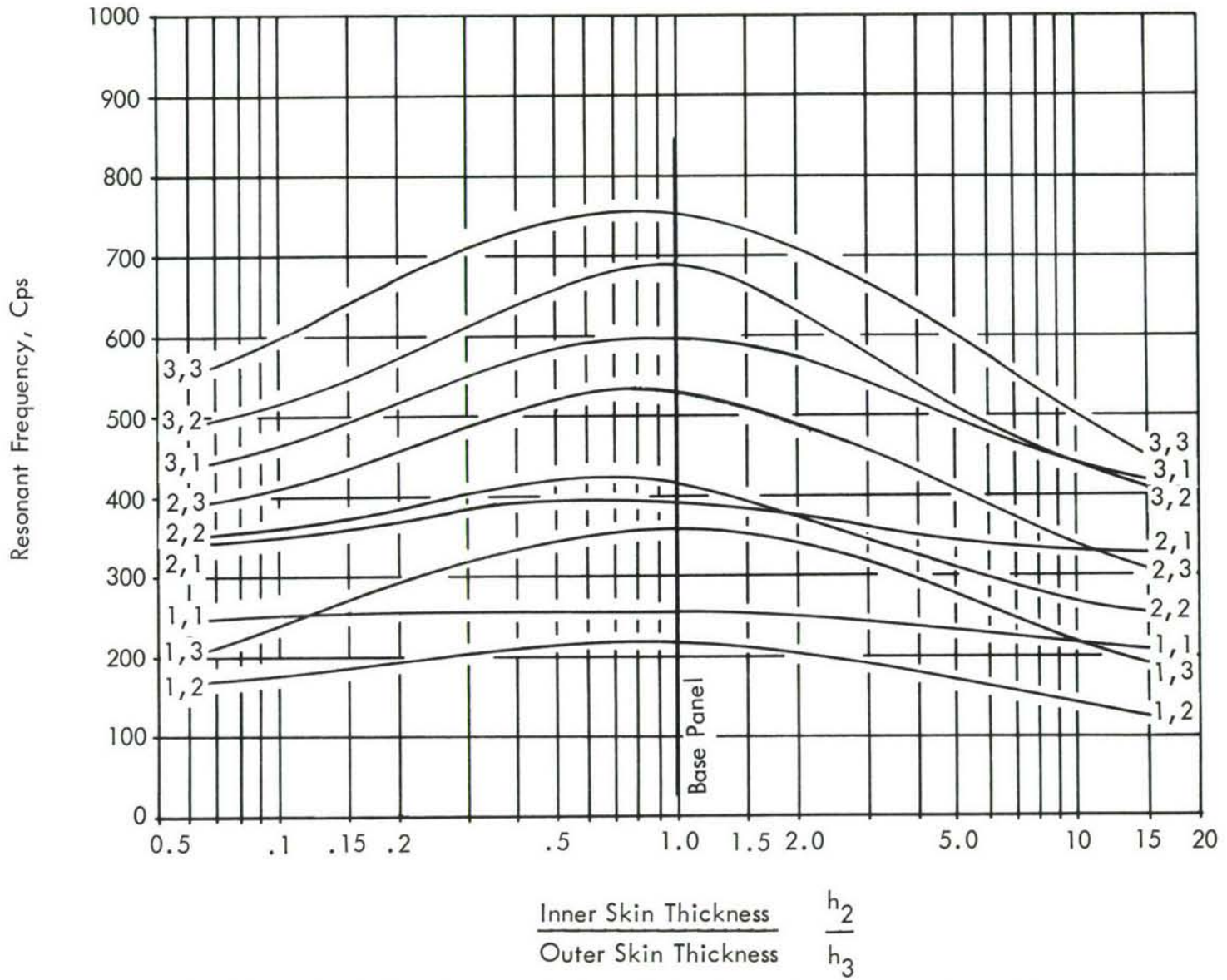

FIGURE 79. EFFECT OF VARYING RATIO OF INNER SKIN THICKNESS TO OUTER SKIN THICKNESS

13, reveals that the near field survey 1/3-octave band levels were higher. The difference is attributed to three things:

- Condenser microphones were used for the near-field noise survey and piezoelectric microphones were used for test monitoring purposes.

- Ambient temperatures were greater for the fatigue tests than for the near-field noise survey so the acoustical noise output of the J-57-P21 turbojet engine was greater during the near-field noise survey.

- The near-field noise survey was made in the absence of reflective surfaces, except the concrete ground plane, whereas the test fixtures provided reflective surfaces during the fatigue tests.

d. Test Specimen Strain Response. A study of Figures 66 through 69 shows four distinct strain response patterns. Figure 66, the specimen response to acoustical noise, shows the greatest response occurred at 160 cps or the (1,1) mode with some activity in the (2,1) mode, 250 cps, and the (1,3) mode, 300 cps. When heat was applied to the test specimen the strain response was diminished in the (1,1) mode, (2,1) mode, and (1,3) mode, as shown in Figure 67. Also, the frequency of each mode was lowered significantly at the 400° F temperature as was the case for the elevated temperature sonic fatigue tests of the simple titanium panels described in Section II.B. Figure 68 shows the response of the low frequency random vibration and acoustical excitation was the response of the test specimen to the low frequency random excitation superimposed on the response due to acoustical excitation. The strain was quite large at 12 cps and the (1,1) mode was about the same as that for acoustical excitation alone. Effect of all three environments is shown in Figure 69. The strain response had the same general appearance as that shown on Figure 67 except the strain at 12 cps is considerably higher because of the low frequency random loading.

The higher modes such as (2,1) and (1,3) had magnitudes almost equal to and in one case greater than the magnitude of the (1,1) mode. The higher modes were influenced by the unequal distribution of acoustical energy in that their excitation was 3 to 5 decibels more than the (1,1) mode excitation.

e. Probability Distribution of Strain Peaks. Probability distribution of strain peaks was determined from strain data recorded during the fatigue tests. Figures 70 through 73 are the probability distribution plots for each of the environmental conditions. It can be deduced from these probability distribution plots that the strain peaks for all environments had a distribution which differed only slightly from a Rayleigh. The strain peaks for the higher modes did not differ appreciably from the fundamental mode, and the strain peak distribution at 12 cps was very nearly Rayleigh.

f. Fatigue Test. There are four possible modes of fatigue failure for honeycomb sandwich. Cracks may form at the fastener holes around the edge of the panel, cracks may form in the facing sheets, the honeycomb core may experience shear fatigue, and the facing sheet may separate from the core (bond failure).

The test specimens experienced two of the four types: core-to-facing sheet bond failure and cracks at fastener holes. The most common type of failure experienced in flight vehicle service, facing sheet cracks, was not produced even though the specimens were subjected to extremely severe test conditions. Only nine of the

twenty-four test specimens were damaged. If fatigue damage is used as a criterion for measuring the severity of each environmental condition, the following categories of severity can be devised. First, the most severe environment, according to the number of fatigue failures and time-to-failure, is heat and acoustical excitation. Three of the nine failures took place under these conditions. Next, the environment of low frequency random vibration and acoustical excitation should be placed in second position even though it also produced three damaged test specimens. (The average time-to-failure was considerably more for this test condition than the average time-to-failure for the environment of heat and acoustical excitation.) Acoustical excitation alone produced two damaged test specimens so this environmental condition should be placed in third position. Finally, one test specimen experienced fatigue cracks when exposed to the three environmental factors simultaneously.

Before the tests were conducted, it was believed that the environment comprised of heat, acoustical excitation, and low frequency random vibration would be the most severe. No explanation can be offered, but there is some evidence that the combined environment is less severe than the other environmental conditions. For example, test specimens 7 and 8, Figure 57, were mounted in Fixture #3 during the first part of the test program and were exposed to the combined environment for over 300 minutes without failure. These specimens were removed and test specimens 23 and 24 were mounted in their place. The electro-hydraulic force system was also removed and then attached to Fixture #1. Consequently, test specimens 23 and 24 were subjected to heat and acoustical excitation only. After 20 minutes of testing, one of the facing sheets of test specimen 23 separated from the honeycomb core producing a core bond failure. When the final inspection was made, test specimen 24 had cracks around the fastener holes.

It was not possible to correlate time-to-failure with the environmental conditions, so sonic fatigue tolerance curves are not included. The honeycomb sandwich design, however, looks very promising for use in design of future aircraft. Due to its light weight, approximately 0.6 pound per square foot, and apparent high resistance to sonic fatigue, it would be desirable for high performance flight vehicle structure.

IV

CONCLUSIONS

1. The curved panel frequency analysis theory derived herein yields accurate results, especially for the higher modes.

2. Curvature greatly increases the sonic fatigue resistance of simple panels.

3. The sonic fatigue design nomograph for skin-rib construction which accounts for structural curvature effects will increase sonic fatigue design capabilities and aid in saving flight vehicle weight.

4. Sonic fatigue tests made on 8Al-1Mo-1V titanium alloy and 17-7PH stainless steel flat panels demonstrated that exposure to heat and acoustical excitation simultaneously was many times more severe than exposure to heat and then acoustical excitation alternately.

5. Stresses resulting from acoustical excitation and thermal buckling were the primary cause of the fatigue of the fatigue cracks developed during the elevated temperature tests of the simple panels, not a degradation of fatigue properties due to elevated temperatures. (See Reference 21.)

6. The frequency theory for curved, tapered-edge, honeycomb sandwich panels derived herein is an accurate first step toward improving honeycomb sandwich sonic fatigue design techniques.

7. The complex specimen test program was an undertaking that was much too ambitious. It should have been conducted in several phases, investigating one environment at a time and then all possible combinations.

8. A jet engine is a poor acoustical noise generator for conducting sonic fatigue research investigations because there is no way of controlling the spectrum.

9. An analytical and experimental program should be devised to increase the reliability and range of application of the existing honeycomb sandwich design nomographs.

10. The complex specimen tests showed that lightweight honeycomb sandwich can be designed to withstand environmental conditions expected to be associated with high performance flight vehicles of the future.

V

REFERENCES

1. Nevius, H. E., and Hillis, B. H., "Strain Measurements of Internal Wing Structure During Static Ground Engine Runs of B58A," FZS-4-224, General Dynamics, Fort Worth, Texas, December 1962.

2. Love, A. E. H., The Mathematical Theory of Elasticity, Dover Press, 1944.

3. Felgar, R. P., Jr., "Formulas for Integrals Containing Characteristic Functions of a Vibrating Beam," Circular No. 14, Bureau of Engineering Research, University of Texas, Austin, 1950.

4. Young, D., "Vibration of Rectangular Plates by the Ritz Method," Journal of Applied Mechanics, Vol. 17, 1950.

5. Young, D., and Felgar, R. P., Jr., "Tables of Characteristic Functions Representing Normal Modes of Vibration of a Beam," Engineering Research Series No. 44, University of Texas, Austin, 1949.

6. Sewell, J. L., unpublished report on curved panel vibration, NASA, Langeley, Va.

7. Sokolnikoff, I. S., Mathematical Theory of Elasticity, Second Edition, McGraw-Hill, New York, 1956.

8. Hurty, W. C., and Rubenstein, M. F., Dynamics of Structures, Prentice-Hall, Inc., 1964.

9. Timoshenko, S. P., and Winowsky-Kreiger, S., Theory of Plates and Shells, Second Edition, McGraw-Hill, Inc., New York, 1959.

10. Plumblee, H. E., et al., "Development of Expected Noise Spectra, Siren Programming Techniques, and Experiment Plans for the ASD Sonic Fatigue Facility," ASD-TDR-63-674, August 1963.

11. Schjelderup, H. C., and Karnesky, A. L., "A Combined Analytical and Experimental Approach to AIF," Shock and Vibration Bulletin, Vol. 25, Part II, 49, 1957.

12. Rucker, C. E., "Some Experimental Effects of Curvature on Response of Simple Panels to Intense Noise," Paper presented to Acoustical Society Meeting, May 1964.

13. Hess, R. W., Herr, R. W., and Mayes, W. H., "A Study of the Acoustic Fatigue Characteristics of Some Flat and Curved Aluminum Panels Exposed to Random and Discrete Noise," NASA TN D-1, 1959.

14. Mead, D. J., and Pretlove, A. J., "On the Vibrations of Cylindrically Curved Elastic Sandwich Plates," Aeronautical Research Council, R & M No. 3363, 1964.

15. Freudenthal, A. M., and Bieniek, M. P., "Forced Vibrations of Sandwich Structures," WADD TR 60-307, January, 1961.

16. Plumblee, H. E., "Free Vibrations of a Cylindrically Curved Honeycomb Sandwich Panel with Clamped Edges," Master's Thesis in preparation, M. S. in Eng. Mech., Georgia Institute of Technology.

17. McGowan, P. R., et al., "Structural Design for Acoustic Fatigue," ASD-TDR-62-820, October 1963.

18. Anon., Strength of Metal Aircraft Elements, MIL-Handbook 5.

19. Sweers, J. E., "Prediction of Response and Fatigue Life of Honeycomb Sandwich Panels Subjected to Acoustical Excitation," Acoustical Fatigue in Aerospace Structures, Syracuse University Press, Syracuse, New York, 1965.

20. Arnold, R. N., and Warburton, G. B., "Flexural Vibrations of the Walls of Thin Cylindrical Shells Having Freely Supported Ends," Proc. Royal Society of London, England, Series A, Vol. 197, 1949.

21. Healy, M. S., et al., "The Fatigue Behavior of Materials for the Supersonic Transport," NASA CR-215, April 1965.

APPENDIX I

DESIGN NOMOGRAM MODIFICATIONS

The effect of curvature on stress ratio, expressed by equation (53), Section II.A.3, can be used in conjunction with existing design charts for flat, rib-skin structure. The theoretical values of the constants C and D in (53) do not, however, yield sufficiently accurate results to be applied to a design analysis. If the results of tests described in Section II.B are used to calculate the constants, then a design chart can be produced empirically.

The constants C and D have the following average values determined experimentally:

$$C = 0.006$$

$$D = 0.412$$

Using the above values (53) is presented as a nomogram in Figure I-1. Using a conventional design nomogram for flat panels such as that shown in Figure I-2 (from Reference 17) an estimation of panel dimensions can be obtained. Using these dimensions, a stress reduction ratio due to curvature is calculated from Figure I-1. The procedure is repeated using the material fatigue curves for reduced stress. The calculation is iterative and 2 to 3 iterations should be sufficient for satisfactory convergence.

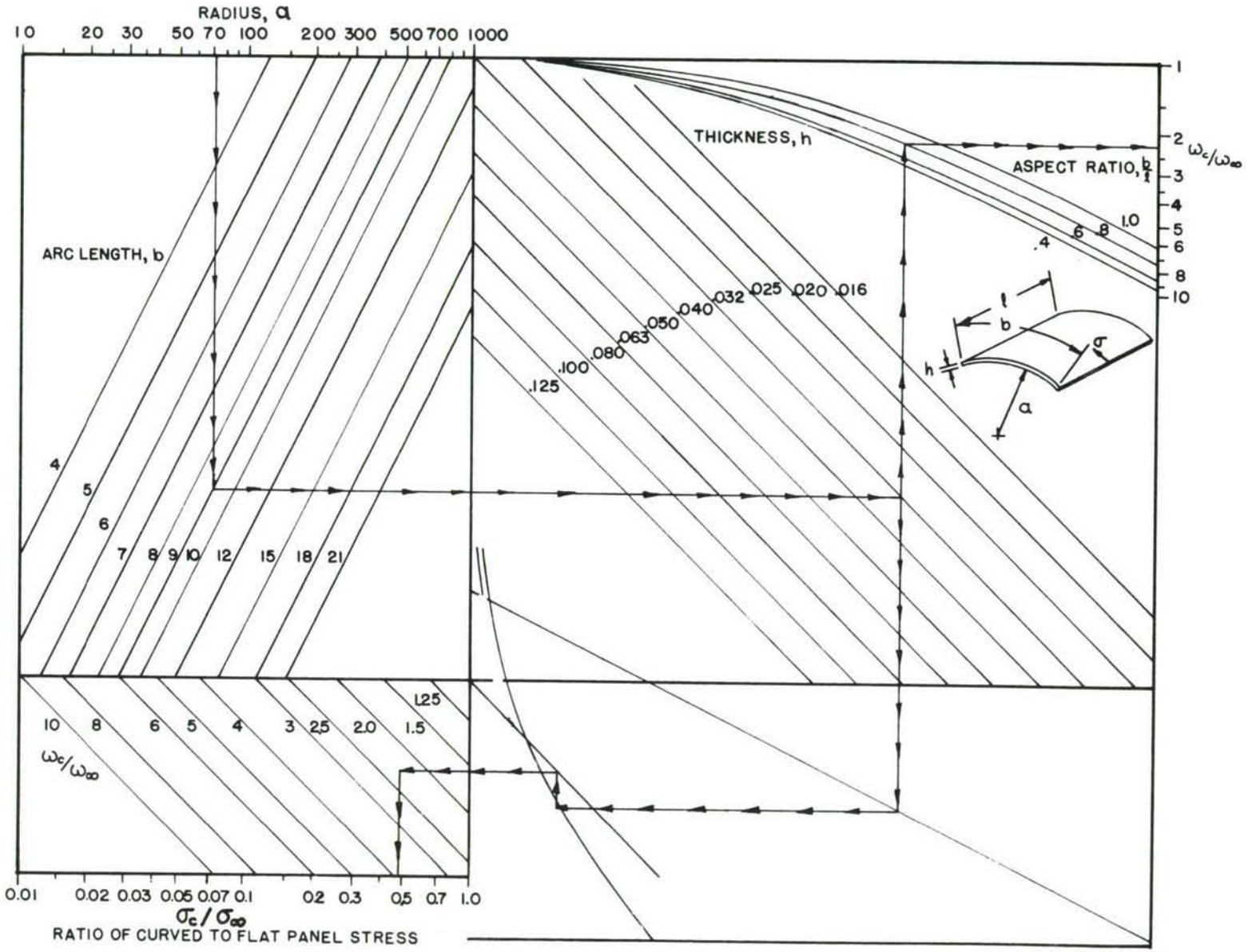

FIGURE 1-1. EFFECT OF CURVATURE ON STRESS RATIO

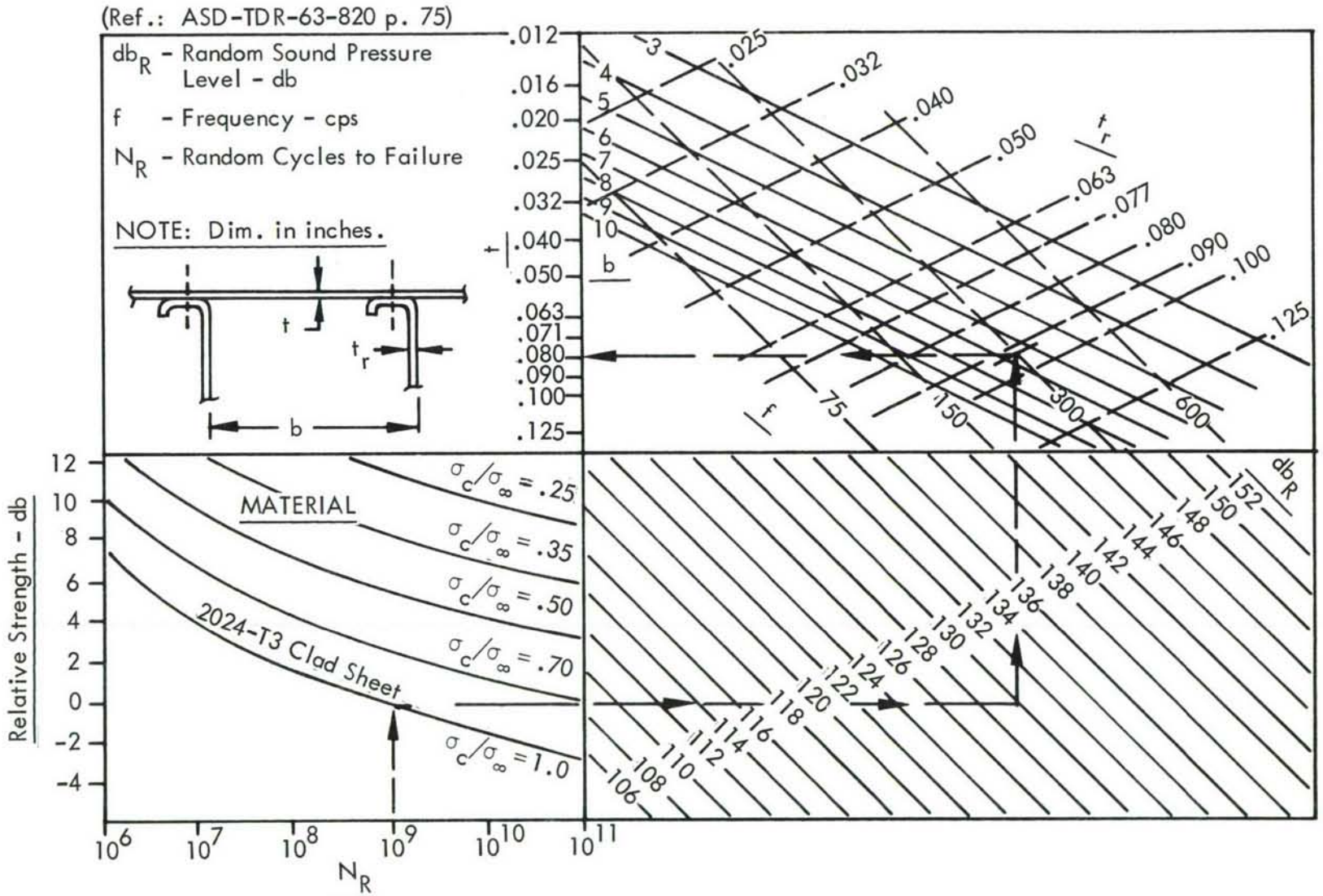

FIGURE I-2 . DESIGN CHART SKIN AND RIB CONSTRUCTION

APPENDIX II

FINAL EQUATIONS

The elements of the K matrices are listed below.

$$
\begin{aligned}
{}_1K_{11} = {} & (2h_1\,{}_1C_{11} + h_2\,{}_2C_{11} + h_3\,{}_3C_{11})\left[\beta_p^2\beta_m^2\,{}_1M_{pm}\left[{}_1N_{qn}\right]\right] \\
& + (2h_1H_1\,{}_1C_{66} + h_2H_6\,{}_2C_{66} + h_3H_{10}\,{}_3C_{66}\left[{}_2M_{pm}\left[{}_2N_{qn}\right]\right]
\end{aligned}
$$

$$
\begin{aligned}
{}_1K_{12} = {} & (2h_1H_2\,{}_1C_{12} + h_2H_5\,{}_2C_{12} + h_3H_8\,{}_3C_{12})\left[\beta_p^2\,{}_1M_{pm}\left[\gamma_n^2\,{}_1N_{qn}\right]\right] \\
& + (2h_1H_2\,{}_1C_{66} + h_2H_5\,{}_2C_{66} + h_3H_8\,{}_3C_{66})\left[{}_2M_{pm}\left[{}_2N_{qn}\right]\right]
\end{aligned}
$$

$$
{}_1K_{13} = -\frac{1}{R}(2h_1H_2\,{}_1C_{12} + h_2H_5\,{}_2C_{12} + h_3H_8\,{}_3C_{12})\left[\beta_p^2\,{}_1M_{pm}\left[{}_1N_{qn}\right]\right]
$$

$$
\begin{aligned}
{}_1K_{14} = {} & -(h_1h_2\,{}_2C_{11} - h_1h_3\,{}_3C_{11})\left[\beta_p^2\,\beta_m^2\,{}_1M_{pm}\left[{}_1N_{qn}\right]\right] \\
& - \left(\frac{4}{3}\frac{h_1^3}{R}\,{}_1C_{66} + h_1h_2H_6\,{}_2C_{66} - h_1h_3H_{10}\,{}_3C_{66}\right)\left[{}_2M_{pm}\left[{}_2N_{qn}\right]\right]
\end{aligned}
$$

$$
\begin{aligned}
{}_1K_{15} = {} & -\left(\frac{2}{3}\frac{h_1^3}{R}\,{}_1C_{12} + h_1h_2H_5\,{}_2C_{12} - h_1h_3H_8\,{}_3C_{12}\right)\left[\beta_p^2\,{}_1M_{pm}\left[\gamma_n^2\,{}_1N_{qn}\right]\right] \\
& - \left(\frac{2}{3}\frac{h_1^3}{R}\,{}_1C_{66} + h_1h_2H_5\,{}_2C_{66} - h_1h_3H_8\,{}_3C_{66}\right)\left[{}_2M_{pm}\left[{}_2N_{qn}\right]\right]
\end{aligned}
$$

$$
\begin{aligned}
{}_1K_{21} = {} & (2h_1H_2\,{}_1C_{21} + h_2H_5\,{}_2C_{21} + h_3H_8\,{}_3C_{21})\left[\beta_m^2\,{}_1M_{pm}\left[\gamma_q^2\,{}_1N_{qn}\right]\right] \\
& + (2h_1H_2\,{}_1C_{66} + h_2H_5\,{}_2C_{66} + h_3H_8\,{}_3C_{66})\left[{}_2M_{pm}\left[{}_2N_{qn}\right]\right]
\end{aligned}
$$

$$
\begin{aligned}
{}_1K_{22} = {} & (2h_1H_1\,{}_1C_{22} + h_2H_6\,{}_2C_{22} + h_3H_{10}\,{}_3C_{22})\left[{}_1M_{pm}\left[\gamma_q^2\gamma_n^2\,{}_1N_{qn}\right]\right] \\
& + \frac{2h_1H_1\,{}_1C_{44}}{R^2}\left[{}_1M_{pm}\left[{}_2N_{qn}\right]\right] \\
& + (2h_1\,{}_1C_{66} + h_2\,{}_2C_{66} + h_3\,{}_3C_{66})\left[{}_2M_{pm}\left[{}_2N_{qn}\right]\right]
\end{aligned}
$$

$$
\begin{aligned}
{}_1K_{23} = {} & -\frac{1}{R}(2h_1H_1\,{}_1C_{22} + h_2H_6\,{}_2C_{22} + h_3H_{10}\,{}_3C_{22})\left[{}_1M_{pm}\left[\gamma_q^2\,{}_1N_{qn}\right]\right] \\
& - \frac{2h_1H_1}{R}\,{}_1C_{44}\left[{}_1M_{pm}\left[{}_2N_{qn}\right]\right]
\end{aligned}
$$

$$
{}_1K_{24} = -\left(\frac{2}{3}\frac{h_1^3}{R}\,{}_1C_{21} + h_1h_2H_5\,{}_2C_{21} - h_1h_3H_8\,{}_3C_{21}\right)\left[\beta_m^2\,{}_1M_{pm}\left[\gamma_q^2\,{}_1N_{qn}\right]\right]
$$

$$
\qquad - \left(\frac{2}{3}\frac{h_1^3}{R}\,{}_1C_{66} + h_1h_2H_5\,{}_2C_{66} - h_1h_3H_8\,{}_3C_{66}\right)\left[{}_2M_{pm}\left[{}_2N_{qn}\right]\right]
$$

$$
{}_1K_{25} = -\left(\frac{4}{3}\frac{h_1^3}{R}\,{}_1C_{22} + h_1h_2H_6\,{}_2C_{22} - h_1h_3\,H_{10}\,{}_3C_{22}\right)\left[{}_1M_{pm}\left[\gamma_q^2\gamma_n^2\,{}_1N_{qn}\right]\right]
$$

$$
\qquad - \frac{2h_1H_1}{R}\,{}_1C_{44}\left[{}_1M_{pm}\left[{}_2N_{qn}\right]\right]
$$

$$
\qquad - (h_1h_2\,{}_2C_{66} - h_1h_3\,{}_3C_{66})\left[{}_2M_{pm}\left[{}_2N_{qn}\right]\right]
$$

$$
{}_1K_{31} = -\frac{1}{R}\,(2h_1H_2\,{}_1C_{21} + h_2H_5\,{}_2C_{21} + h_3H_8\,{}_3C_{21})\left[\beta_m^2\,{}_1M_{pm}\left[{}_1N_{qn}\right]\right]
$$

$$
{}_1K_{32} = -\frac{1}{R}\,(2h_1H_1\,{}_1C_{22} + h_2H_6\,{}_2C_{22} + h_3H_{10}\,{}_3C_{22})\left[{}_1M_{pm}\left[\gamma_n^2\,{}_1N_{qn}\right]\right]
$$

$$
\qquad - \frac{2h_1H_1}{R}\,{}_1C_{44}\left[{}_1M_{pm}\left[{}_2N_{qn}\right]\right]
$$

$$
{}_1K_{33} = \frac{1}{R^2}\,(2h_1H_1\,{}_1C_{22} + h_2H_6\,{}_2C_{22} + h_3H_{10}\,{}_3C_{22})\left[{}_1M_{pm}\left[{}_1N_{qn}\right]\right]
$$

$$
\qquad + 2h_1H_1\,{}_1C_{44}\left[{}_1M_{pm}\left[{}_2N_{qn}\right]\right] + 2h_1\,{}_1C_{55}\left[{}_2M_{pm}\left[{}_1N_{qn}\right]\right]
$$

$$
{}_1K_{34} = \frac{1}{R}\left(\frac{2}{3}\frac{h_1^3}{R}\,{}_1C_{21} + h_1h_2H_5\,{}_2C_{21} - h_1h_3H_8\,{}_3C_{21}\right)\left[\beta_m^2\,{}_1M_{pm}\left[{}_1N_{qn}\right]\right]
$$

$$
\qquad + 2h_1\,{}_1C_{55}\left[{}_2M_{pm}\left[{}_1N_{qn}\right]\right]
$$

$$
{}_1K_{35} = \frac{1}{R}\left(\frac{4}{3}\frac{h_1^3}{R}\,{}_1C_{22} + h_1h_2H_6\,{}_2C_{22} - h_1h_3H_{10}\,{}_3C_{22}\right)\left[{}_1M_{pm}\left[\gamma_q^2\,{}_1N_{qn}\right]\right]
$$

$$
\qquad + 2h_1H_1\,{}_1C_{44}\left[{}_1M_{pm}\left[{}_2N_{qn}\right]\right]
$$

$$
{}_1K_{41} = -(h_1h_2\,{}_2C_{11} - h_1h_3\,{}_3C_{11})\left[\beta_p^2\beta_m^2\,{}_1M_{pm}\left[{}_1N_{qn}\right]\right]
$$

$$
\qquad - \left(\frac{4}{3}\frac{h_1^3}{R}\,{}_1C_{66} + h_1h_2H_6\,{}_2C_{66} - h_1h_3H_{10}\,{}_3C_{66}\right)\left[{}_2M_{pm}\left[{}_2N_{qn}\right]\right]
$$

$$
{}_1K_{42} = -\left(\frac{2}{3}\frac{h_1^3}{R}\,{}_1C_{12} + h_1h_2H_5\,{}_2C_{12} - h_1h_3H_8\,{}_3C_{12}\right)\left[\beta_p^2\,{}_1M_{pm}\left[\gamma_n^2\,{}_1N_{qn}\right]\right]
$$

$$
\qquad - \left(\frac{2}{3}\frac{h_1^3}{R}\,{}_1C_{66} + h_1h_2H_5\,{}_2C_{66} - h_1h_3H_8\,{}_3C_{66}\right)\left[{}_2M_{pm}\left[{}_2N_{qn}\right]\right]
$$

$$
{}_1K_{43} = \frac{1}{R}\left(\frac{2}{3}\frac{h_1^3}{R}\,{}_1C_{12} + h_1h_2H_5\,{}_2C_{12} - h_1h_3H_8\,{}_3C_{12}\right)\left[\beta_p^2\,{}_1M_{pm}\left[{}_1N_{qn}\right]\right]
$$

$$
\qquad + 2h_1\,{}_1C_{55}\left[{}_2M_{pm}\left[{}_1N_{qn}\right]\right]
$$

$$
{}_1K_{44} = \left(\frac{2}{3}h_1^3\,{}_1C_{11} + h_1^2h_2\,{}_2C_{11} + h_1^2h_3\,{}_3C_{11}\right)\left[\beta_p^2\beta_m^2\,{}_1M_{pm}\left[{}_1N_{qn}\right]\right]
$$

$$
\qquad + 2h_1\,{}_1C_{55}\left[{}_2M_{pm}\left[{}_1N_{qn}\right]\right]
$$

$$
\qquad + \left(\frac{2}{3}h_1^3\,{}_1C_{66} + h_1^2h_2H_6\,{}_2C_{66} + h_1^2h_3H_{10}\,{}_3C_{66}\right)\left[{}_2M_{pm}\left[{}_2N_{qn}\right]\right]
$$

$$
{}_1K_{45} = \left(\frac{2}{3}h_1^3\,{}_1C_{12} + h_1^2h_2H_5\,{}_2C_{12} + h_1^2h_3H_8\,{}_3C_{12}\right)\left[\beta_p^2\,{}_1M_{pm}\left[\gamma_n^2\,{}_1N_{qn}\right]\right]
$$

$$
\qquad + \left(\frac{2}{3}h_1^3\,{}_1C_{66} + h_1^2h_2H_5\,{}_2C_{66} + h_1^2h_3H_8\,{}_3C_{66}\right)\left[{}_2M_{pm}\left[{}_2N_{qn}\right]\right]
$$

$$
{}_1K_{51} = -\left(\frac{2}{3}\frac{h_1^3}{R}\,{}_1C_{21} + h_1h_2H_5\,{}_2C_{21} - h_1h_3H_8\,{}_3C_{21}\right)\left[\beta_m^2\,{}_1M_{pm}\left[\gamma_q^2\,{}_1N_{qn}\right]\right]
$$

$$
\qquad - \left(\frac{2}{3}\frac{h_1^3}{R}\,{}_1C_{66} + h_1h_2H_5\,{}_2C_{66} - h_1h_3H_8\,{}_3C_{66}\right)\left[{}_2M_{pm}\left[{}_2N_{qn}\right]\right]
$$

$$
{}_1K_{52} = -\left(\frac{4}{3}\frac{h_1^3}{R}\,{}_1C_{22} + h_1h_2H_6\,{}_2C_{22} - h_1h_3H_{10}\,{}_3C_{22}\right)\left[{}_1M_{pm}\left[\gamma_q^2\gamma_n^2\,{}_1N_{qn}\right]\right]
$$

$$
\qquad - \frac{2h_1H_1}{R}\,{}_1C_{44}\left[{}_1M_{pm}\left[{}_2N_{qn}\right]\right]
$$

$$
\qquad - (h_1h_2\,{}_2C_{66} - h_1h_3\,{}_3C_{66})\left[{}_2M_{pm}\left[{}_2N_{qn}\right]\right]
$$

$$
{}_1K_{53} = \frac{1}{R}\left(\frac{4}{3}\frac{h_1^3}{R}\,{}_1C_{22} + h_1h_2H_6\,{}_2C_{22} - h_1h_3H_{10}\,{}_3C_{22}\right)\left[{}_1M_{pm}\left[\gamma_q^2\,{}_1N_{qn}\right]\right]
$$

$$
\qquad + 2h_1H_1\,{}_1C_{44}\left[{}_1M_{pm}\left[{}_2N_{qn}\right]\right]
$$

$$
{}_1K_{54} = \left(\frac{2}{3}h_1^3\,{}_1C_{21} + h_1^2h_2H_5\,{}_2C_{21} + h_1^2h_3H_8\,{}_3C_{21}\right)\left[\beta_m^2\,{}_1M_{pm}\left[\gamma_q^2\,{}_1N_{qn}\right]\right]
$$

$$
\qquad + \left(\frac{2}{3}h_1^3\,{}_1C_{66} + h_1^2h_2H_5\,{}_2C_{66} + h_1^2h_3H_8\,{}_3C_{66}\right)\left[{}_2M_{pm}\left[{}_2N_{qn}\right]\right]
$$

$$
{}_1K_{55} = \left(\tfrac{2}{3} h_1^3\, {}_1C_{22} + h_1^2 h_2 H_6\, {}_2C_{22} + h_1^2 h_3 H_{10}\, {}_3C_{22}\right)\left[{}_1M_{pm}\left[\gamma_q^2 \gamma_n^2\, {}_1N_{qn}\right]\right]
$$

$$
+ 2h_1 H_1\, {}_1C_{44}\left[{}_1M_{pm}\left[{}_2N_{qn}\right]\right]
$$

$$
+ \left(\tfrac{2}{3} h_1^3\, {}_1C_{66} + h_1^2 h_2\, {}_2C_{66} + h_1^2 h_3\, {}_3C_{66}\right)\left[{}_2M_{pm}\left[{}_2N_{qn}\right]\right]
$$

$$
{}_2K_{11} = h_4\left({}_4C_{11}\left[\beta_p^2 \beta_m^2\, {}_7M_{pm}\left[{}_3N_{qn}\right]\right] + {}_4C_{66}\left[{}_8M_{pm}\left[{}_4N_{qn}\right]\right]\right)
$$

$$
{}_2K_{12} = h_4\left({}_4C_{12}\left[\beta_p^2\, {}_7M_{pm}\left[\gamma_n^2\, {}_3N_{qn}\right]\right] + {}_4C_{66}\left[{}_8M_{pm}\left[{}_4N_{qn}\right]\right]\right)
$$

$$
{}_2K_{13} = -\frac{h_4}{R}\left({}_4C_{12}\left[\beta_p^2\, {}_7M_{pm}\left[{}_3N_{qn}\right]\right]\right)
$$

$$
{}_2K_{21} = h_4\left({}_4C_{21}\left[\beta_m^2\, {}_7M_{pm}\left[\gamma_q^2\, {}_3N_{qn}\right]\right] + {}_4C_{66}\left[{}_8M_{pm}\left[{}_4N_{qn}\right]\right]\right)
$$

$$
{}_2K_{22} = h_4\left({}_4C_{22}\left[{}_7M_{pm}\left[\gamma_q^2 \gamma_n^2\, {}_3N_{qn}\right]\right] + {}_4C_{66}\left[{}_8M_{pm}\left[{}_4N_{qn}\right]\right]\right)
$$

$$
+ \frac{h_4^3}{12R^2}\left({}_4C_{22}\left[{}_7M_{pm}\left[\gamma_q^2 \gamma_n^2\, {}_3N_{qn}\right]\right] + 4\, {}_4C_{66}\left[{}_8M_{pm}\left[{}_4N_{qn}\right]\right]\right)
$$

$$
{}_2K_{23} = -\frac{h_4}{R}\, {}_4C_{22}\left[{}_7M_{pm}\left[\gamma_q^2\, {}_3N_{qn}\right]\right] - \frac{h_4^3}{12R}\left({}_4C_{21}\left[\beta_m^2\, {}_7M_{pm}\left[\gamma_q^2\, {}_3N_{qn}\right]\right]\right.
$$

$$
\left. + {}_4C_{22}\left[{}_7M_{pm}\left[\gamma_q^2 \gamma_n^2\, {}_3N_{qn}\right]\right] + 4\, {}_4C_{66}\left[{}_8M_{pm}\left[{}_4N_{qn}\right]\right]\right)
$$

$$
{}_2K_{31} = -\frac{h_4\, {}_4C_{21}}{R}\left[\beta_m^2\, {}_7M_{pm}\left[{}_3N_{qn}\right]\right]
$$

$$
{}_2K_{32} = -\frac{h_4\, {}_4C_{22}}{R}\left[{}_7M_{pm}\left[\gamma_n^2\, {}_3N_{qn}\right]\right] - \frac{h_4^3}{12R}\left({}_4C_{12}\left[\beta_p^2\, {}_7M_{pm}\left[\gamma_n^2\, {}_3N_{qn}\right]\right]\right.
$$

$$
\left. + {}_4C_{22}\left[{}_7M_{pm}\left[\gamma_q^2 \gamma_n^2\, {}_3N_{qn}\right]\right] + 4\, {}_4C_{66}\left[{}_8M_{pm}\left[{}_4N_{qn}\right]\right]\right)
$$

$$
{}_2K_{33} = \frac{h_4\, {}_4C_{22}}{R^2}\left[{}_7M_{pm}\left[{}_3N_{qn}\right]\right] + \frac{h_4^3}{12}\left({}_4C_{11}\left[\beta_p^2 \beta_m^2\, {}_7M_{pm}\left[{}_3N_{qn}\right]\right]\right.
$$

$$
+ {}_4C_{12}\left[\beta_p^2\, {}_7M_{pm}\left[\gamma_n^2\, {}_3N_{qn}\right]\right] + {}_4C_{21}\left[\beta_m^2\, {}_7M_{pm}\left[\gamma_q^2\, {}_3N_{qn}\right]\right]
$$

$$
\left. + {}_4C_{22}\left[{}_7M_{pm}\left[\gamma_q^2 \gamma_n^2\, {}_3N_{qn}\right]\right] + 4\, {}_4C_{66}\left[{}_8M_{pm}\left[{}_4N_{qn}\right]\right]\right)
$$

$$ {}_iK_{14} = {}_iK_{15} = {}_iK_{24} = {}_iK_{25} = {}_iK_{34} = {}_iK_{41} = {}_iK_{42} = {}_iK_{43} = 0 $$

$$ {}_iK_{44} = {}_iK_{45} = {}_iK_{51} = {}_iK_{52} = {}_iK_{53} = {}_iK_{54} = {}_iK_{55} = 0 $$

$$ i = 2, 3, 4, 5 $$

$$ {}_3K_{11} = h_4 \left({}_4C_{11} \left[\beta_p^2 \beta_m^2 \, {}_7M_{pm} \left[{}_5N_{qn} \right] \right] + {}_4C_{66} \left[{}_8M_{pm} \left[{}_6N_{qn} \right] \right] \right) $$

$$ {}_3K_{12} = h_4 \left({}_4C_{12} \left[\beta_p^2 \, {}_7M_{pm} \left[\gamma_n^2 \, {}_5N_{qn} \right] \right] + {}_4C_{66} \left[{}_8M_{pm} \left[{}_6N_{qn} \right] \right] \right) $$

$$ {}_3K_{13} = - \frac{h_4}{R} \left({}_4C_{12} \left[\beta_p^2 \, {}_7M_{pm} \left[{}_5N_{qn} \right] \right] \right) $$

$$ {}_3K_{21} = h_4 \left({}_4C_{21} \left[\beta_m^2 \, {}_7M_{pm} \left[\gamma_q^2 \, {}_5N_{qn} \right] \right] + {}_4C_{66} \left[{}_8M_{pm} \left[{}_6N_{qn} \right] \right] \right) $$

$$ {}_3K_{22} = h_4 \left({}_4C_{22} \left[{}_7M_{pm} \left[\gamma_q^2 \gamma_n^2 \, {}_5N_{qn} \right] \right] + {}_4C_{66} \left[{}_8M_{pm} \left[{}_4N_{qn} \right] \right] \right) $$
$$ + \frac{h_4^3}{12R^2} \left({}_4C_{22} \left[{}_7M_{pm} \left[\gamma_q^2 \gamma_n^2 \, {}_5N_{qn} \right] \right] + 4 \, {}_4C_{66} \left[{}_8M_{pm} \left[{}_6N_{qn} \right] \right] \right) $$

$$ {}_3K_{23} = - \frac{h_4}{R} \, {}_4C_{22} \left[{}_7M_{pm} \left[\gamma_q^2 \, {}_5N_{qn} \right] \right] - \frac{h_4^3}{12R} \left({}_4C_{21} \left[\beta_m^2 \, {}_7M_{pm} \left[\gamma_q^2 \, {}_5N_{qn} \right] \right] \right. $$
$$ \left. + {}_4C_{22} \left[{}_7M_{pm} \left[\gamma_q^2 \gamma_n^2 \, {}_5N_{qn} \right] \right] + 4 \, {}_4C_{66} \left[{}_8M_{pm} \left[{}_6N_{qn} \right] \right] \right) $$

$$ {}_3K_{31} = - \frac{h_4 \, {}_4C_{21}}{R} \left[\beta_m^2 \, {}_7M_{pm} \left[{}_5N_{qn} \right] \right] $$

$$ {}_3K_{32} = - \frac{h_4 \, {}_4C_{22}}{R} \left[{}_7M_{pm} \left[\gamma_n^2 \, {}_5N_{qn} \right] \right] - \frac{h_4^3}{12R} \left({}_4C_{12} \left[\beta_p^2 \, {}_7M_{pm} \left[\gamma_n^2 \, {}_5N_{qn} \right] \right] \right. $$
$$ \left. + {}_4C_{22} \left[{}_7M_{pm} \left[\gamma_q^2 \gamma_n^2 \, {}_5N_{qn} \right] \right] + 4 \, {}_4C_{66} \left[{}_8M_{pm} \left[{}_6N_{qn} \right] \right] \right) $$

$$ {}_3K_{33} = \frac{h_4 \, {}_4C_{22}}{R^2} \left[{}_7M_{pm} \left[{}_5N_{qn} \right] \right] + \frac{h_4^3}{12} \left({}_4C_{11} \left[\beta_p^2 \beta_m^2 \, {}_7M_{pm} \left[{}_5N_{qn} \right] \right] \right. $$
$$ + {}_4C_{12} \left[\beta_p^2 \, {}_7M_{pm} \left[\gamma_n^2 \, {}_5N_{qn} \right] \right] + {}_4C_{21} \left[\beta_m^2 \, {}_7M_{pm} \left[\gamma_q^2 \, {}_5N_{qn} \right] \right] $$
$$ \left. + {}_4C_{22} \left[{}_7M_{pm} \left[\gamma_q^2 \gamma_n^2 \, {}_5N_{qn} \right] \right] + 4 \, {}_4C_{66} \left[{}_8M_{pm} \left[{}_6N_{qn} \right] \right] \right) $$

$$
{}_4K_{11} = h_4 \left({}_4C_{11} \left[\beta_p^2 \beta_m^2 \, {}_3M_{pm} \left[{}_1N_{qn} \right] \right] + {}_4C_{66} \left[{}_4M_{pm} \left[{}_2N_{qn} \right] \right] \right)
$$

$$
{}_4K_{12} = h_4 \left({}_4C_{12} \left[\beta_p^2 \, {}_3M_{pm} \left[\gamma_n^2 \, {}_1N_{qn} \right] \right] + {}_4C_{66} \left[{}_4M_{pm} \left[{}_2N_{qn} \right] \right] \right)
$$

$$
{}_4K_{13} = -\frac{h_4}{R} \left({}_4C_{12} \left[\beta_p^2 \, {}_3M_{pm} \left[{}_1N_{qn} \right] \right] \right)
$$

$$
{}_4K_{21} = h_4 \left({}_4C_{21} \left[\beta_m^2 \, {}_3M_{pm} \left[\gamma_q^2 \, {}_1N_{qn} \right] \right] + {}_4C_{66} \left[{}_4M_{pm} \left[{}_2N_{qn} \right] \right] \right)
$$

$$
\begin{aligned}
{}_4K_{22} = {} & h_4 \left({}_4C_{22} \left[{}_3M_{pm} \left[\gamma_q^2 \gamma_n^2 \, {}_1N_{qn} \right] \right] + {}_4C_{66} \left[{}_4M_{pm} \left[{}_2N_{qn} \right] \right] \right) \\
& + \frac{h_4^3}{12R^2} \left({}_4C_{22} \left[{}_3M_{pm} \left[\gamma_q^2 \gamma_n^2 \, {}_1N_{qn} \right] \right] + 4 \, {}_4C_{66} \left[{}_4M_{pm} \left[{}_2N_{qn} \right] \right] \right)
\end{aligned}
$$

$$
\begin{aligned}
{}_4K_{23} = {} & -\frac{h_4}{R} \, {}_4C_{22} \left[{}_3M_{pm} \left[\gamma_q^2 \, {}_1N_{qn} \right] \right] - \frac{h_4^3}{12R} \left({}_4C_{21} \left[\beta_m^2 \, {}_3M_{pm} \left[\gamma_q^2 \, {}_1N_{qn} \right] \right] \right. \\
& \left. + {}_4C_{22} \left[{}_3M_{pm} \left[\gamma_q^2 \gamma_n^2 \, {}_1N_{qn} \right] \right] + 4 \, {}_4C_{66} \left[{}_4M_{pm} \left[{}_2N_{qn} \right] \right] \right)
\end{aligned}
$$

$$
{}_4K_{31} = -\frac{h_4 \, {}_4C_{21}}{R} \left[\beta_m^2 \, {}_3M_{pm} \left[{}_1N_{qn} \right] \right]
$$

$$
\begin{aligned}
{}_4K_{32} = {} & -\frac{h_4 \, {}_4C_{22}}{R} \left[{}_3M_{pm} \left[\gamma_n^2 \, {}_1N_{qn} \right] \right] - \frac{h_4^3}{12R} \left({}_4C_{12} \left[\beta_p^2 \, {}_3M_{pm} \left[\gamma_n^2 \, {}_1N_{qn} \right] \right] \right. \\
& \left. + {}_4C_{22} \left[{}_3M_{pm} \left[\gamma_q^2 \gamma_n^2 \, {}_1N_{qn} \right] \right] + 4 \, {}_4C_{66} \left[{}_4M_{pm} \left[{}_2N_{qn} \right] \right] \right)
\end{aligned}
$$

$$
\begin{aligned}
{}_4K_{33} = {} & \frac{h_4 \, {}_4C_{22}}{R^2} \left[{}_3M_{pm} \left[{}_1N_{qn} \right] \right] + \frac{h_4^3}{12} \left({}_4C_{11} \left[\beta_p^2 \beta_m^2 \, {}_3M_{pm} \left[{}_1N_{qn} \right] \right] \right. \\
& + {}_4C_{12} \left[\beta_p^2 \, {}_3M_{pm} \left[\gamma_n^2 \, {}_1N_{qn} \right] \right] + {}_4C_{21} \left[\beta_m^2 \, {}_3M_{pm} \left[\gamma_q^2 \, {}_1N_{qn} \right] \right] \\
& \left. + {}_4C_{22} \left[{}_3M_{pm} \left[\gamma_q^2 \gamma_n^2 \, {}_1N_{qn} \right] \right] + 4 \, {}_4C_{66} \left[{}_4M_{pm} \left[{}_2N_{qn} \right] \right] \right)
\end{aligned}
$$

$$
{}_5K_{11} = h_4 \left({}_4C_{11} \left[\beta_p^2 \beta_m^2 \, {}_5M_{pm} \left[{}_1N_{qn} \right] \right] + {}_4C_{66} \left[{}_6M_{pm} \left[{}_2N_{qn} \right] \right] \right)
$$

$$
{}_5K_{12} = h_4 \left({}_4C_{12} \left[\beta_p^2 \, {}_5M_{pm} \left[\gamma_n^2 \, {}_1N_{qn} \right] \right] + {}_4C_{66} \left[{}_6M_{pm} \left[{}_2N_{qn} \right] \right] \right)
$$

$$
{}_5K_{13} = -\frac{h_4}{R}\left({}_4C_{12}\left[\beta_p^2\, {}_5M_{pm}\left[{}_1N_{qn}\right]\right]\right)
$$

$$
{}_5K_{21} = h_4\left({}_4C_{21}\left[\beta_m^2\, {}_5M_{pm}\left[\gamma_q^2\, {}_1N_{qn}\right]\right] + {}_4C_{66}\left[{}_6M_{pm}\left[{}_2N_{qn}\right]\right]\right)
$$

$$
\begin{aligned}
{}_5K_{22} = h_4\Big({}_4C_{22}\Big[{}_5M_{pm}\Big[\gamma_q^2\gamma_n^2\, {}_1N_{qn}\Big]\Big] + {}_4C_{66}\Big[{}_6M_{pm}\Big[{}_2N_{qn}\Big]\Big]\Big) \\
+ \frac{h_4^3}{12R^2}\Big({}_4C_{22}\Big[{}_5M_{pm}\Big[\gamma_q^2\gamma_n^2\, {}_1N_{qn}\Big]\Big] + 4\, {}_4C_{66}\Big[{}_6M_{pm}\Big[{}_2N_{qn}\Big]\Big]\Big)
\end{aligned}
$$

$$
\begin{aligned}
{}_5K_{23} = -\frac{h_4}{R}\, {}_4C_{22}\Big[{}_5M_{pm}\Big[\gamma_q^2\, {}_1N_{qn}\Big]\Big] - \frac{h_4^3}{12R}\Big({}_4C_{21}\Big[\beta_m^2\, {}_5M_{pm}\Big[\gamma_q^2\, {}_1N_{qn}\Big]\Big] \\
+ {}_4C_{22}\Big[{}_5M_{pm}\Big[\gamma_q^2\gamma_n^2\, {}_1N_{qn}\Big]\Big] + 4\, {}_4C_{66}\Big[{}_6M_{pm}\Big[{}_2N_{qn}\Big]\Big]\Big)
\end{aligned}
$$

$$
{}_5K_{31} = -\frac{h_4\, {}_4C_{21}}{R}\Big[\beta_m^2\, {}_5M_{pm}\Big[{}_1N_{qn}\Big]\Big]
$$

$$
\begin{aligned}
{}_5K_{32} = -\frac{h_4\, {}_4C_{22}}{R}\Big[{}_5M_{pm}\Big[\gamma_n^2\, {}_1N_{qn}\Big]\Big] - \frac{h_4^3}{12R}\Big({}_4C_{12}\Big[\beta_p^2\, {}_5M_{pm}\Big[\gamma_n^2\, {}_1N_{qn}\Big]\Big] \\
+ {}_4C_{22}\Big[{}_5M_{pm}\Big[\gamma_q^2\gamma_n^2\, {}_1N_{qn}\Big]\Big] + 4\, {}_4C_{66}\Big[{}_6M_{pm}\Big[{}_2N_{qn}\Big]\Big]\Big)
\end{aligned}
$$

$$
\begin{aligned}
{}_5K_{33} = \frac{h_4\, {}_4C_{22}}{R^2}\Big[{}_5M_{pm}\Big[{}_1N_{qn}\Big]\Big] + \frac{h_4^3}{12}\Big({}_4C_{11}\Big[\beta_p^2\beta_m^2\, {}_5M_{pm}\Big[{}_1N_{qn}\Big]\Big] \\
+ {}_4C_{12}\Big[\beta_p^2\, {}_5M_{pm}\Big[\gamma_n^2\, {}_1N_{qn}\Big]\Big] + {}_4C_{21}\Big[\beta_m^2\, {}_5M_{pm}\Big[\gamma_q^2\, {}_1N_{qn}\Big]\Big] \\
+ {}_4C_{22}\Big[{}_5M_{pm}\Big[\gamma_q^2\gamma_n^2\, {}_1N_{qn}\Big]\Big] + 4\, {}_4C_{66}\Big[{}_6M_{pm}\Big[{}_2N_{qn}\Big]\Big]\Big)
\end{aligned}
$$

The generalized mass matrix elements follow. Terms not specifically listed are zero.

$$
{}_1M_{11} = (2\rho_1 h_1 + \rho_2 h_2 + \rho_3 h_3)\left[{}_2M_{pm}\left[{}_1N_{qn}\right]\right]
$$

$$
{}_1M_{14} = -(\rho_2 h_1 h_2 - \rho_3 h_1 h_3)\left[{}_2M_{pm}\left[{}_1N_{qn}\right]\right]
$$

$$
{}_1M_{22} = (2\rho_1 h_1 + \rho_2 h_2 + \rho_3 h_3)\left[{}_1M_{pm}\left[{}_2N_{qn}\right]\right]
$$

$$
{}_1M_{25} = -(\rho_2 h_1 h_2 - \rho_3 h_1 h_3)\left[{}_1M_{pm}\left[{}_2N_{qn}\right]\right]
$$

$$
{}_1M_{33} = (2\rho_1 h_1 + \rho_2 h_2 + \rho_3 h_3)\left[{}_1M_{pm}\left[{}_1N_{qn}\right]\right]
$$

$$ {}_1M_{41} = -(\rho_2 h_1 h_2 - \rho_3 h_1 h_3)\left[{}_2M_{pm}\left[{}_1N_{qn}\right]\right] $$

$$ {}_1M_{44} = \left(\frac{2}{3}\rho_1 h_1^3 + \rho_2 h_1^2 h_2 + \rho_3 h_1^2 h_3\right)\left[{}_2M_{pm}\left[{}_1N_{qn}\right]\right] $$

$$ {}_1M_{52} = -(\rho_2 h_1 h_2 - \rho_3 h_1 h_3)\left[{}_1M_{pm}\left[{}_2N_{qn}\right]\right] $$

$$ {}_1M_{55} = \left(\frac{2}{3}\rho_1 h_1^3 + \rho_2 h_1^2 h_2 + \rho_3 h_1^2 h_3\right)\left[{}_1M_{pm}\left[{}_2N_{qn}\right]\right] $$

$$ {}_2M_{11} = \rho_4 h_4 \left[{}_8M_{pm}\left[{}_3N_{qn}\right]\right] $$

$$ {}_2M_{22} = \rho_4 h_4 \left[{}_7M_{pm}\left[{}_4N_{qn}\right]\right] $$

$$ {}_2M_{33} = \rho_4 h_4 \left[{}_7M_{pm}\left[{}_3N_{qn}\right]\right] $$

$$ {}_3M_{11} = \rho_4 h_4 \left[{}_8M_{pm}\left[{}_5N_{qn}\right]\right] $$

$$ {}_3M_{22} = \rho_4 h_4 \left[{}_7M_{pm}\left[{}_6N_{qn}\right]\right] $$

$$ {}_3M_{33} = \rho_4 h_4 \left[{}_7M_{pm}\left[{}_5N_{qn}\right]\right] $$

$$ {}_4M_{11} = \rho_4 h_4 \left[{}_4M_{pm}\left[{}_1N_{qn}\right]\right] $$

$$ {}_4M_{22} = \rho_4 h_4 \left[{}_3M_{pm}\left[{}_2N_{qn}\right]\right] $$

$$ {}_4M_{33} = \rho_4 h_4 \left[{}_3M_{pm}\left[{}_1N_{qn}\right]\right] $$

$$ {}_5M_{11} = \rho_4 h_4 \left[{}_6M_{pm}\left[{}_1N_{qn}\right]\right] $$

$$ {}_5M_{22} = \rho_4 h_4 \left[{}_5M_{pm}\left[{}_2N_{qn}\right]\right] $$

$$ {}_5M_{33} = \rho_4 h_4 \left[{}_5M_{pm}\left[{}_1N_{qn}\right]\right] $$

Unclassified
Security Classification

DOCUMENT CONTROL DATA - R&D

(Security classification of title, body of abstract and indexing annotation must be entered when the overall report is classified)

1. ORIGINATING ACTIVITY *(Corporate author)* Lockheed-Georgia Company South Cobb Drive Marietta, Georgia 30061	2a. REPORT SECURITY CLASSIFICATION Unclassified 2b. GROUP

3. REPORT TITLE

SONIC FATIGUE IN COMBINED ENVIRONMENT

4. DESCRIPTIVE NOTES *(Type of report and inclusive dates)*
Final April 1964 to December 1965

5. AUTHOR(S) *(Last name, first name, initial)*
Ballentine, John R., Plumblee, Harry E. & Schneider, Cecil W.

6. REPORT DATE May 1966	7a. TOTAL NO. OF PAGES 149	7b. NO. OF REFS 21
8a. CONTRACT OR GRANT NO. AF 33(615)-1481 b. PROJECT NO. 1471 c. Task 147101 d.	9a. ORIGINATOR'S REPORT NUMBER(S) AFFDL-TR-66-7 9b. OTHER REPORT NO(S) *(Any other numbers that may be assigned this report)*	

10. AVAILABILITY/LIMITATION NOTICES

Distribution of this document is unlimited.

11. SUPPLEMENTARY NOTES	12. SPONSORING MILITARY ACTIVITY Air Force Flight Dynamics Laboratory Wright-Patterson AFB, Ohio 45433

13. ABSTRACT

Research on sonic fatigue in combined environment is described. Emphasis is placed on determining the effects of structural curvature, low frequency vibratory loads, and heat both singly and collectively on sonic fatigue. The analytical and experimental investigation is presented in two major phases:

1. An investigation of simple structural panels to determine the effect of curvature and heat cycling schemes on dynamic response and fatigue.

2. An investigation to determine the effects of high intensity sound, heat, and low frequency vibratory loads on curved titanium-faced honeycomb sandwich panels.

DD FORM 1 JAN 64 1473

Unclassified
Security Classification

Unclassified

Security Classification

14. KEY WORDS	LINK A ROLE	LINK A WT	LINK B ROLE	LINK B WT	LINK C ROLE	LINK C WT
Sonic Fatigue Dynamic Response Heat Low Frequency Vibratory Loads						

INSTRUCTIONS

1. ORIGINATING ACTIVITY: Enter the name and address of the contractor, subcontractor, grantee, Department of Defense activity or other organization *(corporate author)* issuing the report.

2*a*. REPORT SECURITY CLASSIFICATION: Enter the overall security classification of the report. Indicate whether "Restricted Data" is included. Marking is to be in accordance with appropriate security regulations.

2*b*. GROUP: Automatic downgrading is specified in DoD Directive 5200.10 and Armed Forces Industrial Manual. Enter the group number. Also, when applicable, show that optional markings have been used for Group 3 and Group 4 as authorized.

3. REPORT TITLE: Enter the complete report title in all capital letters. Titles in all cases should be unclassified. If a meaningful title cannot be selected without classification, show title classification in all capitals in parenthesis immediately following the title.

4. DESCRIPTIVE NOTES: If appropriate, enter the type of report, e.g., interim, progress, summary, annual, or final. Give the inclusive dates when a specific reporting period is covered.

5. AUTHOR(S): Enter the name(s) of author(s) as shown on or in the report. Enter last name, first name, middle initial. If military, show rank and branch of service. The name of the principal author is an absolute minimum requirement.

6. REPORT DATE: Enter the date of the report as day, month, year; or month, year. If more than one date appears on the report, use date of publication.

7*a*. TOTAL NUMBER OF PAGES: The total page count should follow normal pagination procedures, i.e., enter the number of pages containing information.

7*b*. NUMBER OF REFERENCES: Enter the total number of references cited in the report.

8*a*. CONTRACT OR GRANT NUMBER: If appropriate, enter the applicable number of the contract or grant under which the report was written.

8*b*, 8*c*, & 8*d*. PROJECT NUMBER: Enter the appropriate military department identification, such as project number, subproject number, system numbers, task number, etc.

9*a*. ORIGINATOR'S REPORT NUMBER(S): Enter the official report number by which the document will be identified and controlled by the originating activity. This number must be unique to this report.

9*b*. OTHER REPORT NUMBER(S): If the report has been assigned any other report numbers *(either by the originator or by the sponsor)*, also enter this number(s).

10. AVAILABILITY/LIMITATION NOTICES: Enter any limitations on further dissemination of the report, other than those imposed by security classification, using standard statements such as:

(1) "Qualified requesters may obtain copies of this report from DDC."

(2) "Foreign announcement and dissemination of this report by DDC is not authorized."

(3) "U. S. Government agencies may obtain copies of this report directly from DDC. Other qualified DDC users shall request through

_____."

(4) "U. S. military agencies may obtain copies of this report directly from DDC. Other qualified users shall request through

_____."

(5) "All distribution of this report is controlled. Qualified DDC users shall request through

_____."

If the report has been furnished to the Office of Technical Services, Department of Commerce, for sale to the public, indicate this fact and enter the price, if known.

11. SUPPLEMENTARY NOTES: Use for additional explanatory notes.

12. SPONSORING MILITARY ACTIVITY: Enter the name of the departmental project office or laboratory sponsoring *(paying for)* the research and development. Include address.

13. ABSTRACT: Enter an abstract giving a brief and factual summary of the document indicative of the report, even though it may also appear elsewhere in the body of the technical report. If additional space is required, a continuation sheet shall be attached.

It is highly desirable that the abstract of classified reports be unclassified. Each paragraph of the abstract shall end with an indication of the military security classification of the information in the paragraph, represented as *(TS)*, *(S)*, *(C)*, or *(U)*.

There is no limitation on the length of the abstract. However, the suggested length is from 150 to 225 words.

14. KEY WORDS: Key words are technically meaningful terms or short phrases that characterize a report and may be used as index entries for cataloging the report. Key words must be selected so that no security classification is required. Identifiers, such as equipment model designation, trade name, military project code name, geographic location, may be used as key words but will be followed by an indication of technical context. The assignment of links, rules, and weights is optional.

GPO 886-551

Unclassified

Security Classification